**University of Granada**
**Department of Mineralogy and Petrology**

# Pre-Variscan magmatism of the Central Iberian Zone: Chemical and isotope composition, geochronology and geodynamic significance

*Cristina Talavera Rodríguez*

Doctoral Thesis
Febrero 2009

Editor: Editorial de la Universidad de Granada
Autor: Cristina Talavera Rodríguez
D.L.: GR. 1774-2009
ISBN: 978-84-692-1438-1



# University of Granada

## Department of Mineralogy and Petrology


# Pre-Variscan magmatism of the Central Iberian Zone: Chemical and isotope composition, geochronology and geodynamic significance


**Cristina Talavera Rodríguez**


Doctoral thesis

Granada, 2009

Universidad de Granada

Departamento de Mineralogía y Petrología

**Pilar G. Montero**

Campus Fuentenueva, 18002 Granada, Spain

Tel +34 958246619; Fax +34 958243368

**pmontero@ugr.es**

**Pilar González Montero**, Catedrático de Petrología y Geoquímica de la Universidad de Granada, certifica:

Que. Dña. **Cristina Talavera Rodríguez** ha realizado bajo mi dirección la Tesis Doctoral que lleva por título: ***Pre-Variscan magmatism of the Central Iberian Zone: Chemical and isotope composition, geochronology and geodynamic significance.***

Y para que así conste, lo firmo en Granada a 13 de Enero de 2009

Fdo. Pilar G. Montero

## ACKNOWLEDGMENTS

"Science has painful roots but has sweet fruits" said Aristóteles and I agree with him. This Thesis is the result of four years of a very hard work in which there have been difficult moments. I would have not been able to overcome them and reach my objective without the help and supportiveness of some people. For that reason, I would like to thank them all.

To Pilar González Montero, my advisor, for introducing me in the wonderful world of the Geochronology and the Isotope Geology, for being always available to answer my questions whenever I had them and for encouraging me in last phase of the Thesis.

To Fernando Bea Barredo, for always having some minutes, in his busy schedule to clarify my geochemical questions and discuss the possible hypothesis of this work.

To Francisco González Lodeiro, for showing me the best outcrops of the pre-Middle Ordovician metagranites of the Sierra de Guadarrama and for his lessons of structural geology.

To Jane Scarrow, for her assistance with the English and to Francisco Molina, for his help with the petrography.

To my colleagues of the Department of Mineralogy and Petrology for receiving me with open arms and for doing this thesis a little more bearable.

To the staff of the Centro de Instrumentación Científica of the University of Granada, for their efficiency and kindness, and also to the staff of the Nordsims of Stockholm and the Australian Geoscience of Canberra.

To Sila Pla and Elvira García, my dear "sherpas", for coming with me to take samples, and for making field campaigns more entertaining.

To my parents, "Maria del Pilar and Jose Luis", for believing in me and encouraging me to realize all my dreams and, above all, for letting me fly.

And finally, to the rest of my family and friends for their comprehension and supportiveness during this Thesis. I know that they have had to bear all my bad days.

This work has been supported by the Spanish grant CLG2005-05863/BTE and the Andalucian grant RNM1595.

# INDEX

# 1. RESUMEN

## RESUMEN

Los estudios geocronológicos de los últimos años indican que el magmatismo Cambro-Ordovícico en Iberia y en el resto de Europa central es mucho más abundante de lo que previamente se creía. En Iberia, y en concreto en la Zona Centroibérica, el basamento pre-Varisco contiene tres alineamientos de rocas ígneas de probable edad Cambro-Ordovícica: las rocas metavolcánicas y metagraníticas de la Formación Ollo de Sapo, los metagranitos y las rocas metavolcánicas de la zona norte del Dominio del Complejo Esquisto-Grauváquico, y más al sur, en el límite con la Zona de Ossa Morena, los granitoides de Carrascal Portalegre y las rocas metavolcánicas de la Formación Urra, mucho menos voluminosos y situados ya en Portugal. La presente Tesis Doctoral trata específicamente de este magmatismo Pre-Varisco y en ella se abordan dos cuestiones fundamentales: por un lado, la datación y el estudio geoquímico e isotópico de los cuerpos ígneos de los bandas situadas más al norte, y por otro lado, la integración de todos los datos en un modelo de generación de magmas durante el Cambro-Ordovícico compatible y extensible al resto de rocas de la misma edad en Europa.

La dificultad que históricamente han tenido estas rocas desde el punto de vista geocronológico radica en que la orogenia Varisca sobreimpuesta ha modificado los sistemas isotópicos en roca total, de forma que la aplicación de métodos de datación como Rb-Sr y Sm-Nd no han dado buenos resultados. Por otra parte, los métodos de datación basados en concentrados de minerales (circones), tampoco han sido eficaces debido a la elevadísima fracción de circones que contienen núcleos pre-magmáticos, algo que solamente se ha puesto de manifiesto en estudios recientes realizados por nuestro grupo de trabajo.

En esta memoria hemos estudiado un total de 26 cuerpos ígneos (volcánicos y plutónicos) de la Formación Ollo de Sapo, los sectores de Guadarrama y Gredos, el domo del Tormes y el Complejo Anatéctico de Toledo. Sobre estos cuerpos hemos llevado a cabo un programa sistemático de datación de circones, complementado con un estudio geoquímico e isotópico (Sr y Nd) de roca total. En primer lugar, hemos estudiado más de 2.000 circones mediante catodoluminiscencia, lo que ha puesto de manifiesto la elevadísima tasa de herencia de estas rocas. En segundo lugar, hemos llevado a cabo la datación sistemática de los circones mediante U-Pb por microsonda iónica (SIMS) y por ICP-MS Ablación Láser, y mediante Pb-Pb por TIMS. Localmente se ha utilizado también el método Rb-Sr en roca

total y una isocrona interna realizada en un megacristal de feldespato potásico. Los resultados geocronológicos se detallan en el capítulo 4 y se resumen en la Tabla 4.1. Además de la edad de la cristalización, mayoritariamente en torno a 480-490 Ma, hemos podido establecer las distintas edades de poblaciones heredadas, que van desde Ediacaran (la más importante en torno a 605-625 Ma), a Toniense, Orosiriense y Mesoarcaica.

Geoquímica e isotópicamente las rocas Cambro-Ordovícicas (tanto las volcánicas como las plutónicas) de los dos dominios de la Zona Centroibérica son muy similares. Geoquímicamente son rocas marcadamente peraluminosas, magnesianas y alcalino-cálcicas (en el sentido de Frost et al., 2001), caracterizadas por el enriquecimiento en los elementos más incompatibles, con una anomalía positiva de Li y negativa de Sr, características típicas de granitos derivados de rocas corticales antiguas. Isotópicamente, estas rocas tienen $(^{87}Sr/^{86}Sr)_{490Ma} \approx 0.707 - 0.713$, y $\varepsilon Nd_{490Ma} \approx -5.8$ a $-3.3$, lo que apunta a que proceden de materiales continentales antiguos con poca o ninguna aportación mantélica excepto, quizá, los metagranitos de Miranda do Douro y San Sebastian, en el dominio del Ollo de Sapo, ligeramente más primitivos $(^{87}Sr/^{86}Sr)_{490Ma} \approx 0.704$, $\varepsilon Nd_{490Ma}$ entre -3.40 y 2.1.

A partir estos datos, y a partir de las edades de las poblaciones heredadas y de la información extraída de los estudios morfológicos y de catodoluminiscencia de los circones se ha establecido la naturaleza de la posible fuente de este magmatismo Cambro-Ordovícico, que ha debido consistir en rocas ígneas félsicas Panafricanas y situadas en el margen norte de Gondwana, posiblemente asociadas espacialmente a las que forman el actual Anti-Atlas marroquí.

La elevadísima proporción de herencia encontrada en los circones de estas rocas es un hecho tan anómalo que ha requerido un estudio específico. Para ello, hemos calculado la temperatura de saturación de circón (≈815 ºC), la temperatura de cristalización de los circones con el termómetro Ti-en-circón (≈ 826 °C) y modelado la cinética de disolución de circón en los magmas Cambro-Ordovícicos usando las ecuaciones de Watson (1996). A partir de estos datos hemos podido extraer información muy valiosa acerca de los mecanismo de fusión que han dado origen a los magmas Cambro-Ordovícicos y su posterior emplazamiento. Se concluye que la fusión del protolito cortical tuvo lugar en la base de la corteza, y fue desencadenada por la afluencia de pulsos de magmas máficos muy calientes en un ambiente geodinámico extensional.

Finalmente, con todos los datos geocronológicos del magmatismo Cambro-Ordovícico de las Zonas Centroibérica, Galicia-Tras-Os-Montes y Ossa-Morena, ha sido posible establecer la edad del rifting Cambro-Ordovícico en Iberia: en las las Zonas Centroibérica y Galicia-Tras-Os-Montes empezó aproximadamente a 500 Ma, alcanzó un máximo a 495-483 y finalizó a 470 Ma. En la Zona de Ossa-Morena la situación es menos clara, la duración del rifting parece haberse extendido desde 515 hasta 460 Ma, sin que exista un máximo bien definido.

# 1. INTRODUCTION

# 1. INTRODUCTION

## 1.1. Problem definition and objectives

### 1.1.1. The problem

Growing geochronological evidence indicates that the Cambro-Ordovician magmatism of South and Central Europe was more voluminous than earlier believed (e.g., Delaperriere and Respaut, 1995; Schaltegger and Gebauer, 1999; Valverde-Vaquero and Dunning, 2000; Barbey et al., 2001; Deloule et al., 2002; Schaltegger et al., 2003; Friedl et al., 2004; Mazur et al., 2004; Roger et al., 2004; Helbing and Tiepolo, 2005). Igneous rocks of this age are well represented in the Central Iberian Zone where pre-Middle Ordovician felsic volcanic rocks and granitoids, strongly deformed and variably metamorphosed during Varis-

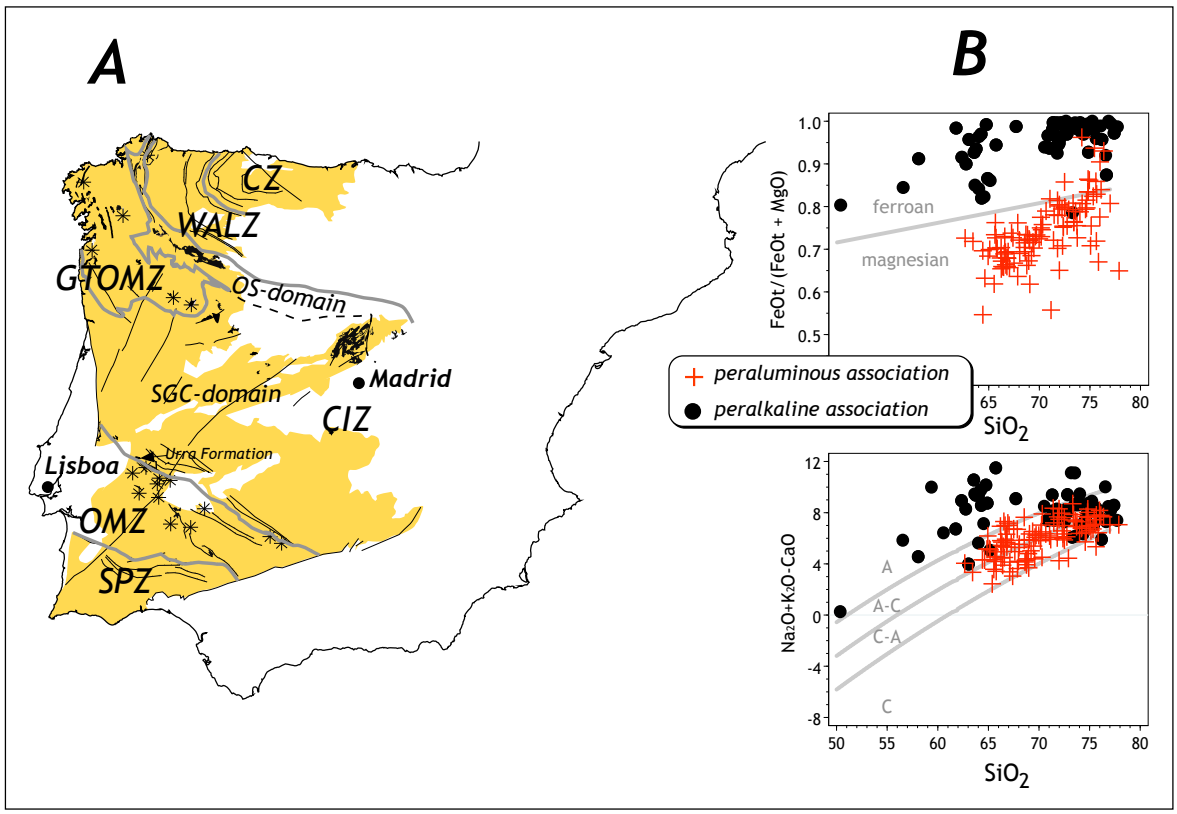


Figure 1.1: A) Exposures of the Cambro-Ordovician igneous rocks in the Iberian Massif. Black spots represent the peraluminous association; stars represent bodies of the peralkaline Association. CZ: Cantabrian Zone; WALZ: West Asturian Leonese Zone; CIZ: Central Iberian Zone, OS and SGC: Ollo de Sapo and Schist-Graywacke Complex domains; GTOMZ: Galicia Tras-os-Montes Zone; OMZ: Ossa-Morena Zone; SPZ: South Portuguese Zone. B) Frost et al. (2001) plots of the Cambro-Ordovician igneous rocks of Iberia revealing the contrasting composition of the peraluminous and peralkaline associations (see text for discussion).

can times, crop out following three NW-SE roughly parallel curved lineaments (Fig. 1.1A): The first, and most voluminous, comprises the Ollo de Sapo Formation, located near the boundary with the West Asturian Leonese Zone; the second comprises the orthogneisses of the northern part of the Schist-Graywacke Complex Domain, and the third, and less voluminous, includes the Urra Formation (Portugal), and is located at the boundary with the Ossa-Morena Zone.

All these rocks are augen-gneisses mostly derived from igneous rocks, either volcanic or plutonic, so that all of them can be properly named orthogneisses. To avoid confusion and distinguish between those derived from volcanic rocks from those derived from plutonic rocks, we shall use the terms "metavolcanic rocks" and "metagranites". Obviously, this last term does not mean "a granite of metamorphic origin" but a "metamorphosed granite".

The study of the Cambro-Ordovician igneous rocks of the Central Iberian Zone has historically raised much interest because of the following two main reasons:

- First, they represent the largest pre-Variscan magmatic episode in the Central Iberian Zone, the significance of which is still poorly understood. Whereas there is a general agreement that the Cambro-Ordovician peralkaline rocks and associated gabbros of the Ossa Morena Zone originated in a rifting environment (e.g., Ribeiro, 1987; Ribeiro and Floor, 1987; Santos Zalduegui et al., 1995; Montero and Bea, 1998; Sánchez García et al., 2003; Montero and Floor, 2004a), the Cambro-Ordovician peraluminous to calc-alkaline rocks of Central Iberia, solely by virtue of their chemical signature, have been interpreted by several authors as evidence for an active margin setting (e.g., Gebauer et al., 1993; Valverde-Vaquero and Dunning, 2000; von Raumer et al., 2003).

- Second, they are an important component of the source layer of the Iberian Variscan granites (Villaseca et al., 1998; Castro et al., 1999; Castro et al., 2000; Dias et al., 2002; Bea et al., 2003).

However, the study of the Iberian Cambro-Ordovician magmatism has been plagued with difficulties, most of them arising from the lack of precisely determined ages, which in the literature have been variously estimated, from Early Ediacaran to Late Ordovician.

Stratigraphically, the position of the metavolcanic rocks is poorly constrained. In the case of the Ollo de Sapo Formation, they are located below a siliciclastic series of probable Arenig age, the Armorican Quartzite, and overlie a non-fossiliferous series of unknown age which has been variously interpreted as Early Paleozoic or Late Proterozoic. Radiometrically, no attempt to date the Ollo de Sapo metavolcanic rocks by Rb-Sr, Sm-Nd or conventional U-Pb on zircon concentrates has succeeded so far. Only the El Cardoso gneiss in the eastern Guadarrama mountains (to the south of Riaza, Fig. 1.3), which although it does not belong to the Ollo de Sapo Formation bears many similarities to it, has been dated at 480 ± 2 Ma, U-Pb on zircons (Valverde-Vaquero and Dunning, 2000). Equally problematic is the age of the metagranites, especially those of the Ollo de Sapo Domain, in which U-Pb dating of zircon concentrates has characteristically yielded highly discordant and very imprecise ages, from 618 Ma (Lancelot et al., 1985) to 440 Ma (Fernández-Suárez et al., 1999).

The reasons for these difficulties may be summarized as follows:

- The lack of initial isotopic homogeneity and the disturbances produced during the Variscan metamorphism cause many difficulties when applying Rb-Sr and Sm-Nd methods.

- The zircons of these rocks are very complex, as revealed by our previous studies. Cathodoluminescence imaging revealed that a significant fraction of grains contain inherited cores which record different ages, from Ediacaran up to Archean (Bea et al., 2006; Montero et al., 2007; Bea et al., 2007; Sola et al., 2008; Talavera et al., in press). The simultaneous occurrence of two or more different age components make dating methods like conventional U-Pb in zircon concentrates useless, single crystal methods are the only way to properly date these rocks.

### 1.1.2. Objectives

The main goal of this work is to make a systematic study of the geochronology, Sr and Nd isotope geology, and geochemistry of the Lower-than-Middle Ordovician magmatism of the Central Iberian Zone. In particular, we aimed at the following objectives:

- To date, using zircon U-Pb ion microprobe and LA-ICPMS analyses, single-grain Pb-Pb stepwise evaporation analyses and, occasionally, whole rock and internal Rb-Sr isochrons, (i) the metavolcanic and metagranitic rocks of the Ollo de Sapo

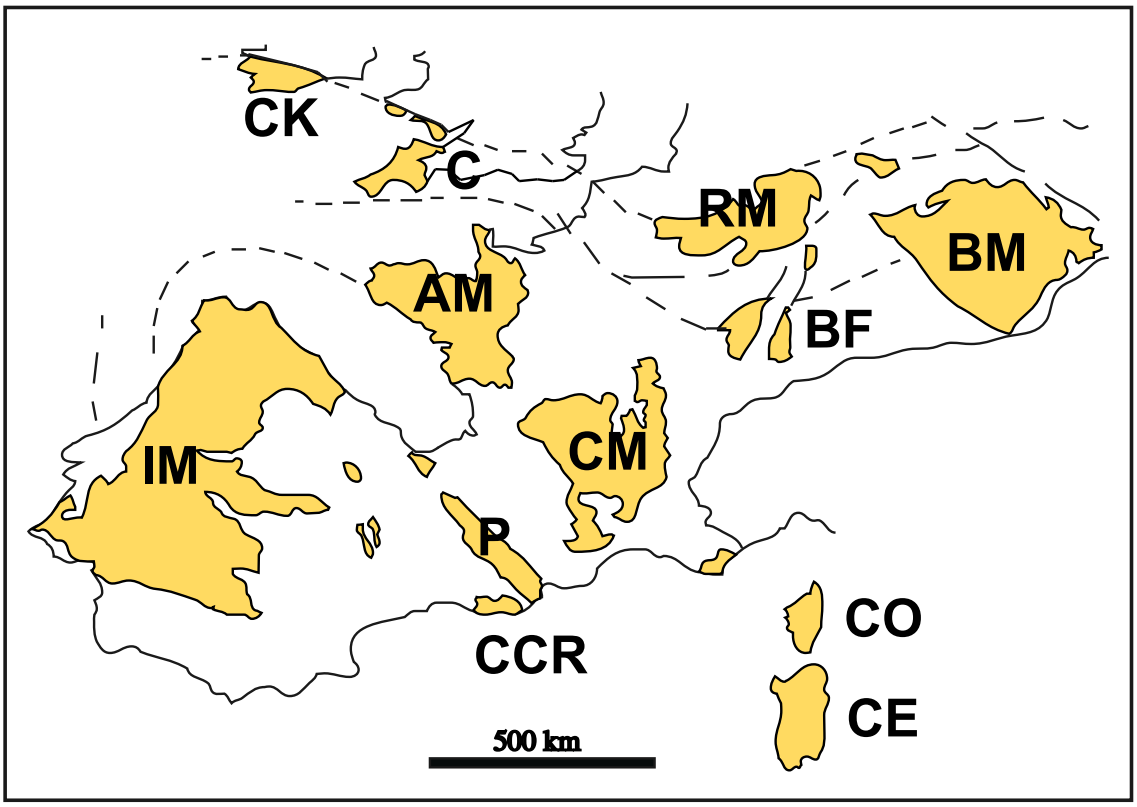


Figure 1.2. Main segments of the Variscides during the Early Carboniferous. IM, Iberian Massif; CCR, Catalan Coastal Ranges; P, Pyrenees; CM, Central Massif; AM, Armorican Massif; C, Cornubia; CK, Cork; RM, Renish Massif; BF, Black Forest; BM, Bohemian Massif. (Taken from http://www.geofys.uu.se/eprobe/Projects/iberia/SWIberia.htm).

Domain, and (ii) the pre-Middle Ordovician metagranites and metavolcanic rocks of the Schist-Graywacke Complex Domain.

- To study the major and trace element geochemistry and the Sr and Nd isotope geology of all these materials.

- To understand the reasons for the abnormally elevated zircon inheritance of these rocks, which largely exceeds what is to be expected for common felsic volcanic rocks and granites (e.g., Miller et al., 2003). To do this, we developed a numerical model based on zircon solubility and solution kinetics that constrains the minimum heating and cooling rates of the melting event that caused the Cambro-Ordovician anatexis.

- Finally, to propose a geodynamic model compatible with these data that may explain the origin of the Cambro-Ordovician magmatism of Central Iberia.

## 1.2 Geological setting

### 1.2.1. The Iberian Massif

The Iberian Massif is one of the largest exposures of the European Variscan Orogen (Fig. 1.2) occupying the west and northwest areas of the Iberian Peninsula (Fig. 1.1A). Lotze (1945), based on stratigraphic, structural, metamorphic and magmatic features, divided it into six paleogeographic zones which from the north to the south are: Cantabrian, West Asturian Leonese, Castellan-Galician, Alcudian-Lusitanian, Ossa Morena and South Portuguese Zones. Afterwards, Julivert et al. (1972) joined the Castellan-Galician Zone and the Alcudian-Lusitanian Zone together to form the Central Iberian Zone. Some years later, Farias et al. (1987) and Arenas et al. (1988) identified a new zone within the Central Iberian Zone which they called the Galicia Tras-os-Montes Zone.

The internal regions of the Iberian Massif: the Ossa Morena, Galicia-Tras-os-Montes and Central Iberian Zones stand out because of the abundance of pre-Middle Ordovician magmatic rocks. These form two different geochemical associations. The most abundant is composed of intermediate to silicic peraluminous rocks (mol. $Al_2O_3/(CaO + Na_2O + K_2O) \approx 1.34 \pm 0.23$) which according to the classification scheme of Frost et al. (2001) are magnesian, and alkaline-calcic to calc-alkaline (Fig. 1.1B). The less abundant association is composed of ferroan, alkaline to calc-alkaline, and predominantly high-silica rocks (Fig. 1.1B) which often contain Na pyroxenes and/or amphiboles. Whereas the latter unequivocally form an A-type association, the former, despite having most features similar to S-type rocks including the occasional presence of cordierite and garnet, cannot be correctly termed so because, according to zircon evidence, they do not represent melts of sedimentary rocks, which strongly suggests that their magmatic source was predominantly composed of Pan-African igneous materials (Montero et al., 2007; Bea et al., 2007). Therefore, for the sake of simplicity, in this work we shall refer to these two different rock associations as “peraluminous” and “peralkaline”, noting that a few rocks of the first group have mol. $Al_2O_3/(CaO + Na_2O + K_2O) < 1.05$ and about 50-70% of the rocks of the second group, depending on the massif, have mol. $(Na_2O+K_2O)/Al_2O_2 \leq 1$, i.e., they are not strictly peralkaline. Whereas in Ossa-Morena and Galicia-Tras-os Montes Zones, the two associations are well represented, in the Central Iberian Zone, despite of hosting the most voluminous pre-Middle Ordovician magmatism, only the peraluminous association is found.

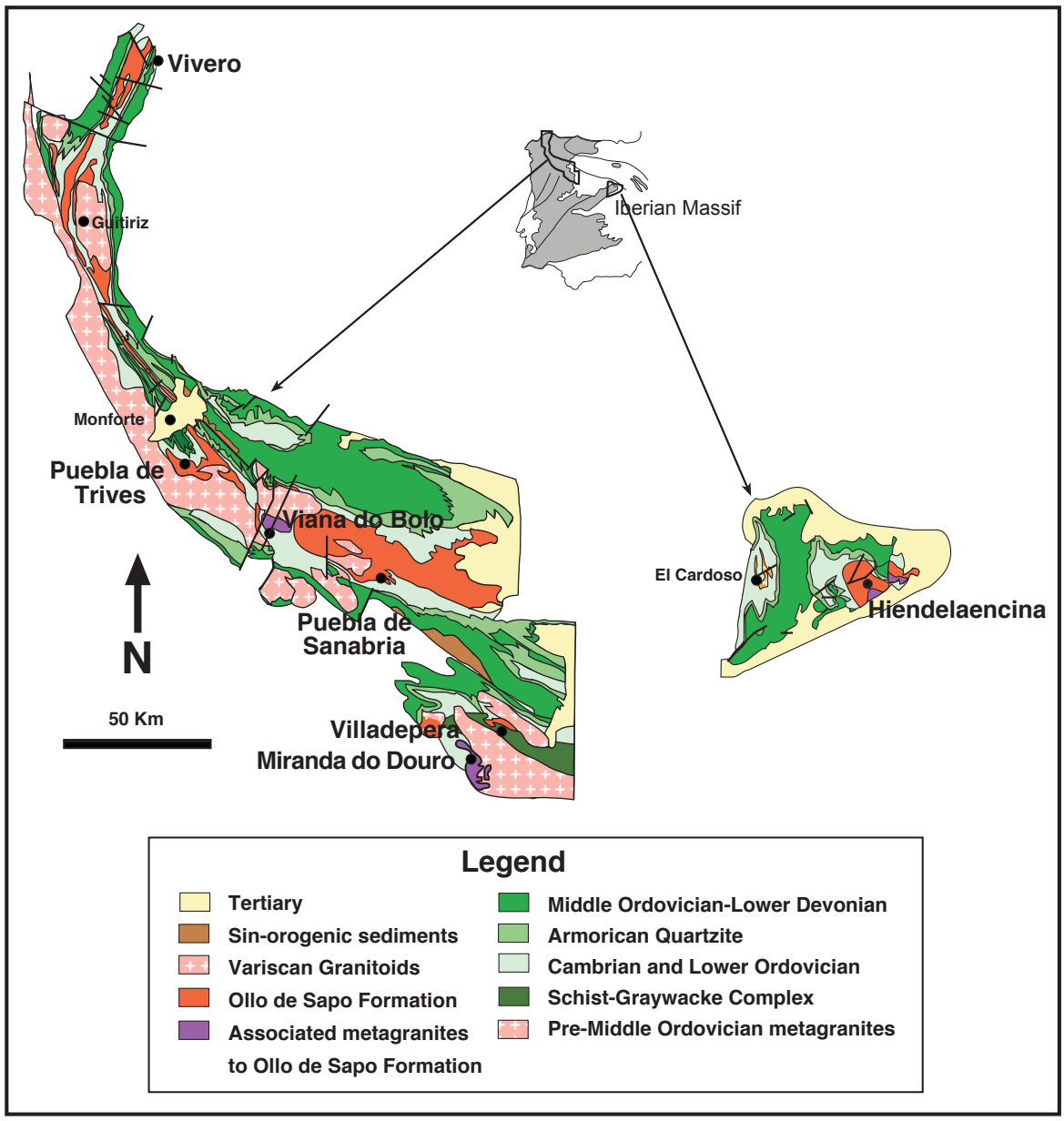


Figure 1.3: Geological scheme of the Ollo de Sapo Domain (Martínez Catalán et al., 2004).

The following section describes the features of the Central Iberian Zone which are relevant to the present work.

### 1.2.2. The Central Iberian Zone

The Central Iberian Zone is located in the central part of the Iberian Massif. Its boundaries are the Vivero fault and the Courel and Peñalba synclines in the north (Martínez Catalán, 1985), and the Badajoz-Córdoba shear zone in the south (Díez Balda et al., 1990; Azor et al., 1994). Rock formations in this area mostly consist of Late Proterozoic to Early

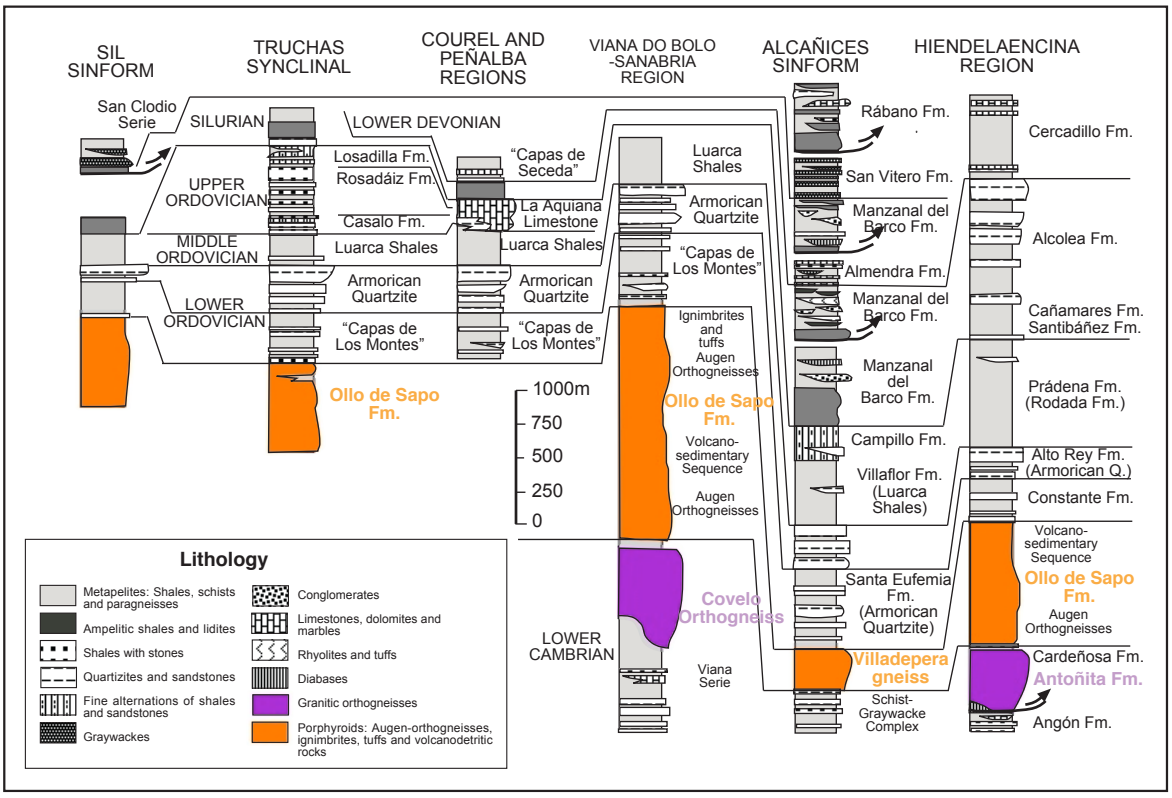


Figure 1.4: The most representative stratigraphical columns of the Ollo de Sapo Domain (Martínez Catalán et al., 2004)

Paleozoic metasediments and minor pre-Middle Ordovician metagranites intruded by numerous syn- or late-kinematic Variscan granitoids. Discordant Carboniferous deposits are common in the cores of large synclines.

The Central Iberian Zone can be subdivided into two domains: the Ollo de Sapo Domain to the north and the Schist-Graywacke Complex Domain to the south (Pérez-Estaún et al., 2004). The most important features of these areas are as follows:

### *1.2.2.1. The Ollo de Sapo Domain*

The Ollo de Sapo Domain is a narrow zone located in the north of the Central Iberian Zone (Fig. 1.3), limited by the Vivero fault and Peñalba and Courel synclines to the east and northeast, which mark the boundary with the West Asturian Leonese Zone (Fig. 1.1A) (Martínez Catalán, 1985).

The Ollo de Sapo Domain is defined by the presence of the Ollo de Sapo Formation, which extends for about 570 kilometers, from the northeast Galician coast to the Sanabria region. From this region to the southeast, it is covered by the Tertiary deposits of the Duero

Basin to reappear again in the Hiendelaencina region (Fig. 1.3). This domain consists of: (i) a pre-Ordovician sequence, (ii) the Ollo de Sapo Formation, (iii) an Ordovician-Lower Devonian sequence, (iv) an Upper Devonian-Upper Carboniferous sequence (Fig. 1.4).

- **The pre-Ordovician sequence** crops out below the Ollo de Sapo Formation (Fig. 1.4), in the cores of large antiforms in the Hiendelaencina and Viana do Bolo region. In the last region this series has been called the Porto-Villavieja Series (Martínez García and Corretgé, 1970), Porto Series (Martínez García, 1973) or Viana Series (Ferragne, 1968). From bottom to top the series consists of: (i) quartzites and quartzitic micro-conglomerates, (ii) limestones associated with quartzites, (iii) schists and migmatitic gneisses in which Covelo and San Sebastián metagranites are intercalated, and (iv) limestones and calcic-silicate rocks. In Hiendelaencina, the sequence is very similar and from bottom to top it consists of: (i) a sequence of schists, quartzites, micro-conglomerates, marbles and amphibolites (the Angón Formation: González Lodeiro, 1980; Fernández Rodríguez, 1991), (ii) the sill-like Antoñita metagranite (Schäfer, 1969), and (iii) a sequence of calcic-silicate rocks and marbles with a few meters of feldspathic quartzites and schists (the Cardeñosa Formation). In Galicia the base of the Ollo de Sapo Formation is not exposed.

- **The Ollo de Sapo Formation** is intercalated between a pre-Ordovician sequence and the Lower Ordovician shales and quartzites, called "Capas de los Montes" in Galicia (Riemer, 1963), Puebla de Sanabria Formation in the Sanabria region (Martínez García, 1971, 1973), Santa Eufemia Formation in the Villadepera region (Vacas and Martínez Catalán, 1987) and Constante Formation in the Hiendelaencina region (Schäfer, 1969; González Lodeiro, 1980, 1981a, 1981b) (Fig. 1.4). The lower contact is always very deformed and is metamorphosed to medium or high grade. The upper contact is locally discordant. Two facies of the Ollo de Sapo Formation are often distinguished, one coarse-grained and the other fine-grained, these form alternating layers of variable thickness (Parga-Pondal et al., 1964; Navidad, 1978) :

  - *Coarse-grained facies.* The coarse-grained facies is preferentially, but not exclusively, in the lower part of the formation. It is composed of K-feldspar megacrysts (Ø ≈ 5-7 cm, locally up to 15 cm) and phenocrysts of plagioclase


Figure 1.5: Facies of the Ollo de Sapo Formation: A) Coarse-grained facies in the Ria del Barquero (Lugo); B) Coarse-grained facies in the Hiendelaencina region; C) Fine-grained facies in the Ria del Barquero (Lugo); D) Fine-grained facies in Mañon (A Coruña).

and quartz (Ø ≈ 0.5-3 cm) in a gray to greenish fine-grained groundmass (Fig. 1.5, A and B). K-feldspar megacrysts are usually euhedral or subhedral, locally rapakivi, and contain abundant inclusions of plagioclase, quartz, biotite and zircon. Plagioclase phenocrysts ($An_{15-25}$) are euhedral or subhedral. Quartz phenocrysts tend to be subhedral, locally rounded, and often show embayed contours. The groundmass is composed of quartz, K-feldspar, muscovite, biotite, rare albite, chlorite and sericite. The accessory mineral assemblage is often composed of apatite, zircon, Fe-Ti-oxides, monazite, xenotime, ilmenite and Fe-Cu-sulfides.

- *Fine-grained facies*. The fine-grained facies is typically located in the upper part of the Ollo de Sapo Formation. It consists of small phenocrysts of K-feldspar (up to 2 cm) and quartz (up to 1.5-2 cm) inside a groundmass with a modal composition identical to that of the coarse-grained facies (Fig. 1.5, C and D). Often the fine-grained facies is intercalated with layers of metasediments, mostly schists, quartzites and quartz-feldspatic schists. In some areas, such as the Sanabria and Hiendelaencina regions, both facies are finely intercalated, so forming the "mixed facies".

- **The Ordovician-Lower Devonian sequence** overlies the Ollo de Sapo Formation. It is composed of pre-orogenic deposits from the Lower Ordovician to the Lower Devonian (Fig. 1.4). The Ordovician deposit consists of: (i) alternating quartzites and black shales with minor intercalations of micro-conglomerates (Matte, 1968; Pérez Estaún, 1978), and a quartzitic formation, both of which are Lower Ordovician, (ii) a formation of gray-bluish shales with minor quartzitic intercalations which is Middle Ordovician (Gutiérrez-Marco et al., 1999), and (iii) gray and gray-greenish shales with intercalations of sandstones and quartzites, and sometimes beds of limestones and dolomites, which are Upper Ordovician.

  According to Schäfer (1969), Bultynck and Soers (1971), Soers (1972), Carls (1977) and Gutiérrez-Marco and Robardet (1991), the Silurian rocks are composed of: (i) few quartzitic beds, (ii) black carbonaceous shales (ampelites), and (iii) gray shales, thin beds of gray and white quartzites, lidites, black and very fine-grained silicious and carbonaceous rocks and thin beds of limestones.

Finally, as described by Drot and Matte (1967), Carls (1969) and Bultynck and Soers (1971), the Lower Devonian is made up of shales and limestones.

- **The Upper Devonian-Upper Carboniferous sequence** is formed of a succession of syn-orogenic flysch facies, mostly turbiditic deposits of argillites, graywackes and micro-conglomerates (Martínez Catalán and González Clavijo, 2004).

Spatially associated with the metavolcanic rocks of the Ollo de Sapo Formation there are some augen-gneisses that undoubtedly represent intrusive granite bodies. They appear as sills or lacoliths up to 300 m thick (González Lodeiro, 1981b; Iglesias Ponce de Leon and Ribeiro, 1981) that intrude the metasedimentary sequence underlying the Ollo de Sapo metavolcanic rocks. The best known are: (i) the Antoñita metagranite in the Hiendelaencina region, (ii) the Miranda do Douro metagranite in the Villadepera region, and (iii) the Covelo and San Sebastián metagranites in the Viana do Bolo area. These rocks are coarse-grained augen-gneisses that differ from those of the Ollo de Sapo in having a coarser groundmass, a lack of blue quartz crystals and the presence of intrusive contacts, aplopegmatitic dikes and metapelitic enclaves. They are composed of large K-feldspar megacrysts (Ø ≈ 5-12 cm) within a coarse-grained foliated groundmass of quartz, oligoclase, K-feldspar, biotite, muscovite, and rare tourmaline, cordierite and garnet. The K-feldspar megacrysts frequently have multiple tiny inclusions of plagioclase and biotite aligned following crystallographic contours (Frals inclusions), and also often have rapakivi structures. The accessory minerals are apatite, ilmenite ± magnetite, zircon, monazite and xenotime.

#### *1.2.2.2. The Schist-Graywacke Complex Domain*

The Schist-Graywacke Complex Domain occupies the major part of the Central Iberian Zone (Fig. 1.6). It is bounded by the Badajoz-Córdoba shear zonein the south, marking the boundary with the Ossa Morena Zone. At the northeast boundary of this domain, to the west of Zamora, there are recumbent folds with northeast vergence which define a transitional zone to the Ollo de Sapo Domain. The main sedimentary units of this domain are: (i) The Schist-Graywacke Complex, (ii) the Cambrian transgressive deposits, and (iii) the post-Cambrian-Paleozoic sequence.

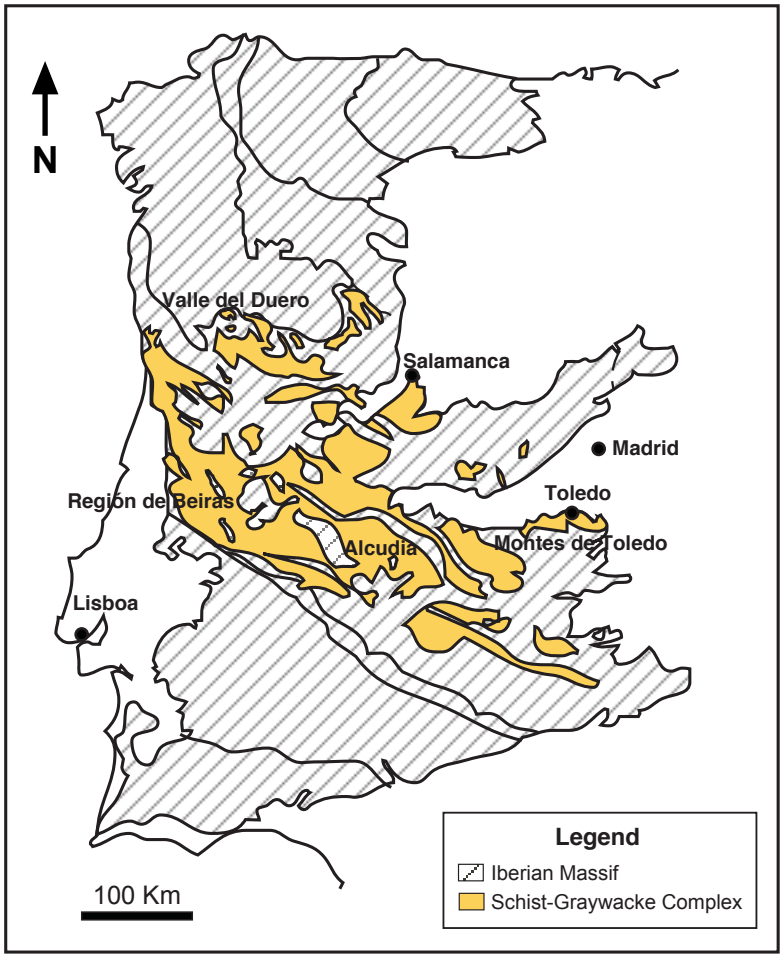


Figure 1.6: Outcrops of the Schist-Graywacke Complex in the Central Iberian Zone (Bernardo de Sousa, 1984).

- **The Schist-Graywacke Complex.** This term refers to important Ediacaran to Cambrian monotonous non-fossiliferous pelitic and psammitic successions (Carrington da Costa, 1950) which crop out in the core of large antiforms in central Portugal (Valle del Duero and región de Beiras), Salamanca, Extremadura, Montes de Toledo and Alcudia (Fig. 1.6). The Schist-Graywacke Complex can be separated into two units which have different names depending on the places where they have been defined (Fig. 1.7). According to Rodríguez Alonso et al. (2004) and Diez Balda (1986) these units can be described as follows:

  - The lower unit, often called the Monterrubio unit. This is a monotonous succession consisting of lutites and sandstones with minor intercalations of conglomerates, chaotic beds and few volcanoclastic beds, which appear in the upper part of the series. It crops out throughout all the Central Iberian Zone ex-

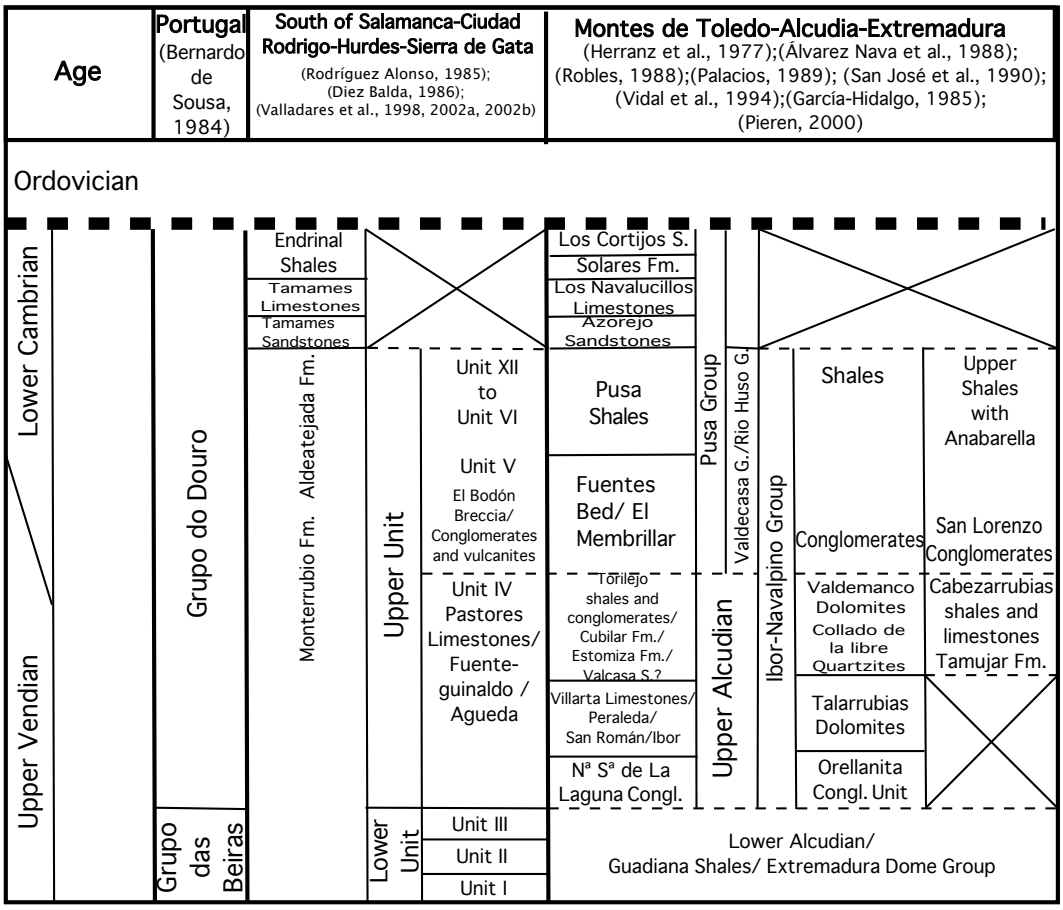


Figure 1.7: Scheme of the chronostratigraphy and the correlation of the units, groups and formations which have been defined in different areas of the Schist-Graywacke Complex Domain for pre-Ordovician sequence to the north of Los Pedroches batholith (Rodríguez Alonso et al., 2004).

cept in the northwest of the domain (in the areas of Salamanca, Fregeneda and Douro). Its thickness is unknown because the lower boundary is not exposed.

- The upper unit, often called the Aldeatejada unit. This occurs on top of the Lower unit and it is mainly composed of pelites with some beds of black lutites, conglomerates and sandstones, together with limestones and discontinuous olistostromic beds and intercalations of phosphates and volcanic and volcanoclastic rocks. This unit has been divided into a several litostratigraphic units which mainly crop out in the anticlines of Alcudia, Ibor, Navalpino and Valdelacasa, at the edge of the Ciudad Rodrigo-Hurdes-Sierra de Gata area and in the Douro-Fregeneda-Salamanca area and its eastern prolongation.

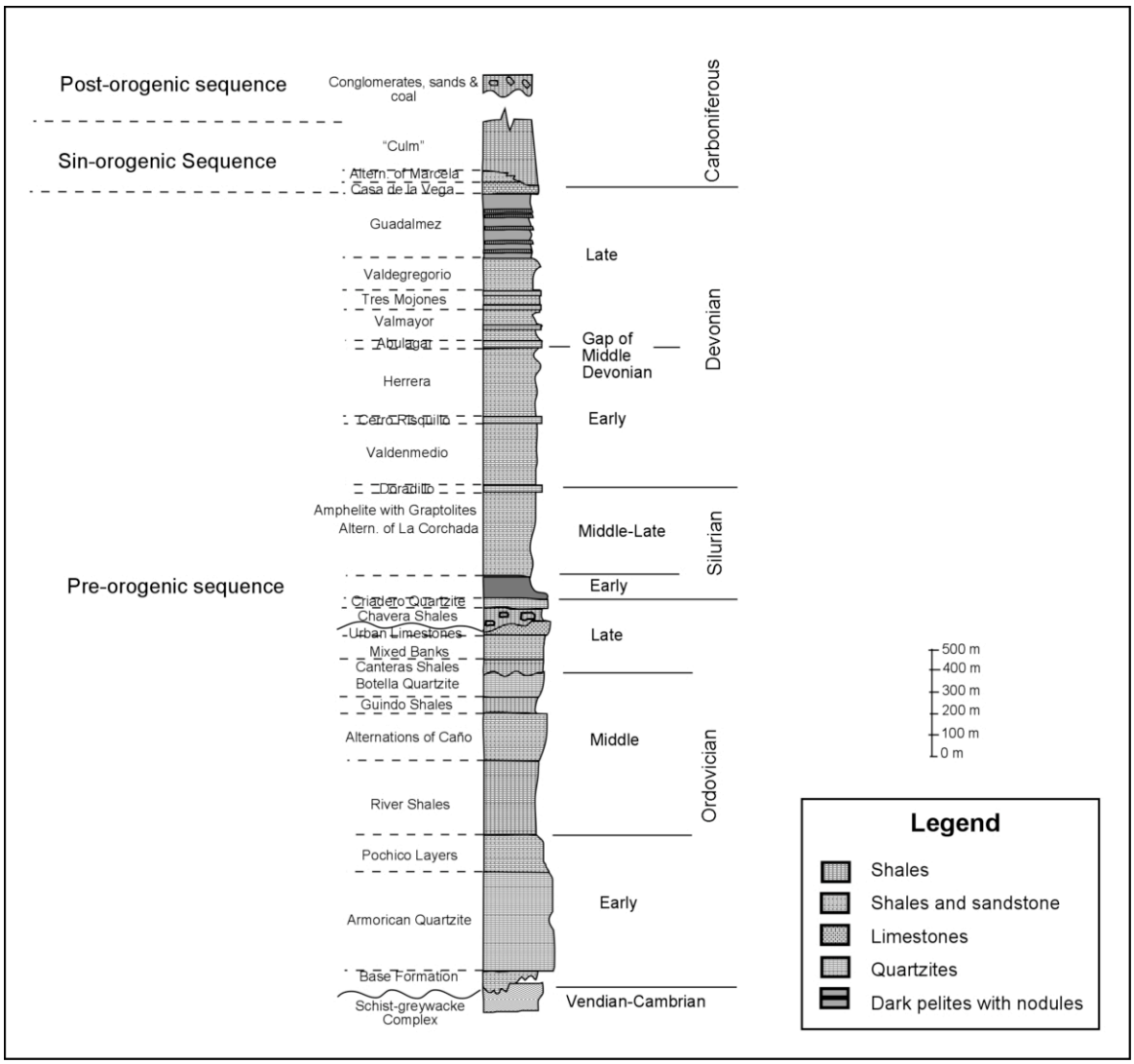


Figure 1.8: Stratigraphic column of the Ordovician-Carboniferous rocks of the Schist-Graywacke Complex Domain to the north of Los Pedroches Batholith (Martínez Poyatos et al., 2004).

These units can be recognized throughout all the Central Iberian Zone except to the south of the Pedroches Batholith, where the Cambrian-Ediacaran sedimentary sequence bears more similarities to the sequences of the same age found in the Ossa Morena Zone to the south (Fig. 1.1A).

- **The Cambrian transgressive deposits** crop out discontinuously throughout the Schist-Graywacke Complex Domain, except in the southeast and the central-eastern areas of the Central Iberian Zone, and the Portuguese region of the Douro. In the central and eastern areas of the Central Iberian Zone, this sequence consists of shallow marine sandy deposits overlain by platform carbonates. In the

Fregeneda and the Portuguese region of the Douro, the sequence is composed of a pelitic-psammitic succession with calcic-silicate and conglomeratic beds.

- **The post-Cambrian Paleozoic sequence**. The post-Cambrian Paleozoic sequence crops out in the cores of synclines with northwest-southeast orientation and in the southern part of the Schist-Graywacke Complex Domain. According to Martínez Poyatos et al. (2004), it can be divided in three sequences (Fig. 1.8): pre-orogenic, sin-orogenic and post-orogenic.

  - **Pre-orogenic sequence**. This mainly consists of a succession of detritic formations deposited in a shallow-marine siliciclastic platform environment. These sediments are discordantly deposited over the Cambrian deposits (Lotze, 1956; Gutierrez Marco et al., 2002). In detail, the sequence is composed of: (i) conglomerates, sandstones and silts, Armorican Quartzite, and alternating quartzites and shales which are Lower Ordovician, (ii) dark shales, alternating sandstones and shales, gray shales, and quartzites which are Middle Ordovician, (iii) shales (at the base of which there is a conglomeratic bed with phosphates), alternating shales and sandstones, discontinuous calcareous bed, a disconformity related to an erosive event (Robardet, 1981), and diamictites which are Upper Ordovician, (iv) orthoquartzites at the top of which is the Ordovician-Silurian boundary, (v) black shales with volcanic beds and alternating Silurian shales, sandstones, and orthoquartzites; vi) alternating shales and sandstones, orthoquartzites and ferruginous sandstones, alternating shales and sandstones with intercalated bioclastic limestones in the lower part which are Lower Devonian; vii) a stratigraphic gap (Puschmann, 1967) which covers almost all the Middle Devonian; viii) a quartzitic unit, orthoquartzites interlayered within two important units of alternating shales and sandstones, dark gray shales with nodules, limestones, and, finally, shales and sandstones, which are Upper Devonian-Lower Carboniferous.

    To the south of the Alburquerque-Pedroches magmatic lineation, the Devonian pre-orogenic sequence is different. It has disconformities between the Devonian series and the previous series, and the extension of the stratigraphic gap is bigger.

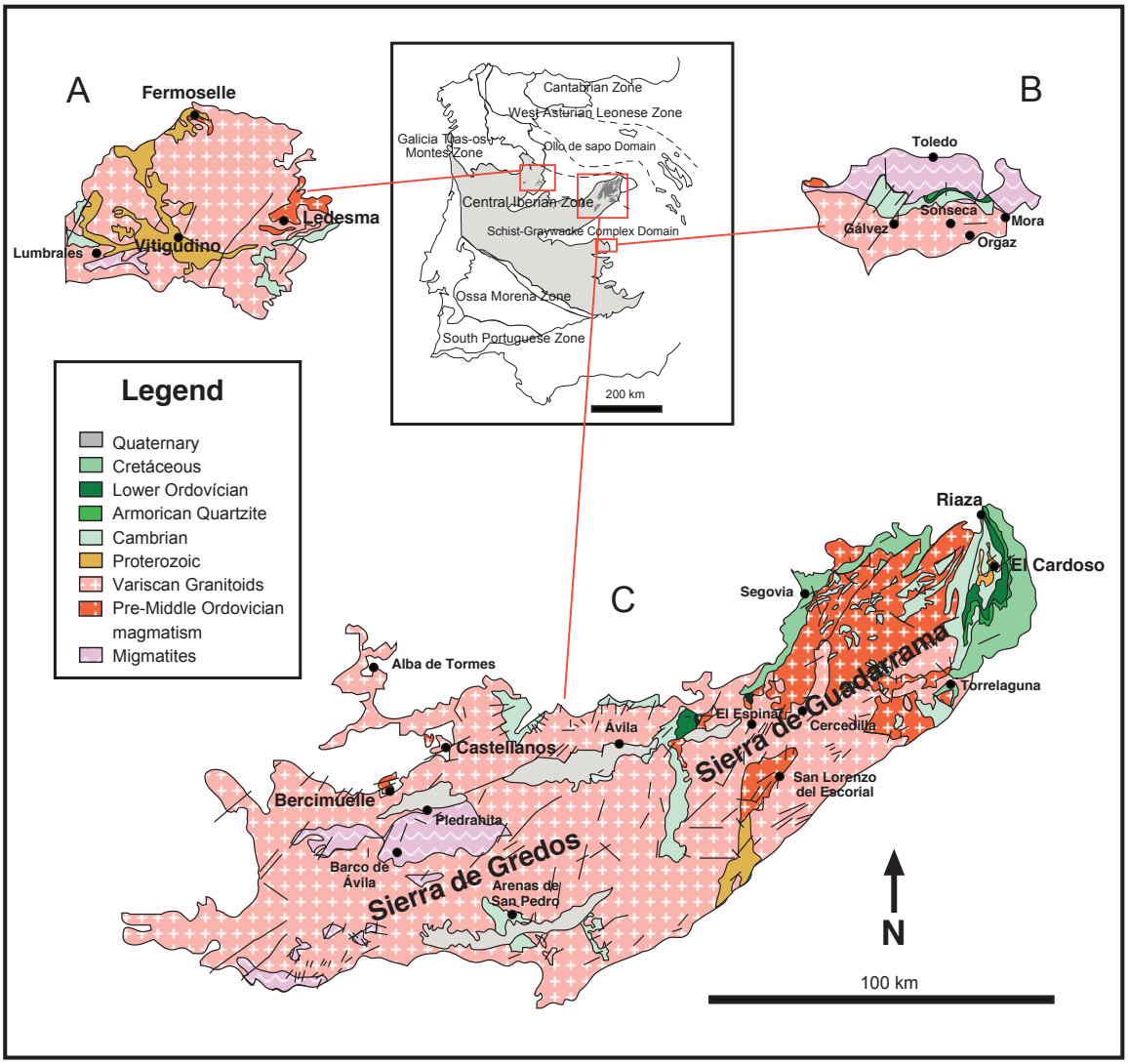


Figure 1.9: Geological Scheme of areas of the Schist-Graywacke Complex Domain where pre-Middle Ordovician metagranites and metavolcanic rocks crop out. The geological scheme represents a section of the geological map of Spain (Álvaro et al., 1994).

- **Sin-orogenic sequence**. It crops out in the south of the Schist-Graywacke Complex Domain and is arranged in northwest-southeast bands. It consists of alternating Lower-Middle Carboniferous shales and graywackes in the Culm facies with intercalations of conglomerates, acid and basic volcanic rocks and minor limestones, which are preferentially found at the bottom of this sequence (García-Alcalde et al., 1984; Rodríguez et al., 1990). At the southern edge, there are two outcrops of sin-orogenic sequences (Mamet and Martínez, 1981; Andreis and Wagner, 1983; Cózar and Rodríguez, 1999), one of them

has paralic sedimentation and the another limnic sedimentation and cyclic sedimentation of conglomerates, sands, silts and coal.

- **Post-orogenic sequence.** This is a sub-horizontal cyclical discordant sequence composed of Upper Carboniferous conglomerates, sands, silts and coal beds (Wagner and Utting, 1967) which crops out in few isolated intra-mountain basins.

The pre-Middle Ordovician magmatism in the Schist-Graywacke Complex Domain is mostly represented by (i) intrusive granitoids and metavolcanic rocks cropping out in the northern sector of the domain, in the areas of Salamanca, Ávila, Toledo and, especially, Guadarrama (Fig. 1.9), and (ii) the Urra Formation, totally analogous to the Ollo de Sapo Formation albeit much less voluminous, which crops out in the south, just at the boundary with the Ossa Morena Zone.

#### *1.2.2.3. Deformation in the Central Iberian Zone*

The pre-Variscan and Variscan deformation in the Central Iberian Zone can be summarized as follows:

- **The pre-Variscan deformation** is revealed by three discordancies in the Schist-Graywacke Complex Domain, named Alcudian, Cadomian and Toledanic. The first two formed during the Cadomian or Pan-African orogeny, and the last one during a Middle-Upper Cambrian low intensity tectonic event (González Lodeiro et al., 2004).

  - The **Alcudian discordance** is found in the southern part of the Schist-Graywacke Complex Domain between the Lower and Upper Alcudian. It is an angular discordance which was identified by the higher dip of the intersection lineation in the Lower Alcudian than in the Upper Alcudian (Ortega Gironés and González Lodeiro, 1986).

  - The **Cadomian discordance** has only been observed in the Peraleda Anticline of the southern Schist-Graywacke Complex Domain, (Llopis, 1970; Capdevila et al., 1971), where a schistosity, dated at 550 ± 10 Ma (Blatrix and Burg, 1981) is found in the "Serie Negra". This schistosity does not affect the overlying Ordovician succession.

- The **Toledanic discordance** is at the bottom of the Ordovician succession. It is affected by minor folds without associated foliation and metamorphism (Díez Balda et al., 1990), it is recognizable because the Ordovician succession lies on top of different formations of the underlying succession. This discordance has been called "Sardic" (Lotze, 1945) and was attributed to the effects of pre-Ordovician movements in a block-tectonic regime. The Toledanic discordance is always between the Armorican Quartzite and the Ollo de Sapo Formation, and affects the Central Iberian and Ossa-Morena Zones.

- **The Variscan deformation** took place through the Late Devonian-Late Carboniferous and was developed in three phases. The most remarkable features of these phases are:

  - **First phase (D1)**. The first phase is characterized by the formation of recumbent folds with east and northeast vergence and an S1 cleavage in the Ollo de Sapo Domain (Matte, 1968) and the north and southeast area of the Schist-Graywacke Complex Domain (Macaya et al., 1991; Azor et al., 1994). In the central area of the Schist-Graywacke Complex Domain, folds have sub-vertical axial planes (Díez Balda et al., 1990).

  - **Second phase (D2)**. The second phase is distinguished by the development of the thrust faults which cut the aforementioned recumbent folds. In the Ollo de Sapo Domain, these thrust faults generally form within Silurian metapelites, with abundant graphite-rich layers (González Clavijo and Martínez Catalán, 2002).

  - **Third phase (D3)**. The third phase is recognized by the formation of back-folding structures whose superposition formed several large folds in the Ollo de Sapo Domain, for instance the El Cardoso Antiform and the Majaelrayo Synform (González Lodeiro et al., 1988; Macaya et al., 1991). In the central and south areas of the Schist-Graywacke Complex Domain the previous recumbent folds and thrust faults were bent by folds with a vertical axial plane or northeast vergence and northwest-southeast direction.

- Moreover, **some late-orogenic extensional structures** have been identified in both domains. These structures are generally described as extensional shear

zones and crop out in the deeper structural levels of antiforms and domes (Escuder Viruete et al., 1994; Escuder Viruete et al., 2000; Diez Balda et al., 1995).

## 1.3. Previous work

Numerous researchers have studied the stratigraphy, petrology, structural geology and geochronology of the Cambro-Ordovician magmatism of the Central Iberian Zone. What follows is a brief summary of the most important studies.

### 1.3.1. The Ollo de Sapo Formation and associated metagranites

#### *1.3.1.1. General geology and lithology*

The term "Ollo de Sapo" derives from the presence of quartz phenocrysts that, when the metamorphic grade is medium or low, have a deep-blue color, probably due to inclusions of sagenitic rutile. The study of the rocks currently grouped under the name of Ollo de Sapo started at the end of the nineteenth century with Cortázar (1874) and Macpherson (1883). The first author considered the Ollo de Sapo of the Mombuey region (Zamora province) as a poligenetic psefite. The second author also proposed a detritic origin for the Ollo de Sapo from Ria del Barquero (Lugo) and suggested that certain fragments of this detritic formation may have come from granitic rocks.

In the first part of the twentieth century, Hernández Sampelayo (1922) described a micaceous nodular gneiss in the Colleira island (Lugo province) which was called "Ollo de Sapo" by the villagers of this region. This gneiss had abundant feldspar crystals from 2 millimeters to 8 centimeters and bluish quartz phenocrysts. Schroeder (1930) described the upper part of the Hiendelaencina formations and considered these rocks as conglomeratic gneisses. Finally, Lotze (1945) studied the porphyric formation of the Sanabria region and considered it to be of volcanic origin, similar to volcanic gneisses of Azuaga, in the Ossa Morena Zone.

In the second part of the twentieth century, numerous researchers have studied the Ollo de Sapo Formation. San Miguel de la Cámara and Lobato Díez (1955) working in the area surrounding the Sanabria lake described the presence of an augen-gneiss. Riemer (1963) in the south of the Lugo province described a volcanic acid association of lavas, tuffs and variably metamorphosed sub-volcanic rocks and named it the Vilachá complex, nowadays known as part of the Ollo de Sapo. Parga-Pondal et al. (1964) provided the first description of the Ollo de Sapo as a whole. These authors defined the Ollo de Sapo as a complex for-

mation consisting of two types of rocks: (i) Detritic rocks consisting of arkosic conglomerates, schistose arkoses, arkoses s.s. with some intercalations of schists and quartzites, which were probably derived from granites and gneisses, and (ii) Tuffaceous volcanic rocks of predominantly rhyolitic composition.

Anthonioz and Ferragne (1967), on the other hand, reached a contrasting conclusion. These authors suggested that in the Sanabria area the Ollo de Sapo showed features of a sedimentary complex: the fact that the coarse-grained facies are located at the bottom of the complex and the fine-grained facies on top was considered to be due to stratigraphic polarity. Furthermore shear structures that often affect these rocks were consider to reflect sedimentary characteristics such as grain selection and crossed stratification. The authors also concluded that most of the detritic material of the Ollo de Sapo came from Galician orthogneisses. Finally, Ferragne (1968) studied the pre-Cambrian basement of the Viana do Bolo region (Southern Galicia) nothing the presence of orthogneisses and paragneisses.

In the 1970s, Martínez García and Corretgé (1970) listed the most distinctive features of the different petrographic units of the Porto-Villavieja Series, including the San Sebastián and Porto gneisses. Martínez García (1973) recognized two facies in the Ollo de Sapo Formation of the Sanabria region and concluded that although the sedimentary contribution was important in some areas, the origin was basically volcanic. Navidad (1978), in agreement with Parga-Pondal et al. (1964) and Martínez García (1973), differentiated two facies: the first one was composed of metavulcanites and metaarkoses preferentially located in the lower part of the formation, and the second one consisted of graywackes and pelites preferentially located in the upper part of the formation. Navidad (1978) suggested an igneous-sedimentary origin for the Ollo de Sapo Formation based on geochemical data.

In the 1980s, Navidad and Peinado (1981) studied the orthogneisses and the metasediments underlying the Ollo de Sapo Formation, that is to say the Angón Formation, the Antoñita gneiss and the Cardeñosa Formation. They concluded that the Antoñita gneiss was a banded and very homogenous augen-gneiss and, based on its chemical-mineralogical features, it was classified as an S-type granitoid belonging to the very differentiated terms of the S-type granitoids with abundant primary muscovite and low-An plagioclase. This gneiss also has associated aplitic and pegmatitic leucogneisses. Iglesias Ponce de León and Ribeiro (1981) carefully mapped the Miranda do Douro and San Vitero-Carbajales regions, and described the Ollo de Sapo Formation as a monotonous series of feldspathic meta-

graywackes and rhyolites with blue quartz crystals with massive layers except at the base where they show grain selection. These authors also identified some decimetric lens of pelites and orthoquartzites placed at the bottom of this formation. González Lodeiro (1981b) studied the Lower-than-Ordovician Series of the eastern Central System (From bottom to top: the Angón Formation, the Antoñita Formation, the Cardeñosa Formation, the Hiendelaencina Formation and La Constante Formation) and their correlation. This author concluded that the Hiendelaencina Formation, which was composed of coarse-grained gneisses at the bottom and fine-grained gneisses at the top, could be correlated with the Ollo de Sapo Formation of the northwest of the Iberian Peninsula and Sanabria region. By contrast the Antoñita Formation, which is composed of quite homogenous augen-gneisses, was very difficult to correlate.

Finally, Díez Montes (2006), in detailed research about the Ollo de Sapo Formation in the Sanabria region, described this formation as a series of lithologic groups composed of augen orthogneisses and a volcanic and volcanosedimentary sequence whose textural, structural and compositional features suggested a common origin.

#### *1.3.1.2. Stratigraphic position*

Some of the first researchers who studied the stratigraphy of the Ollo de Sapo Formation were Parga-Pondal et al. (1964). These authors attributed a Lower-than-Cambrian age to this formation by analogy with similar formations of the Iberian Peninsula and France. Later, Iglesias Ponce de León and Ribeiro (1981) carefully mapped the Miranda do Douro y S. Vitero-Carbajales regions, and concluded that the Ollo de Sapo Formation is between the Lower Ordovician Puebla Formation and the Lower Cambrian Schist-Graywacke Complex. Arias et al. (2002) mapped the Viana do Bolo-A Gudiña region and deduced that the Ollo de Sapo Formation was intercalated with the Upper Cambrian-Lower Ordovician "Serie de los Cabos". Finally, Díez Montes (2006) attributed a Lower Ordovician age to this formation placing it between the Viana do Bolo Series and "Las Capas de Los Montes".

#### *1.3.1.3. Structural geology*

The first study of the structural geology of the Ollo de Sapo Formation was made by Matte (1963), who described the Variscan Deformation of Galicia. This author included the Anticlinorium of the Ollo de Sapo in the domain of the Recumbent and Bend Folds during

the Variscan orogeny. He also assigned names to several antiform structures in whose cores the Ollo de Sapo Formation crops out. Martínez García (1973) studied the deformation and the metamorphism of the Zamora region. In agreement with previous authors, he recognized two facies in the Ollo de Sapo Formation of the Sanabria region and concluded that the differences between both facies were not due to a different origin but a different metamorphic history. Facies with feldspar megacrysts had suffered more intense metamorphism that facies without feldspar megacrysts. González Lodeiro (1981b) analyzed the Ollo de Sapo anticline in the Hiendelaencina region (Central System) and deduced that it was a recumbent fold with east vergence produced during the first phase of the Variscan orogeny. Finally, Capote et al. (1981) looked at large ductile thrust faults of the Central System generated during the second phase of the Variscan deformation. According to these authors, this phase of thrust faults was mainly syn-metamorphic and modified the distribution of the regional metamorphism isotherms causing important thermal inversions.

#### *1.3.1.4. Radiometric dating and isotope geology*

The first radiometric studies of the Ollo de Sapo Formation and associated metagranites using U-Pb in zircon concentrates were done by Lancelot et al. (1985) in the Sanabria-Villadepera region. These authors studied the Viana do Bolo (which was actually the San Sebastián metagranite) and Miranda do Douro orthogneisses and two samples from the middle and upper facies of the Ollo de Sapo gneisses. The results were highly discordant in all cases, with upper intersections at 618 ± 9 Ma and 465 ± 10 Ma for the Miranda do Douro and Viana do Bolo orthogneisses, respectively, which they interpreted as the crystallization ages of these orthogneisses. In the Ollo de Sapo sequence, they obtained a discordia with an upper intersection at 1797 ± 30 Ma and a lower intersection at 325 ± 3 Ma. They concluded that the upper intersection represented an inherited population of zircons and the lower intersection yielded the age of the Variscan main thermal event. The authors proposed a model based on the U-Pb system of the Ollo de Sapo in which there was mixing of pre-Cambrian detrital zircons (older than 1.8 Ga) with zircons originating in subvolcanic rocks formed at 500-600 Ma. The mixing was produced during the deposit in the Ollo de Sapo Formation. Later, during the Variscan thermal event, they suggested these zircons were affected by a substantial loss of radiogenic lead.

Wildberg et al. (1989) studied U-Pb in zircon concentrates from the Hiendelaencina series (La Constante augen-gneiss, the Bustares augen-gneiss and the Antoñita gneiss) and

obtained the following results: (i) a discordia with an upper intersection at 2055 Ma and a lower intersection at 378 ± 6 for the Antoñita gneiss, and (ii) a group of data for the Constante augen-gneiss and the Bustares augen-gneiss which did not plot a discordia. The Constante augen-gneiss data plotted above and below the Antoñita reference line and Bustares augen-gneiss data marked a curve which moved away from the Antoñita reference line.

The above-mentioned results reveal the enormous difficulties in dating these rocks with U-Pb zircon concentrates. The first spot U-Pb zircon data for the Ollo de Sapo Formation and associated metagranites were done by Gebauer et al. (1993) who, in an abstract presented at the 1993 Annual Meeting of the Geological Society of America, suggested a crystallization age of 488 Ma for Ollo de Sapo Formation, and indicated the presence of concordant ages at 2670 and 578 Ma in some inherited cores. Fernández-Suárez et al. (1999) investigated the geochronology of the northwest outcrops of the Ollo de Sapo Formation using LA-ICPMS. They detected the presence of four age groups: 440-460 Ma, 590-620 Ma, 1.2 Ga and 1.9-2.0 Ga and concluded that the youngest group (440-460 Ma) was the age of the magmatic component of the Ollo de Sapo Formation and the other age groups (590-620 Ma, 1.2 Ga y 1.9-2.0 Ga) represented recycled zircon populations.

Full understanding of the reasons for the highly discordant nature of the zircons from these rocks comes from the first studies that combined cathodoluminescence imaging and single grain or spot analysis (e.g., Bea et al., 2006a). These authors revealed that most zircon grains consist of a Cambro-Ordovician rim growth over a pre-Cambrian core (see Fig. 4.1 in Chapter 4) and obtained a concordant crystallization age of 483 ± 3 Ma for the Miranda do Douro orthogneiss. They also detected abundant inherited concordant or subconcordant populations at 605 Ma and ca. 3.2 Ga. Zeck et al. (2007) also dated the Miranda do Douro orthogneiss using U-Pb ion microprobe and found a slightly older crystallization age of 496 ± 3 Ma and observed the presence of inherited cores with ages between c. 2700 - 550 Ma from assimilated country rock, or more probably, from anatectic source rock which was melted to produce the granitic magma that intruded to give parent rocks of the gneiss formation. Within these inherited cores, three prevailing inherited age components are 628, 580 ± 9 Ma, and c. 557 Ma.

Díez Montes (2006) dated the augen orthogneiss and the ignimbrites of the Ollo de Sapo Formation from the Sanabria region using U-Pb analysis in zircon concentrates. As

expected, the results were highly discordant. This author obtained: (i) two discordias for the augen orthogneiss which had the same lower intersection, at 472 ± 14 Ma, and different upper intersection, at 2.03 Ga and 1.53 Ga, and (ii) two discordias for the ignimbrites, one had a lower intersection at 66 ± 75 Ma and an upper intersection at 488 ± 6 Ma and the other had a lower intersection at 488 ± 6 Ma and an upper intersection at 2.14 Ga.

Recently, Montero et al. (2007) have studied the metavolcanic rocks of the Ollo de Sapo Formation in Villadepera, near the Miranda do Douro metagranite, and in Hiendelaencina, as well as the spatially-related Antoñita metagranite, using spot U-Pb ion microprobe, LA-ICPMS and Pb-Pb stepwise analysis. The results are as follows: (i) the 2000 m thick metavolcanic rocks of the Ollo de Sapo Formation in the Hiendelaencina region show a noticeable difference in the crystallization age between top, 483 ± 3 Ma, and base, 495 ± 5 Ma. They, however, contain similar inherited populations at 603 Ma (by far the most abundant), 650-700 Ma, 850-900 Ma and ca. 2000 Ma, and (ii) the spatially-related Antoñita metagranite is younger still, with a well-defined Pb-Pb plateau-age of 474 ± 4 Ma, which is considered to be the age of crystallization.

Regarding, isotope geology, the lack of precise crystallization ages has caused the Sr and Nd isotope geology of the Ollo de Sapo materials to be poorly known.

Ortega et al. (2000) using a crystallization age of 490 Ma, calculated a $(^{87}Sr/^{86}Sr)_{init}$ between 0.7084 and 0.7122 and a εNd between -2.0 and -2.8 for homogeneous augen-gneisses of the northern and central sectors of the Ollo de Sapo Formation. They observed that samples with the best preserved igneous features presented the lowest values of $(^{87}Sr/^{86}Sr)_{init}$ and concluded that the Ollo de Sapo rocks could be late-orogenic magmatism.

Fernández-Suárez et al. (1999) studied the Nd isotopes of the volcanosedimentary rocks of the northwest sector of the Ollo de Sapo Formation and noticed that the Ollo de Sapo rocks had a narrow range of $T_{DM}$ ages in spite of the multi-age zircon population they contained. They concluded that this reflected a relatively homogeneous mixture of crustal components (Icartian, Grenville, Cadomian and a c. 440-460 Ma component) over a large area which was consistent with the proposed proximal nature of the crustal sources.

Montero et al. (2007) studied the Sr and Nd isotope geology of the Ollo de Sapo Formation in Villadepera and Hiendelaencina, and found important differences in Sr isotopes: whereas at Villadepera $(^{87}Sr/^{86}Sr)_{init}$ is always lower than 0.7075, in Hiendelaencina this

ratio is always higher than 0.7098. Nd isotopes do not show meaningful regional variations, but there are differences between the Nd isotopes of the metavolcanic rocks and the metagranites, especially in Villadepera. In Hiendelaencina, the $(^{87}Sr/^{86}Sr)_{init}$ are 0.71039 and 0.70985 for the metavolcanic rocks, and 0.71054, 0.71105 and 0.71168 for the metagranite. In Villadepera, the $(^{87}Sr/^{86}Sr)_{init}$ are 0.70700 and 0.70755 for the metavolcanic rocks, and 0.70442 and 0.70521 for the metagranite. The $Nd_{(CHUR)}$ model age for the Miranda do Douro metagranite, which has the most primitive isotope and chemical composition, is 0.69 Ga, slightly older than the zircon age of the source, whereas for the Villadepera metavolcanic rocks the $Nd_{(CHUR)}$ model age is 1.0 Ga. In Hiendelaencina, both rock types yielded the same value of 0.94 Ga.

### 1.3.2. The pre-Middle Ordovician metagranites of the Schist-Graywacke Complex Domain

#### *1.3.2.1. General geology and composition*

The metagranites of the Schist-Graywacke Complex Domain were extensively studied in the 1970s, when their analogy with the materials of the Ollo de Sapo was established by Bard et al. (1970). These authors suggested that some augen-gneisses, for example the Santa María de la Alameda outcrop, might be the source of the Ollo de Sapo Formation. Fernández Casals and Capote (1971) studied the petrology of the augen-gneisses of Eastern Guadarrama and proposed they are part of a thick formation made of augen-gneisses with intercalated banded gneisses and granoblastic rocks at the base and micro-augen gneisses at the top, similar therefore to the distribution of coarse-grained and fine-grained facies in the Ollo de Sapo. For this reason, they concluded that this formation could be the Ollo de Sapo intensely migmatized. Additionally, they placed this formation below the Cambrian metamorphic series and assigned it an Upper pre-Cambrian age. Fernández Casals (1974) investigated the gneissic formation of La Morcuera and differentiated: (i) a basal complex of augen-gneisses which represented orthogneisses derived from porphyritic granites with enclaves and aplitic dikes, (ii) a thinner succession of several types of gneisses derived from volcanic and sedimentary rocks. Finally, this author concluded that the gneissic formation of La Morcuera was beneath the Cambrian sedimentary formation and was pre-Cambrian. García de Figuerola and Franco González (1975) mapped and studied the petrology of the metamorphic terranes cropping out to the east of Guijuelo (Salamanca province). In this area, the Bercimuelle gneiss, the origin of which was unclear, crops out. They suggested that it either represents an older Variscan granodiorite intruded in the Mo-

rille series before the second phase of deformation or was derived from a volcanic formation interlayered within the metasediments. Capote et al. (1977) studied the pre-Cambrian series of the Montes de Toledo and the Central System. In the Montes de Toledo, they distinguished a lower formation of shales and graywackes and an upper turbidite formation composed of metapelites. In the Central System, they also differentiated two main formations: (i) the first dominantly composed of augen-gneisses, and (ii) the other mostly composed of metasediments. Navidad (1979) carried out a study of the augen series of western and central Guadarrama. This author differentiated two different facies of augen-gneisses: (i) Homogenous augen-gneisses and (ii) Heterogeneous augen-gneisses, and concluded that their petrological and compositional features suggested that they were derived from a vulcano-sedimentary series.

Navidad and López Ramos (1981) studied the augen-gneisses of El Vellón and Pedrezuela massifs located in the Sierra de Guadarrama. The Vellón massif was composed of three facies: (i) feldspathic gneisses with megacrysts, which represent the most internal facies, (ii) biotitic orthogneisses, which represent the intermediate facies, and (iii) feldspathic micro-augen-gneisses, which represent the most external facies. The Pedrezuela massif consists of two-mica augen-gneisses and different types of leucogneisses. They inferred that both massifs were ancient metagranitic massifs which had different ages, the Pedrezuela massif being younger than El Vellón massif or, at least, younger than the intermediate facies of El Vellón massif. In the same year, Peinado and Álvaro (1981) studied the gneisses of the metamorphic area of "El Escorial" (Central System) and they differentiated two types of gneisses: the biotitic orthogneisses of the Santa Maria de la Alameda and the Abantos orthogneisses. The former were interpreted as I-type porphyritic biotite granites with a homogenous composition and quartz-dioritic enclaves. These granites formed as low volume stratiform bodies intruded in a relatively cold host rock producing an aureole of contact metamorphism that was subsequently affected by the second phase of Variscan deformation. The Abantos orthogneisses, by contrast, represent S-type two-mica granites characterized by the presence of aluminous silicates and abundant associated leucogranites, aplites and pegmatites. These were more voluminous and intruded into the Upper pre-Cambrian-Lower Cambrian regional metasedimentary series at different levels. Saavedra et al. (1984) studied the petrography and the geochemistry of the granitoids and metamorphic rocks of the Morille-Martinamor area (Salamanca province). One of these metamorphic

rocks was the San Pelayo gneiss whose composition is intermediate between the composition of granitoids and the non-calcic metamorphic rocks.

Finally, Bea et al. (1990) described the migmatization processes that occurred in the Almohalla Formation (Anatectic Complex of Pena Negra, Ávila Batholith). This formation is composed of three lithotypes: (i) a pre-Variscan, orthoderived, coarse-grained augen-gneiss, (ii) opthalmitic and diktynonitic migmatites developed from the orthogneiss, (iii) a garnet-bearing leucogranite of Variscan age, which crops out in the orthogneiss as a small, irregular, subauthochtonous body with transitional contacts with the host. Bea et al. (1990) concluded that the two processes of partial fusion that occurred in this formation were very different although they had been generated from the same material.

#### *1.3.2.2. Stratigraphic position*

The stratigraphy of the pre-Middle Ordovician metagranites of the Schist-Graywacke Complex Domain was studied for the first time by Capote and Fernández Casals (1975). They identified several pre-Ordovician gneissic formations which have different age and lithology and concluded that : (i) the lower pre-Ordovician Formation was an augen-gneiss with xenoliths (La Morcuera) and could represent a metamorphosed and deformed porphyritic granite or could have derive from a granitic pluton which intruded the surrounding meta-sediments, (ii) a series which overlays the Morcuera 1 and from bottom to top consisted of: (a) pelitic and psammitic metasediments with amphibolitic and calcareous intercalations, in whose base there were rocks with volcanic participation, (b) a lithologic group which came from acid lavas and sediments related to these lavas, (the Hiendelaencina gneiss could be included in this group), and (c) pelitic-psammitic group with salic-silicate rocks and without limestones. Furthermore, the lower pre-Ordovician Formation in Salamanca are below Lower Cambrian formations and for that reason, these authors considered them to be pre-Cambrian formations, although pre-Ordovician series in the Ávila province could be considered to be Lower Cambrian formations.

#### *1.3.2.3. Structural geology*

Concerning the structural geology of the pre-Middle Ordovician metagranites of the Schist-Graywake Complex Domain, one of the most important papers is that ofMacaya et al. (1991). These authors described the deformational structures generated in the cover and the basement of the Sierra de Guadarrama through the Variscan orogeny. The gneisses of

the Schist-Graywake Complex Domain reveal structures attributable to the first and third Variscan deformation phases but they do not display pre-Variscan structures, perhaps because they were obliterated by the intense deformation and high grade metamorphism developed during the Variscan orogeny. Escuder Viruete et al. (1994) studied the tectono-thermic evolution of the Tormes Dome in which two units were distinguished: (i) The Lower Unit which consisted of glandular orthogneisses, ortho-derived leucogneisses and aluminous paragneisses with lenses of marble and calc-silicate rocks, and (ii) the Upper Unit which was a monotonous sequence of slates and quartzose schists. According to these authors, two events could be distinguished in the tectono-thermic evolution of the Tormes Dome. The first event is well represented by a clockwise segment of the P-T path, characteristic of the thickening and stacking of crustal units during the continental collision. The second event was related to the gravitational collapse of the crust, giving way to a short stage of prograde decompression and, then, to a nearly isothermal decompression. The uplift of deep and hot rocks was accompanied by the development of anatectic processes and controlled by extensional ductile deformation which gave rise to their juxtaposition with an Upper Unit that underwent nearly isobaric heating. Following this, both units, as a whole, already at a high crustal level, experienced cooling and a weak decompression.

#### *1.3.2.4. Radiometric dating and isotope geology*

The first geochronological research about the pre-Middle Ordovician metagranites of the Schist-Graywacke Complex Domain were by Priem et al. (1970) who dated the Variscan and pre-Variscan plutonic rocks of the western Iberian Peninsula using the Rb-Sr method. They obtained Rb-Sr ages between 460 and 430 Ma for pre-Variscan rocks and concluded that they were Upper Ordovician. Bischoff et al. (1978) undertook a geochemical and geochronological study of the metarhyolites and orthogneisses of eastern Guadarrama. The results confirmed the existence of a thermal event in the transition Carboniferous-Permian period but did not identify a crystallization age for the gneisses due to the homogenization of the Rb-Sr system.

In the 1980s, several important investigations were carried out on the pre-Middle Ordovician metagranites of the Schist-Graywacke Complex Domain. Linares et al. (1987) dated the San Pelayo orthogneiss using the Rb-Sr method and obtained an age of 430 ± 30 Ma that they considered a minimum age of metamorphism, probably produced by the intrusion of the neighboring Variscan granites. Vialette et al. (1987) dated some gneisses from the

Sierra de Guadarrama using the Rb-Sr method. The results were as follows: (i) a crystallization age of 471 ± 12 Ma and a $(^{87}Sr/^{86}Sr)_{init}$ of 0.7093 ± 0.010 for the El Villar de Pradena gneiss, (ii) a crystallization age of 474 ± 7 Ma and a $(^{87}Sr/^{86}Sr)_{init}$ of 0.7070 ± 0.0017 for the Abantos gneiss, and (iii) a crystallization age of 494 ± 10 Ma and a $(^{87}Sr/^{86}Sr)_{init}$ of 0.7087 ± 0.0011 for the Otero de Herreros gneiss. And finally, Wildberg et al. (1989) tried to reconstruct the pre-Variscan and Variscan histories of the Sierra de Guadarrama using U-Pb in zircon concentrates from the El Cardoso and Madarquillos gneisses. These authors obtained a discordia with an upper intersection at approximately 2435 Ma and a lower intersection at 540 +31/-35 Ma for the El Cardoso gneiss, and a discordia with an upper intersection at 1970 Ma and a lower intersection at 370 ± 8 Ma for the Madarquillos gneiss.

Following this, Valverde-Vaquero and Dunning (2000) dated the El Cardoso, Riaza, Buitrago and La Morcuera gneisses of the Sierra de Guadarrama using U-Pb in zircon concentrates. The results were as follows: (i) a discordia with an upper intersection at 2.64 Ga and a lower intersection at 480 ± 2 Ma for El Cardoso gneiss, (ii) a discordia with an upper intersection at 468 +16/-8 Ma for the Riaza gneiss, (iii) a discordia with an upper intersection at 488 +10/-8 Ma for the Buitrago gneiss, and finally, (iv) a discordia with an upper intersection at 477 ± 4 Ma for La Morcuera gneiss.

The most recently published geochronological data for this area are for the "La Almohalla" gneiss located in the Sierra de Gredos (Central System). The first study was by Bea et al. (2003) which obtained a stepwise evaporation Pb-Pb age of 543 ± 6 Ma, the second study was carried out by Zeck et al. (2004) and obtained an ion-microprobe U-Pb age of 546 ± 3 Ma.

# 2. SAMPLES AND METHODS

# 2. SAMPLES AND METHODS

## 2.1. Samples

For this work we collected a total of seventy four samples of pre-Middle Ordovician magmatic rocks from the Central Iberian Zone. The number of samples suitable for chemical and isotopic studies was severely limited by the scarcity of fresh-rock outcrops, despite the fact that we used a portable drilling machine wherever the alteration was

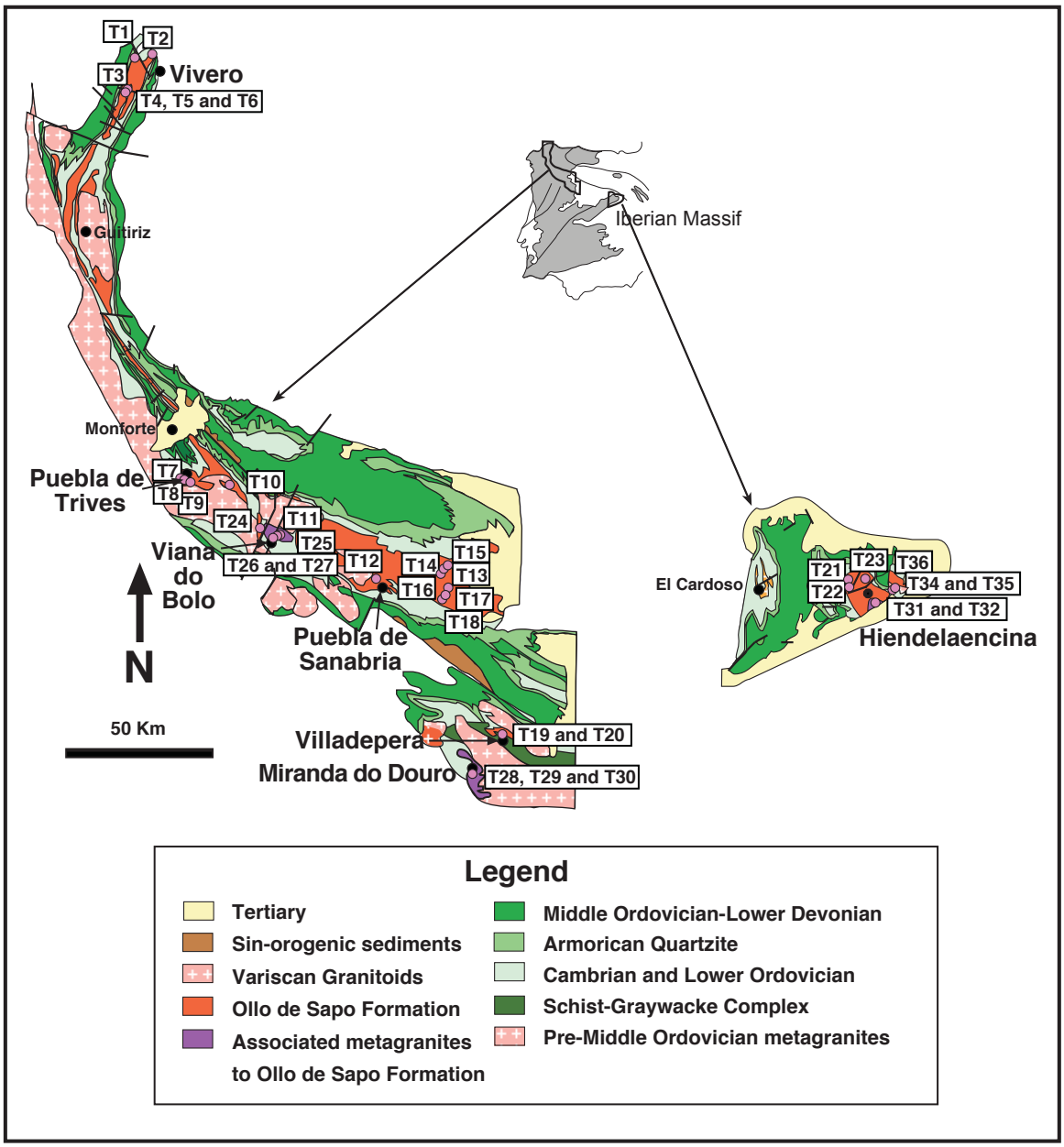


Figure 2.1: Geological scheme of the Ollo de Sapo Domain (Martínez Catalán et al., 2004) in which sampled metavolcanic and metagranitic rocks are located and represented by letter T.

particularly intense. The samples were collected from two main areas: the Ollo de Sapo Domain and the northern part of the Schist-Graywacke Complex Domain. Sixty three samples were analyzed for major and trace elements, including 14 REE, Th and U. A subset of forty two samples was also analyzed for Sr and Nd isotopes. Zircon was separated from thirty five samples, and analyzed using single-grain stepwise Pb-Pb evaporation, and U-Pb ion microprobe and LA-ICPMS methods.

We sampled the metavolcanic rocks of the Ollo de Sapo Formation in five selected areas that represent the whole domain: Vivero-Mañón, Trives, Sanabria, Villadepera and Hiendelaencina (Fig. 2.1). We also sampled four spatially associated metagranites: the Antoñita metagranite in Hiendelaencina, the Miranda do Douro metagranite in Villadepera, and the Viana do Bolo and San Sebastián metagranites in Sanabria. The location and relevant field information about these samples is shown in Table 2.1.

Table 2.1: Samples of the Ollo de Sapo Domain. The letter between parentheses in the column "Rock type" is the sample reference. The coordinates are geographic coordinates.

| Locality | Rock type | Coordinates | Description |
|---|---|---|---|
| Vivero | Fine grained Ollo de Sapo (T1) | N 43°43'53.2" W 7°41'56.9" | Deformed gneiss with blue quartz and feldspar phenocrysts. Phenocrysts with pressure shadows Fine-grained matrix. It is located in the upper part of the Ollo de Sapo Formation. |
| | Coarse-grained Ollo de Sapo (T2). | N 43°44'45.7" W 7°38'55.6" | Deformed gneiss with K-feldspar megacrysts and blue quartz phenocrysts. It is located in the lower part of the Ollo de Sapo Formation. |
| Mañon | Fine-grained Ollo de Sapo (T3) | N 43°41'24.5" W 7°43'06.7" | Gneiss without feldspar megacrysts. It is located in the upper part of the Ollo de Sapo Formation. |
| | Coarse-grained Ollo de Sapo (T4, T5, T6) | N 43°41'12.5" W 7°43'21.5" | Intensely deformed gneiss with feldspar megacrysts and blue quartz phenocrysts. It is located in the lower part of the Ollo de Sapo Formation. |
| Puebla de Trives | Fine grained Ollo de Sapo (T7) | N 42°23'04.0" W 7°27'41.6" | Very deformed gneiss with enclaves and deformed dikes. Blue quartz phenocrysts. Very micaceous matrix. Without feldspar megacrysts. It is located in the upper part of the Ollo de Sapo Formation. |
| | Coarse-grained Ollo de Sapo (T8, T9, T10) | N 42°23'06.9" W 7°29'30.6" N 42°22'40.0" W 7°26'21.6" N 42°19'50.0" W 7°13'05.7" | Variably deformed gneiss. Feldspar megacrysts. It is located in the lower part of the Ollo de Sapo Formation. |

| Locality | Rock type | Coordinates | Description |
|---|---|---|---|
| Sanabria | Coarse-grained Ollo de Sapo (T11) | N 42°09'25.9" W 6°54'38.4" | Very deformed gneiss with enclaves and deformed dikes. Feldspar megacrysts. It is located in the lower part of the Ollo de Sapo Formation. |
| | Fine-grained Ollo de Sapo (T12) | N 42°07'50.3" W 6°38'45.3" | Very deformed gneiss with feldspar and quartz phenocrysts. It is located in the middle part of the Ollo de Sapo Formation. |
| | Mixed Facies (T13, T14, T15, T16, T17, T18) | N 42°06'04.9" W 6°24'33.4" N 42°06'42.1" W 6°24'03.3" N 42°06'59.8" W 6°22'30.6" N 42°03'40.7" W 6°19'25.7" N 42°01'25.7" W 6°20'39.3" | Coarse-grained facies. Gneiss with feldspar megacrysts, quartz phenocrysts and black fragments. Fine-grained facies. Gneiss with quartz phenocrysts and without feldspar megacrysts. It is located in the upper part of the Ollo de Sapo Formation. |
| Villadepera | Fine-grained Ollo de Sapo (T19, T20) | N 41°33'37.3" W 6°07'51.6" | Migmatized, extremely deformed gneiss. Cut by dikes and pegmatoid stocks. |
| Hiendelaencina | Coarse-grained Ollo de Sapo (T21) | N 41°08'20.6" W 3°03'27.3" | Gneiss with feldspar megacrysts and blue quartz phenocrysts. It is located in the lower part of the Ollo de Sapo Formation. |
| | Fine grained Ollo de Sapo (T22) | N 41°06'28.1" W 3°04'15.4" | Gneiss with blue quartz phenocrysts and without feldspar megacrysts. More micaceous than the coarse grained Ollo de Sapo. It is located in the middle part of the Ollo de Sapo Formation. |
| | Coarse-grained Ollo de Sapo (T23) | N 41°05'06.0" W 2°59'53.1" | Gneiss with feldspar megacrysts and blue quartz phenocrysts. It is located in the upper part of the Ollo de Sapo Formation. |
| Viana do Bolo | Viana do Bolo metagranite (T24, T25) | N 42°08'34.6" W 6°56'58.8" N 42°13'52.1" W 7°06'28.8" | Very deformed and migmatized medium-coarse-grained gneiss without feldspar megacrysts. |
| Porto | San Sebastián metagranite (T26, T27) | N 42°07'54.9" W 6°59'06.9" | Deformed fine-grained gneiss without feldspar megacrysts. |
| Miranda do Douro | Miranda do Douro metagranite (T28, T29, T30) | N 41°29'29.1" W 6°16'24.6" | Biotitic mesocratic medium-fine grained gneiss with feldspar phenocrysts. |
| Hiendelaencina | Antoñita metagranite (T31, T32) | N 41°03'24.0"7 W 2°59'10.0" | Deformed coarse-grained gneiss. Feldspar phenocrysts with SC structures. Associated aplitic dikes. |
| La Bodera | Antoñita metagranite (T33, T34, T35) | N 41°07'13.9"/ W 41°07'13.9" N 41°07'18.9" W 2°54'23.4" | Deformed gneiss with feldspar phenocrysts. Phenocrysts with pressure shadows. |

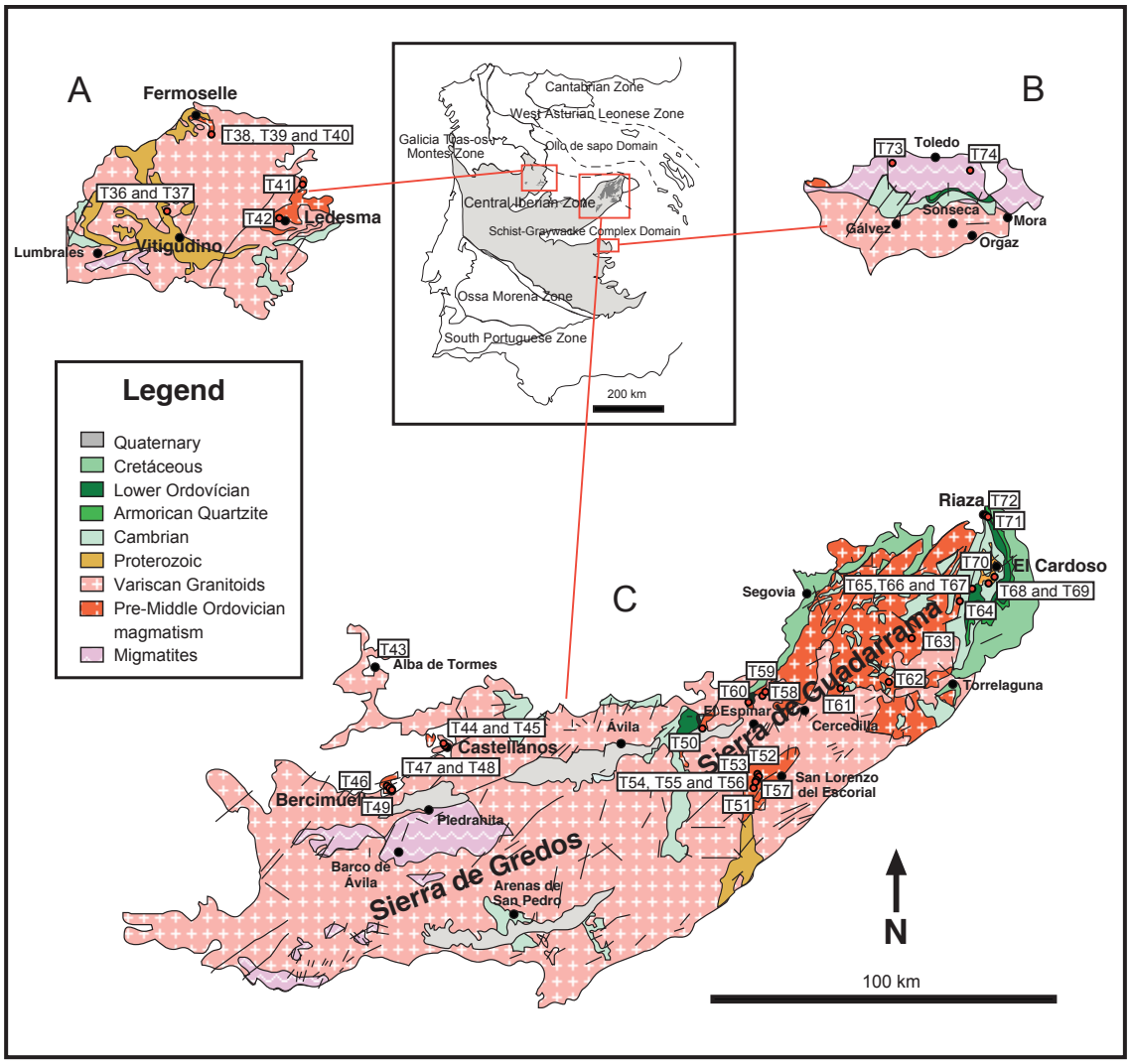


Figure 2.2: Geological scheme of the outcrops of the pre-Middle Ordovician metagranites and metavolcanic rocks of the north of the Schist-Graywacke Complex Domain. Sampled metagranites are represented by letter T. The geological scheme represents sections of the geological map of Spain (Álvaro et al., 1994).

We also sampled the pre-Middle Ordovician metagranites and metavolcanic rocks in four areas of the northern part of the Schist-Graywacke Complex Domain (Fig. 2.2):

- In the Tormes Dome: the Fermoselle, Vitigudino and Ledesma metagranites.
- In the northwest part of the Sierra de Gredos: the San Pelayo, Bercimuelle and Castellanos metagranites.

- In the Sierra de Guadarrama: La Cañada, La Hoya, La Estación I, La Estación II, El Caloco, Vegas de Matute, La Morcuera and Buitrago de Lozoya metagranites, and La Berzosa, El Cardoso and Riaza metavolcanic rocks.

- In the Anatectic Complex of Toledo: the Polán and Mohares metagranites.

The location and relevant field information for the pre-Middle Ordovician metagranites is shown in the Table 2.2.

Table 2.2: Samples of the metagranites and metavolcanic rocks from the north of the Schist-Graywacke Complex Domain. The letter between parentheses in the column "Rock type" is the sample reference. The coordinates are geographic coordinates.

| Locality | Rock type | Coordinates | Description |
|---|---|---|---|
| Barceíno | Vitigudino metagranite (T36, T37) | N 41°05'01.9" W 6°27'14.5" | Slightly migmatized medium-grained gneiss with few feldspar megacrysts. |
| Sardón de los Frailes | Fermoselle metagranite (T38, T39, T40) | N 41°14'44.7" W 6°16'22.1" N 41°14'23" W 6°16'32" | Slightly migmatized and deformed medium-coarse grained gneiss with few feldspar megacrysts. |
| Almeida | Ledesma metagranite (T41) | N 41°19'16.6" W 5°53'14.9" | Deformed and migmatized biotitic gneiss with feldspar megacrysts. |
| Ledesma | Ledesma metagranite (T42) | N 41°06'15.6" W 6°01'28.0" | Biotitic gneiss with feldspar megacrysts. |
| Martinamor | San Pelayo metagranite (T43) | N 40°47'36.6" W 5°34'32.1" | Deformed coarse-grained gneiss. Cut by late pegmatoid dikes. |
| Diegoálvaro | Castellanos metagranite (T44, T45) | N 40°38'48.9" W5°18'43.0" N 40°39'02.4" W 5°18'46.7" | Deformed biotitic fine-grained gneiss with enclaves. |
| Bercimuelle | Bercimuelle metagranite (T46, T47, T48, T49) | N 40°31'34.3" W 5°30'30.5" N 40°31'26.6" W 5°30'05.3" N 40°31'25.9" W 5°29'47.8" | Deformed biotitic augen-gneiss. |
| La Cañada | La Cañada metagranite (T50) | N 40°42'06.4" W 4°26'50.4" | Biotitic augen-gneiss with meta-sedimentary enclaves. Cut by aplitic and pegmatoid dikes. |
| Navas del Marqués | Navas del Marqués metagranite (T51) | N 40°33'14.4" W 4°16'14.4" | Slightly migmatized augen-gneiss. |
| Santa María de la Alameda | Santa María de la Alameda metagranite (T52) | N 40°35'24.0" W 4°15'34.2" | Deformed and slightly migmatized biotitic augen-gneiss with enclaves. |
| Santa María de la Alameda | La Hoya metagranite (T53) | N 40°34'34.7" W 4°15'30.0" | Very migmatized biotitic augen-gneiss. |

| Locality | Rock type | Coordinates | Description |
|---|---|---|---|
| La Estación | La Estación I metagranite (T54, T55, T56) | N 40°34'30.6" W 4°15'53.3" | Very deformed biotitic augen-gneiss. |
| La Estación | La Estación II metagranite (T57) | N 40°34'20.1" W 4°15'55.8" | Deformed biotitic augen-gneiss. Cut by late aplitic dikes. |
| Vegas de Matute | Vegas de Matute metagranite (T58, T59) | N 40°47'56.1" W 4°14'29.1" N 40°47'34.5" W 4°15'01.3" | Biotitic mesocratic augen-gneiss with calco-silicate enclaves and garnet. |
| Vegas de Matute | El Caloco metagranite (T60) | N 40°47'21.0" W 4°17'24.9" | Fine-grained leucogneiss. |
| La Morcuera | La Morcuera metagranite (T61, T62) | N 40°48'21.5" W 3°58'11.9" N 40°49'41.3" W 3°49'49.1" | Deformed biotitic augen-gneiss. Exhibits rapakivi texture and pressure shadows. |
| Buitrago de Lozoya | Buitrago metagranite (T63) | N 40°56'37.4" W 3°43'03.1" | Slightly migmatized biotitic medium-grained gneiss with few enclaves. Cut by a few leucocratic stocks. |
| Prádena del Rincón | Prádena del Rincón metagranite (T64) | N 41°02'03.9" W 3°33'07.1" | Slightly migmatized medium-grained leucogneiss with biotite and garnet. Cut by pegmatoid stocks and ptygmatic veins |
| Montejo de la Sierra | La Berzosa metavolcanic rock(T65, T66, T67) | N 41°03'41.7" W3°30'25.0" N 41°03'41.7" W3°30'22.0" | Deformed micaceous augen-gneiss |
| El Cardoso de la Sierra | El Cardoso metavolcanic rock (T68, T69, T70) | N 41°04'28.2" W 3°27'29.3" N 41°05'04.9" W 3°25'45.6" | Deformed biotitic fine-grained gneiss |
| Riaza | Fine-grained metavolcanic rocks (T71)<br><br>Coarse-grained metavolcanic rocks (T72) | N 41°16'49.8" W 3°28'13.8"<br><br>N 41°16'05.6" W 3°27'45.2" | Deformed two-mica gneiss.<br><br>Deformed augen gneiss with a few leucocratic dikes parallel to the foliation. |
| Guajaraz | Polán metagranite(T73) | N 39°51'38.9" W 4°09'07.7" | Deformed micaceous augen-gneiss. |
| Toledo | Mohares metagranite (T74) | N 39°50'05.0" W 3°53'12.2" | Deformed micaceos augen-gneiss. |

## 2.2. Analytical methods

### 2.2.1. Whole-rock major and trace element analyses

Major and trace elements of sixty three samples were analyzed at the Centro de Instrumentación Científica (CIC) of the University of Granada. Major-element and Zr determinations were performed by X-ray fluorescence after fusion with lithium tetraborate.

Typical precision was better than ± 1.5% for an analyte concentration of 10 wt.%, and ± 5% for 100 ppm Zr. Trace elements, except Zr, were determined by ICP-mass spectrometry (ICP-MS) after $HNO_3$ + HF digestion in a Teflon-lined vessel, evaporation to dryness, and subsequent dissolution in 100 ml of 4 vol.% $HNO_3$. Instrument measurements were carried out in triplicate with a PE SCIEX ELAN-5000A spectrometer using Rh as internal standard. Precision was better than ± 5% for analytical concentrations of 10 ppm. As standards we used the natural rocks UBN, WSE, PME, BCR, BRN, DRN, GSP, GA and GH with the values recommended by Govindaraju (1994) and Govindaraju et al. (1994).

Table 2.3: Values of the standards used in a routine run from the Granada laboratory. The subscript M and C represent the measured and the certificated values respectively.

| Elements | $PMS_M$ | $PMS_C$ | $WSE_M$ | $WSE_C$ | $UBN_M$ | $UBN_C$ | $BEN_M$ | BENC | $BR_M$ | $BR_C$ | $AGV_M$ | $AGV_C$ |
|---|---|---|---|---|---|---|---|---|---|---|---|---|
| Li | 7.5 | 7.3 | 13.5 | 13.6 | 27 | 27 | 12.4 | 13 | 14.2 | 13 | 11 | 12 |
| Rb | 0.9 | 1 | 25 | 25 | 3.3 | 4 | 47.4 | 47 | 46.9 | 47 | 68.2 | 67.3 |
| Cs | 0.5 | 0.4 | 0.6 | 0.5 | 10.1 | 10 | 0.8 | 0.8 | 0.7 | 0.8 | 1.3 | 1.3 |
| Be | 0.2 | 0.5 | 0.9 | 1.1 | 0.1 | 0.2 | 1.9 | 1.9 | 1.6 | 1.5 | 2.2 | 2.1 |
| Sr | 271 | 280 | 405 | 410 | 7 | 9 | 1370 | 1370 | 1323 | 1320 | 671 | 662 |
| Ba | 142 | 148 | 330 | 338 | 25 | 27 | 1001 | 1025 | 1054 | 1050 | 1213 | 1226 |
| Sc | 34.3 | 34 | 26.9 | 28 | 13.3 | 13 | 22.3 | 22 | 22.1 | 25 | 12 | 12.2 |
| V | 192 | 192 | 335 | 340 | 65 | 75 | 235 | 235 | 239 | 235 | 125 | 121 |
| Cr | 320 | 314 | 108 | 99 | 2267 | 2300 | 365 | 360 | 369 | 380 | 27 | 10 |
| Co | 49 | 49 | 44 | 44 | 100 | 100 | 61 | 60 | 58 | 52 | 15 | 15 |
| Ni | 122 | 115 | 56 | 55 | 1983 | 2000 | 264 | 267 | 260 | 260 | 17 | 16 |
| Cu | 61 | 59 | 69 | 65 | 25 | 28 | 73 | 72 | 72 | 72 | 58 | 60 |
| Zn | 69 | 60 | 129 | 117 | 81 | 85 | 133 | 133 | 171 | 160 | 95 | 88 |
| Ga | 16 | 16 | 22 | 23 | 2 | 3 | 18 | 17 | 18 | 19 | 21 | 20 |
| Y | 11 | 11 | 31 | 30 | 3 | 3 | 28 | 30 | 28 | 30 | 19 | 20 |
| Nb | 2.1 | 2.6 | 15.9 | 18 | 0.1 | 0.1 | 103.1 | 105 | 102.8 | 98 | 13 | 15 |
| Ta | 0.3 | 0.2 | 1.3 | 1.2 | 0.1 | 0 | 5.7 | 6.2 | 6.1 | 6.2 | 0.9 | 0.9 |
| Zr | 37 | 39 | 194 | 195 | 4 | 4 | 259 | 260 | 261 | 260 | 222 | 227 |
| Hf | 1.07 | 1.12 | 5.19 | 5.3 | 0.22 | 0.1 | 5.87 | 5.6 | 5.91 | 5.6 | 5.3 | 5.1 |
| Mo | 1.86 | 1.9 | 3.74 | 3.7 | 0.25 | 0.55 | 2.78 | 2.8 | 2.45 | 2.4 | 2.29 | 2.7 |
| Sn | 2.97 | 3 | 17.93 | 18 | 0.3 | 0 | 1.89 | 2 | 2.27 | 2 | 4.31 | 4.2 |
| Tl | 0.04 | 0.04 | 0.13 | 0.16 | 0.03 | 0.06 | 0.02 | 0.04 | 0.05 | 0.05 | 0.29 | 0.34 |
| Pb | 2.06 | 2.5 | 13.52 | 13.8 | 12.53 | 13 | 4 | 4 | 4.67 | 5 | 36.67 | 36 |
| U | 0.014 | 0.03 | 0.631 | 0.65 | 0.071 | 0.07 | 2.371 | 2.4 | 2.438 | 2.5 | 1.963 | 1.92 |
| Th | 0.043 | 0.05 | 3.039 | 3 | 0.103 | 0.07 | 10.946 | 10.4 | 10.958 | 11 | 6.792 | 6.5 |
| La | 2.737 | 2.8 | 26.204 | 27 | 0.37 | 0.35 | 81.147 | 82 | 81.265 | 82 | 38.823 | 38 |
| Ce | 6.704 | 6.8 | 59.384 | 61 | 0.818 | 0.8 | 148.724 | 152 | 148.5 | 151 | 68.292 | 67 |
| Pr | 1.03 | 1.08 | 7.668 | 7.8 | 0.123 | 0.12 | 16.844 | 17.5 | 17.109 | 17 | 8.307 | 7.6 |
| Nd | 5.342 | 5.5 | 32.082 | 33 | 0.608 | 0.6 | 63.92 | 67 | 66.363 | 65 | 33.05 | 33 |
| Sm | 1.749 | 1.75 | 8.461 | 8.8 | 0.192 | 0.2 | 12.029 | 12.2 | 12.106 | 12.2 | 5.995 | 5.9 |
| Eu | 1.019 | 1.07 | 2.106 | 2.25 | 0.069 | 0.08 | 3.657 | 3.6 | 3.668 | 3.7 | 1.647 | 1.64 |
| Gd | 2.053 | 2 | 7.059 | 7.2 | 0.333 | 0.3 | 9.752 | 9.7 | 9.831 | 9.5 | 4.757 | 5 |
| Tb | 0.342 | 0.36 | 1.1 | 1.1 | 0.065 | 0.06 | 1.396 | 1.3 | 1.399 | 1.25 | 0.736 | 0.7 |
| Dy | 1.93 | 2 | 5.915 | 6 | 0.386 | 0.38 | 6.141 | 6.4 | 6.029 | 6.4 | 3.543 | 3.6 |
| Ho | 0.409 | 0.42 | 1.186 | 1.2 | 0.085 | 0.09 | 1.075 | 1.1 | 1.079 | 1.1 | 0.71 | 0.67 |
| Er | 1.085 | 1.1 | 2.865 | 3 | 0.269 | 0.28 | 2.277 | 2.5 | 2.415 | 2.5 | 1.724 | 1.7 |
| Tm | 0.165 | 0.17 | 0.405 | 0.43 | 0.037 | 0.045 | 0.295 | 0.34 | 0.315 | 0.34 | 0.239 | 0.34 |
| Yb | 0.926 | 1 | 2.441 | 2.5 | 0.275 | 0.28 | 1.722 | 1.8 | 1.716 | 1.8 | 1.572 | 1.72 |
| Lu | 0.145 | 0.15 | 0.356 | 0.37 | 0.043 | 0.045 | 0.233 | 0.24 | 0.24 | 0.25 | 0.251 | 0.27 |

The accuracy of the analytical results can be estimated from the comparison of the results of analyzing these standards as samples in a routine run, and their certified values (Table 2.3)

### 2.2.2. Sr and Nd isotope analyses

Sr and Nd isotopes of forty seven samples were analyzed at the CIC of the University of Granada. Theses samples (0.1000 g) were digested with $HNO_3$ + HF in a Teflon-lined vessel and analyzed by thermal ionization mass spectrometry (TIMS) in a Finnigan Mat 262 RPQ spectrometer after separation with ion-exchange resins using conventional procedures. All reagents were ultra clean. Normalization values were $^{86}Sr/^{88}Sr = 0.1194$ and $^{146}Nd/^{144}Nd = 0.7219$. Blanks were 0.6 and 0.09 nanograms for Sr and Nd. The external precision (2σ), estimated by analyzing 10 replicates of the standard WS-E (Govindaraju et al., 1994), was better than ± 0.003% for $^{87}Sr/^{86}Sr$ and ± 0.0015% for $^{143}Nd/^{144}Nd$. $^{87}Rb/^{86}Sr$ and $^{147}Sm/^{144}Nd$ were directly determined by ICP-MS at Granada following the method developed by Montero and Bea (1998), with a precision better than ± 1.2% and ± 0.9% (2σ) respectively.

### 2.2.3. Zircon separation and dating

Zircons of thirty five samples were separated using conventional magnetic and heavy-liquid techniques. Once mounted and polished, zircon grains were studied by cathodoluminescence imaging using a ZEISS DSM 950 and LEO 1430-VP scanning electronic microscopes (SEM) at the CIC of the University of Granada. Subsequently they were analyzed:

- For U-Th-Pb, using the Cameca IMS1270 ion microprobe of the NORDSIM facility in Stockholm and the SHRIMP II of the Australian Geoscience of Canberra.
- For U-Th-Pb and for Ti and Zr/Hf using the LA-ICPMS of the CIC of the University of Granada.
- For Pb-Pb using the stepwise evaporation method at the TIMS facility of the CIC of the University of Granada.

### *2.2.3.1. Zircon U-Pb ion microprobe analyses*

Ion microprobe analyses were done in a CAMECA IM-1270 instrument at the NORDSIM facility (Stockholm) and in a SHRIMP II at the Australian National University (Canberra). Analytical methods broadly follow those described by Whitehouse et al. (1999) and references mentioned therein. U/Pb and Th/Pb ratios were calibrated using the Geostandards 91500 reference zircon (1065 Ma; Wiedenbeck et al., 1995) and include a propagated error component from replicate analyses of 91500 during the analytical session. Errors on $^{207}Pb/^{206}Pb$ ratios are either the observed analytical uncertainly or the counting statistics error, whichever is highest. Common Pb corrections assume that most contaminant Pb is present on the surface of the analyzed grains, introduced from the sample preparation process, and has a composition that can be approximated using the Stacey and Kramers (1975) model for the present day. For grains with ages <1000 Ma, common lead was corrected using the "207-correction" which is calculated by projecting the uncorrected analyses onto concordia from the assumed common $^{207}Pb/^{206}Pb$ present day composition. In most cases, however, the amount of common Pb, revealed by monitoring $^{204}Pb$, is relatively small and has little influence on the interpreted age. For grains with ages > 1000 Ma, factors for common lead correction were calculated by iteration from the $^{204}Pb/^{206}Pb$ and $^{204}Pb/^{207}Pb$ ratios provided by the Stacey and Kramers (1975) model at the calculated age, until convergence to a constant value. All ages are calculated using the decay constant recommendations of Steiger and Jäger (1977).

### *2.2.3.2. Zircon U-Th-Pb, Zr/Hf and Ti laser ablation ICP-MS analyses*

LA-ICPMS analyses of Ti, Zr, Hf, Th, U and Pb isotopes were carried out with a Nd-YAG 213 nm Mercantek laser and a torch-shielded quadrupole Agilent 7500 ICP-MS spectrometer. To avoid the isobaric interference caused by $^{96}Zr^{+2}$, Ti was determined on the isotope $^{49}Ti$ (5.5%) instead of the most abundant $^{48}Ti$ (73.8%). The laser beam was set at a diameter of 60 μm, with a repetition rate of 10 Hz and an output energy of 75%. The ablation time was 60 s and the spot was pre-ablated during 45 s with a laser output energy of 50%. The ablation was done in a He atmosphere. $^{91}Zr$ was used as an internal standard. The external standard was the NIST-610 glass, which contains 434 ppm Ti, 439.9 ppm Zr, 417.7 ppm Hf, 409 ppm Pb, 457.1 ppm U and 450.6 ppm Th (Pearce et al., 1997). The following isotope ratios, determined by TIMS at the University of Granada, were also used: $^{204}Pb/^{206}Pb = 0.06$, $^{207}Pb/^{206}Pb = 0.9127$, $^{208}Pb/^{206}Pb = 2.1898$, $^{206}Pb/^{238}U = 0.2501$, $^{208}Pb/^{232}Th = 0.5402$. U-Pb LA-ICPMS ages are in good agreement with ion-microprobe

data but show more dispersion and tend to be more discordant. The precision (1σ) estimated on ten replicates of the NIST-610 analyzed in the same run was better than 2.5% for element ratios and ca. 0.3% for isotope ratios. Common lead interferences are significantly higher than in ion microprobe analyses, owing to the larger spot diameter. Data with a discordance factor ($^{206}Pb/^{238}U$)age/($^{207}Pb/^{235}U$)age < 0.9 were always rejected, except they plot in a well-defined discordia line. In the rest, common lead was corrected using the same methods as described in the previous section. The detection limit for Ti was about 0.4 ppm, and the precision (1σ) estimated on the standards NIST-610, NIST-612 and a homemade glass, was 4%, 8% and 20% for Ti concentrations of 434 ppm, 48 ppm, and 12 ppm. Ti-in-zircon temperatures were estimated with the formula of Watson and Harrison (2005): T (°K)= 5080/(6.01 - log10(ppm Ti)) assuming a $TiO_2$ activity = 1.

#### *2.2.3.3. Zircon Pb-Pb stepwise evaporation analyses*

Single-zircon evaporation analyses (Kober, 1987) were performed using a SEM-RPQ multicollector Finnigan Mat 262 thermal ionization mass spectrometer with a double filament ion-source arrangement, operated with the RunIt262 Spectromat™ software. The zircon grain was mounted on a canoe-shaped Re evaporation filament and heated until the lead beam was intense enough (~200-400 $^{206}Pb$ ions per second). The lead was collected on the ionization filament for 20-30 min, and was then analyzed in 5 blocks with 7 scans per block. Once the analysis was finished, a new step was started by heating the zircon on the evaporation filament at a higher temperature than in the previous step (usually increasing the current by 50-100 mA) and analyzing as before the Pb deposited anew on the ionization filament. The procedure was repeated until all the lead was exhausted from the zircon. The number of steps depended on the size and lead content of each zircon. Data acquisition was performed in dynamic mode (peak hopping), using a secondary electron multiplier as detector with the 206-204-206-207-208 mass sequence. The mass-ratio 204/206 was monitored to detect and, if necessary, correct for common lead. Factors for common lead correction were calculated by iteration from the $^{204}Pb/^{206}Pb$ and $^{204}Pb/^{207}Pb$ ratios provided by the Stacey and Kramers (1975) model at the calculated age, until convergence to a constant value. Mass fractionation in the detector was corrected by multiplying by √(207/206). Standard errors for each step were calculated according to the formula: SE = 2*σ/√n. The confidence interval for the final age is calculated for the 95% confidence level of the mean of all steps.

# 3. PETROGRAPHY AND MINERALOGY

# 3. PETROGRAPHY AND MINERALOGY

Detailed description of the petrography and mineralogy of the Cambro-Ordovician rocks of Central Iberia studied by many authors (see section 1.3). The fact that all these materials were variably metamorphosed during the Variscan has resulted in a large variety of textures and mineral assemblages which, when the metamorphic grade is high, obliterates the primary pre-metamorphic features of the rocks. Therefore, since the primary purpose of this work has been to study the geochronology and isotope geology of the magmatic protoliths from which these rocks were derived, our sampling has been markedly biased in favor of low-grade samples. It should also be noted that the ranges of mineral compositions mentioned in the next section are refer exclusively to the samples studied in this work. Our intention has been to provide a description of the rocks from which we studied zircons, rather than discussing the compositional spectrum or the metamorphic evolution of the studied bodies. The reader interested in these aspects can find more information in the literature mentioned in section 1.3

## 3.1 Ollo de Sapo Domain

### 3.1.1. The Ollo de Sapo Formation gneisses

As noted previously, the Ollo de Sapo Formation is composed of coarse-grained and fine-grained augen gneisses. Whereas the former tend to be located in the lower part of the formation, the later tend to be placed in the upper part. Locally the two types appear as alternating thin (< 1m) layers forming what is customarily known as the mixed facies.

#### *3.1.1.1. The Ollo de Sapo coarse-grained gneisses*

These are mesocratic gneisses with large augen within a medium- to fine-grained groundmass (Fig. 3.1). The augen often consist of isolated crystals of K-feldspar, plagioclase or quartz. Less frequently they are made of polycrystalline (though usually monomineralic) aggregates of these minerals.

The augen of K-feldspar are subhedral, or rarely euhedral, stubby prism to ovoidal crystals, locally rapakivi, which may reach up to 15 cm in diameter (Fig. 3.1). When the metamorphic grade is very low, they show Carlsbad twinning and are markedly perthitic indicating that they originally contained an elevated fraction of albite component. They often have inclusions of other minerals, especially plagioclase, quartz, biotite and,

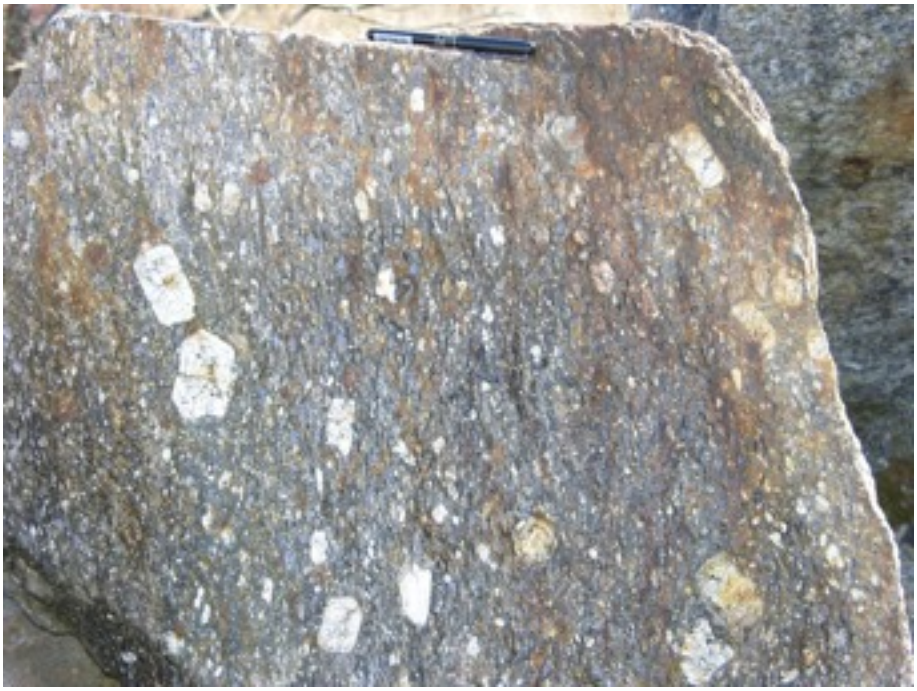

Figure 3.1: Field appearance of the coarse-grained facies of the Ollo de Sapo metavolcanic rocks at Hiendelaencina region. Note the rapakivi texture of some megacrysts.

remarkably, zircon. For this reason, in an area of the Hiendelaencina region where the rock's weathering makes it possible to hand-pick K-feldspar megacrysts, we have been able to extract zircon from them (see section 4.1.1.5.2.).

Subhedral or anhedral, often rounded, quartz phenocrysts are also very abundant. Their size is about 1-3 cm, being, therefore, notably smaller than the K-feldspar megacrysts. If the metamorphic grade is low they often have a characteristic bluish color (Fig. 3.1, see also Fig. 3.5) attributed to the presence of sagenitic needles of rutile. Under the microscope they frequently appear as hexagonal prismatic sections with embayed borders, which strongly suggest a volcanic origin (Fig. 3.2A). As the metamorphic grade increases, the quartz phenocrysts become polygonized, recrystallizing into polycrystalline aggregates that in most cases still keep the original shape of the crystal (Fig. 3.2B)

The phenocrysts of plagioclase consist of subhedral stubby prisms up to 1-2 cm long, of oligoclase or oligoclase-albite, scarcely zoned and often with a marked albite twinning.

Besides these three types of phenocrysts, the low-grade coarse-grained gneisses of the Ollo de Sapo can also locally contain small (≈ 5-10 mm) lithic fragments composed of quartz, plagioclase, biotite, zircon and Fe-Ti oxides (Fig 3.3).

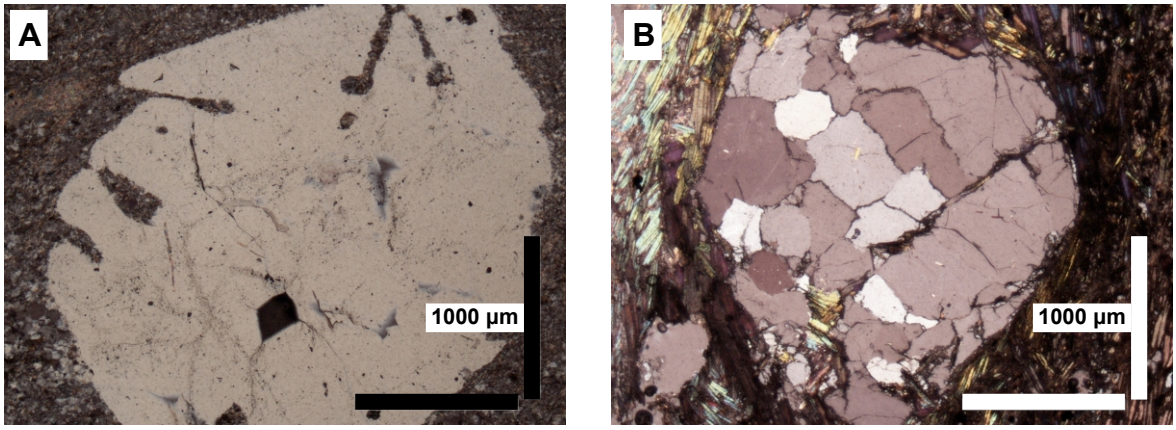


Figure 3.2: A) Quartz phenocrystal with embayed borders of the coarse-grained facies, in parallel nichols); B) Quartz phenocrystal which has been recrystallized forming fine-grained aggregates due to the metamorphism, in crossed nichols.


Figure 3.3: Lithic fragments (black angular specks) in coarse-grained low-grade metavolcanic rocks of the Ollo de Sapo in Sanabria.

The groundmass is fine-grained and variably deformed, the grain size increases with the metamorphic grade. In the samples with the lowest grade of metamorphism, it consists of quartz, oligoclase-albite, K-feldspar, retrograded crystal of biotite, chlorite, illite and, locally, prehnite-pumpellite, epidote-zoisite, carbonates and pseudomorphs of Fe-Mg minerals, the primary nature of which cannot currently be ascertained (Fig. 3.4). As the metamorphic grade increases, the groundmass becomes increasingly recrystallized and strongly foliated, with conspicuous SC structures defined by alternating muscovite + biotite-rich and quartz + feldspar-rich layers. The phenocrysts develop pressure shadows. The most deformed samples have abundant quartz and plagioclase ribbons, the internal structure of which is granoblastic.

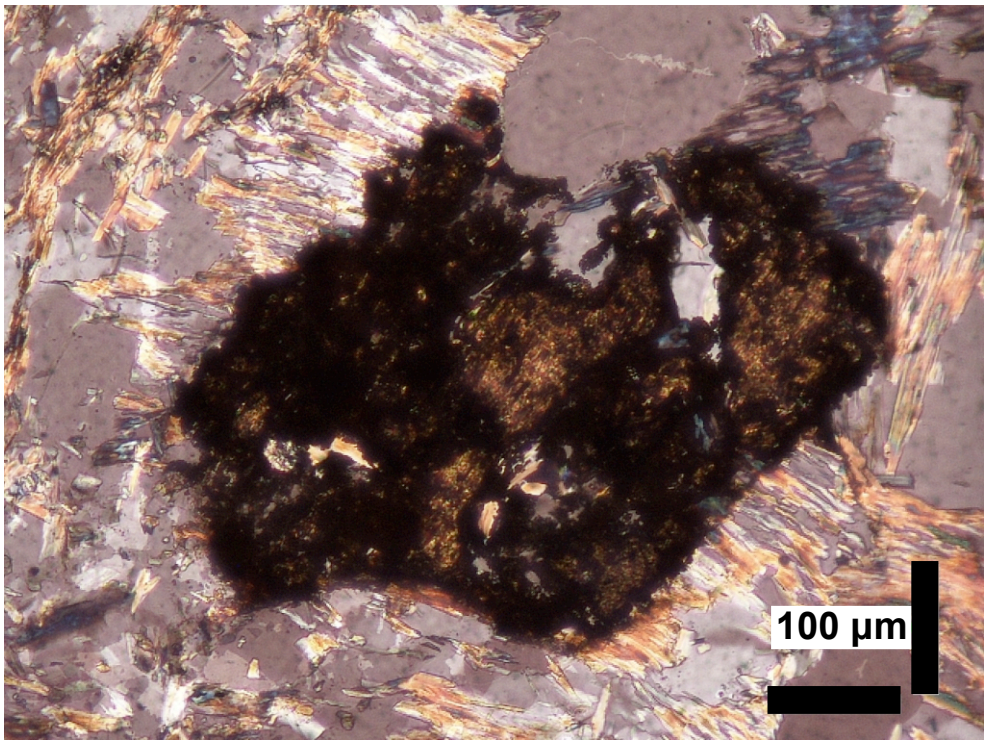


Figure 3.4: Pseudomorph of a Fe-Mg mineral, probably amphibole in the Ollo de Sapo Formation at Sanabria. Crossed nichols.

The accessory mineral assemblage consists of apatite, zircon, monazite, xenotime, titanite, ilmenite, rutile, Fe-oxides, occasional tourmaline, and rare uraninite. The most abundant are apatite and zircon. Apatite comprises stubby subhedral, up to 1 mm, prismatic crystals. Zircon consists of euhedral to subhedral, rarely rounded anhedral, crystals up to 350 µm, of short bipyramidal prism, seldom long prisms or needle-like. Titanite consists of subhedral to anhedral yellow-brown crystals up to 500 µm often closely associated with biotite, thus suggesting it might be secondary. Monazite and xenotime are subhedral and are present as isolated crystals or aggregates up to 300 µm in diameter. Tourmaline is subhedral and has a pleochroism from pale yellow to blue and size up to 250 µm.

The Ollo de Sapo gneisses are often altered, so that the primary mineralogy is, in most cases partially, transformed to secondary, low-temperature. The alteration is especially intense in the lower grade metamorphic samples.

#### *3.1.1.2. The Ollo de Sapo fine-grained gneisses*

These are formed of mesocratic to leucocratic augen gneisses (Fig. 3.5) that differ from these described in the previous section by the small size of the augen. The rocks contain

small phenocrysts of K-feldspar, quartz or plagioclase embedded in a fine-grained matrix (see Fig. 1.5C and 1.5D in Chapter 1). The gneisses are commonly deformed showing SC structures (Fig. 3.5).

The phenocrysts of K-feldspar are subhedral short prisms up to 1 cm in length. They often appear twinned and some have perthitic intergrowths. The phenocrysts of quartz are subhedral or rounded anhedral, up to 1-1.5 cm long, often with a characteristic bluish color (Fig. 3.4). The phenocrysts of plagioclase (oligoclase) are subhedral and are up to 6 mm long.

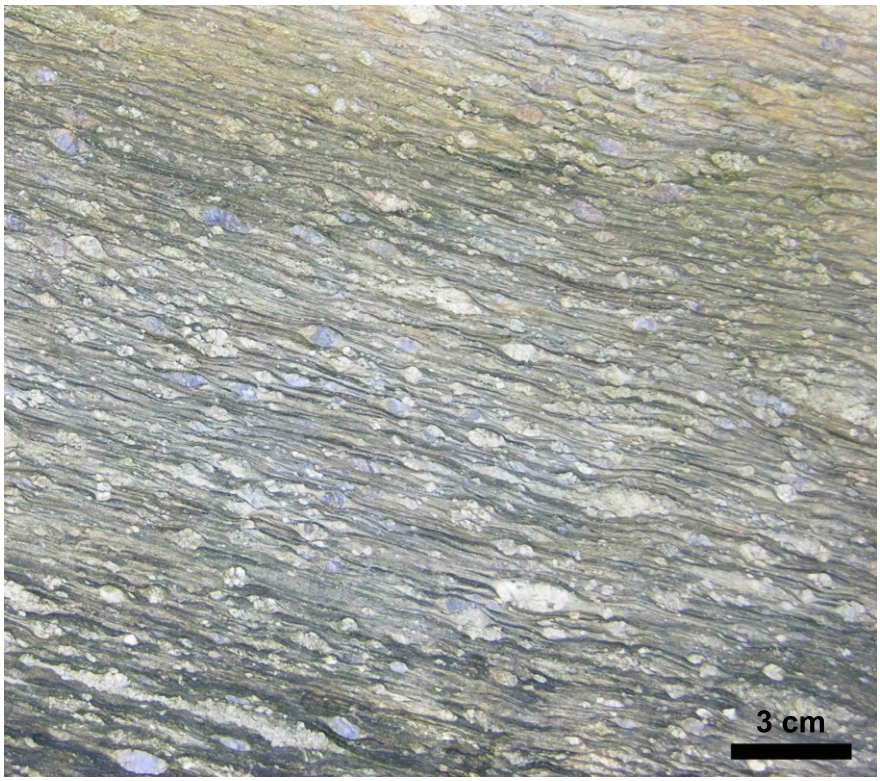


Figure 3.5: Field appearance of the fine-grained facies of the Ollo de Sapo metavolcanic rocks at Vivero. Note the bluish color of quartz phenocrysts.

The groundmass of the Ollo de Sapo fine-grained gneisses is identical to that of the coarse-grained gneisses both in texture and mineralogy. To avoid tedious repetitions, therefore, the reader is referred to section 3.1.1.1.

### 3.1.2. The Ollo de Sapo Formation metagranites

As mentioned in previous sections, we have studied the four most representatives metagranites associated with the Ollo de Sapo Formation: Viana do Bolo, San Sebastián,

Miranda do Douro and Antoñita. Currently, these rocks are mesocratic to leucocratic augen-gneisses characterized by large subhedral K-feldspar megacrysts, up to 15 cm, although often between 3 and 8 cm, with conspicuous aplopegmatitic dikes (Fig. 3.6) and enclaves (Fig. 3.7).

Some petrographic characteristics are common to all the metagranites. The K-feldspar megacrysts often show Carlsbad twinning and locally have Frals inclusions. They are embedded in a medium to coarse-grained (up to 1 cm) foliated groundmass which mainly consists of quartz, plagioclase, K-feldspar, biotite and rare muscovite. Quartz is present as anhedral or subhedral, slightly rounded, crystals. K-feldspar appears as anhedral crystals often with microcline twinning and perthitic intergrowths. Plagioclase is often oligoclase, rarely andesine or albite, which forms subhedral tabular crystals that may reach up to 4 cm and commonly display albite twinning. They are always zoned. The varietal mineralogy is biotite and muscovite, rarely biotite alone, which are present as subhedral, often deformed crystals. When the metamorphic grade reaches the anatexis isograde, these rocks often contain cordierite + sillimanite ± garnet.

The accessory mineral assemblage is composed of apatite, zircon, monazite, xenotime, tourmaline, ilmenite and Fe-sulfides. The most abundant is apatite, which forms short euhedral prisms up to 600 μm long. Zircon consists of short, occasionally long, bipyramidal, pale-pink to brownish-orange prisms with a maximum dimension up to 300 μm, although sometimes pale-yellow. Monazite and xenotime are subhedral isolated crystals with a maximum dimension up to 30 and 10 μm respectively. Tourmaline appears as euhedral or subhedral crystals with a maximum dimension up to 1.5 mm and has a pleochroism from colorless to yellow-pale blue.

The Viana do Bolo metagranite (Fig. 3.7) is leucocratic and coarse-grained with quartz + K-feldspar + plagioclase + biotite + muscovite as major minerals. Apatite, zircon, monazite and Fe-oxides are accessory minerals.

The San Sebastián metagranite appears forming strongly deformed narrow (< 2 m thick) dikes. It is a fine-grained leucocratic gneiss with quartz + K-feldspar + plagioclase + biotite as major minerals and apatite, zircon, monazite and Fe-Ti-oxides as accessories.

The Miranda do Douro metagranite (Fig. 3.8) is mesocratic and coarse-grained with quartz + plagioclase + biotite + K-feldspar as major minerals and apatite, zircon, monazite,

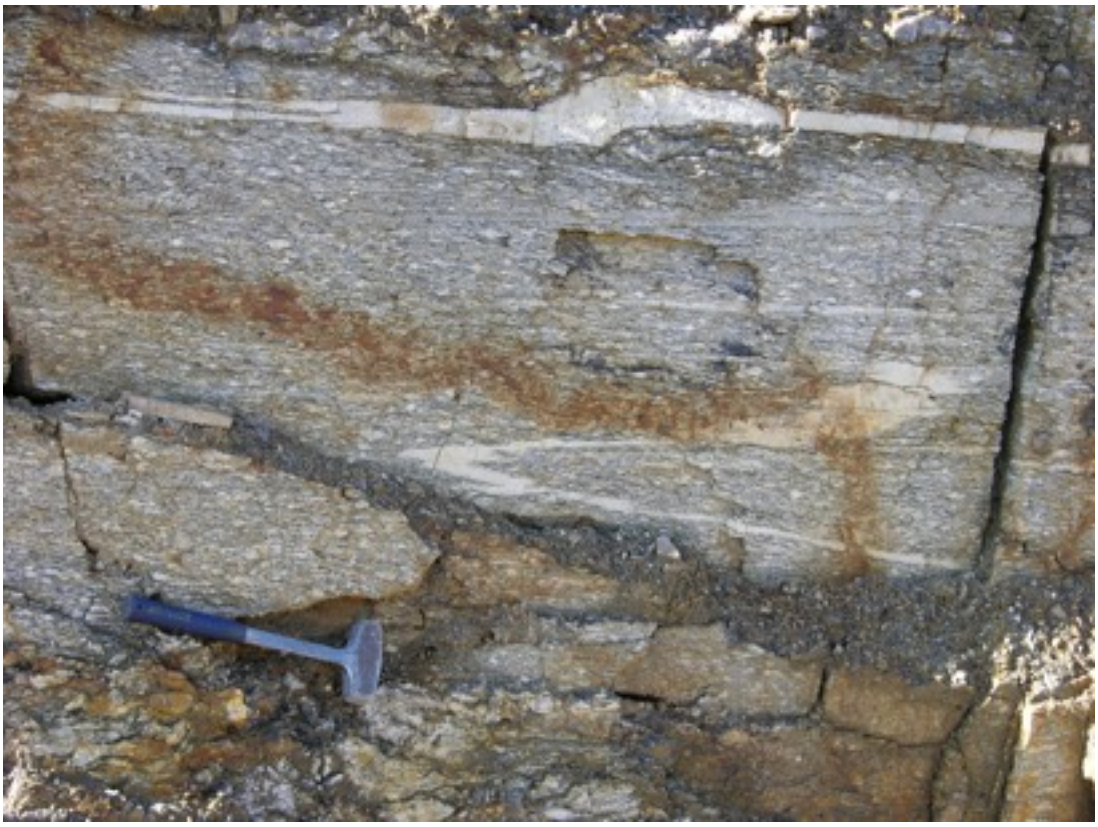

Figure 3.6: Field appearance of the metagranites associated to the Ollo de Sapo Formation. Note the folded aplites in the Antoñita metagranite of Hiendelaencina

Figure 3.7: Field appearance of the metagranites associated to the Ollo de Sapo Formation. Note the microgranular enclave in the Viana do Bolo metagranite

xenotime, Fe-Ti-oxides and Fe-sulfides as accessory minerals.

Figure 3.8: Field appearance of the Miranda do Douro metagranite.

The Antoñita metagranite (Fig. 3.6) is leucocratic and coarse-grained with quartz + plagioclase + K-feldspar + plagioclase + biotite + muscovite as major minerals and tourmaline, apatite, zircon, monazite and xenotime as accessory minerals.

## 3.2. The Schist-Graywacke Complex Domain

The pre-Middle Ordovician metagranites and metavolcanic rocks of the Schist-Graywacke Complex Domain are mostly found in four areas located in the northern part of the domain. These are the Tormes Dome, Sierra de Gredos, Sierra de Guadarrama and the Anatectic Complex of Toledo. The most relevant petrographic features of the pre-Middle Ordovician rocks of these four areas are as follows:

### *3.2.1. The Tormes Dome*

The pre-Middle Ordovician metagranites of the Tormes Dome studied here, Fermoselle, Vitigudino and Ledesma are leucocratic augen gneisses. The augen comprise subhedral to euhedral prisms of K-feldspar megacrysts with a maximum dimension up to 6 cm. They show Carlsbald twinning and perthitic intergrowths and contain numerous minute inclusions of other minerals such as biotite and quartz. In areas where the deformation has been more intense, they also show fractures perpendicular to major axis and asymmetric pressure shadows.

Figure 3.9: Field appearance of the Fermoselle metagranite.

Figure 3.10: Field appearance of the Vitigudino metagranite.

Figure 3.11: Field appearance of the Ledesma metagranite. Note the asymmetric pressure shadows

The megacrysts are included in a medium-grained and variably metamorphosed groundmass. When the metamorphic grade is low, the groundmass mainly consists of quartz + K-feldspar + plagioclase (oligoclase-albite) + biotite ± muscovite defining a hypidiomorphic texture. As the metamorphic grade increases, biotite is partially replaced by sillimanite ± cordierite. Locally, the metagranites reached anatexis and produced small leucocratic stocks of Variscan anatectic leucogranites.

The accessory mineral assemblage consists of apatite, zircon, monazite, xenotime, tourmaline, Fe-sulphide and Fe-oxides. Apatite is colorless euhedral crystals with a maximum dimension up to 300 μm. Zircon comprises short, occasionally long, bipyramidal, pale-pink to brownish crystals with a maximum dimension of 450 μm. It can also sometimes be colorless or yellow. Monazite and xenotime are isolated subhedral crystals with a maximum dimension of 200 μm and 170 μm respectively. Tourmaline consists of up to 1 mm long subhedral crystals, and shows a slight pleochroism from yellow-greenish to pale blue.

The Fermoselle metagranite (Fig. 3.9) is leucocratic and coarse-grained with quartz + K-feldspar + plagioclase + biotite ± muscovite ± sillimanite ± cordierite as major minerals and apatite, zircon, monazite, xenotime and Fe-oxides as accessory minerals.

The Vitigudino metagranite (Fig. 3.10) is leucocratic and fine-grained with quartz + K-feldspar + plagioclase + biotite ± muscovite as major minerals and apatite, zircon, monazite, xenotime, Fe-oxides and Fe-sulfides as accessory minerals.

The Ledesma metagranite (Fig. 3.11) is leucocratic and coarse-grained with quartz + K-feldspar + plagioclase + biotite ± muscovite ± cordierite ± sillimanite as major minerals and apatite, zircon, monazite, ilmenite and occasional sulfides as accessory minerals.

### 3.2.2. The Sierra de Gredos

The pre-Middle Ordovician metagranites of the Sierra de Gredos studied in this work are Bercimuelle, Castellanos and San Pelayo, all of them located in the northwest of the Sierra. These metagranites are strongly metamorphosed, even partially migmatized. They are typically mesocratic and coarse grained, though fine-grained leucocratic facies are also common, especially in Castellanos. The augen consist of subhedral prismatic K-feldspar phenocrysts with dimensions between 3-5 cm, that often have tiny inclusions of quartz and biotite. They usually show Carlsbad twinning and perthitic intergrowths.

Figure 3.12: Field appearance of the Bercimuelle metagranite.

The K-phenocrysts are embedded in a medium to coarse-grained groundmass mainly composed of quartz + plagioclase + K-feldspar + biotite ± muscovite ± sillimanite ± cordierite ± rare garnet.

The accessory mineral assemblage comprises apatite, zircon, tourmaline, monazite, xenotime, rutile, sulfides and Fe-Ti-oxides. Zircon consist of short, sometimes long or slightly rounded, bipiramidal, usually pale-pink to brownish-orange prisms with a maximum dimension of 450 μm, although sometimes is colorless or pale-yellow. Apatite comprises colorless subhedral crystals up to 200 μm. Tourmaline consists of subhedral crystals with a maximum dimension of 4 mm and pleochroism from yellow-blue to pale-yellow-pale-blue. Monazite and xenotime comprise either isolated subhedral crystals or fine-grained aggregates with a maximum dimension of 80 and 120 μm respectively.

The San Pelayo metagranite is mesocratic and coarse-grained composed of K-feldspar + quartz + oligoclase + biotite + muscovite + abundant tourmaline. Apatite, zircon, monazite, xenotime, Fe-Ti-oxides and sulfides are accessory minerals.

The Castellanos metagranite is mesocratic to leucocratic and coarse to fine-grained with quartz + K-feldspar + plagioclase + biotite + muscovite ± cordierite as major minerals and tourmaline, apatite, zircon, monazite and xenotime as accessories.

The Bercimuelle metagranite (Fig. 3.12) is also mesocratic to leucocratic, coarse-grained, and always appears variably migmatized. The major minerals are quartz + K-feldspar + albite-oligoclase + biotite ± cordierite. The accessory assemblage comprises apatite, zircon, monazite, xenotime, Fe-Ti-oxides and sulfides.

### 3.2.3. The Sierra de Guadarrama

As mentioned in section 1.2.2.2., the Sierra de Guadarrama contains the most voluminous accumulation of pre-Middle Ordovician metagranites and metavolcanic rocks in the Central Iberian Zone. The most relevant petrographic features are as follows:

#### *3.2.3.1. Metagranites*

The metagranites of the Sierra de Guadarrama sampled for this work are La Cañada, Santa Maria de la Alameda, La Hoya, La Estación I, La Estación II, Vegas de Matute (melanocratic and leucocratic metagranites), La Morcuera, Buitrago de Lozoya and Prádena del Rincón (see Table 2.2, chapter 2). All these rocks are mesocratic to leucocratic granitic gneisses, either augen or fine-grained, that have been variably deformed and metamorphosed, often to anatexis.

Some petrographic characteristics are common to all the metagranites. The augen consist either of K-feldspar megacrysts, plagioclase phenocrysts or monomineralic aggregates of quartz or plagioclase. K-feldspar megacrysts are subhedral to euhedral prisms, rarely ovoidal, with a maximum dimension up to 8-12 cm. They show Carlsbad twinning and perthitic intergrowths, and may have rapakivi textures. The plagioclase phenocrysts are subhedral crystals of oligoclase-andesine with a maximum dimension up to 6 mm.

The major mineral assemblage of the groundmass consists of K-feldspar + plagioclase + quartz + biotite ± muscovite forming a hypidiomorphic aggregate. At low metamorphic grade, biotite is altered to relicts of biotite and chlorite and an aggregate of illite and other phillosilicates. As the metamorphic grade increases, garnet, cordierite and sillimanite appear as a consequence of the breakdown of biotite.

Figure 3.13: Mesoscopic appearance of the La Cañada metagranite.

Figure 3.14: Mesoscopic appearance of the La Hoya metagranite.

Figure 3.15: Field appearance of the La Estación I metagranite.

Figure 3.16: Field appearance of the La Estación II metagranite.

Figure 3.17: Field appearance of the melanocratic metagranite of Vegas de Matute.

Figure 3.18: Field appearance of the leucocratic metagranite of Vegas de Matute.

The accessory mineral assemblage consists of apatite, zircon, monazite, xenotime, rutile, Fe-Ti-oxides and Fe-Cu sulfides. Apatite occurs as subhedral to euhedral colorless crystals with a maximum dimension of 1 mm. Zircon consists of short, rarely long or acicular, bipyramidal prisms with a maximum dimension up to 450 μm. It is usually pale-pink to brownish and sometimes yellowish or orange. Monazite and xenotime occurs as subhedral to euhedral isolated crystals or aggregates with a maximum dimensions up to 500 and 200 μm respectively.

The La Cañada metagranite (Fig. 3.13) is mesocratic and coarse-grained with quartz + plagioclase + K-feldspar + biotite ± cordierite ± garnet ± muscovite as major minerals. Apatite, zircon, monazite and Fe-oxides are the accessory minerals.

The La Hoya metagranite (Fig. 3.14) is mesocratic and coarse-grained with K-feldspar + plagioclase + quartz + biotite ± muscovite. Apatite, zircon, monazite, xenotime and Fe-Ti oxides are the accessory minerals.

The La Estación I metagranite (Fig. 3.15) is mesocratic, coarse-grained, with K-feldspar + oligoclase + quartz + biotite ± sillimanite ± chlorite ± cordierite. Apatite, zircon, tourmaline, monazite, xenotime, Fe-Ti-oxides and Fe-sulfides are the accessory minerals.

The La Estación II metagranite (Fig. 3.16) is mesocratic and coarse-grained with K-feldspar + quartz + oligoclase + biotite ± chlorite ± muscovite. Apatite, zircon, monazite, xenotime and Fe-Ti-oxides are the accessory minerals.

The melanocratic metagranite of Vegas de Matute (Fig. 3.17) is coarse-grained with quartz + plagioclase + K-feldspar + biotite ± muscovite ± chlorite ± sillimanite ± garnet. Apatite, zircon, monazite, xenotime, Fe-Ti oxides and Fe-Cu sulfides are the accessory minerals.

The leucocratic metagranite of Vegas de Matute (Fig. 3.18) is fine-grained with quartz + plagioclase + K-feldspar + biotite + muscovite as major minerals and apatite, zircon, monazite, xenotime and Fe-Ti oxides as accessories.

The La Morcuera metagranite (Fig. 3.19) is mesocratic and coarse-grained with K-feldspar + plagioclase + quartz + biotite ± muscovite as major minerals and apatite, zircon, monazite, xenotime, rutile and Fe-Ti oxides as accessories.

Figure 3.19: Field appearance of the La Morcuera metagranite. Note the rapakivi textures of some megacryts.

Figure 3.20: Mesoscopic appearance of the Buitrago de Lozoya metagranite cut by pegmatite and aplite veins.

Figure 3.21: Field appearance of the Prádena del Rincón metagranite.

The Buitrago de Lozoya metagranite (Fig. 3.20) is mesocratic and coarse-grained with K-feldspar + plagioclase + quartz + biotite ± sillimanite ± muscovite. Apatite, zircon, monazite, xenotime and Fe-sulfides are the accessory minerals.

The Prádena del Rincón metagranite (Fig. 3.21) is leucocratic and fine-grained with quartz + K-feldspar + plagioclase + biotite ± muscovite ± garnet as major minerals and apatite, zircon, monazite, Fe-Ti oxides as accessories.

### *3.2.3.2. Metavolcanic rocks*

In the Sierra de Guadarrama there are three gneissic bodies, La Berzosa, El Cardoso and Riaza, with features similar to the metavolcanic rocks of the Ollo de Sapo Formation (García Cacho, 1973; Capote and Fernández Casals, 1975). As in the latter formation, a coarse-grained and a fine-grained facies are identified depending on the size of the augen.

The **coarse-grained facies** (Fig. 3.22) is formed of gneisses with abundant augen. These are either K-feldspar megacrysts, phenocrysts of plagioclase and quartz, or

Figure 3.22: Field aspect of the coarse-grained metavolcanites of the Sierra de Guadarrama.

Figure 3.23: Field aspect of the fine-grained metavolcanites of the Sierra de Guadarrama.

polycrystalline aggregates of plagioclase and quartz. The K-feldspar megacrysts are subhedral prisms with a maximum dimension up to 6-8 cm; they show Carlsbad twinning, perthitic intergrowths and numerous small inclusions of biotite and quartz. The phenocrysts of plagioclase are subhedral platty crystals of oligoclase ($An_{21-18}$) with conspicuous albite twinning. The phenocrysts of quartz are subhedral, often rounded, crystals with a maximum dimension of 2 mm.

The major mineral assemblage of the groundmass depends on the metamorphic grade. In general it consists of a fine grained hypidiomorphic aggregate of quartz, plagioclase, K-feldspar, biotite and muscovite, which are locally partially replaced by subhedral to anhedral crystals of cordierite.

The accessory mineral assemblage consists of apatite, zircon, monazite, xenotime, rutile, Fe-Ti-oxides and Fe-Cu sulfides. Apatite is present as subhedral to euhedral colorless crystals with a maximum dimension up to 500 μm. Zircon consists of short, bipiramidal, pale pink to brownish prisms with a maximum dimension up to 450 μm. Monazite and xenotime occur as subhedral to euhedral isolated crystals with maximum dimensions up to 20 and 15 μm respectively, or as aggregates.

The **fine-grained facies** (Fig. 3.23) do not have K-feldspar megacrysts and the phenocrysts are always less than 1 cm. In general, the gneisses of the fine-grained facies are less metamorphosed than the coarse-grained gneisses. For that reason, the original shapes of the phenocrysts of quartz and embayed borders in quartz can be distinguished. The rest of the features of the fine-grained facies are similar to the features of the coarse-grained facies described above.

### 3.2.4. The Anatectic Complex of Toledo

As mentioned in the previous section, in the Anatectic Complex of Toledo samples from two metagranitic orthogneisses, Polán and Mohares, located in the north part of the complex (see Table 2.2 in chapter 2) have been studied. In both cases they are mesocratic to leucocratic fine-grained gneisses, locally augen, which were strongly metamorphosed during the Variscan orogeny (Fig. 3.24). The augen consist of K-feldspar megacrysts and quartz phenocrysts. The megacrysts of K-feldspar are subhedral with a maximum dimension of 3-5 cm. They show Carlsbad twinning and small inclusions of plagioclase.

Figure 3.24: Field aspect of the Mohares metagranite of the Anatectic Complex of Toledo. Note the lack of augen and the elevated migmatization.

The phenocrysts of quartz are anhedral or slightly rounded, and are rare rarely larger than 1 cm.

The augen are embedded in a medium-grained groundmass with a major mineral assemblage mainly composed of quartz, plagioclase, K-feldspar and biotite. Plagioclase appears as subhedral to anhedral albite-twinned crystals. K-feldspar is present as anhedral crystals. Biotite appears as subhedral, often deformed, crystals. In the most metamorphosed samples, biotite is partially replaced by subhedral to euhedral crystals of garnet and cordierite.

The accessory mineral assemblage is composed of apatite, zircon, monazite and Fe-oxides. Apatite appears as euhedral crystals with a maximum dimension up to 300 μm. Zircon consists of short, although occasionally long, bipiramidal, yellowish to brownish prisms with a maximum dimension up to 450 μm. Monazite appears as pale-brown euhedral crystals with a maximum dimension of 160 μm.

# 4. GEOCHRONOLOGY

# 4. GEOCHRONOLOGY

For this study more than two thousand zircon grains were hand-picked under the binocular microscope, mounted and studied by cathodoluminescence imaging. A selection of them were dated using spot U-Th-Pb and stepwise evaporation Pb-Pb methods as described in Chapter 2. The cathodoluminiscence studies have also been used for calculating the proportion of inherited cores contained in the zircons. The crystallization ages of all studied bodies are summarized in Table 4.1, at the end of this chapter.

## 4.1. The Ollo de Sapo Domain

### 4.1.1. The Ollo de Sapo Formation

We separated zircon from ten different samples of the metavolcanic rocks of the Ollo de Sapo Formation. The exact location and coordinates of the studied samples are given in Table 2.1. The zircons from all samples show many similarities. Most of them are euhedral or subhedral short prisms, rarely long prisms or needle-like, often with pale-pink-brownish, rarely grayish, or colorless. The average size is about 200 x 90 μm; occasionally they may reach sizes up to 350 x 135 μm. The cathodoluminescence imaging reveal that these zircons stand out because of the ubiquitous presence of inherited cores (Figs. 4.1z1, 4.1z2, 4.1z3, 4.1z6, 4.1z7, 4.1z8, 4.1z10, 4.1z11, 4.1z12, 4.1z13 and 4.1z14), present in no less than 70-80%, locally up to 100% of the grains (Fig. 4.2). Most cores show magmatic oscillatory zoning. Most rims also display typical magmatic oscillatory zoning, though it is

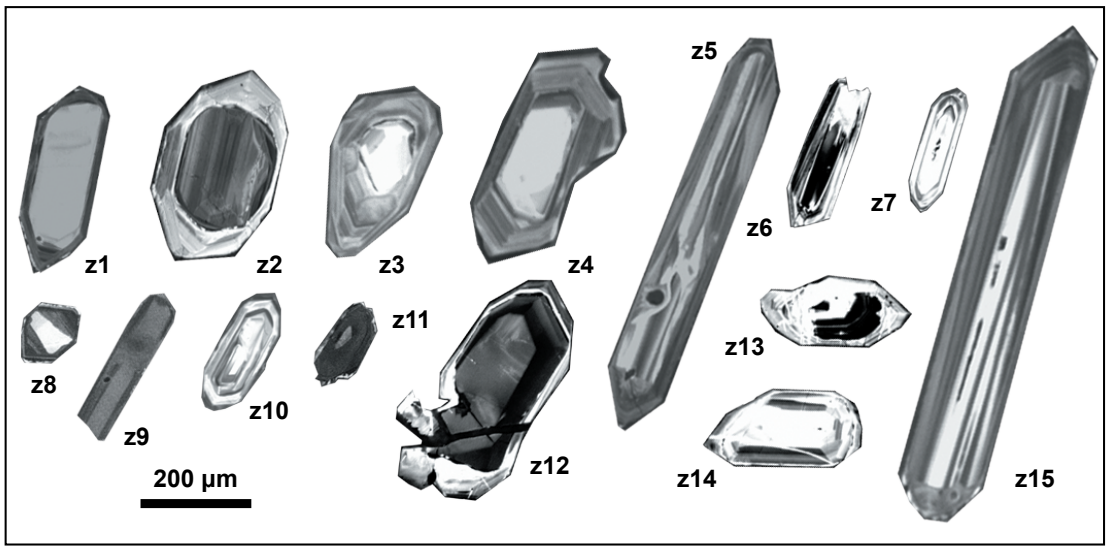


Figure 4.1: Cathodoluminescence images of the most representative internal textures of the metavolcanic rocks of the Ollo de Sapo Formation.

often sharply discordant with the cores (Fig. 4.1z4, 4.1z5, 4.1z9 and 4.1z15); convolute zoning is also found locally in some grains.

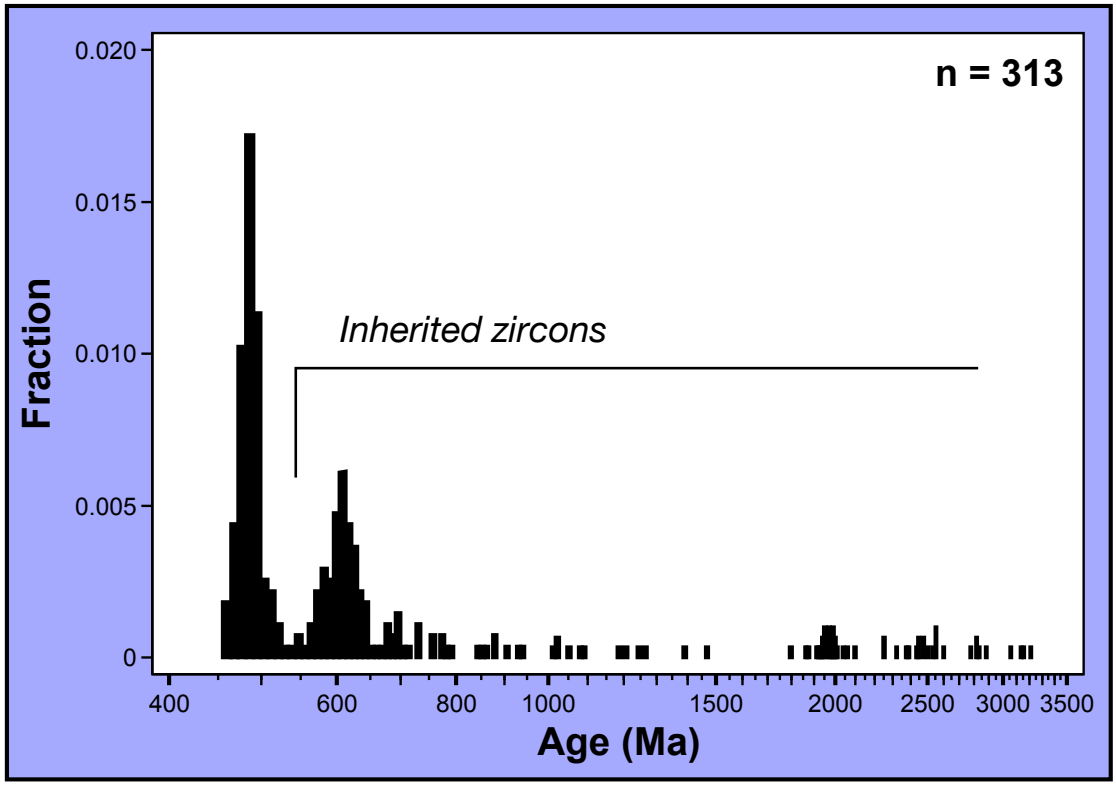


Figure 4.2: Age distribution pattern found in zircons of the metavolcanic and metagranitic rocks of the Ollo de Sapo Domain. Built from the U-Pb SIMS, SHRIMP and LA-ICPMS data.

The results of zircon dating in the Ollo de Sapo Formation can be summarized as follows:

#### *4.1.1.1. Vivero*

In the Vivero region we studied three samples of metavolcanic rocks, two (one coarse-grained, another fine-grained) from the Ria del Barquero in the Cantabric Coast and one fine-grained facies from the Mañón area. The three samples were studied using U-Pb LA-ICPMS (Table 4.2) and Pb-Pb stepwise evaporation (Table 4.3). U-Pb dating of the three samples yielded the same results (Figs. 4.3A and 4.3C): a very abundant concordant to subconcordant Cambro-Ordovician population with a mean age of 486 ± 3 Ma (Fig. 4.3B), another also abundant concordant to subconcordant population with a mean age of 608 ± 16 Ma, two concordant points at ca. 1000 Ma, several concordant points at ca. 2000 Ma, and a discordia line with an upper intercept at ca. 2600 Ma.

Twelve zircon grains were analyzed by the Pb-Pb evaporation method. Seventeen out of 48 evaporation steps yielded a plateau-age at 486 ± 3 Ma, identical to the U-Pb age of the youngest concordant population (Fig. 4.3D), which we therefore consider the crystallization age of the Ollo de Sapo in Vivero. It is remarkable that most crystals contain inherited cores. The most common ages for these cores are ca. 540 and ca. 600 Ma and minimum ages of ca, 800, 2000 and 2800 Ma are also present.

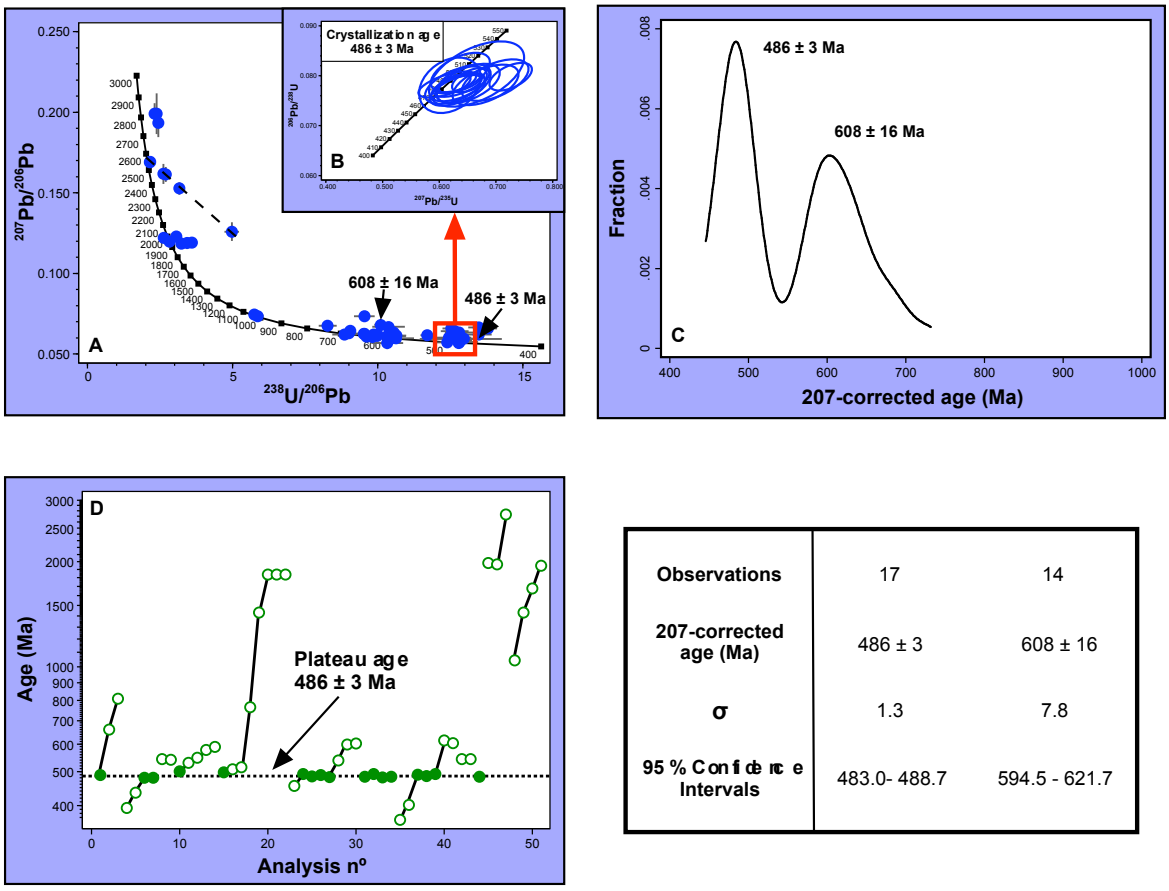


| | | |
|---|---|---|
| Observations | 17 | 14 |
| 207-corrected age (Ma) | 486 ± 3 | 608 ± 16 |
| σ | 1.3 | 7.8 |
| 95 % Confidence Intervals | 483.0- 488.7 | 594.5 - 621.7 |

Figure 4.3: Geochronological data of the Vivero metavolcanic rocks: A) Tera-Wasserburg concordia; B) Wetherill concordia; C) Distribution of concordant 207-corrected ages and the statistical data of the two most abundant populations; and D) Pb-Pb stepwise evaporation age.

According to the cathodoluminescence images, the Cambro-Ordovician population (486 ± 3 Ma) was present in rims of grains containing older cores (Fig. 4.4LAz17) and in grains with uniform ages from core to rim (Fig. 4.4LAz3). The Ediacaran population (608 ± 16 Ma), however, was present in the cores of zircons (Fig. 4.4LAbz1), most of which were overgrown by Cambro-Ordovician rims (Fig. 4.4LAz17). The older-than-Ediacaran ages always correspond to restitic cores (Fig. 4.4LAz9).

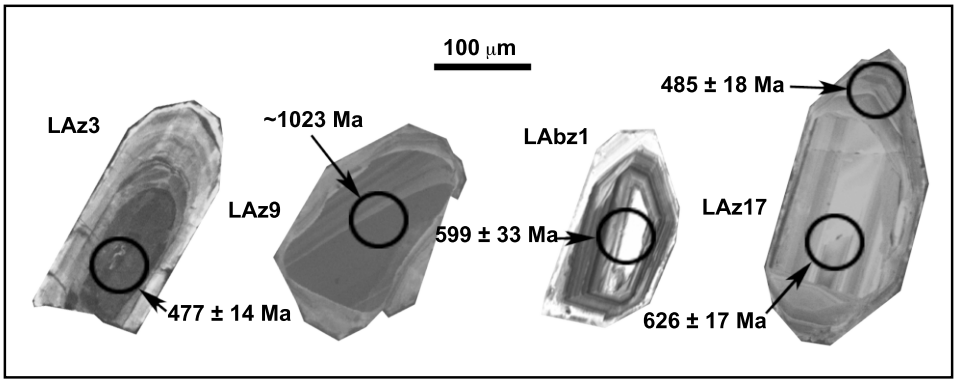


Figure 4.4: Cathodoluminescence images and ages of selected zircons from the Vivero metavolcanic rocks.

### *4.1.1.2. Trives*

In the Trives region, a coarse-grained metavolcanic rock was dated using U-Pb ion microprobe and LA-ICPMS (Fig. 4.5 and Table 4.4). These data reveal the presence of three concordant population (Fig. 4.5A and 4.5C). The first one, very abundant, is at 458-499 Ma, yields a mean age of 486 ± 5 Ma and is considered the age of crystallization (Fig. 4.5B). The second population, also abundant, at 605-616 Ma yields a mean age of 610 ± 9 Ma. Between these two populations are two points at 558 and 562 Ma which probably represent a mixing age between them. The third population, less numerous and

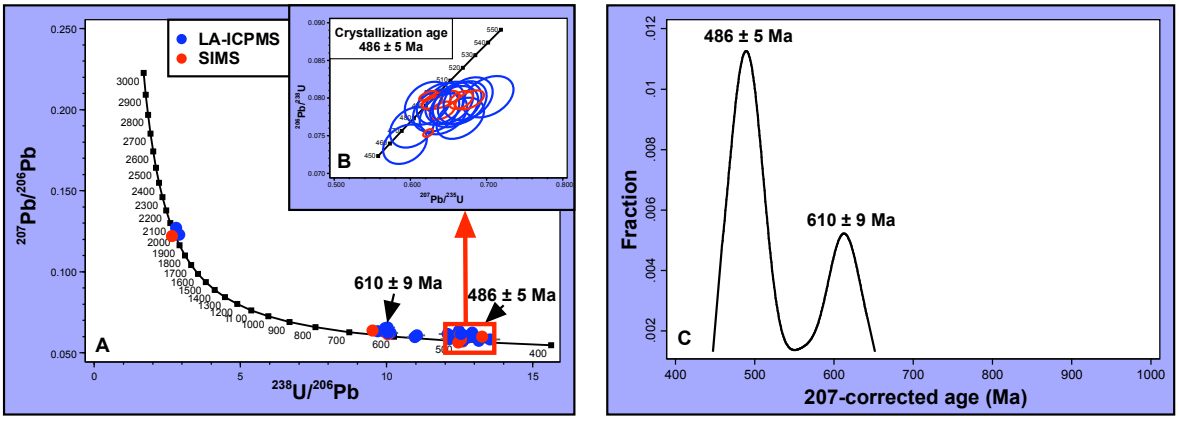


| Observations | 207-corrected age (Ma) | σ | 95 % Confidence Intervals |
|---|---|---|---|
| 20 | 486 ± 5 | 2.3 | 481.2 - 490.8 |
| 8 | 610 ± 9 | 4.8 | 607.5 - 613.0 |

Figure 4.5: Geochronological data of the Trives metavolcanic rocks: A) Tera-Wasserburg concordia; B) Wetherill concordia; and C) Distribution of concordant 207-corrected ages and the statistical data of the two most abundant populations.

also concordant, yielded ages between 1988 Ma and 2059 Ma, with a mean of 2015 ± 40 Ma.

As revealed by the cathodoluminescence images, the Cambro-Ordovician population (486 ± 5 Ma) is present in rims of grains containing older cores and in grains with uniform ages from core to rim (Fig. 4.6z10 and 4.6z12). The Ediacaran (610 ± 9 Ma) (Fig. 4.6z4) and the Orosirian (1988 Ma and 2059 Ma populations) (Fig. 4.6z1) were always obtained in cores of zircons with Cambro-Ordovician rims.

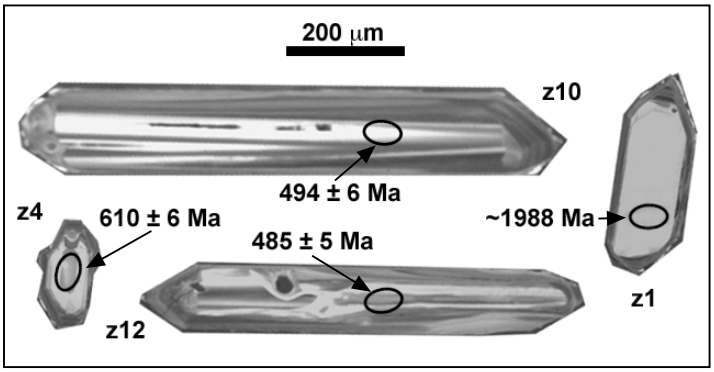


Figure 4.6: Cathodoluminescence images and ages of selected zircons from the Trives metavolcanic rocks.

### *4.1.1.3. Sanabria*

In the Sanabria region, the metavolcanic rocks form a sequence with a thickness of about 1500 m (Díez Montes et al., 2006). To determine the time span recorded in the sequence, we analyzed samples located at different stratigraphic positions: one from the lowermost coarse-grained facies, another from the uppermost fine-grained facies and another from the upper mixed facies.

#### *4.1.1.3.1. Lower metavolcanic rocks*

The sample from the lower metavolcanic rocks was analyzed by U-Pb ion-microprobe and LA-ICPMS (Table 4.5). The results revealed a complex age distribution with two concordant populations and several grains scattered at older ages (Figs. 4.7A and 4.7C). The most abundant concordant population is Cambro-Ordovician, with a precise mean age of 492 ± 4 Ma which is therefore interpreted as the crystallization age of the lower metavolcanic rocks of the Ollo de Sapo Formation in the Sanabria region (Fig. 4.7B). The second most abundant concordant population is Ediacaran, with a mean age of 605 ± 4 Ma.

There are also two points at 680 Ma, another two at 1.0 Ga, one at ca. 2.0 Ga and some others defining a discordia line with an upper interception at ca. 2.6 Ga.

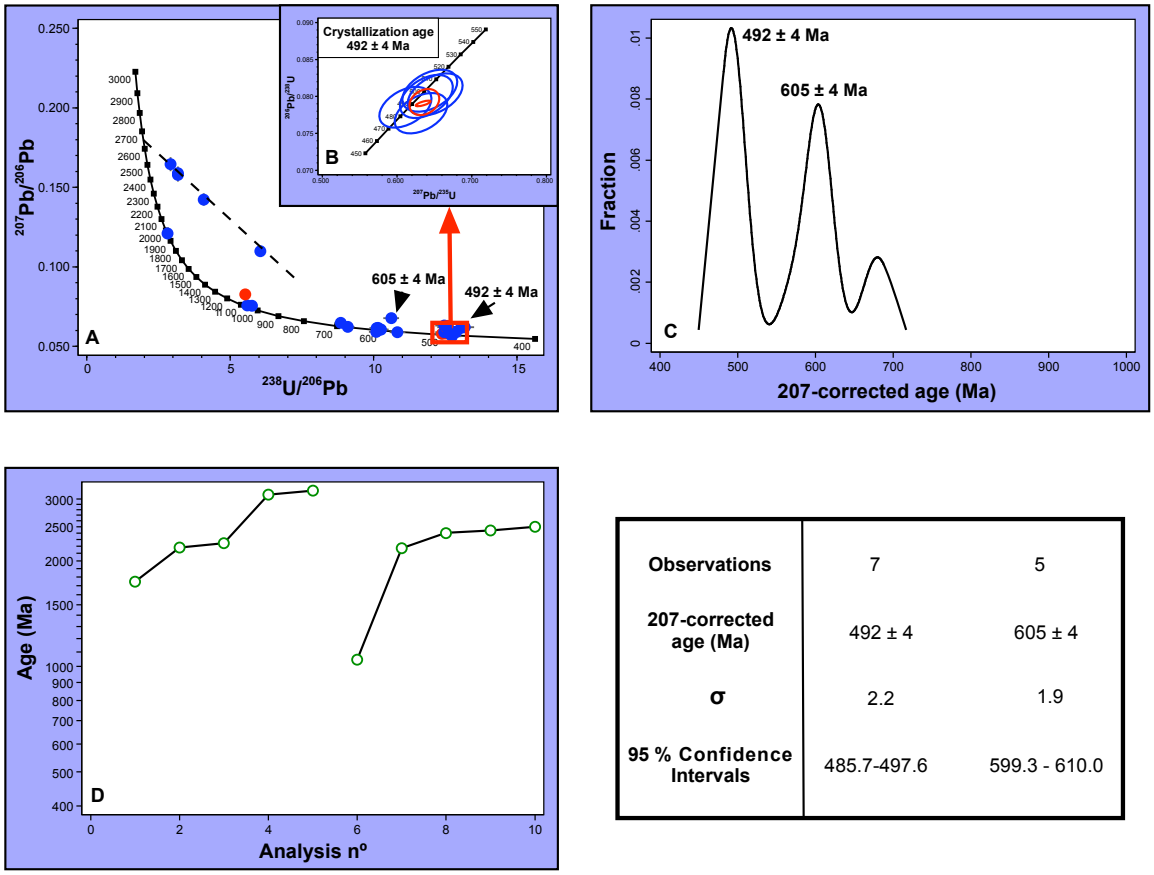


| | | |
|---|---|---|
| **Observations** | 7 | 5 |
| **207-corrected age (Ma)** | 492 ± 4 | 605 ± 4 |
| **σ** | 2.2 | 1.9 |
| **95 % Confidence Intervals** | 485.7-497.6 | 599.3 - 610.0 |

Figure 4.7: Geochronological data of the lower metavolcanic rocks of the Sanabria region: A) Tera-Wasserburg concordia; B) Wetherill concordia; C) Distribution of concordant 207-corrected ages and the statistical data of the two most abundant populations; and D) Pb-Pb stepwise evaporation age.

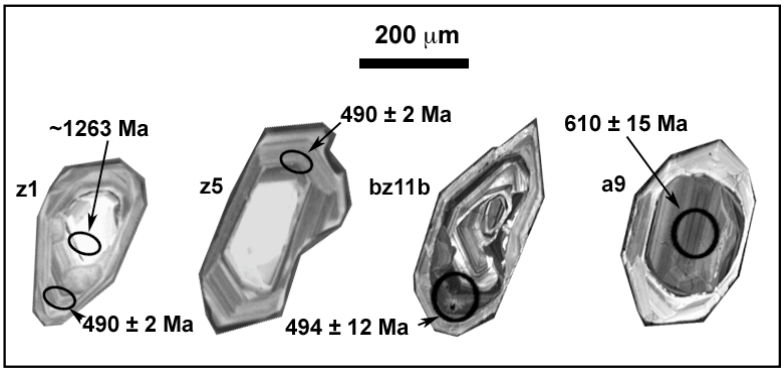


Figure 4.8: Cathodoluminescence images and ages of selected zircons from the lower meta-volcanic rocks of Sanabria region.

Some zircon grains analyzed with the Pb-Pb evaporation method did not yield a suitable estimation of the crystallization age, but revealed the presence of Archean cores with minimum ages of 3-3.2 Ga (Fig. 4.7D and Table 4.6).

The Cambro-Ordovician ages, according to the cathodoluminescence imaging, are represent as rims of grains containing older restitic cores (Fig. 4.8z1) and in uniform grains (Figs. 4.8z5 and 4.8bz11b). The Ediacaran ages were obtained in cores of grains rimmed by Cambro-Ordovician overgrowths (Fig. 4.8a9) or in scarce totally restitic zircons. All older-than-Ediacaran ages were obtained in restitic zircons and, more often, in cores rimmed by Cambro-Ordovician overgrowths (Fig. 4.8z1).

*4.1.1.3.2. Upper metavolcanic rocks*

The two samples belonging to the upper metavolcanic rocks and mixed facies were analyzed with the U-Pb (ion-microprobe and LA-ICPMS) and Pb-Pb stepwise evaporation methods (Tables 4.7 and 4.8). The two samples have exactly the same U-Pb age

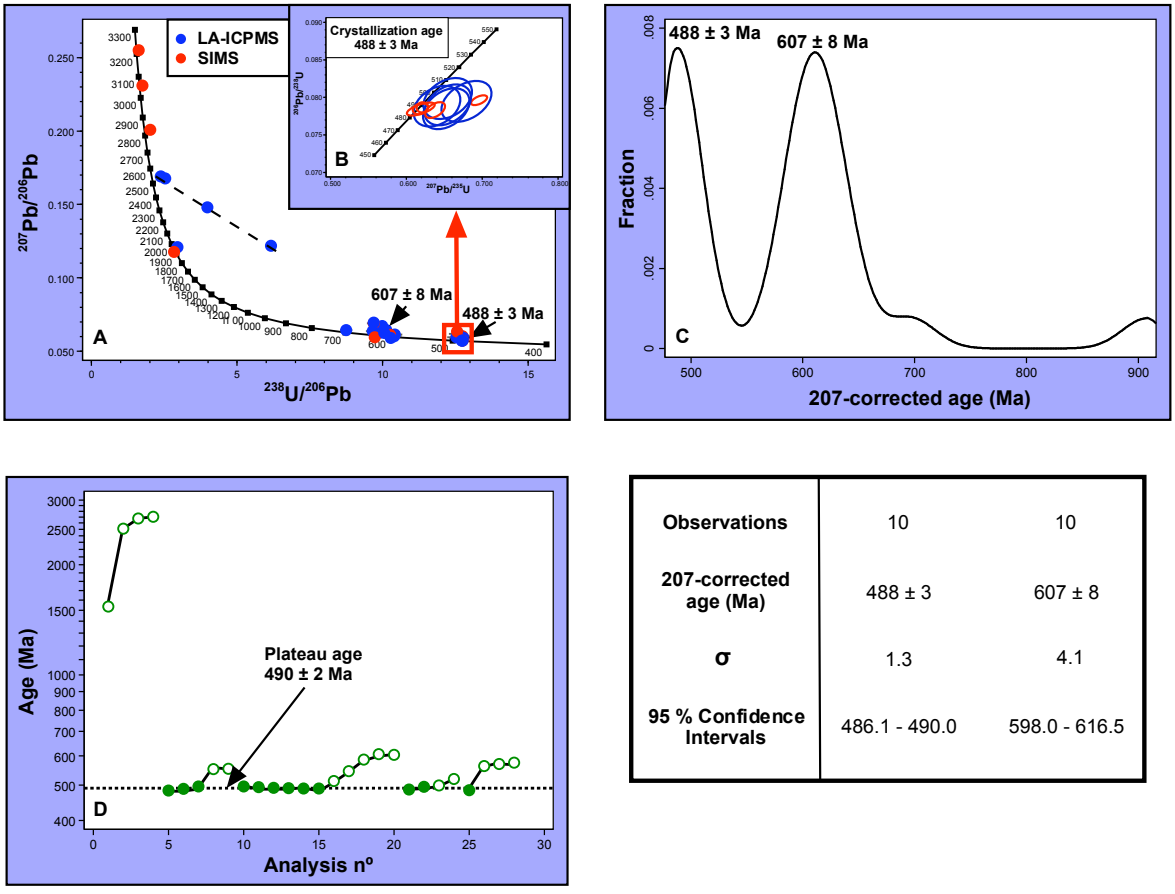


| | | |
|---|---|---|
| Observations | 10 | 10 |
| 207-corrected age (Ma) | 488 ± 3 | 607 ± 8 |
| σ | 1.3 | 4.1 |
| 95 % Confidence Intervals | 486.1 - 490.0 | 598.0 - 616.5 |

Figure 4.9: Geochronological data of the upper metavolcanic rocks of the Sanabria region: A) Tera-Wasserburg concordia; B) Wetherill concordia; C) Distribution of concordant 207-corrected ages and the statistical data of the two most abundant populations; and D) Pb-Pb stepwise evaporation age.

distribution, with abundant concordant Cambro-Ordovician and Ediacaran populations, a few concordant Orosirian ages, and several points yielding a discordia line with an upper interception at ca. 2.6 Ga (Figs. 4.9A and 4.9C).

The Cambro-Ordovician population is the most abundant. It yielded a precise mean age of 488 ± 3 Ma which represents, therefore, the crystallization age of the upper metavolcanic rock in the Sanabria region (Fig. 4.9B). The Ediacaran zircons yielded a mean age of 607 ± 8 Ma and, as in previous cases, made up the main inherited population.

Six zircon grains were analyzed by the Pb-Pb stepwise evaporation method. Twelve of 28 evaporation steps yielded a precise plateau-age of 490 ± 2 Ma (Fig. 4.9D) which represents, therefore, the best estimate of the crystallization age of these rocks.

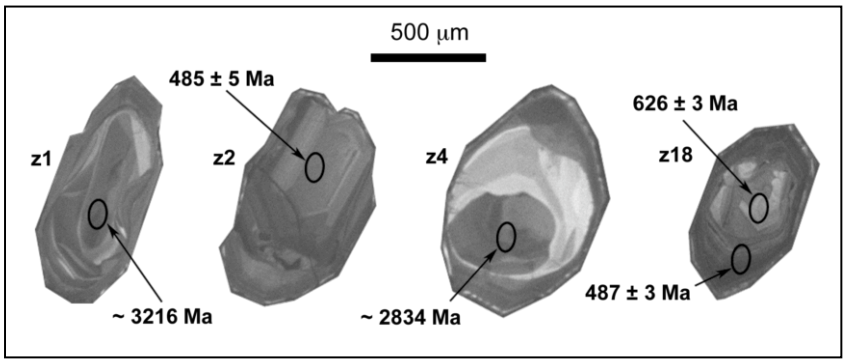


Figure 4.10: Cathodoluminescence images and ages of selected zircons from the upper metavolcanic rocks of the Sanabria region.

According to the cathodoluminescence images, the Cambro-Ordovician population is present in rims that overgrow over older cores (Fig. 4.10z18) and, less frequently, from grains with uniform ages (Fig. 4.10z2). The Ediacaran and older populations were obtained in cores of grains rimmed by Cambro-Ordovician overgrowths (Figs. 4.10z4 and 4.10z18).

#### *4.1.1.4. Villadepera*

The metavolcanic rocks of the Villadepera region were dated using U-Pb ion-microprobe and LA-ICPMS (Table 4.9). Both techniques yielded similar results (Fig. 4.11A and 4.11C) and reveal the presence of two concordant populations and few older ages. As before, the most abundant is Cambro-Ordovician and the second Ediacaran. There are also two concordant points about 2000 Ma, and some discordant points that define a discordia line with an upper interception at ca. 3000 Ma.

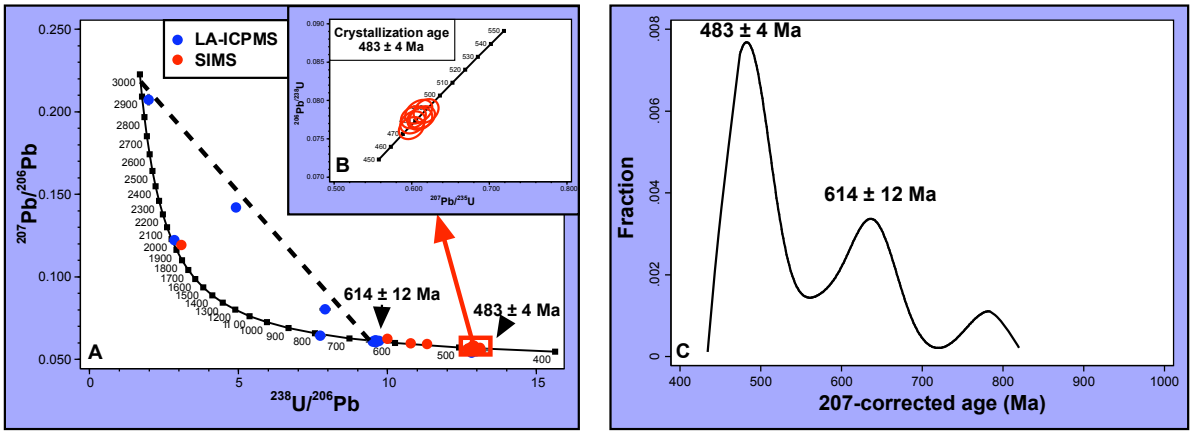


| Observations | 207-corrected age (Ma) | σ | 95 % Confidence Intervals |
|---|---|---|---|
| 7 | 483 ± 4 | 1.8 | 486.5 - 496.6 |
| 4 | 614 ± 12 | 6.2 | 586.8 - 620.4 |

Figure 4.11: Geochronological data of the Villadepera metavolcanic rocks: A) Tera-Wasserburg concordia; B) Wetherill concordia; and C) Distribution of concordant 207-corrected ages and the statistical data of the two most abundant populations.

The Cambro-Ordovician population yielded a precise mean age of 483 ± 4 Ma which represents, therefore, the crystallization age of the Ollo de Sapo Formation in the this region (Fig. 4.11B). The Ediacaran, has an mean age of 614 ± 12 Ma. The former, according to cathodoluminescence imaging, resulted either from rims of grains with inherited cores or from grains with uniform ages (Fig. 4.12z6). The later (Fig. 4.12z5), as well as the older ages (Fig. 4.12z7), were obtained from the restitic cores of zircons rimmed by Cambro-Ordovician overgrowths.

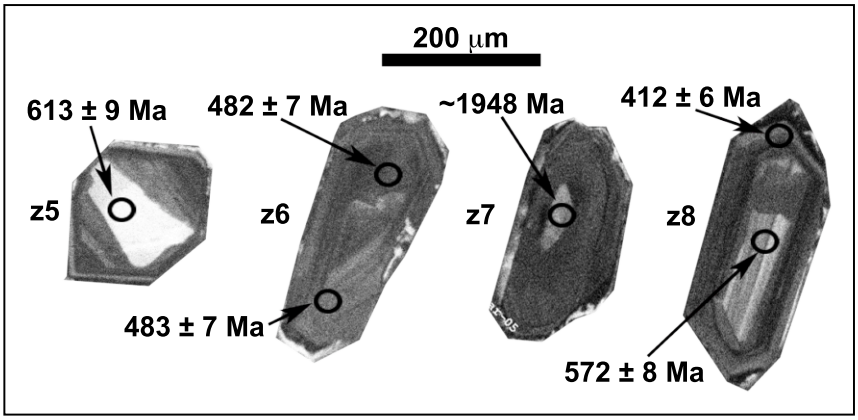


Figure 4.12: Cathodoluminescence images and ages of selected zircons from the Villadepera metavolcanic rocks.

### *4.1.1.5. Hiendelaencina*

In the Hiendelaencina region, as in Sanabria, the metavolcanic rocks form a thick sequence of about 2000 m (González Lodeiro, 1981b). In order to determine the time span recorded in this sequence, three samples in different stratigraphic positions were analyzed: two samples from the lower metavolcanic rocks, one augen and one fine-grained, and one sample from the upper metavolcanic rocks.

#### *4.1.1.5.1. Lower metavolcanic rocks*

U-Pb ion microprobe and LA-ICPMS data from the two samples from the lower metavolcanic rocks are indistinguishable, so that they will be discussed together (Table 4.10). These data reveal the presence of several concordant or nearly concordant populations and few older ages (Figs. 4.13A and 4.13C). The first concordant population is Cambro-Ordovician, with a mean age of 495 ± 5 Ma which is interpreted as the crystallization age of the lower metavolcanic rocks of the Ollo de Sapo in the

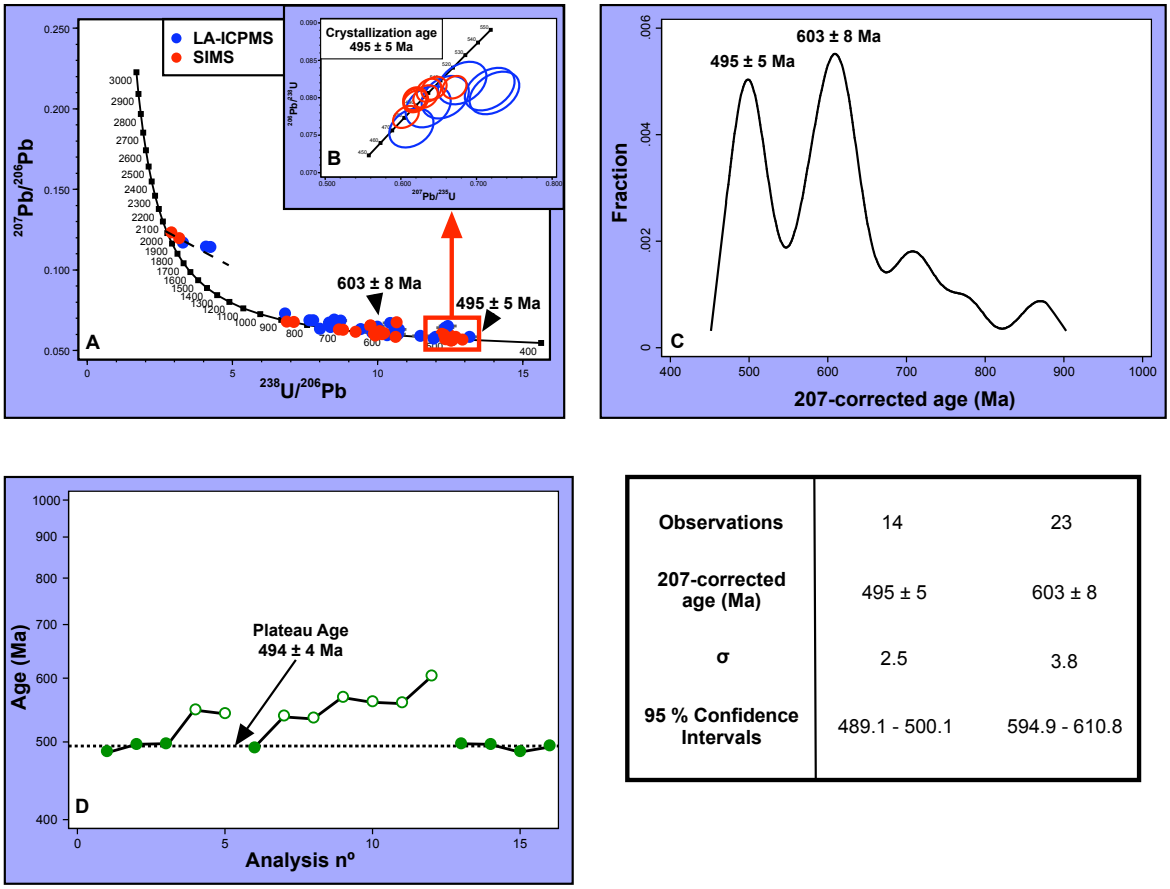


| | | |
|---|---|---|
| **Observations** | 14 | 23 |
| **207-corrected age (Ma)** | 495 ± 5 | 603 ± 8 |
| **σ** | 2.5 | 3.8 |
| **95 % Confidence Intervals** | 489.1 - 500.1 | 594.9 - 610.8 |

Figure 4.13: Geochronological data of the lower metavolcanic rocks of the Hiendelaencina region: A) Tera-Wasserburg concordia; B) Wetherill concordia; C) Distribution of concordant 207-corrected ages and the statistical data of the two most abundant populations; and D) Pb-Pb stepwise evaporation age.

Hiendelaencina region (Fig. 4.13B). The second concordant population has a mean age of 603 ± 8 Ma and represents, therefore, the main inherited population. The third concordant population spreads from 662 Ma to 695 Ma and the last one from 864 Ma to 878 Ma. The older ages are discordant and yield a discordia line with an upper interception at 2016 ± 49 Ma. It must be considered that the 662 Ma to 695 Ma population may be an artifact, owing to mixed Ediacaran and Tonian ages.

Three zircons were analyzed by the Pb-Pb stepwise evaporation method (Table 4.11 and Fig. 4.13D). Eight of the 16 performed evaporation steps yielded a plateau-age of 494 ± 4 Ma, which matches the age obtained by U-Pb analysis. Two of these grains had a restitic core with a minimum age of 540 and about 600 Ma.

The crystallization ages were obtained in uniform grains and, more often, in rims over older cores (Fig. 4.14z32). The 572-627 Ma (Fig. 4.14z32), the 662-695 Ma and the 864-878 Ma populations (Fig. 4.14z28) were mainly obtained in cores of rimmed grains or, less frequently, in totally restitic zircons, and the ≈2000 Ma ages were obtained in totally restitic grains (Fig. 4.14z26).

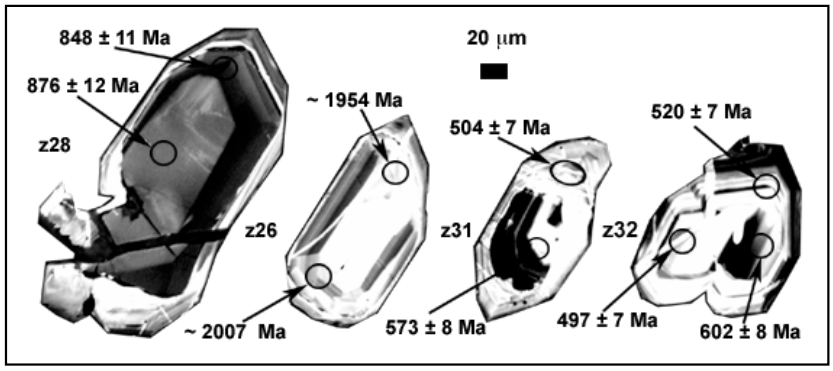


Figure 4.14: Cathodoluminescence images and ages of selected zircons from the lower metavolcanic rocks of the Hiendelaencina region.

*4.1.1.5.2. Upper metavolcanic rocks*

To date the upper part of the Hiendelaencina sequence we extracted zircons from a concentrate of fresh K-feldspar megacrysts from the coarse-grained facies. These zircons were analyzed by the U-Pb ion microprobe and LA-ICPMS and Pb-Pb stepwise evaporation method (Table 4.12 and Table 4.13)

U-Pb data revealed the presence of two main concordant or nearly concordant populations (Figs. 4.15A and 4.15C), the most abundant at 463-504 Ma, yielded a mean

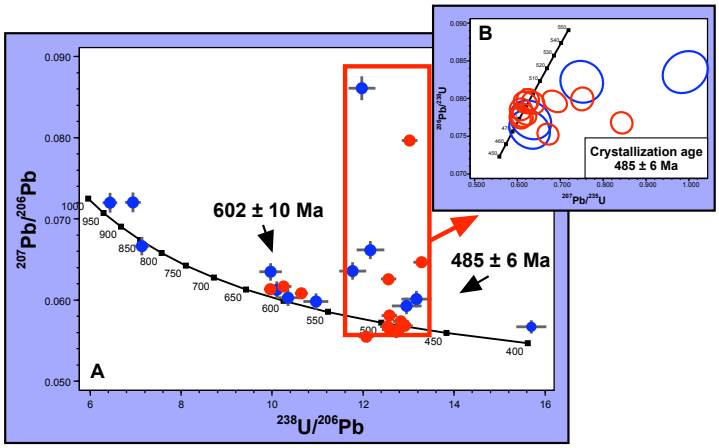


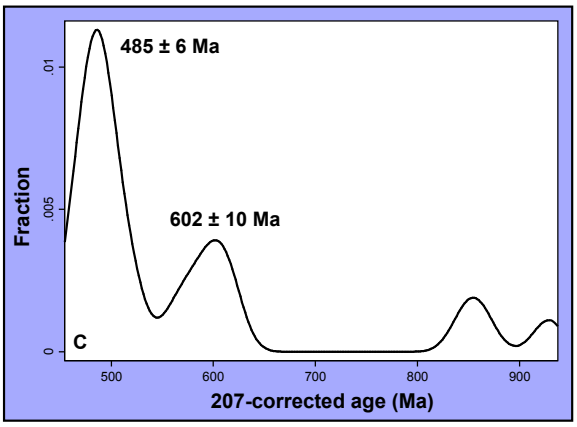


| | | |
|---|---|---|
| **Observations** | 15 | 7 |
| **207-corrected age (Ma)** | 485 ± 6 | 602 ± 10 |
| σ | 3.2 | 5.0 |
| **95 % Confidence Intervals** | 477.9 - 491.4 | 590.0 - 614.3 |

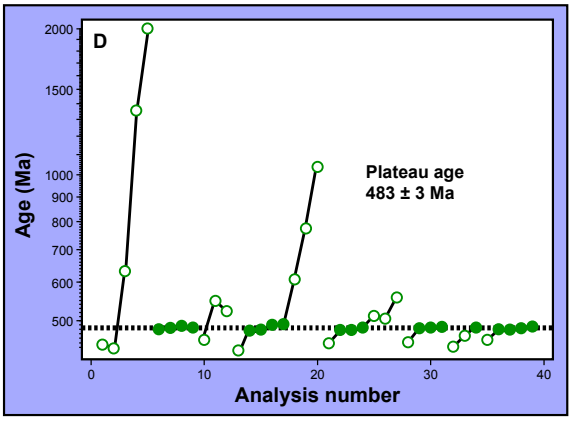


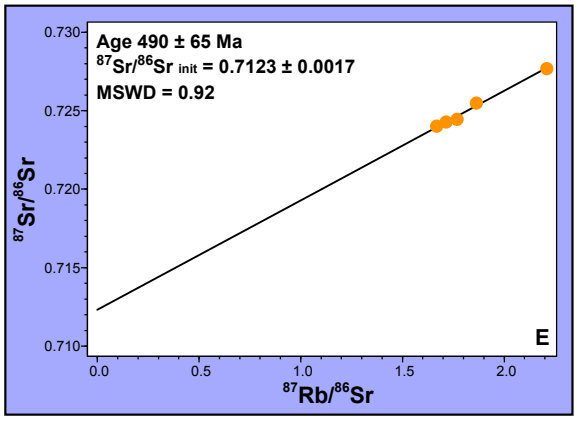


Figure 4.15: Geochronological data of the upper metavolcanic rocks of the Hiendelaencina region: A) Tera-Wasserburg concordia; B) Wetherill concordia; C) Distribution of concordant 207-corrected ages and the statistical data of the two most abundant populations; D) Pb-Pb stepwise evaporation age; and E) Rb-Sr internal isochron of a sliced K-feldspar megacryst.

age of 485 ± 6 Ma and represents the time of crystallization (Fig. 4.15B). The second population at 578-616 Ma, has a mean age of 602 ± 10 Ma and represents the main inherited population. There are also a few concordant or nearly-concordant grains yielding ages between 850 and 900 Ma and finally there is a younger-than-crystallization age which corresponds to texturally discontinuous rims, the significance of which will be discussed in section 4.3.3.

Eight zircon grains were also studied with the Pb-Pb stepwise evaporation method. Nineteen out of 39 evaporation steps yielded a very precise plateau age of 483 ± 3 Ma (Fig. 4.15D). Since this value totally agrees with the U-Pb data, it is considered the best estimate of the crystallization age. Seven grains yielded younger overgrowths with a minimum age of ca. 445 Ma and four grains also had older cores, in one case with a minimum age of ca. 2000 Ma.

Also, five slabs sliced from one of these megacrysts have sufficient Rb/Sr variation to obtain a Rb/Sr internal isochron (Table 4.14). This yielded an age of 490 ± 65 Ma with $(^{87}Sr/^{86}Sr)_{init}$ = 0.7123 ± 0.0017 and MSWD = 0.92 (Fig. 4.15E). Although the confidence interval is large, because the $^{87}Sr/^{86}Sr$ coordinate only ranges from 1.67 to 2.21, the excellent fit and the coincidence with U-Pb and Pb-Pb zircon data permits consideration of isochron as a good estimate of the crystallization age of the K-feldspar megacryst.

The 463-504 Ma ages obtained in rims of grains overgrowing over older restitic cores and in uniform grains (Figs. 4.16z27 and 4.16z32). The 578-616 Ma ages were mainly obtained in the core of 463-504 Ma rimmed zircons (Figs. 4.16z23 and 4.16z24).

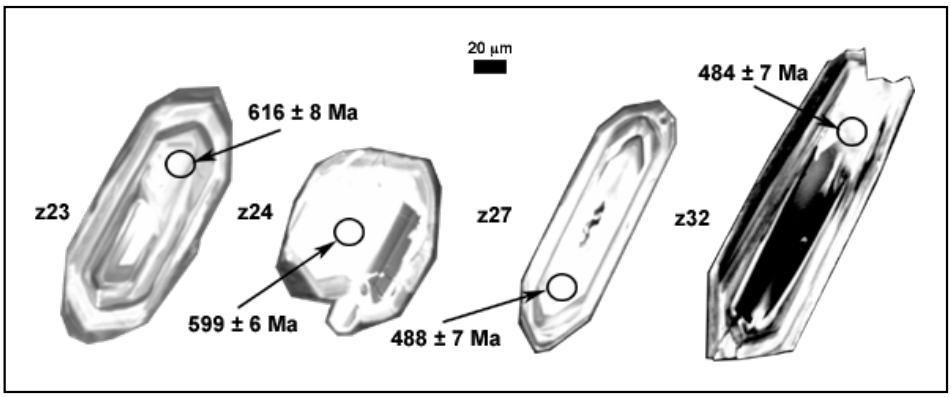


Figure 4.16: Cathodoluminescence images and ages of selected zircons from the upper metavolcanic rocks of the Hiendelaencina region.

### 4.1.2. The metagranites of the Ollo de Sapo Formation

Zircon grains from the four metagranites associated with the Ollo de Sapo Formation, Antoñita, Miranda do Douro, San Sebastián and Viana do Bolo are often pale-pink to yellow or, less frequent, orange to brownish or colorless. Most are short prismatic, euhedral or subhedral and only a few are long prismatic or acicular. Their average size is about 180 x 75 μm, and the maximum up to 450 x 180 μm. As in the metavolcanic rocks, cathodoluminescence imaging reveals that a significant fraction of them, no less than 70%, except in the San Sebastián metagranite with less than 20%, contain restitic cores (Fig. 4.2) which in most cases display a oscillatory zoning (Figs. 4.17z5, 4.17z8, 4.17z12, 4.17z13 and 4.17z14).

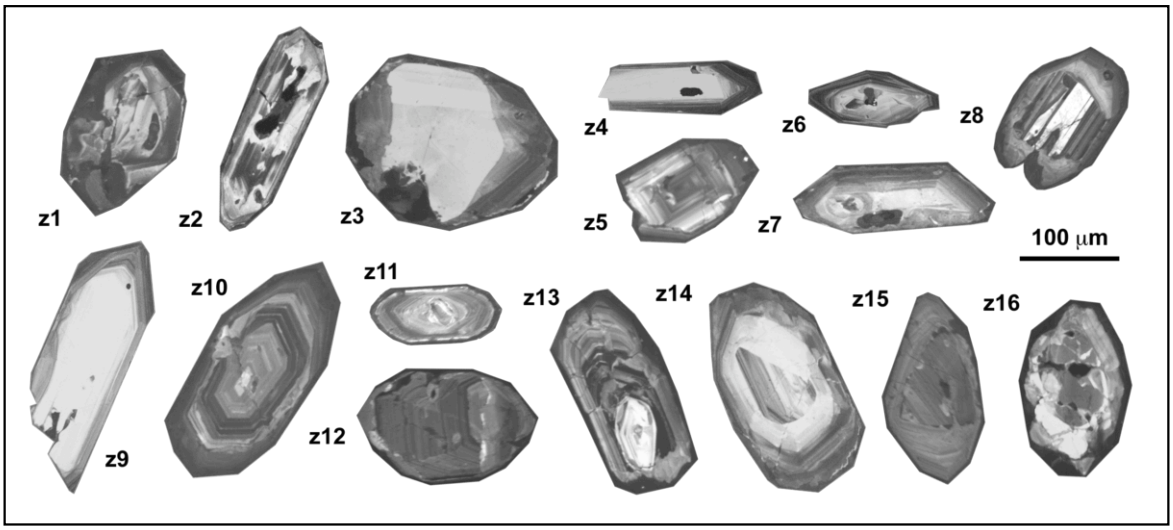


Figure 4.17: Cathodoluminescence images of the most representative internal textures of the metagranites of the Ollo de Sapo Domain.

#### *4.1.2.1. Viana do Bolo*

The Viana do Bolo metagranite outcrops in the Sanabria region and is spatially associated to the Ollo de Sapo metavolcanic rocks (see Fig. 3 in Lancelot et al., 1985). We have dated the common facies at Covelo using the U-Pb LA-ICPMS (Table 4.15) and Pb-Pb stepwise evaporation methods (Table 4.16). The U-Pb data revealed the existence of two concordant populations, one Cambro-Ordovician and the other Ediacaran, and few older ages defining a discordia line with an upper interception at ca. 2.6 Ga (Figs. 4.18A and 4.18C). The Cambro-Ordovician population is the most abundant and concordant. It is present either in rims or in totally uniform grains (Figs. 4.19LA050a and 4.19LA024a). Its mean age is 487 ± 4 Ma (Fig. 4.18B) which we consider, therefore, the crystallization age

of the Viana do Bolo metagranite. The Ediacaran population is less abundant and also less concordant. It comes entirely from zircon cores (Figs. 4.19LA018a and 4.19LA048a) and yielded a mean age of 609 ± 10 Ma.

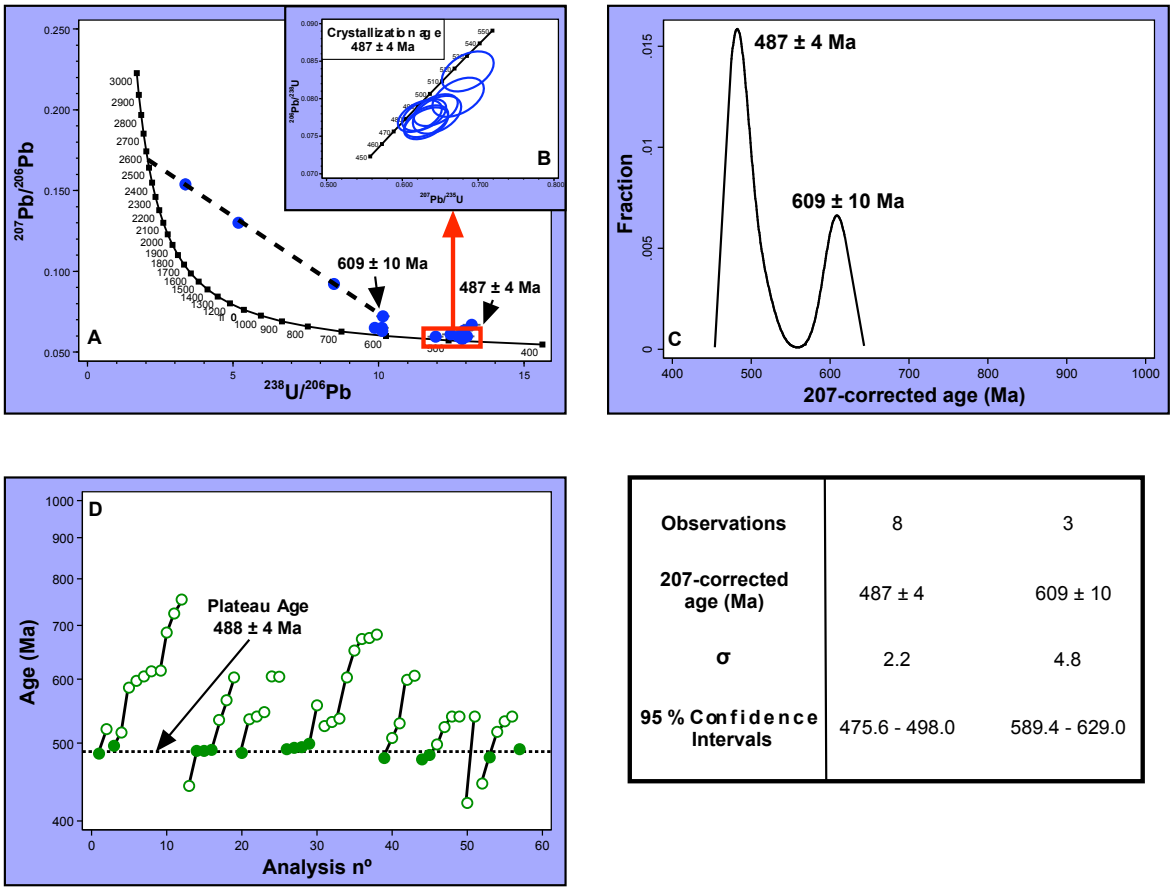


| | | |
|---|---|---|
| Observations | 8 | 3 |
| 207-corrected age (Ma) | 487 ± 4 | 609 ± 10 |
| σ | 2.2 | 4.8 |
| 95 % Confidence Intervals | 475.6 - 498.0 | 589.4 - 629.0 |

Figure 4.18: Geochronological data of the Viana do Bolo metagranite: A) Tera-Wasserburg concordia; B) Wetherill concordia; C) Distribution of concordant 207-corrected ages and the statistical data of the two most abundant populations; D) Pb-Pb stepwise evaporation age.

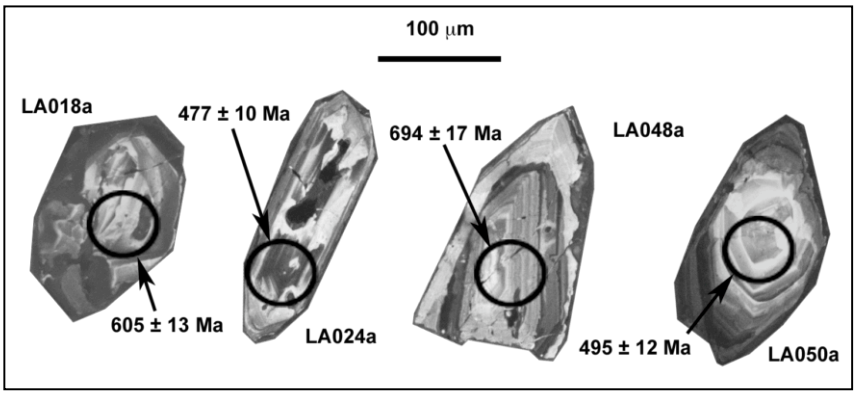


Figure 4.19: Cathodoluminescence images and ages of selected zircons from the Viana do Bolo metagranite.

Thirteen zircon grains were analyzed by the Pb-Pb stepwise evaporation method. Fifteen out of 58 evaporation steps provided a plateau age of 488 ± 4 Ma (Fig. 4.18D), which is practically identical to the youngest U-Pb concordant population. We consider this value, therefore, as the best estimate of the crystallization age of the Viana do Bolo metagranite. Again, the fraction of grains with a pre-magmatic core (minimum age ≈540-600 Ma) is remarkably elevated.

### *4.1.2.2. San Sebastián*

The San Sebastián metagranite is spatially associated with the Viana do Bolo metagranite and the volcanic rocks of Sanabria. In contrast with them, the San Sebastián metagranite has little zircon inheritance, being to date, so far, the only known case of Central Iberian Cambro-Ordovician rocks with a percentage of zircon grains with pre-magmatic core less than 20%. Not surprisingly, therefore, Lancelot et al. (1985) using zircon concentrate analyses were able to determine an upper intercept at 465 ± 10 Ma. We studied this metagranite by U-Pb ion microprobe (Table 4.17), and found that most grains

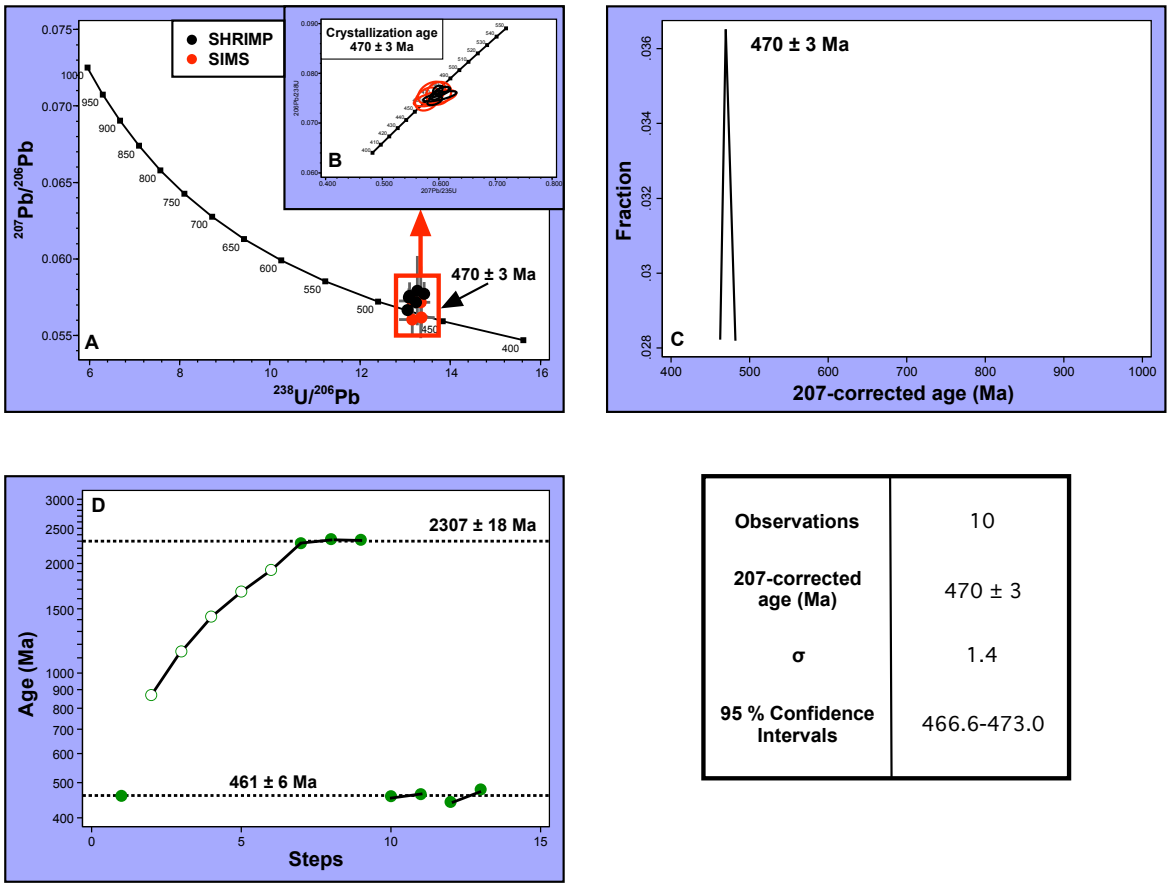


Figure 4.20: Geochronological data of the San Sebastián metagranite: A) Tera-Wasserburg concordia; B) Wetherill concordia; C) Distribution of concordant 207-corrected ages and the statistical data of the crystallization population; D) Pb-Pb stepwise evaporation age.

are concordant with an average 207-corrected age of 470 ± 3 Ma (Figs. 4.20A, 4.20B and 4.20C). The San Sebastián metagranite, therefore, is the youngest dated Cambro-Ordovician magmatic body of the Ollo de Sapo formation, about 15 Ma younger than any other from the Sanabria region.

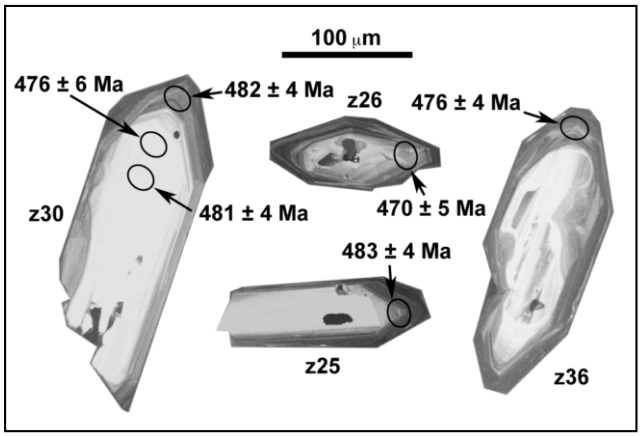


Figure 4.21: Cathodoluminescence images and ages of selected zircons from the San Sebastián metagranite.

Pb-Pb data for four zircons (Table 4.18) yielded a badly defined plateau at 461 ± 6 Ma and a plateau corresponding to the age of the restitic core of one of the zircons at 2307 ± 18 Ma (Fig. 4.20D).

### *4.1.2.3. Miranda do Douro*

The Miranda do Douro metagranite is spatially associated with the metavolcanic rocks of the Villadepera region. It has been dated by U-Pb ion microprobe and LA-ICPMS obtaining two main concordant or nearly concordant populations (Figs. 4.22A and 4.22C and Table 4.19). The first and most abundant population is Cambro-Ordovician with a mean age of 483 ± 3 Ma which represents, therefore, the age of crystallization (Fig. 4.22B). The second most abundant population is Ediacaran, with a mean age of 605 ± 13 Ma. The latter represents the main inherited population. There are also other younger and highly discordant points at about 350 Ma, and a few older discordant ages which yielded a discordia line with an upper interception at 3.167 Ma +57/−48 Ma.

The crystallization ages were acquired in uniform grains (Fig. 4.23z10) and in rims of crystals that contain premagmatic cores. The Ediacaran population comprises a few grains with uniform ages and, more often, cores of crystals rimmed by large Cambro-Ordovician

overgrowths (Fig. 4.23z18). As in previous cases, younger-than-crystallization ages are mostly found in narrow discontinuous rims. Regarding the older ages, one corresponds to a core rimmed by an Ordovician overgrowth and the other two are the rim and the core of a single Archean grain (Fig. 4.23z19).

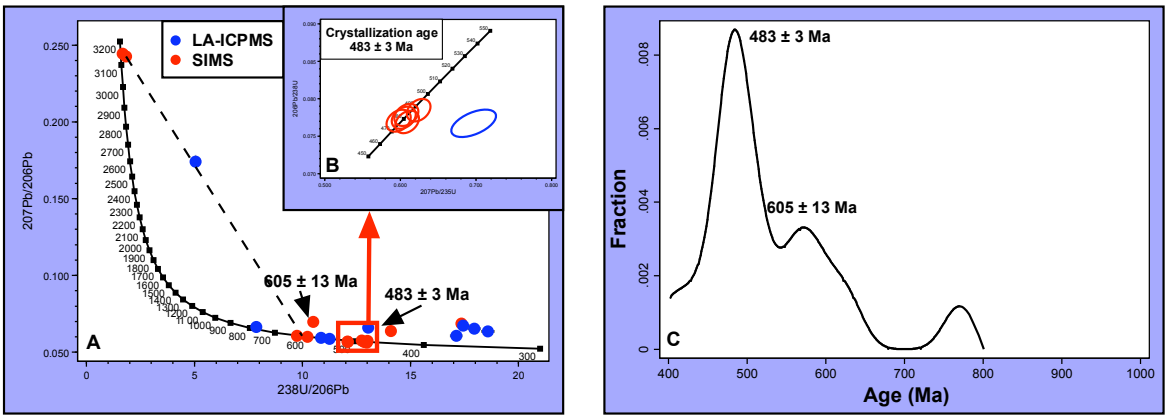


| Observations | 207-corrected age (Ma) | σ | 95 % Confidence Intervals |
|---|---|---|---|
| 6 | 483 ± 3 | 1.7 | 477.4 - 488.9 |
| 3 | 603 ± 13 | 6.7 | 539.8 - 666.4 |

Figure 4.22: Geochronological data of the Miranda do Douro metagranite: A) Tera-Wasserburg concordia; B) Wetherill concordia; C) Distribution of concordant 207-corrected ages and the statistical data of the two most abundant populations.

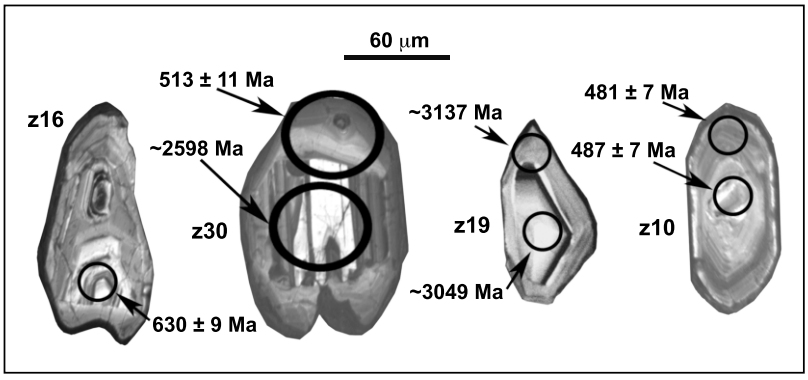


Figure 4.23: Cathodoluminescence images and ages of selected zircons from the Miranda do Douro metagranite.

### *4.1.2.4. Antoñita*

The Antoñita metagranite is spatially associated with the metavolcanic rocks of the Hiendelaencina region. Our attempts to date the Antoñita metagranite using U-Pb either by

LA-ICPMS or ion microprobe were not successful due to high discordance. However, we succeed using the Pb-Pb stepwise evaporation method. Ten zircon grains yielded 46 evaporation steps, 19 of which define a plateau with a mean age of 474 ± 4 Ma (Table 4.20 and Fig. 4.24A). Most zircon grains also have older cores, the precise age of which cannot be estimated because of the lack of plateaus, except in one case that yielded a Neo-Archaean age of 2.68 Ga. Six grains also have younger overgrowths with ages down to 400 Ma, a value that roughly agrees with the ca. 380 Ma U-Pb lower intercept previously found by Wildberg et al. (1989). These anomalous younger ages are frequent in Hiendelaencina despite not being migmatized during the Variscan. Their significance is discussed in section 4.3.3.

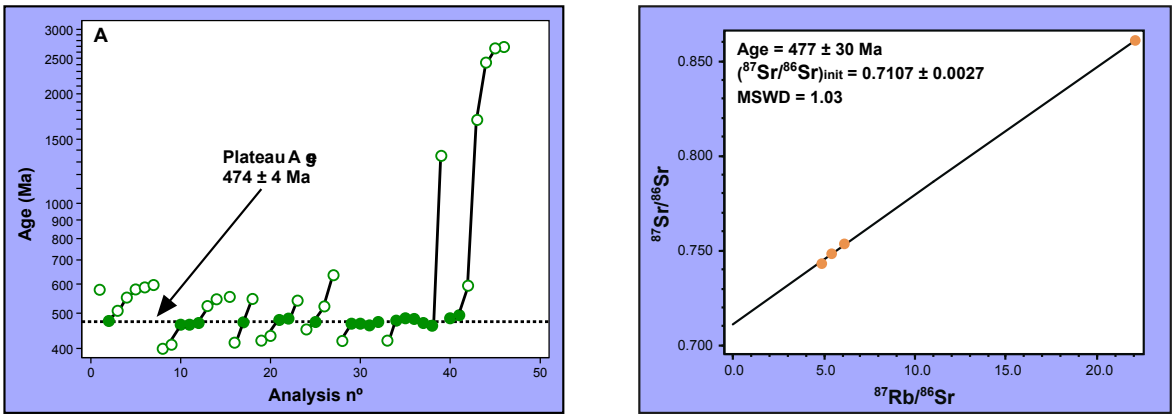


Figure 4.24: Geochronological data of the Antoñita metagranite: A) Pb-Pb stepwise evaporation age; and B) Rb-Sr isochron.

Four whole-rock samples from the Antoñita metagranite were analyzed for Sr isotopes (Table 4.21). Surprisingly, despite the intense Variscan deformation that affected them, the five samples fit well into a Rb-Sr isochron (Fig. 4.24B) that yielded an age of 477 ± 30 Ma, with $(^{87}Sr/^{86}Sr)_{init}$ = 0.7107 ± 0.0027 and a MSWD = 1.03. This value is very close to the 474 Ma Pb-Pb age, and we considered it, therefore, as a good estimate of the crystallization age of the Antoñita gneiss.

## 4.2. The Schist-Graywacke Complex Domain

More than five hundred zircons from the metagranites and metavolcanic rocks of the northern part of the Schist-Graywacke Complex Domain have been studied using optical and cathoduluminescence imaging. These zircons show a great variety of colors: pale-pink, yellow, orange, brownish and colorless. Most are short prismatic, euhedral or subhedral and only a few are long prismatic or acicular. Their average size is about 180 x 75 μm, and the maximum up to 450 x 180 μm.

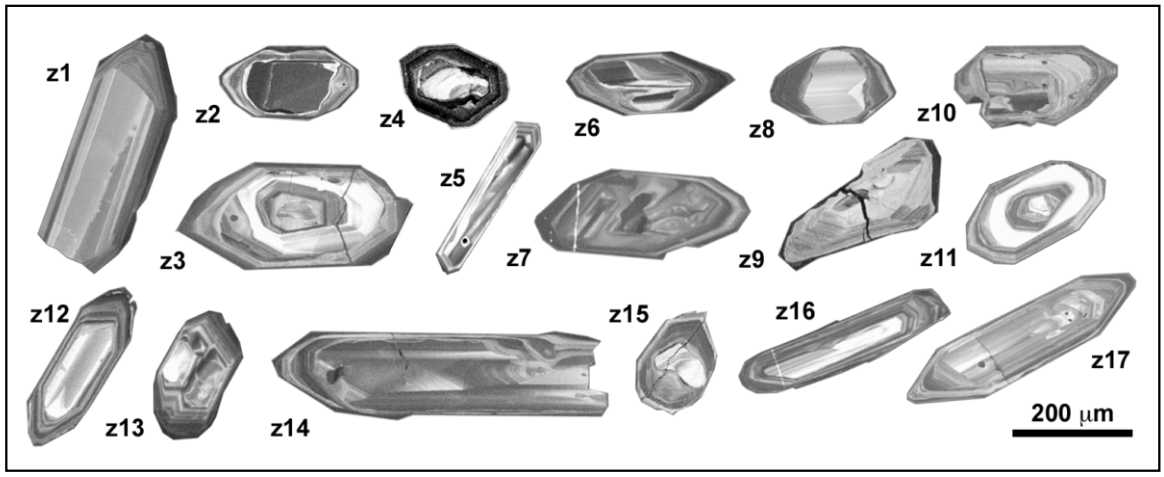


Figure 4.25: Cathodoluminescence images of the most representative internal textures of the metagranites and metavolcanic rocks of the north of the Schist-Graywacke Complex Domain.

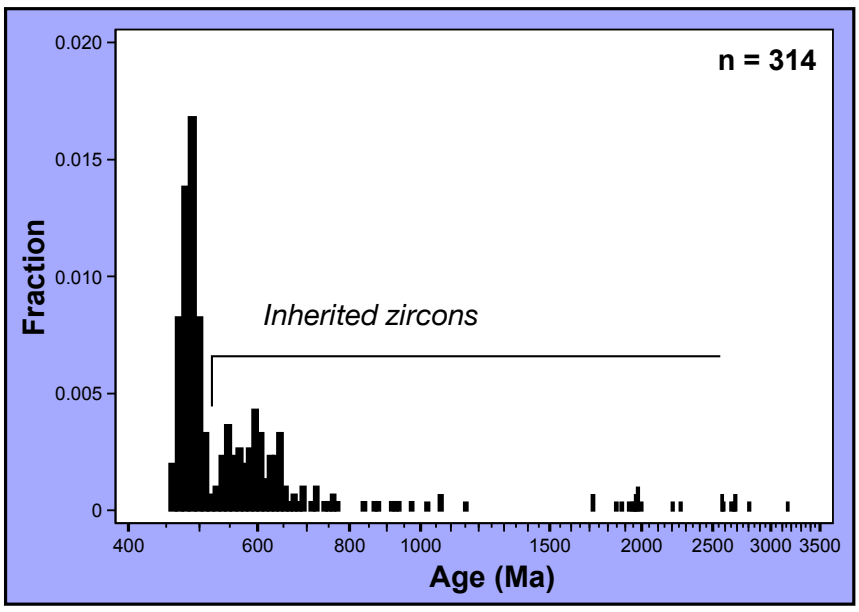


Figure 4.26: Age distribution pattern found in zircons of the metagranites and metavolcanic rocks of the north of the Schist-Graywacke Complex Domain. Built from U-Pb SIMS, SHRIMP and LA-ICPMS data.

Cathodoluminescence images reveal that most of the zircons have well-defined oscillatory zoning (Figs. 4.25z1, 4.25z5, 4.25z12, 4.25z13, 4.25z14, 4.25z16 and 4.25z17) and few also have convolute zoning (Figs. 4.25z6 and 4.25z7). Between 70 and 90 % of these zircons contain inherited cores (Fig. 4.26), except in the Sierra de Guadarrama where the percentage of inherited cores decreases up to 50-70%. These inherited cores often show a marked zoning discordant with that of the rims (Figs. 4.25z3, 4.25z4, 4.25z8, 4.25z9 and 4.25z11).

In the northern of the Schist-Graywacke Complex Domain, there are numerous small bodies of Cambro-Ordovician metagranites that define a broad band roughly parallel to the boundary with the Ollo de Sapo Formation. These rocks have been sampled in four areas: (1) the Tormes Dome, (2) the Gredos sector and (3) the Guadarrama sector of the Ávila batholith, and (4) Toledo.

### 4.2.1. The Tormes Dome

In the Tormes Dome, we sampled three metagranites: Fermoselle, Vitigudino and Ledesma. These metagranites have been dated using U-Pb ion microprobe.

#### *4.2.1.1. Fermoselle*

Here we obtained ten concordant to subconcordant ages (Figs. 4.27A and 4.27C and Table 4.22). Six of them are Cambro-Ordovician, with a mean age of 486 ± 6 Ma which is

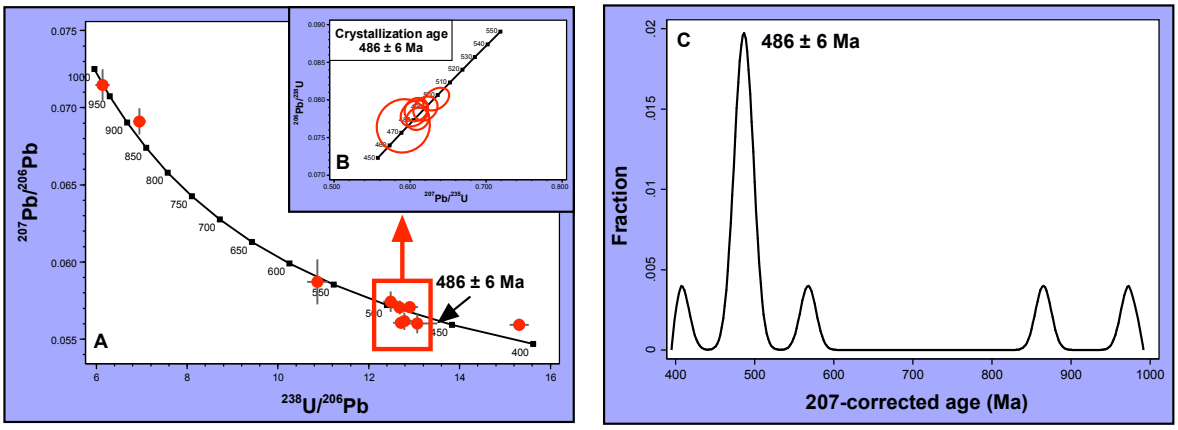


| Observations | 207-corrected age (Ma) | σ | 95 % Confidence Intervals |
|---|---|---|---|
| 6 | 486 ± 6 | 3.0 | 478.6 - 493.8 |

Figure 4.27: Geochronological data of the Fermoselle metagranite: A) Tera-Wasserburg concordia; B) Wetherill concordia; and C) Distribution of concordant 207-corrected ages and the statistical data of the crystallization population.

therefore considered as the age of crystallization (Fig. 4.27B). The other three are subconcordant older points at 568 Ma, 865 Ma and 973 Ma and finally there is a younger point at approximately 407 Ma. According to the cathodoluminescence images, the crystallization ages were obtained either in uniform grains (Fig. 4.28z33) or in rims over older cores. The three older points were all obtained in the core of grains rimmed by 486 ± 6 overgrowth (Fig. 4.28z23) or in totally restitic grains (Fig. 4.28z22).

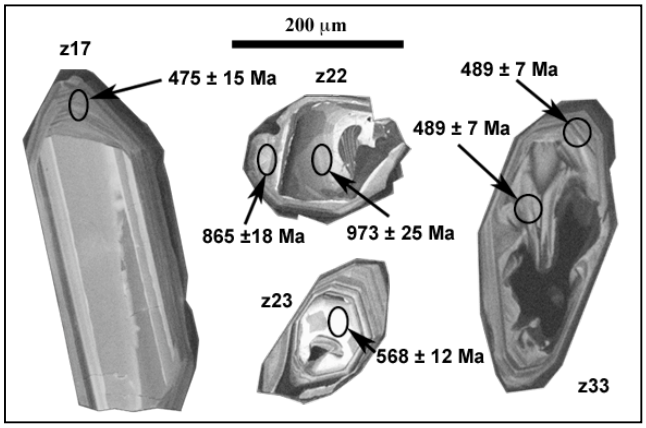


Figure 4.28: Cathodoluminescence images and ages of selected zircons from the Fermoselle metagranite.

### *4.2.1.2. Vitigudino*

The U-Pb data of the Vitigudino metagranite reveal the existence of two nearly concordant populations, one Cambro-Ordovician and the other Ediacaran, and two

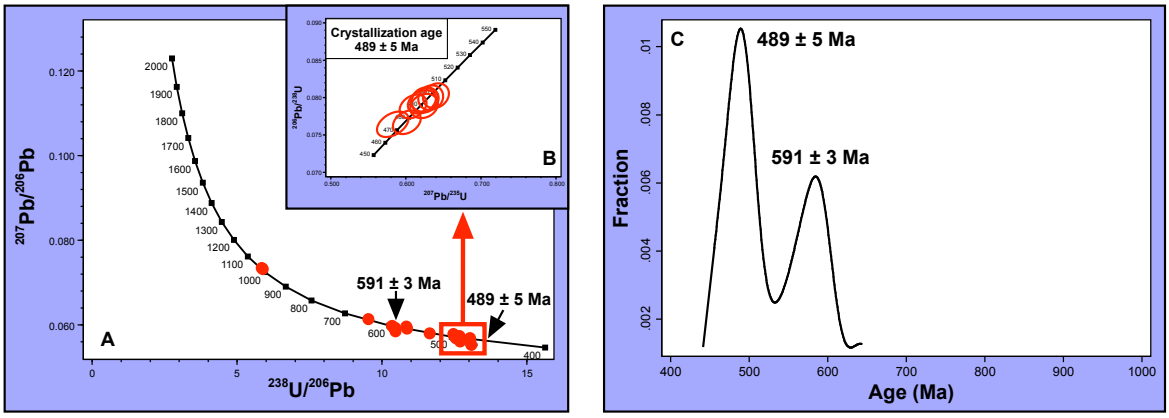


| Observations | 207-corrected age (Ma) | σ | 95 % Confidence Intervals |
|---|---|---|---|
| 9 | 489 ± 5 | 2.7 | 483.2 - 495.7 |
| 4 | 591 ± 3 | 1.3 | 587.1 - 595.5 |

Figure 4.29: Geochronological data of the Vitigudino metagranite: A) Tera-Wasserburg concordia; B) Wetherill concordia; and C) Distribution of concordant 207-corrected ages and the statistical data of the two populations.

concordant points at ca. 1.0 Ga (Figs. 4.29A and 4.29C and Table 4.23). The Cambro-Ordovician population is the most abundant, with a mean age of 489 ± 5 Ma, which we consider the age of crystallization (Fig. 4.29B). The Ediacaran population, less numerous, has a mean age of 591 ± 3 Ma. There are also two points at 531 Ma and 643 Ma that probably resulted from analyzing the transition between the main components. The Ordovician ages were obtained in the rim of grains with inherited cores (Fig. 4.30z10) or grains with uniform ages (Fig. 4.30z1) and older ages were obtained in the cores of rimmed zircons (Figs. 4.30z7, 4.30z10 and 4.30z15).

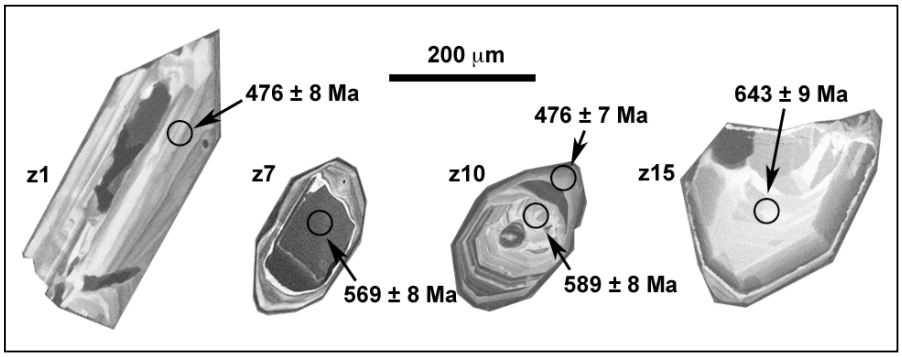


Figure 4.30: Cathodoluminescence images and ages of selected zircons from the Vitigudino metagranite.

### *4.2.1.3. Ledesma*

The U-Pb data of the Ledesma metagranite also reveal the occurrence of two nearly

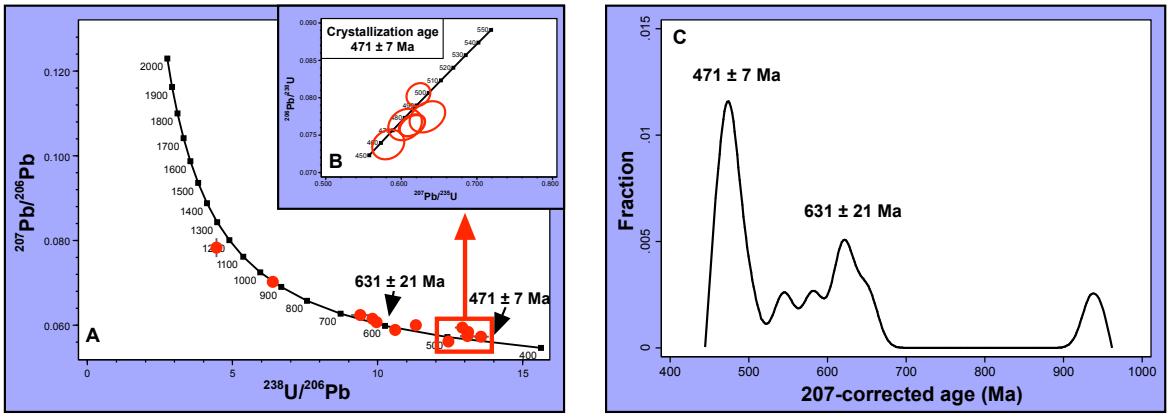


| Observations | 207-corrected age (Ma) | σ | 95 % Confidence Intervals |
|---|---|---|---|
| 5 | 471 ± 7 | 3.6 | 461.5 - 481.3 |
| 3 | 631 ± 21 | 10.4 | 585.9 - 675.7 |

Figure 4.31: Geochronological data of the Ledesma metagranite: A) Tera-Wasserburg concordia; B) Wetherill concordia; and C) Distribution of concordant 207-corrected ages and the statistical data of the two populations.

concordant populations, one Cambro-Ordovician and the other Ediacaran, and older ages at 938 Ma and 1156 Ma (Figs. 4.31A and 4.31C and Table 4.24). The Cambro-Ordovician population is the most abundant and the most concordant, with a mean age of 471 ± 7 Ma (Fig. 4.31B), which is therefore regarded as the crystallization age of the Ledesma metagranite. The Ediacaran population has a mean age of 631 ± 21 Ma. The two nearly concordant points at 545 and 582 Ma probably represent mixed ages resulting from analyzing an internal boundary. According to the cathodolumisnescence images, whereas the Cambro-Ordovician population was obtained in rims of zircons containing inherited cores (Figs. 4.32z22, 4.32z29 and 4.32z30) and in grains with uniform ages (Fig. 4.32z17), the Ediacaran population and older grains were always obtained in the core of rimmed grains (Figs. 4.32z29 and 4.32z30).

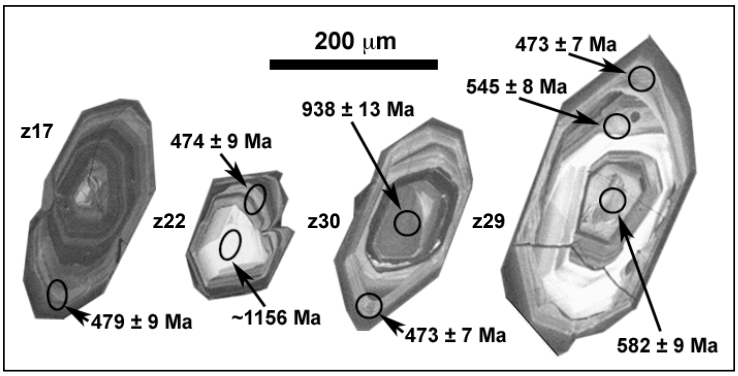


Figure 4.32: Cathodoluminescence images and ages of selected zircons from the Ledesma metagranite.

### 4.2.2. The Gredos Sector

In the northwest of the Sierra de Gredos, we sampled three metagranites: Bercimuelle, Castellanos and San Pelayo. The exact location and coordinates of the samples are given in Table 2.2. They have been dated using U-Pb ion microprobe and LA-ICPMS. The results are detailed as follows:

#### *4.2.2.1. San Pelayo*

As in all other cases, the San Pelayo metagranite contains two concordant populations, one Cambro-Ordovician and the other Ediacaran, and a few isolated older grains (Figs. 4.33A and 4.33C and Table 4.25). The Cambro-Ordovician population yields a mean age of 492 ± 4 Ma, which represents the age of crystallization (Fig. 4.33B). The Ediacaran population has a mean age of 604 ± 15 Ma. Besides this, there are several older concordant

ages: one point at about 717 Ma, one point at about 912 Ma, four points at about 2000 Ma and one point at about 2.6 Ga. Finally, as in previous cases, there are younger-than-crystallization ages (see discussion in section 4.3.3).

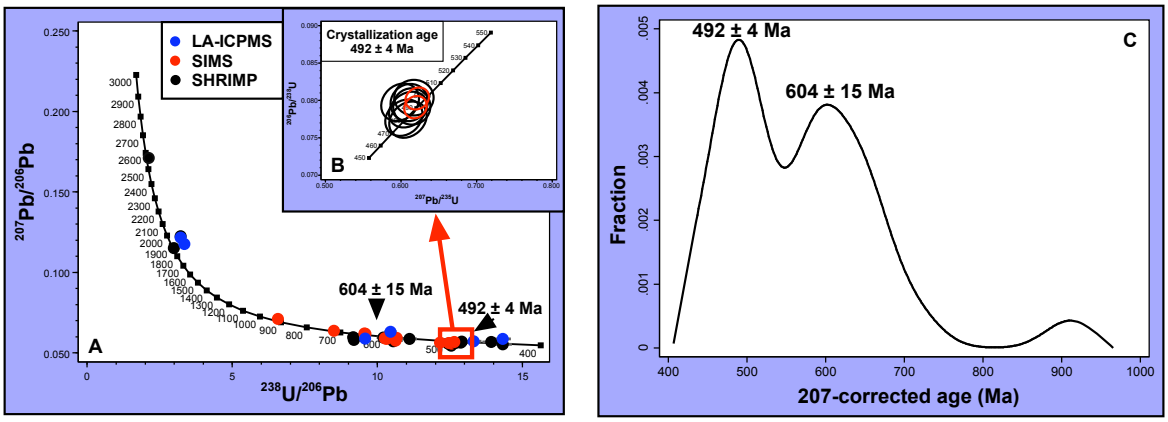


| Observations | 207-corrected age (Ma) | σ | 95 % Confidence Intervals |
|---|---|---|---|
| 9 | 492 ± 4 | 2.2 | 486.5 - 496.6 |
| 11 | 604 ± 15 | 7.6 | 586.8 - 620.4 |

Figure 4.33: Geochronological data of the San Pelayo metagranite: A) Tera-Wasserburg concordia; B) Wetherill concordia; and C) Distribution of concordant 207-corrected ages and the statistical data of the two most abundant populations.

The Cambro-Ordovician population comes from rims of grains with inherited cores (Fig. 4.34z28) and, less frequently, from uniform zircons. The Ediacaran population comes either from cores of rimmed grains or from totally restitic zircons (Fig. 4.34z27 and 4.34z30). The oldest ages were obtained, in all cases, from cores of zircons rimmed by Cambro-Ordovician overgrowths (Fig. 4.34z29).

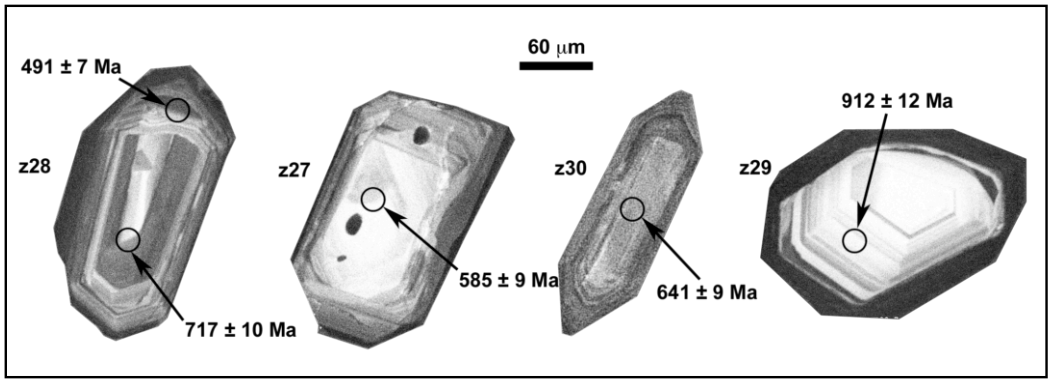


Figure 4.34: Cathodoluminescence images and ages of selected zircons from the San Pelayo metagranite.

### *4.2.2.2. Castellanos*

The U-Pb data of the Castellanos metagranite demonstrate the existence of three main concordant populations (Figs. 4.35A and 4.35C and Table 4.26). The most abundant is also the youngest; it is Cambro-Ordovician, with a mean age of 498 ± 4 Ma, and represents the age of crystallization of this body (Fig. 4.35B). The second most abundant population, in contrast to all previous bodies, is not Ediacaran but Early Cambrian, with a mean age of 548 ± 10 Ma. The third is Ediacaran, with a mean age of 612 ± 10 Ma. Besides this, we found some other concordant or nearly concordant points: one at 683 Ma, another at 1.8 Ga and another about 3.2 Ga.

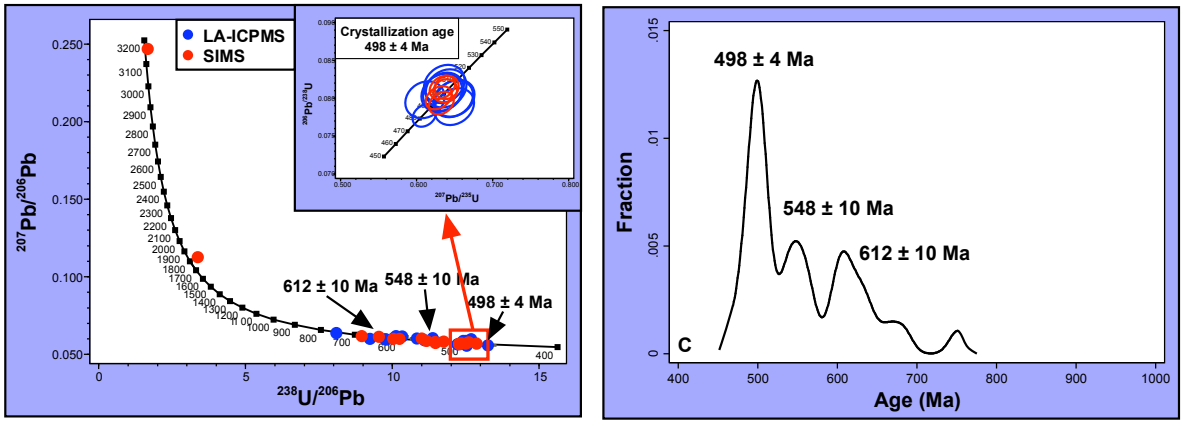


| Observations | 207-corrected age (Ma) | σ | 95 % Confidence Intervals |
|---|---|---|---|
| 14 | 498 ± 4 | 1.9 | 493.9 - 502.3 |
| 8 | 548 ± 10 | 4.8 | 536.7 - 559.4 |
| 7 | 612 ± 10 | 5.0 | 599.6 - 624.1 |

Figure 4.35: Geochronological data of the Castellanos metagranite: A) Tera-Wasserburg concordia; B) Wetherill concordia; and C) Distribution of concordant 207-corrected ages and the statistical data of the three most abundant populations.

According to the cathodoluminescence images, the 498 ± 4 Ma population comes either from the rims of zircons that have inherited cores, or from uniform grains (Fig. 4.36z20). The 548 ± 10 Ma population also comes either from cores or rims of older grains (Fig. 4.36z11). Remarkably this is the crystallization age of the neighboring Almohalla orthogneiss (543 ± 6 Ma, Bea et al., 2003). The older ages were acquired in inherited cores and totally restitic zircons (Figs. 4.36z11, 4.36 z14 and 4.36 15).

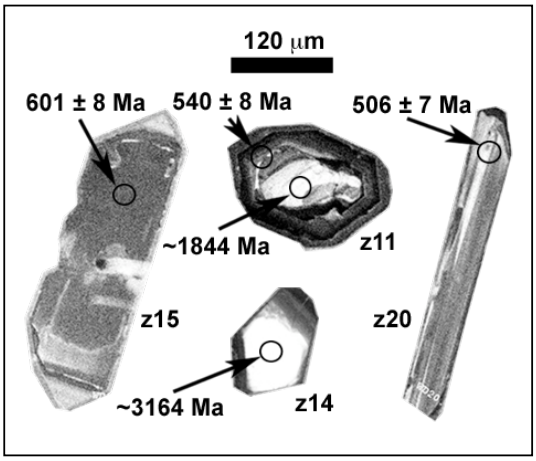


Figure 4.36: Cathodoluminescence images and ages of selected zircons from the Castellanos metagranite.

### *4.2.2.3. Bercimuelle*

The U-Pb ion microprobe data of the Bercimuelle metagranite reveals a highly complex age distribution, with four concordant populations (Figs. 4.37A and 4.37C and Table 4.27). The youngest is Cambro-Ordovician, with a mean age of 488 ± 3 Ma (Fig. 4.37B). It is preceded by another population at 545 ± 3 Ma, which as in the Castellanos metagranite, is coincident with the age of the neighboring Almohalla orthogneiss. The third is Ediacaran,

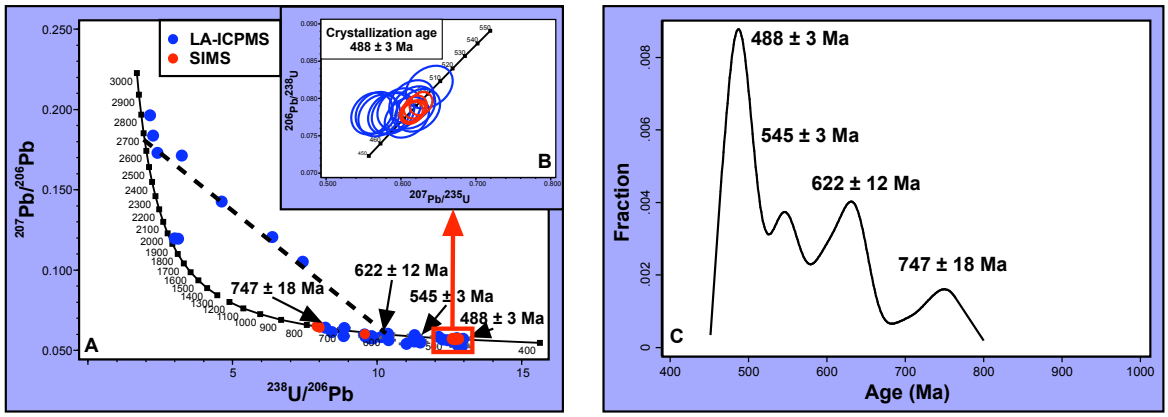


| Observations | 207-corrected age (Ma) | σ | 95 % Confidence Intervals |
|---|---|---|---|
| 16 | 488 ± 3 | 1.4 | 485.1 - 491.1 |
| 6 | 545 ± 3 | 1.5 | 540.9 - 548.7 |
| 11 | 622 ± 12 | 6.0 | 608.3 - 634.9 |
| 4 | 747 ± 18 | 8.9 | 718.8 - 775.3 |

Figure 4.37: Geochronological data of the Bercimuelle metagranite: A) Tera-Wasserburg concordia; B) Wetherill concordia; and C) Distribution of concordant 207-corrected ages and the statistical data of the four most abundant populations.

with a mean age of 622 ± 12 Ma. And the fourth is Cryogenian, clustering around 747 ± 18 Ma. Besides this, there are some data clustering around 2.0 Ga, and a discordia line with upper interception close to 2.7 Ga, all very similar to what was found in the metavolcanic rocks of the Ollo de Sapo Formation.

According to cathodoluminescence imaging, crystallization ages were obtained in uniform grains (Fig. 4.38z7) and in rims of grains with inherited cores (Fig. 4.38z3). The other Cambrian, Ediacaran and Cryogenian populations were obtained in inherited cores and, rarely, in rims of grains with inherited cores (Fig. 4.38z2).

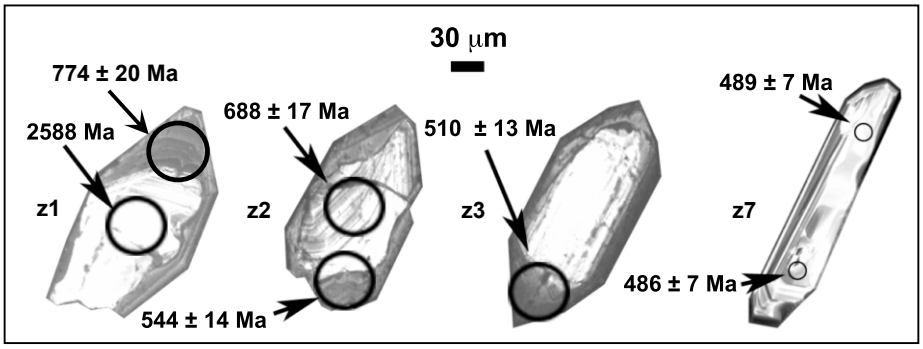


Figure 4.38: Cathodoluminescence images and ages of selected zircons from the Bercimuelle metagranite.

### 4.2.3. The Guadarrama Sector

In the Sierra de Guadarrama, where the largest accumulation of Cambro-Ordovician granitoids of Iberia occur, we sampled the following orthogneisses of probable metagranitic origin: La Cañada, La Hoya, La Estación I, La Estación II, Vegas de Matute, El Caloco, La Morcuera and Buitrago de Lozoya. The exact location and coordinates of the samples are given in Table 2.2. We also sampled three orthogneisses that probably derived from metavolcanic rocks: La Berzosa, El Cardoso and Riaza. All of them were dated using U-Pb ion microprobe and LA-ICPMS. The results are described below:

#### *4.2.3.1. La Cañada*

U-Pb ion microprobe and LA-ICPMS data from La Cañada metagranite display the presence of two concordant or nearly concordant populations and some isolated ages (Figs. 4.39A and 4.39C and Table 4.28). The first population is Cambro-Ordovician and yields a mean age of 489 ± 9 Ma that represents the age of crystallization of this body (Fig. 4.39B). The second population is Ediacaran, with a mean age of 571 ± 14 Ma. There are two older

concordant ages, at 1718 and 2670 Ma and, again, several younger-than-crystallization ages between about 338 and 440 Ma.

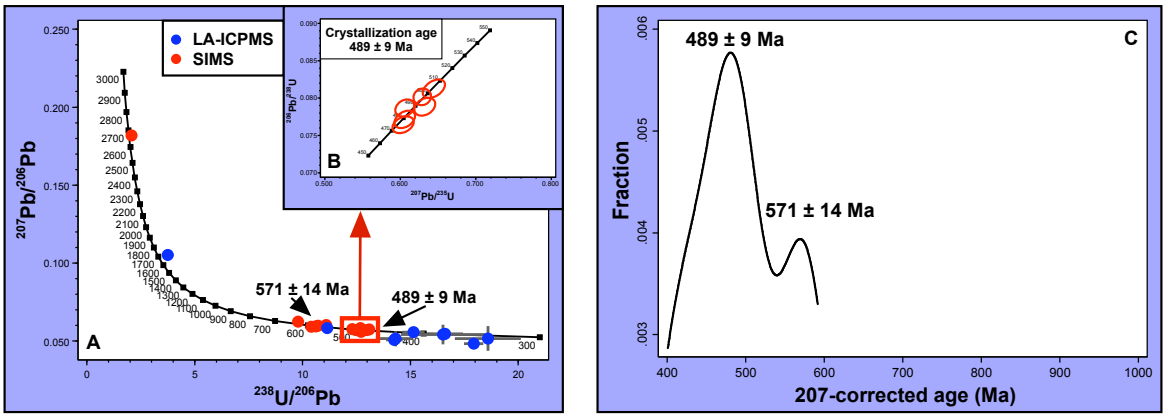


| Observations | 207-corrected age (Ma) | σ | 95 % Confidence Intervals |
|---|---|---|---|
| 6 | 489 ± 9 | 4.4 | 477.1 - 500.0 |
| 5 | 571 ± 14 | 7.2 | 551.3 - 591.4 |

Figure 4.39: Geochronological data of La Cañada metagranite: A) Tera-Wasserburg concordia; B) Wetherill concordia; and C) Distribution of concordant 207-corrected ages and the statistical data of the two most abundant populations.

The crystallization ages were usually obtained in the rims of grains containing inherited cores (Figs. 4.40z45 and 4.40z49) and, rarely, in uniform grains (Fig. 4.40z41). The inherited population was always obtained in cores of zircons rimmed by Cambro-Ordovician overgrowths (Figs. 4.40z45 and 4.40z50), as well as the two older ages (Fig. 4.40z49). Younger-than-crystallization ages were, in all cases, obtained in the outermost part of some grains.

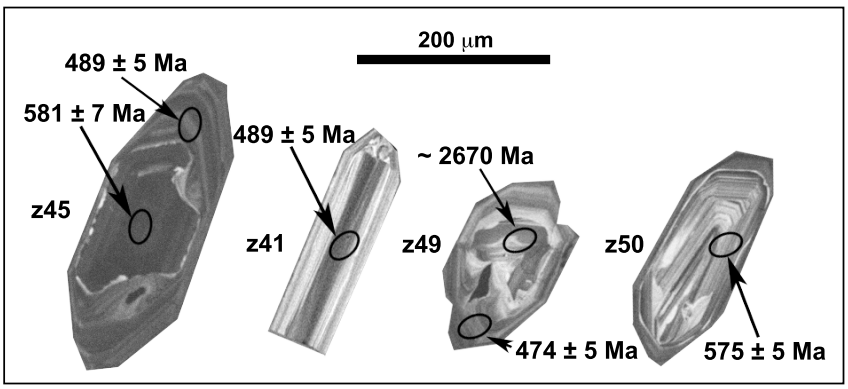


Figure 4.40: Cathodoluminescence images and ages of selected zircons from La Cañada metagranite.

### *4.2.3.2. La Hoya*

The U-Pb ion microprobe data of La Hoya metagranite reveal the existence of a Cambro-Ordovician nearly concordant population with a mean age of 478 ± 7 Ma that we interpret as representing the age of crystallization (Fig. 4.41 and Table 4.29). There is also a subconcordant point at 710 Ma and a younger-than-crystallization age at 393 Ma.

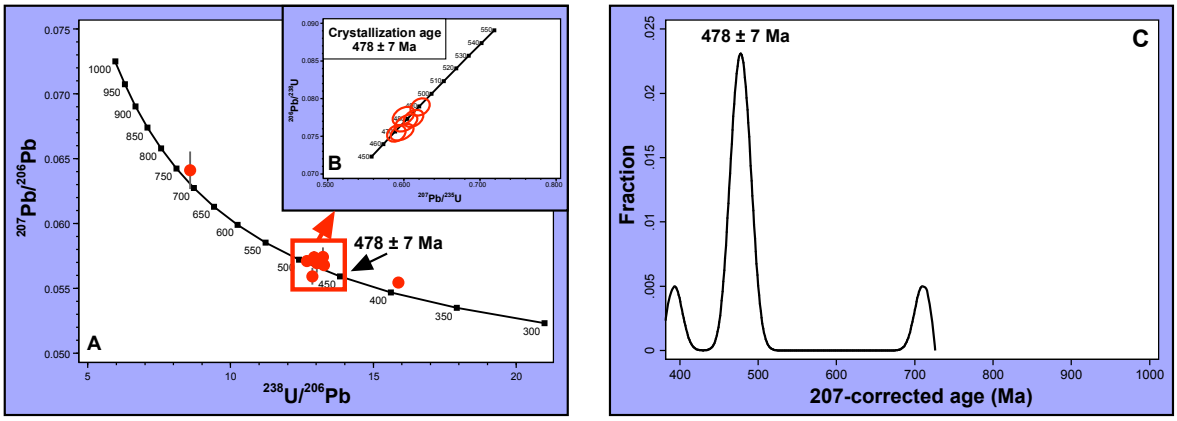


| Observations | 207-corrected age (Ma) | σ | 95 % Confidence Intervals |
|---|---|---|---|
| 6 | 478 ± 7 | 3.4 | 468.9 - 486.4 |

Figure 4.41: Geochronological data of La Hoya metagranite: A) Tera-Wasserburg concordia; B) Wetherill concordia; and C) Distribution of concordant 207-corrected ages and the statistical data of the crystallization population.

According to the cathodoluminescence images, the crystallization population was obtained in uniform grains (Fig. 4.42z2) and, less frequently, in rims of zircons with older cores (Fig. 4.42z16). The 710 Ma age was obtained in a core of a grain with a Cambro-Ordovician rim (Fig. 4.42z16).

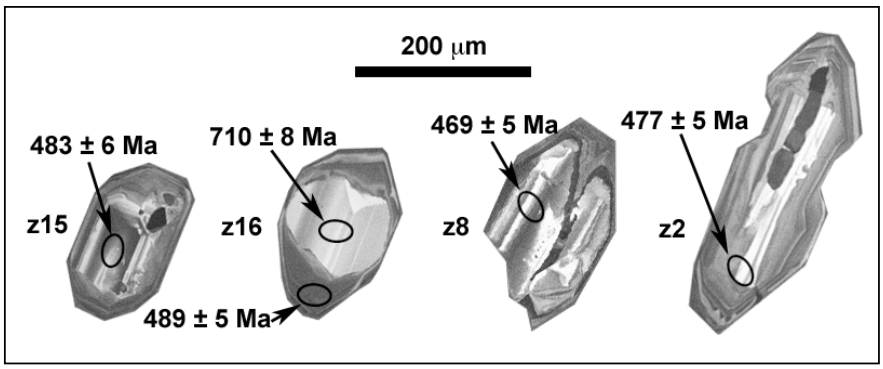


Figure 4.42: Cathodoluminescence images and ages of selected zircons from La Hoya metagranite.

### *4.2.3.3. La Estación*

In La Estación I metagranite, the U-Pb data reveal the existence of a concordant and abundant population and few older ages (Fig. 4.43A and 4.43C and Table 4.30). The concordant population is Cambro-Ordovician, with a mean age of 490 ± 5 Ma, which represents the age of crystallization of this metagranite (Fig. 4.43B). There are also two concordant points at about 600 Ma, another point at 646 and another, also concordant, at about 924 Ma.

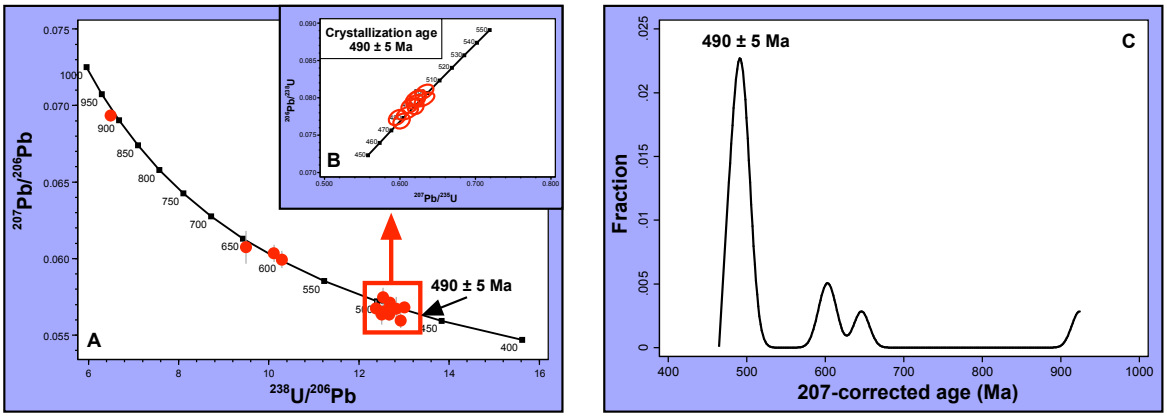


| Observations | 207-corrected age (Ma) | σ | 95 % Confidence Intervals |
|---|---|---|---|
| 10 | 490 ± 5 | 2.4 | 484.9 - 496.8 |

Figure 4.43: Geochronological data of La Estación I metagranite: A) Tera-Wasserburg concordia; B) Wetherill concordia; and C) Distribution of concordant 207-corrected ages and the statistical data of the crystallization population.

The Cambro-Ordovician population was obtained in uniform grains (Fig. 4.44z30) and in rims of grains containing older cores (Figs. 4.44z29, 4.44z33 and 4.44z36). All the older ages were obtained in cores of zircons rimmed by Cambro-Ordovician overgrowths (Figs. 4.44z29, 4.44z33 and 4.44z36).

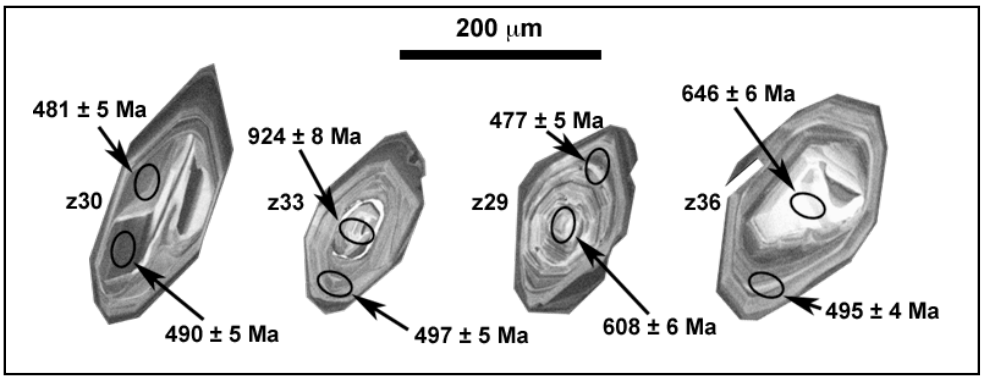


Figure 4.44: Cathodoluminescence images and ages of selected zircons from La Estación I metagranite.

### *4.2.3.4. La Estación II*

In La Estación II metagranite, the U-Pb data from five zircons reveal the presence of a nearly concordant population, Cambro-Ordovician (Figs. 4.45A and 4.45C and Table 4.31), with a mean age of 473 ± 8 Ma, which seems to be the best estimate of the age of crystallization of this body (Fig. 4.45B). No older inherited cores were found, nevertheless, according to the cathodoluminescence images, there are inherited cores (Fig. 4.46).

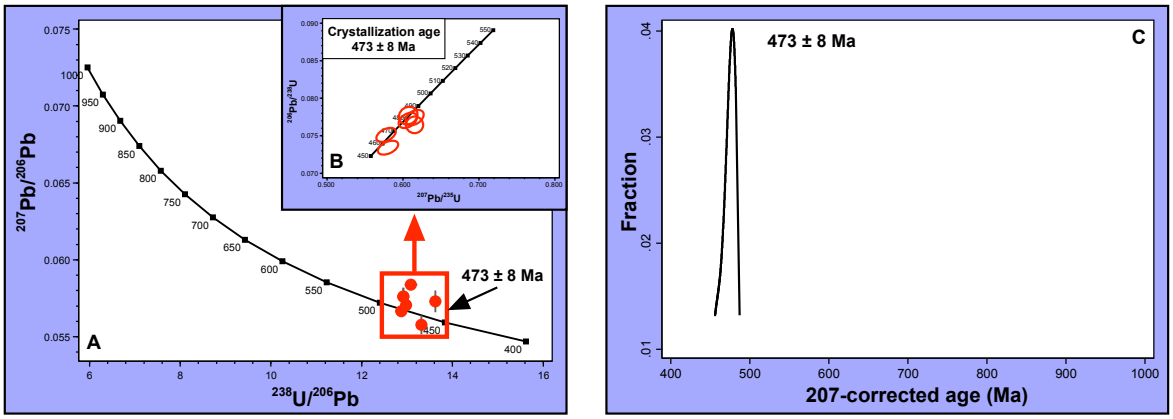


| Observations | 207-corrected age (Ma) | σ | 95 % Confidence Intervals |
|---|---|---|---|
| 6 | 473 ± 8 | 4.0 | 465.2-483.3 |

Figure 4.45: Geochronological data of La Estación II metagranite: A) Tera-Wasserburg concordia; B) Wetherill concordia; and C) Distribution of concordant 207-corrected ages and the statistical data of the crystallization population.

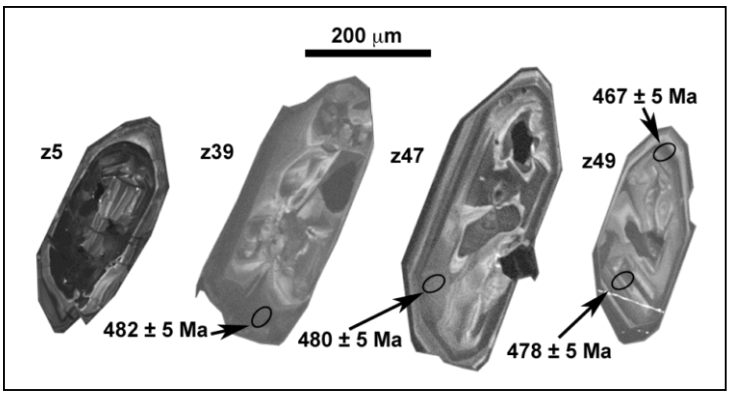


Figure 4.46: Cathodoluminescence images and ages of selected zircons from La Estación II metagranite.

According to the cathodoluminescence images, all crystallization ages were obtained in uniform grains (Figs. 4.46z39, 4.46z47 and 4.46z49), but some images also reveal the existence of inherited cores although they have not appeared in the analyzed zircons (Fig. 4.46z5).

### *4.2.3.5. Vegas de Matute (Melanocratic metagranites)*

The U-Pb ion microprobe data from the Vegas de Matute metagranite reveal the presence of one concordant population, another nearly concordant one and two isolated points (Figs. 4.47A and 4.47C and Table 4.32). The first population is Cambro-Ordovician, with a mean age of 476 ± 5 Ma which represents the age of crystallization (Fig. 4.47B). The second population, which is less abundant than the previous, is Ediacaran ranging from 545 to 609 Ma with a mean age of 574 ± 17 Ma. Between these two population there is a point with an age of 530 Ma which, although concordant, can result from the mixture of the last two concordant components. Apart from that, there are two older ages, one at 1024 Ma and the other at 1971 Ma.

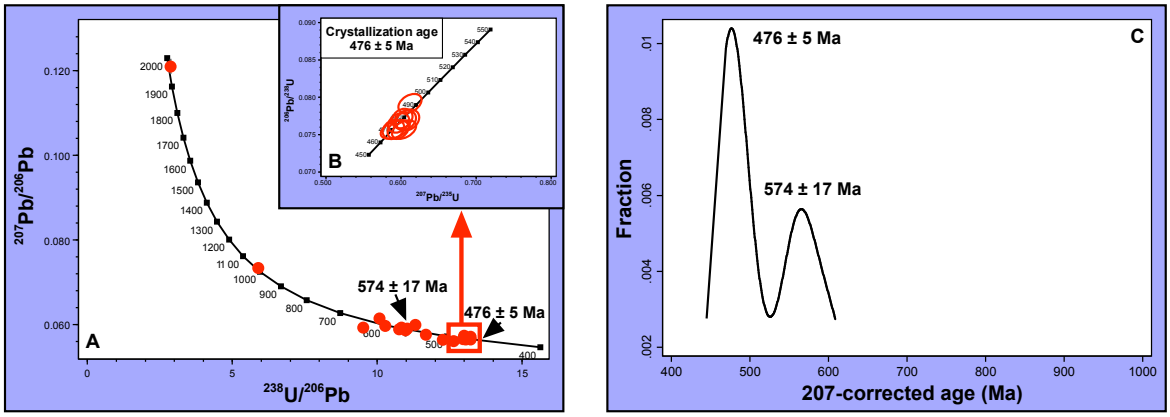


| Observations | 207-corrected age (Ma) | σ | 95 % Confidence Intervals |
|---|---|---|---|
| 9 | 476 ± 5 | 2.4 | 470.2 - 481.2 |
| 7 | 574 ± 17 | 8.5 | 552.7 - 594.4 |

Figure 4.47: Geochronological data of the Vegas de Matute (Melanocratic metagranites): A) Tera-Wasserburg concordia; B) Wetherill concordia; and C) Distribution of concordant 207-corrected ages and the statistical data of the two populations.

As usual, the crystallization ages were obtained in rims of crystals containing older cores (Figs. 4.48z48 and 4.48z50) and also in uniform crystals (Fig. 4.48z57). The inherited population (545-609 Ma) was always obtained in cores of crystals rimmed by

Cambro-Ordovician overgrowths (Fig. 4.48z48). The two older ages were also obtained in restitic cores (Figs. 4.48z50 and 4.48z54) rimmed by Cambro-Ordovician overgrowths.

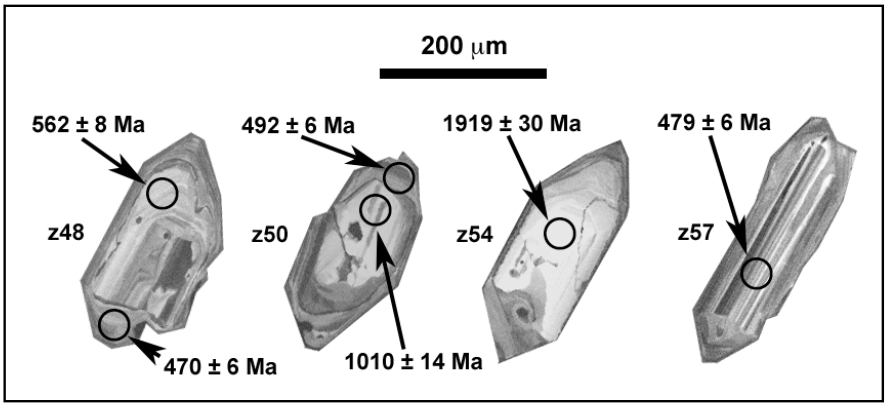


Figure 5.48: Cathodoluminescence images and ages of selected zircons from the Vegas de Matute (Melanocratic metagranites).

### *4.2.3.6. Vegas de Matute (Leucocratic metagranites: El Caloco)*

In the leucocratic El Caloco metagranite we found a single population, Cambro-Ordovician (Figs. 4.49A and 4.49C and Table 4.33), with a mean age of 484 ± 6 Ma (Fig. 4.49B) which represents the crystallization age. Most grains have narrow Variscan rims caused by the intense migmatization that affects this body. Owing to the thinness of these rims, the ages close to 360 Ma shown in Fig. 4.49A must be considered maximum estimates.

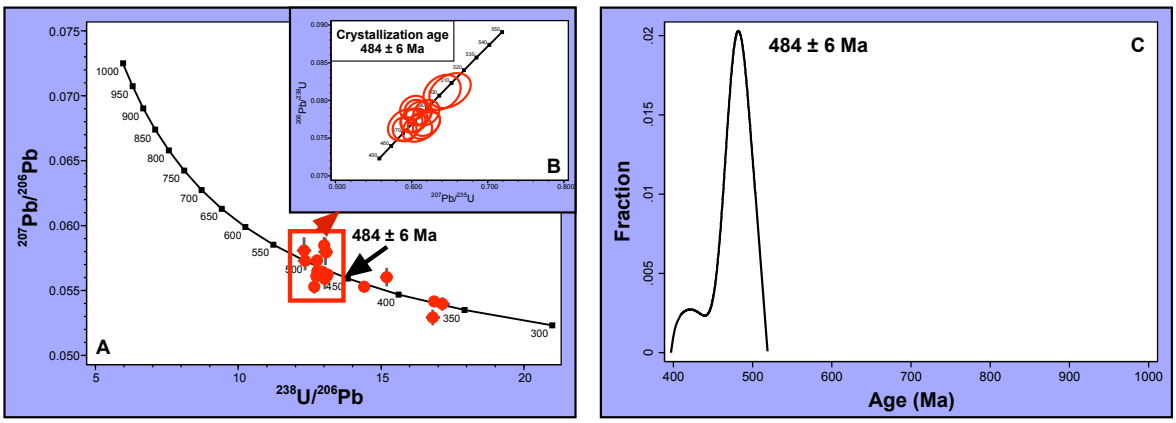


| Observations | 207-corrected age (Ma) | σ | 95 % Confidence Intervals |
|---|---|---|---|
| 13 | 484 ± 6 | 2.9 | 477.9 - 490.1 |

Figure 4.49: Geochronological data of the Vegas de Matute (Leucocratic metagranites): A) Tera-Wasserburg concordia; B) Wetherill concordia; and C) Distribution of concordant 207-corrected ages and the statistical data of the crystallization population.

No inherited cores were found and all data were acquired in uniform zircons (Figs. 4.50z33, 4.50z43 and 4.50z45). Despite this, the cathodoluminescence images reveal the presence of inherited cores (Fig. 4.50z4).

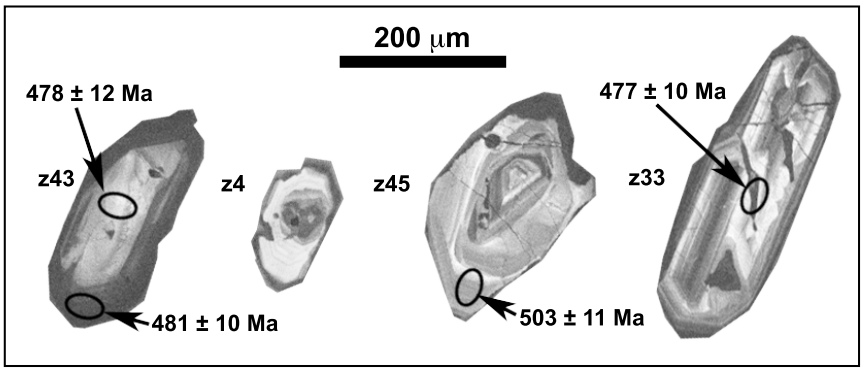


Figure 4.50: Cathodoluminescence images and ages of selected zircons from the Vegas de Matute (Leucocratic metagranites).

### *4.2.3.7. La Morcuera*

The U-Pb ion microprobe data from La Morcuera metagranite reveal the presence of two nearly concordant populations (Figs. 4.51A and 4.51C and Table 4.34). The first one, Cambro-Ordovician, yields a mean age of 482 ± 8 Ma that represents the best estimate of the crystallization age (Fig. 4.51B). The second population, Ediacaran, yields a mean age of 639 ± 13 Ma. Between these two populations are two nearly concordant point at 516 and 572 Ma, which probably represent mixed ages between the two populations mentioned before. There is also another nearly concordant point at about 725 Ma.

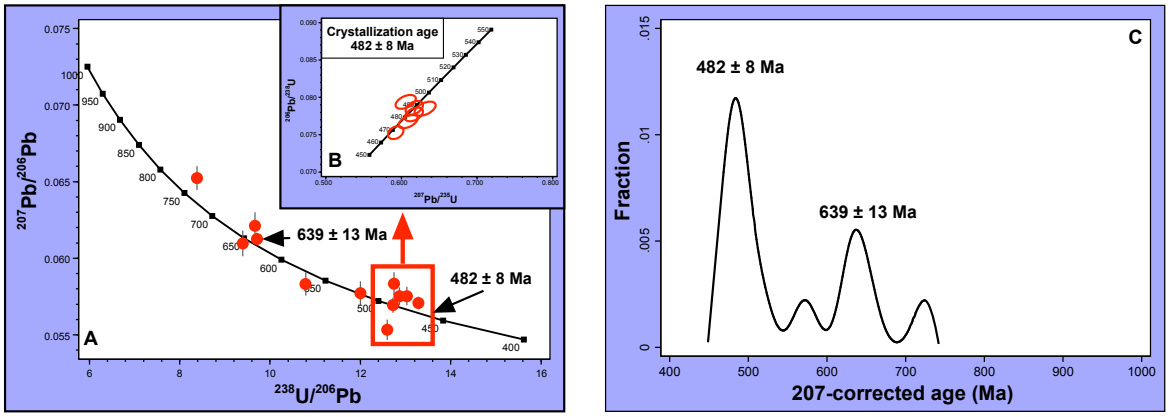


| Observations | 207-corrected age (Ma) | σ | 95 % Confidence Intervals |
|---|---|---|---|
| 6 | 482 ± 8 | 3.8 | 472.5 - 491.9 |
| 3 | 639 ±13 | 6.7 | 610.3 - 667.8 |

Figure 5.51: Geochronological data of La Morcuera metagranite: A) Tera-Wasserburg concordia; B) Wetherill concordia; and C) Distribution of concordant 207-corrected ages and the statistical data of the two populations.

According to the cathodoluminescence images, the Cambro-Ordovician population is present in the rims of grains having inherited cores (Figs. 4.52z48 and 4.52z54) and in uniform grains (Fig. 4.52z57). The inherited population was, in all cases, acquired in the core of crystals rimmed by Cambro-Ordovician overgrowths (Figs. 4.52z48, 4.52z50 and 4.52z54).

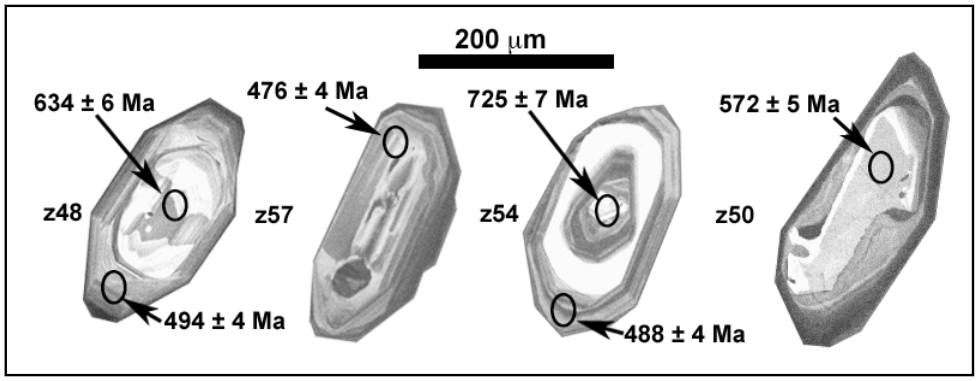


Figure 4.52: Cathodoluminescence images and ages of selected zircons from La Morcuera metagranite.

The 482 ± 8 Ma age matches the crystallization age obtained by Valverde-Vaquero and Dunning (2000) using conventional U-Pb dating on zircon concentrates (477 ± 4 Ma).

### *4.2.3.8. Buitrago de Lozoya*

In the Buitrago de Lozoya metagranite, the U-Pb ion microprobe data reveal the occurrence of two concordant populations and few isolated ages (Figs. 4.53A and 4.53C

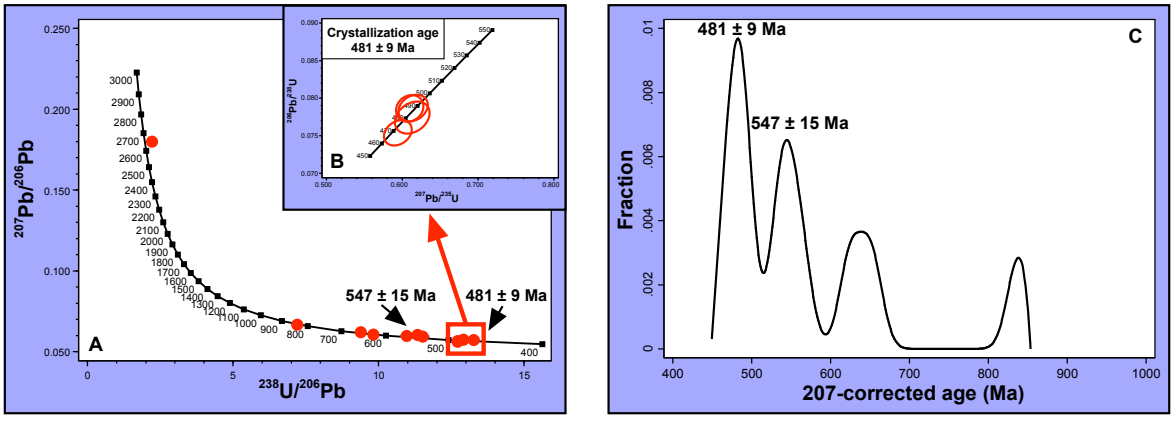


| Observations | 207-corrected age (Ma) | σ | 95 % Confidence Intervals |
|---|---|---|---|
| 4 | 481 ± 9 | 4.8 | 465.8 - 496.6 |
| 3 | 547 ± 15 | 7.7 | 514.0 - 580.4 |

Figure 4.53: Geochronological data of the Buitrago de Lozoya metagranite: A) Tera-Wasserburg concordia; B) Wetherill concordia; and C) Distribution of concordant 207-corrected ages and the statistical data of the two most abundant populations.

and Table 4.35). The first population is Cambro-Ordovician, with a mean age of 481 ± 9 Ma that represents the age of crystallization (Fig. 4.53B). The second population is Early Cambrian, with a mean age of 547 ± 15 Ma and represents the main inherited population. There are also two more concordant points at 625 and 652 Ma, a third point at 839 Ma and an another one at 2653 Ma .

The crystallization ages were acquired in rims of crystals with restitic cores (Figs. 4.54z17 and 4.54z23). The main inherited population was obtained in uniform zircons (Fig. 4.54z11). All other older ages were acquired in cores of rimmed crystals (Fig. 4.54z16, 4.54z17 and 4.54z23).

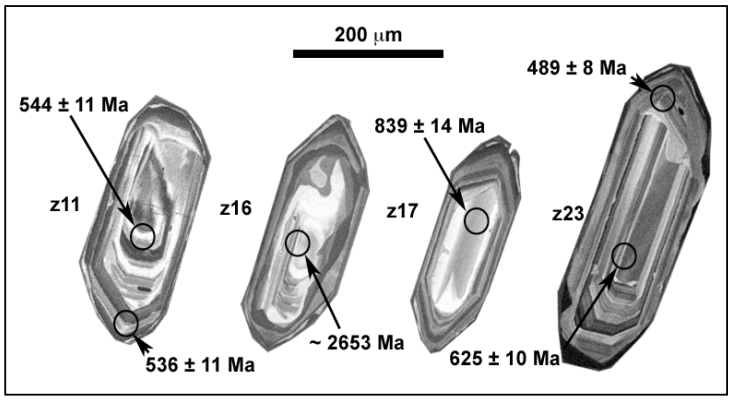


Figure 4.54: Cathodoluminescence images and ages of selected zircons from the Buitrago de Lozoya metagranite.

The 481 ± 9 Ma age matches, within error range, the crystallization age obtained by Valverde-Vaquero and Dunning (2000) using conventional U-Pb dating on zircon concentrates (488+10/-8 Ma).

### *4.2.3.9. La Berzosa*

The U-Pb ion microprobe data of La Berzosa metavolcanic rocks reveal the existence of two nearly concordant populations (Fig. 4.55A and 4.55C and Table 4.36). The first population is Cambro-Ordovician, with a mean age of 462 ± 11 Ma (Fig. 4.55B). It should be emphasized that only four of these determinations were close to concordia ($^{206Pb/238U}$age/ $^{206Pb/238U}$age > 0.95) so that this value must be simply considered as a provisional estimate of the crystallization age of La Berzosa rocks. The second, less abundant, population has between 593 and 635 Ma and has a mean age of 613 ± 15 Ma. There are also three older concordant ages at 721, 1965 and 2682 Ma.

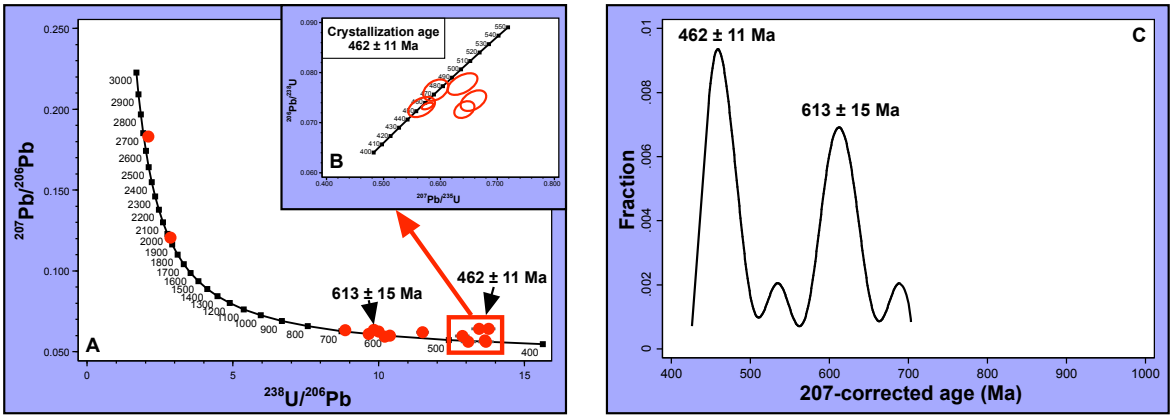


| Observations | 207-corrected age (Ma) | σ | 95 % Confidence Intervals |
|---|---|---|---|
| 6 | 462 ± 11 | 5.3 | 448.3 - 475.7 |
| 5 | 613 ± 15 | 7.3 | 592.7 - 633.4 |

Figure 4.55: Geochronological data of La Berzosa metagranite: A) Tera-Wasserburg concordia; B) Wetherill concordia; and C) Distribution of concordant 207-corrected ages and the statistical data of the two populations.

The crystallization ages were obtained in uniform zircons (Figs. 4.56z1 and 4.56z8) and in rims of grains containing restitic cores. The inherited population was obtained in uniform zircons (Fig. 4.56z16) and in cores of rimmed zircons. The older ages correspond to inherited cores (Fig. 4.56z14).

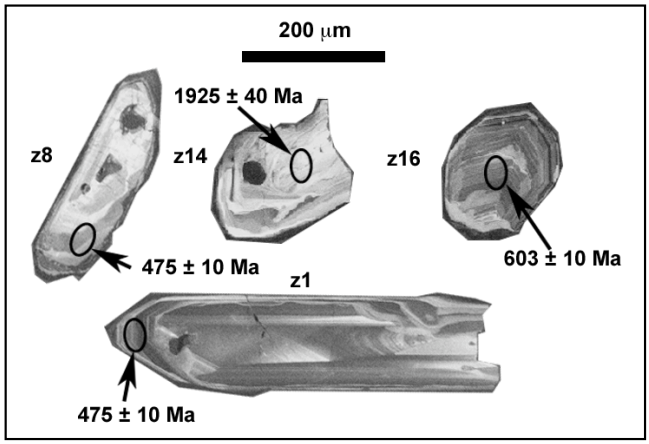


Figure 4.56: Cathodoluminescence images and ages of selected zircons from La Berzosa metagranite.

### *4.2.3.10. El Cardoso*

The U-Pb dating of El Cardoso metavolcanic rocks (Figs. 4.57A and 4.57C and Table 4.37) yielded a Cambro-Ordovician concordant population with a mean age of 483 ± 6 Ma

which represents the crystallization age (Fig. 4.57B). There are also some subconcordant points at 599, 609, 658 and 866 Ma and a discordant point near 1.95 Ga.

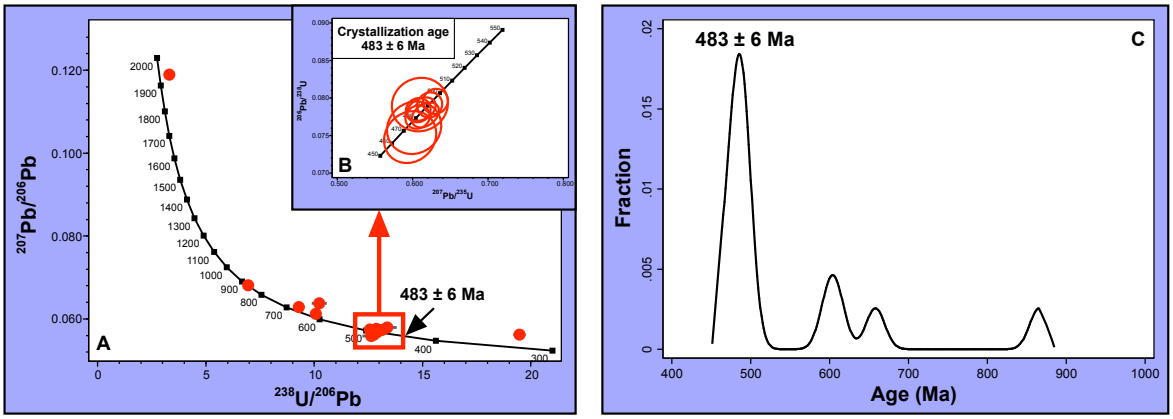


| Observations | 207-corrected age (Ma) | σ | 95 % Confidence Intervals |
|---|---|---|---|
| 9 | 483 ± 6 | 3.2 | 475.7-490.7 |

Figure 4.57: Geochronological data of El Cardoso metagranite: A) Tera-Wasserburg concordia; B) Wetherill concordia; and C) Distribution of concordant 207-corrected ages and the statistical data of the crystallization population.

According to the cathodoluminescence images, the crystallization ages were acquired in uniform grains (Fig. 4.58z11) and rims of grains with inherited cores (Fig. 4.58z2). The inherited populations were obtained in cores of rimmed zircons (Figs. 4.58z2 and 4.58z16) and in uniform zircons (Fig. 4.58z1).

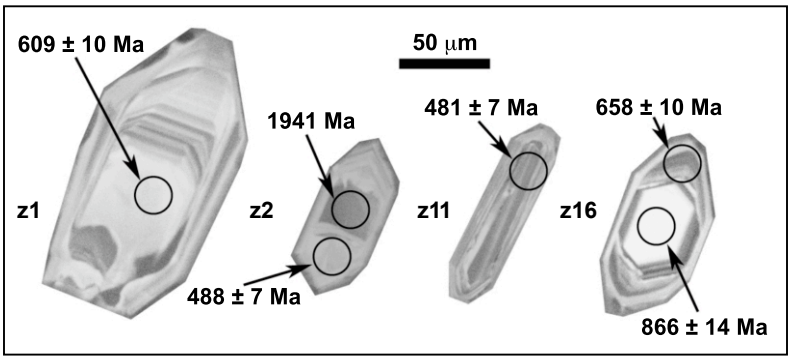


Figure 4.58: Cathodoluminescence images and ages of selected zircons from El Cardoso metagranite.

The 483 ± 6 Ma age matches, within error range, the crystallization age obtained by Valverde-Vaquero and Dunning (2000) using conventional U-Pb dating on zircon concentrates (480 ± 2 Ma).

### *4.2.3.11. Riaza*

The U-Pb ion microprobe data of the Riaza metavolcanic rocks reveal three concordant populations (Fig. 4.59A and 4.59C and Table 4.38). The youngest is Cambro-Ordovician, with a mean age of 475 ± 5 Ma, which represents the crystallization age (Fig. 4.59B). The second is Early Cambrian, with a mean age of 545 ± 11 Ma. The oldest is Ediacaran, clustering at around 599 ± 6 Ma.

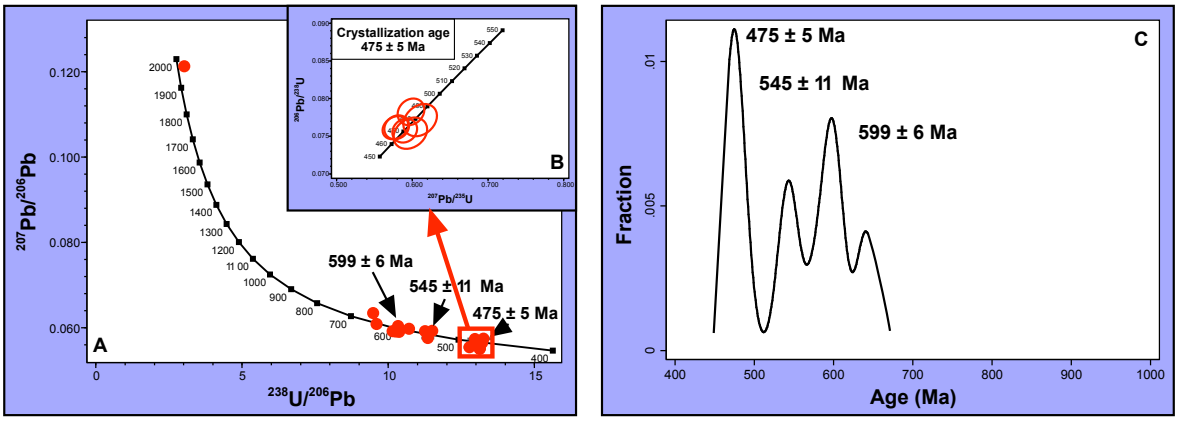


| Observations | 207-corrected age (Ma) | σ | 95 % Confidence Intervals |
|---|---|---|---|
| 6 | 475 ± 5 | 2.7 | 468.3 - 482.3 |
| 4 | 545 ± 11 | 5.5 | 530.4 - 565.2 |
| 4 | 599 ± 6 | 2.8 | 590.0 - 607.7 |

Figure 4.59: Geochronological data of La Riaza metagranite: A) Tera-Wasserburg concordia; B) Wetherill concordia; and C) Distribution of concordant 207-corrected ages and the statistical data of the three populations.

The crystallization ages, according to the cathodoluminescence images, were obtained in uniform grains and in rims of grains with inherited cores (Fig. 4.60z5). The inherited populations were acquired in cores of rimmed grains (Figs. 4.60z5 and 4.60z4) and in uniform grains (Fig. 4.60z13).

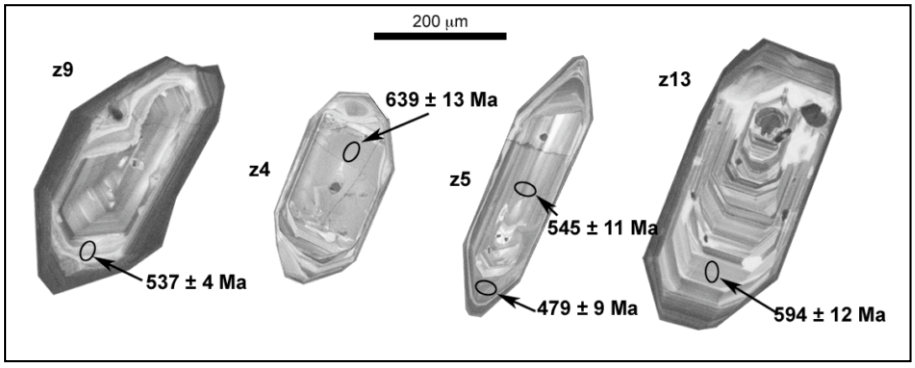


Figure 4.60: Cathodoluminescence images and ages of selected zircons from the Riaza metagranite.

The 475 ± 5 Ma age is different from, but still within error range, of the value obtained by Valverde-Vaquero and Dunning (2000) using conventional U-Pb dating on zircon concentrates (468 +19/-8 Ma).

### 4.2.4. The Anatectic Complex of Toledo

In the Anatectic Complex of Toledo we sampled two metagranites: Polán and Mohares. They were dated using U-Pb ion microprobe with the following results:

#### *4.2.4.1. Polán*

The Polán metagranite has a concordant Cambro-Ordovician population, two older concordant points at 521 and 587 Ma and one younger-than-crystallization ages at 429 Ma

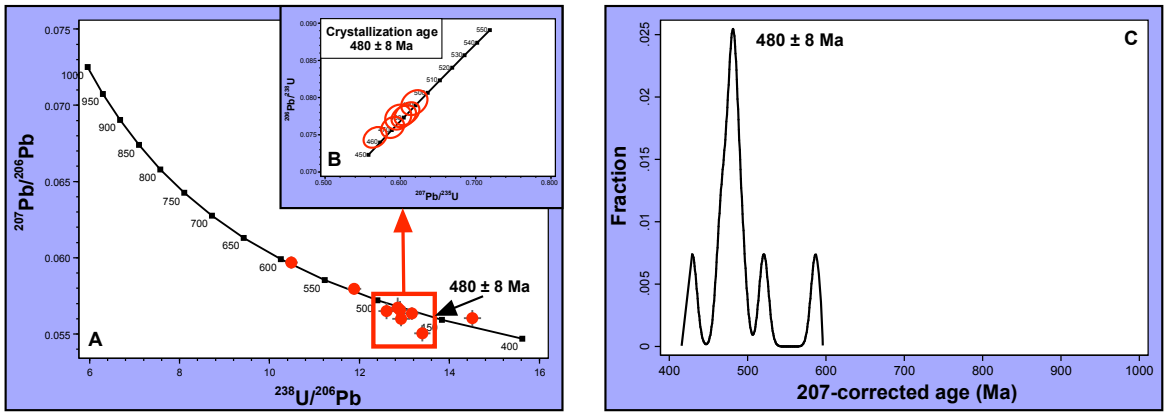


| Observations | 207-corrected age (Ma) | σ | 95 % Confidence Intervals |
|---|---|---|---|
| 6 | 480 ± 8 | 3.9 | 469.0 - 489.2 |

Figure 4.61: Geochronological data of the Polán metagranite: A) Tera-Wasserburg concordia; B) Wetherill concordia; and C) Distribution of concordant 207-corrected ages and the statistical data of the crystallization population.

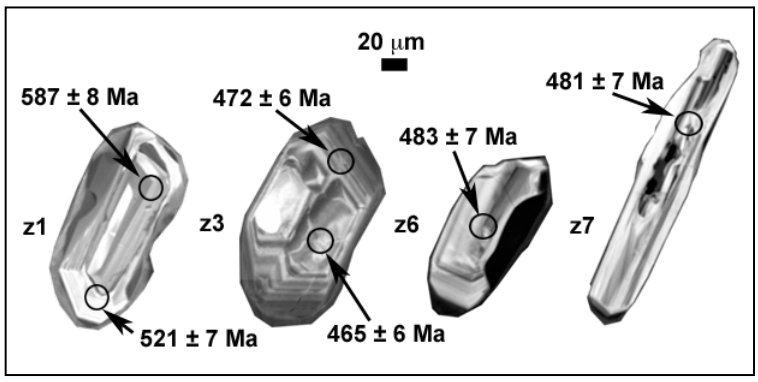


Figure 4.62: Cathodoluminescence images and ages of selected zircons from the Polán metagranite.

(Fig. 4.61A and 4.61C and Table 4.39). The Cambro-Ordovician population has a mean age of 480 ± 8 Ma, which represents the crystallization age (Fig. 4.61B). All ages from the crystallization population were acquired in uniform zircons (Figs. 4.62z3, 4.62z6 and 4.62z7) and the same occurred with the rest of the ages, except the 587 Ma age, which corresponds to an inherited core of a rimmed crystal (Fig. 4.62z1).

### *4.2.4.2. Mohares*

The U-Pb dating of the Mohares metagranite reveal the presence of an unique, small and concordant Cambro-Ordovician population with a mean age of 489 ± 7 Ma (Figs. 4.63A and 4.63C and Table 4.40), which we regard as the crystallization age (Fig. 4.63B). No inherited cores were found and all data were obtained in uniform crystals (Fig. 4.64).

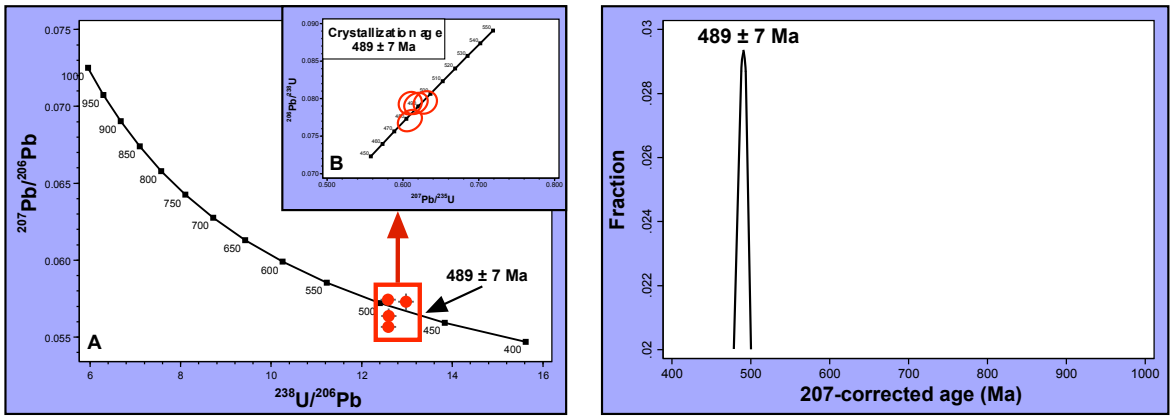


| Observations | 207-corrected age (Ma) | σ | 95 % Confidence Intervals |
|---|---|---|---|
| 4 | 489 ± 7 | 3.7 | 477.6 - 501.1 |

Figure 4.63: Geochronological data of the Mohares metagranite: A) Tera-Wasserburg concordia; B) Wetherill concordia; and C) Distribution of concordant 207-corrected ages and the statistical data of the crystallization population.

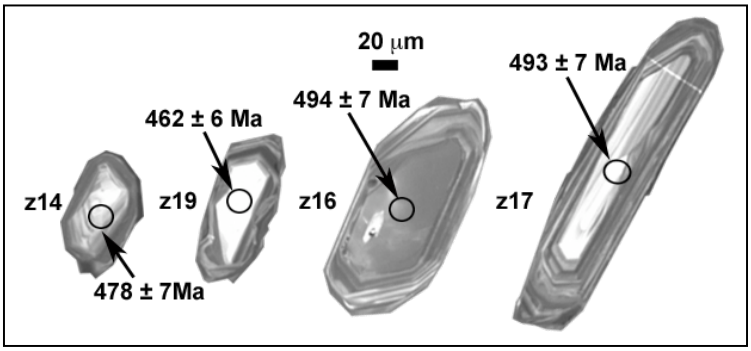


Figure 4.64: Cathodoluminescence images and ages of selected zircons from the Mohares metagranite.

## 4.3. Summary

### 4.3.1. The Ollo de Sapo Domain

The geochronological data of the Ollo de Sapo Formation and the associated metagranites, reveal that here the magmatism was synchronous and short lived, except in the Hiendelaencina area, where it was exceptionally long lived. In the northwestern area of the Ollo de Sapo Domain all the magmatic activity occurred between 492 Ma and 486 Ma, an age span comparable to the Urra Formation (495 Ma to 488 Ma, Sola et al., 2008) located in the western extreme of the Central Iberian Zone. The crystallization age is more variable in the southeastern area of the formation. In the Hiendelaencina region there are at least two volcanic episodes, one at 495 Ma and the other at 483 Ma, followed by a plutonic episode at 474 Ma accounting, in total, for about 20 million years of episodic magmatic activity. In the Villadepera region, the volcanic and intrusive rocks have the same age, 483 Ma, coincidental with the youngest volcanism in Hiendelaencina.

As mentioned before, one of the most remarkable features of the Cambro Ordovician rocks of Central Iberia is the elevated percentage of zircons with premagmatic cores, usually about 70-80%, in occasions up to near 100%. In the Ollo de Sapo metavolcanic rocks and metagranites about 80% of the inherited zircons components are Ediacaran, with a mean age of 609 ± 3 Ma (Fig. 4.2). This population was found in all rocks types, irrespective of their locality or whether they are metavolcanic or metagranitic. The Cryogenian (650-700 Ma) and Tonian (850-900 Ma) populations are only well-represented in Hiendelaencina, which is, therefore, another unique feature of this region. The second most important inherited population is Orosirian, with concordant ages clustering around 2.0 Ga. It is far less abundant that the Ediacaran and is much better represented in metavolcanic rocks than in metagranites. Orosirian ages appear mostly in the cores of Cambro-Ordovician zircons, though crystals with a Cambro-Ordovician rim enclosing a large Ediacaran core that contains an internal Orosirian core are also found. There are also two small and poorly defined Archean populations (Fig. 4.2), one Neoarchean (approximately 2.6 Ga), discordant, present in Sanabria and Vivero, and the other Mesoarchean, with concordant ages around 3.0-3.2 Ga, which appears in all studied regions except in Trives and Hiendelaencina.

Finally, apart from these inherited populations, there are sometimes younger, and always discordant, ages fluctuating between 450 Ma and 350 Ma which, at least in part,

correspond to mixed Cambro-Ordovician and Variscan ages (see section 4.3.3), the later caused by incipient migmatization.

Table 4. 1. Summary of the crystallization ages of the metavolcanic rocks and metagranites of the Ollo de Sapo Domain and the north of the Schist-Graywacke Complex Domain. Note that the $(^{206}Pb/^{238}U)_{cor}$ ages have been obtained using LA-ICPMS, SIMS and SHRIMP methods, $(^{207}Pb/^{206}Pb)$ ages using stepwise evaporation method and (Rb/Sr)ages using TIMS method.

| **Ollo de Sapo Domain** | | | |
|---|---|---|---|
| | **Ages (Ma)** | | |
| | **$(^{206}Pb/^{238}U)_{cor}$** | **$(^{207}Pb/^{206}Pb)$** | **(Rb/Sr)** |
| *Ollo de Sapo Formation* | | | |
| Vivero | 486 ± 3 | 486 ± 3 | - |
| Trives | 486 ± 5 | - | - |
| Sanabria (Lower) | 492 ± 4 | - | - |
| Sanabria (Upper) | 488 ± 3 | 490 ± 2 | - |
| Villadepera | 483 ± 4 | - | - |
| Hiendelaencina (Lower) | 495 ± 5 | 494 ± 4 | - |
| Hiendelaencina (Upper) | 485 ± 6 | 483 ± 3 | 490 ± 65 |
| *Associated metagranites* | | | |
| San Sebastián | 470 ± 3 | 461 ± 3 | - |
| Viana do Bolo | 487 ± 4 | 488 ± 4 | - |
| Miranda do Douro | 483 ± 3 | - | - |
| Antoñita | - | 474 ± 4 | 477 ± 30 |
| **Schist-Graywacke Complex Domain** | | | |
| *The Tormes Dome* | | | |
| Fermoselle | 486 ± 6 | - | - |
| Vitigudino | 489 ± 5 | - | - |
| Ledesma | 471 ± 7 | - | - |
| *The Sierra de Gredos* | | | |
| San Pelayo | 492 ± 4 | - | - |
| Castellanos | 498 ± 4 | - | - |
| Bercimuelle | 488 ± 3 | - | - |
| *The Sierra de Guadarrama* | | | |
| La Cañada | 489 ± 9 | - | - |
| La Hoya | 478 ± 7 | - | - |
| La Estación I | 490 ± 5 | - | - |
| La Estación II | 473 ± 8 | - | - |
| Vegas de Matute (Melanocratic) | 476 ± 5 | - | - |
| Vegas de Matute (Leucocratic) | 484 ± 6 | - | - |
| La Morcuera | 482 ± 8 | - | - |
| Buitrago de Lozoya | 481 ± 9 | - | - |
| La Berzosa | 462 ± 11 | - | - |
| El Cardoso | 483 ± 6 | - | - |
| Riaza | 475 ± 5 | - | - |
| *The Anatectic Complex of Toledo* | | | |
| Polán | 480 ± 8 | - | - |
| Mohares | 489 ± 7 | - | - |

### 4.3.2. The Schist-Graywacke Complex Domain

Though the high metamorphic grade affecting most Cambro-Ordovician rocks of the Schist-Graywacke Complex Domain makes it difficult to recognize their protolith, it seems that in most cases it was plutonic. Only in the Sierra del Guadarrama there are some gneisses: El Cardoso, Riaza, and La Berzosa, which were probably derived from volcanic rocks. The duration of the magmatic activity was not the same in the four studied areas. The magmatic activity occurred between: (i) 489 Ma and 471 Ma in the Tormes Dome; (ii) 498 Ma and 488 Ma in the Sierra de Gredos; (iii) 489 Ma and 480 Ma, in the Anatectic Complex of Toledo; (iv) 490 Ma and 462 Ma in the Sierra de Guadarrama, though this lower limit should be considered cautiously because of the imprecision in the determination of the crystallization age of the La Berzona orthogneiss (see section 4.2.3.9). It seems, therefore, that whereas the magmatism in the Tormes Dome and Toledo was fully coeval with the Ollo de Sapo, in Sierra de Gredos started a little earlier and in the Sierra de Guadarrama started later and lasted longer.

A high fraction of zircon grains from the Cambro-Ordovician rocks of the northern Schist-Graywacke Complex Domain also have inherited cores. In the small bodies of the Sierra de Gredos, Toledo and the Tormes Dome, the inheritance is similar to that of the metavolcanic rocks and metagranites of the Ollo de Sapo Formation, but in the Sierra del Guadarrama the fraction of the zircons with pre-magmatic cores is smaller, oscillating between 50 and 70 %. The distribution of ages of these restitic cores is slightly different from what was found in the Ollo de Sapo Formation (Fig. 4.26). There are three main Neoproterozoic populations (521-646 Ma) that represent about 73 % of the inherited cores. The first two have mean ages of 540 ± 3 Ma and 571 ± 4 Ma, and have been found in the four sampled areas. The third has a mean age of 617 ± 5 Ma and has been found in the Tormes Dome, Sierra de Gredos and Sierra de Guadarrama. There are also other less abundant populations with ages Cryogenian (650-700 Ma), Tonian (850-950 Ma) and Orosirian (1900-2000). Cryogenian and Tonian populations have been observed in the Tormes Dome, Sierra de Gredos and Sierra de Guadarrama, and Orosirian population only has been found in Sierra de Gredos and Sierra de Guadarrama. Finally, there are some nearly concordant Neoarchean ages (2.5-2.6 Ga), which have been obtained in the Sierra de Gredos and Sierra de Guadarrama, and a nearly concordant Mesoarchean age which has only been found in the Castellanos metagranite (Sierra de Gredos).

As in the Ollo de Sapo Formation, there is a small population of younger and almost always discordant ages fluctuating between 338 Ma and 450 Ma which may correspond to mixed ages between Cambro-Ordovician and Variscan ages (see next section).

### 4.3.3. The significance of the younger ages

Many studied zircons have small overgrowths, rarely thicker than 20 µm, with younger-than-Ordovician ages. They are often highly discordant, with 207-corrected values between 450 Ma and 338 Ma. We have found that these younger ages are the consequence of two different processes: (i) solid-state overgrowths on zircons included in Zr-rich feldspars probably caused by the exsolution of Zr (Bea et al., 2006b); and (ii) Variscan overgrowths probably caused by incipient migmatization. In the first case (Fig. 4.65A) the overgrowths are highly cathodoluminescent due to the low concentrations of U, Th and HREE. In the second case, they show a low cathodoluminescence (Fig. 4.65B) due to elevated concentrations of U. To discuss the origin of these overgrowths in detail is beyond the scope of this work. Here it is sufficient to consider that most often the overgrowths yielded highly discordant ages from which no useful information can be derived. For that reason, they will not be considered further.

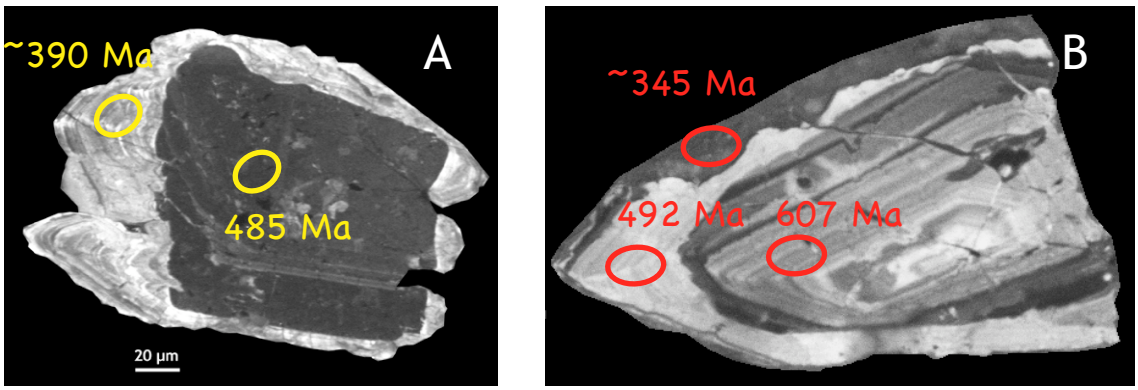


Figure 5.65.- The reason for younger ages. A) Overgrowth in a zircon included in a K-feldspar megacryst from the upper metavolcanic rocks of Hiendelaencina. The elevated cathodoluminescence is caused by low contents of U, Th and HREE. Bea et al. (2006b) attributed them to the exsolution of Zr from Zr-rich feldspars. B) U-rich overgrowth caused by incipient migmatization in the Viana do Bolo metagranite. Ellipses represent zones analyzed with the ion-microprobe. The results for either overgrowth are highly discordant ages.

# 5. CHEMICAL COMPOSITION AND Sr-Nd ISOTOPE GEOLOGY

# 5. CHEMICAL COMPOSITION AND Sr-Nd ISOTOPE GEOLOGY

As mentioned before, the Cambro-Ordovician felsic rocks of Iberia form two contrasting geochemical associations (Fig. 1.1A). The most abundant comprises intermediate to silicic peraluminous rocks (mol. $Al_2O_3/(CaO + Na_2O + K_2O) \approx 1.34 \pm 0.23$) which according to the classification of Frost et al. (2001) are magnesian and alkaline-calcic to calc-alkaline (Fig. 1.1B). The less abundant association is composed of ferroan, alkaline to calc-alkaline, and predominantly high-silica rocks (Fig. 1.1B) which often contain Na pyriboles. Accordingly, Montero et al., (in press and in rev.) named these two different rock associations as peraluminous and peralkaline, with it being well understood that a few rocks of the first group have mol. $Al_2O_3/(CaO + Na_2O + K_2O) < 1.05$ and about 50-70% of the rocks of the second group, depending on the massif, have mol. $(Na_2O + K_2O)/Al_2O_3 \leq 1$, that is, they are not strictly peralkaline.

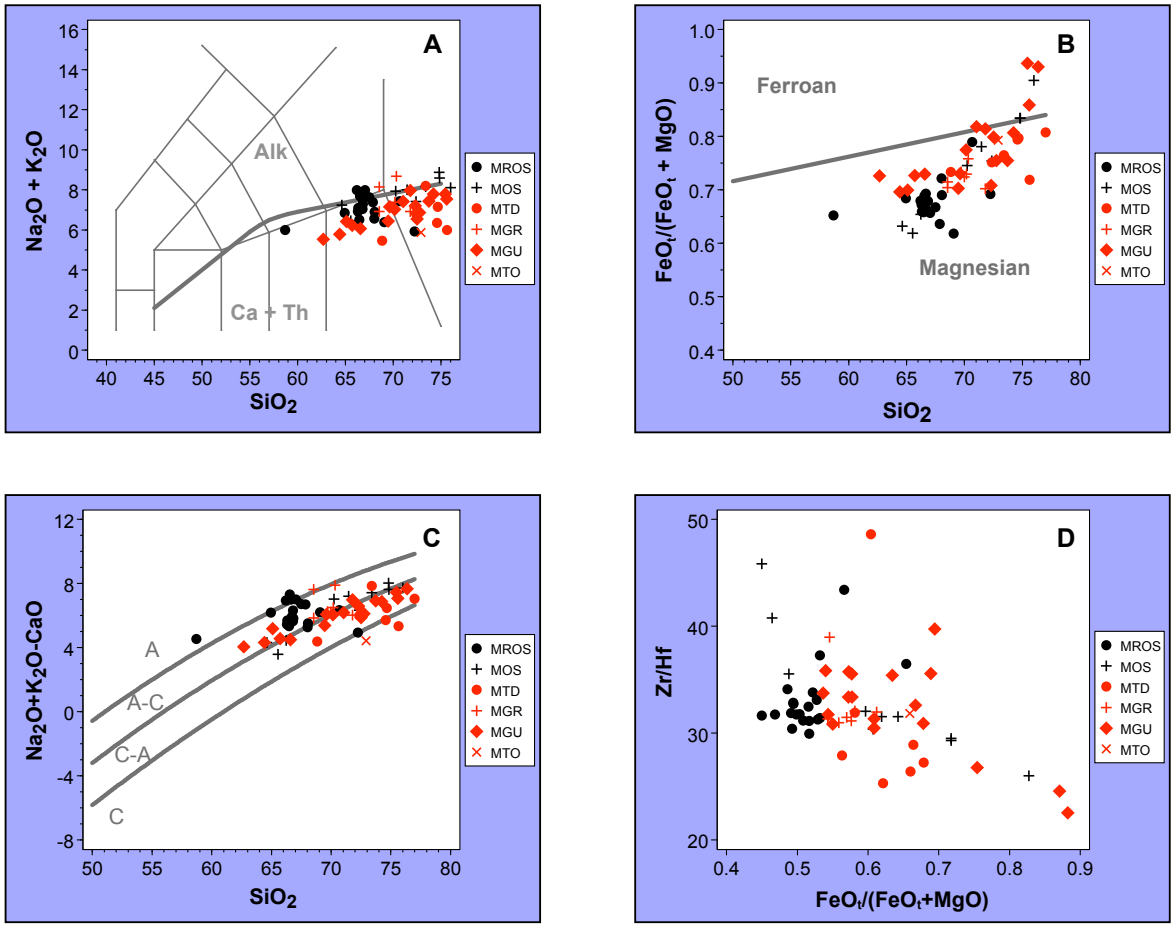


Figure 5.1: A) TAS plot; B and C) Frost et al. (2001) plots; D) Zr/Hf-FeO/(FeO$_t$+MgO) plot. The meaning of the abbreviations of the legend is: MROS: Metavolcanic rocks of the Ollo de Sapo Domain; MOS: Metagranites of the Ollo de Sapo Domain; MGR: Metagranites of the Sierra de Gredos; MGU: Metagranites and metavolcanic rocks of the Sierra de Guadarrama; MTD: Metagranites of the Tormes Dome; MTO: Metagranites of the Anatectic Complex of Toledo.

All metavolcanic rocks and metagranites of the Central Iberian Zone belong to the peraluminous association. Those of the Ollo de Sapo Domain have ASI (mol. $Al_2O_3/(CaO+Na_2O+K_2O)$) clustering around 1.15 in the metagranites and around 1.50 in the metavolcanic rocks and all of them are magnesian and alkaline-calcic (Fig. 5.1). The metavolcanic rocks have a relatively homogeneous major element composition which corresponds to K-rich peraluminous dacites (Fig. 5.1). The metagranites are more variable, either less silicic (granodioritic) or more silicic (leucogranitic) than the metavolcanic rocks. The trace element composition of both metavolcanic rocks and metagranites is characterized by marked enrichments in alkali elements, especially Li, and precipitous negative anomalies in Sr (Fig. 5.2). The chondrite-normalized REE patterns decrease smoothly from La to Sm, have a marked negative Eu anomaly, and decrease again from Gd to Lu, the slope being steeper in the metagranites than in the metavolcanic rocks (Fig. 5.3). The latter showing a large variation in HREE. When compared to averages of Palaeozoic European S-type collision-related granites and I-type subduction-related granites (Fig. 5.2C), the trace element compositions of both the metagranites and the metavolcanic rocks of the Ollo de Sapo Formation bear a stronger resemblance with the former.

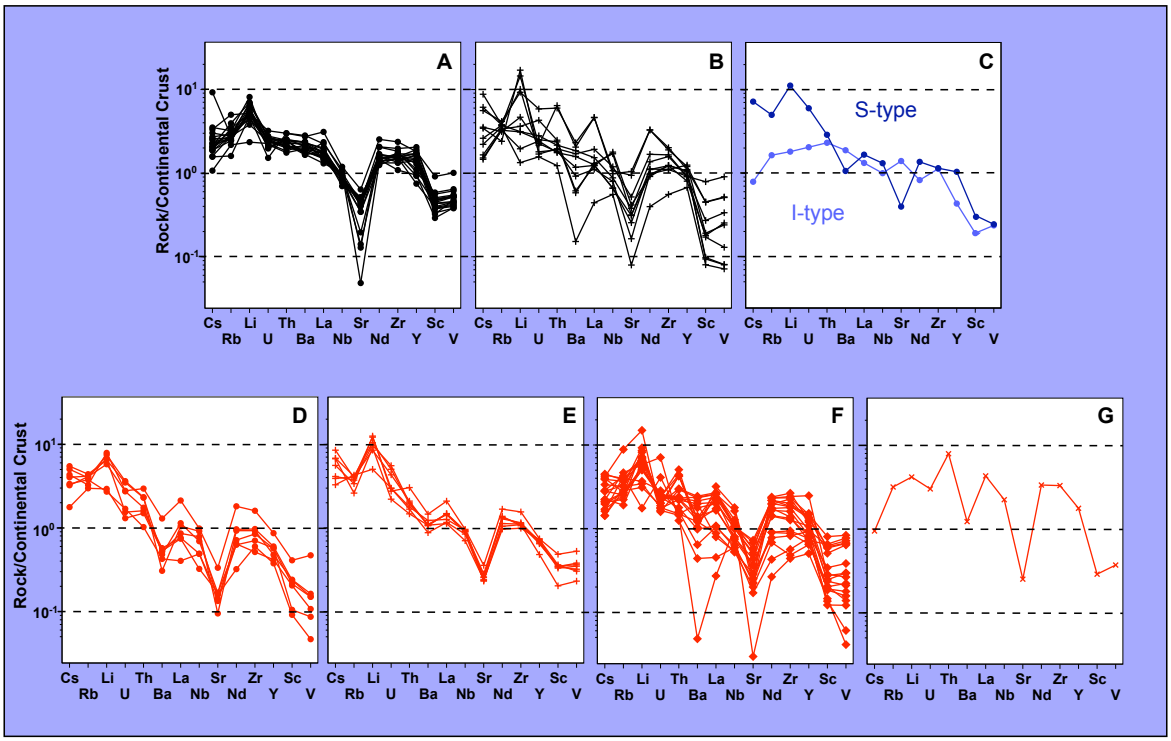


Figure 5.2: Continental-crust normalized trace-element plots of: A) Metavolcanic rocks of the Ollo de Sapo Domain; B) Metagranites of the Ollo de Sapo Domain; C) References averages of the Paleozoic European I and S types granites; D) Metagranites of the Tormes Dome; E) Metagranites of the Sierra de Gredos; F) Metagranites and metavolcanic rocks of the Sierra de Guadarrama; G) Metagranites of the Anatectic Complex of Toledo.

The metagranites and the metavolcanic rocks of the northern Schist-Graywacke Complex Domain do not show any significant difference from the rocks of the Ollo de Sapo Formation. They are equally peraluminous (ASI ≈ 1.4, Table 5.1), and equally alkaline-calcic to calc-alkaline and magnesian, so that in the Frost et al. (2001) diagrams the rocks from the two domains plot in the same area (Fig. 5.1). The evolution from magnesian to ferroan as $SiO_2$ increases (Fig. 5.1B) is due to the effects of magmatic differentiation, as evidenced by the sympathetic decrease of the differentiation index e.g., Zr/Hf (Fig. 5.1D). The trace element composition of the metagranites and metavolcanic rocks of the northern Schist-Graywacke Complex Domain is also nearly identical to the metagranites of the Ollo de Sapo Formation, characterized by the enrichment in Li and a strong depletion in Sr (Fig. 5.2). In Guadarrama, the metagranites show the largest compositional spectrum, from granodioritic to leucogranitic, the later showing depleted chondrite-normalized REE-patterns with precipitous negative Eu anomalies and secondary Nd negative anomalies (Fig. 5.3).

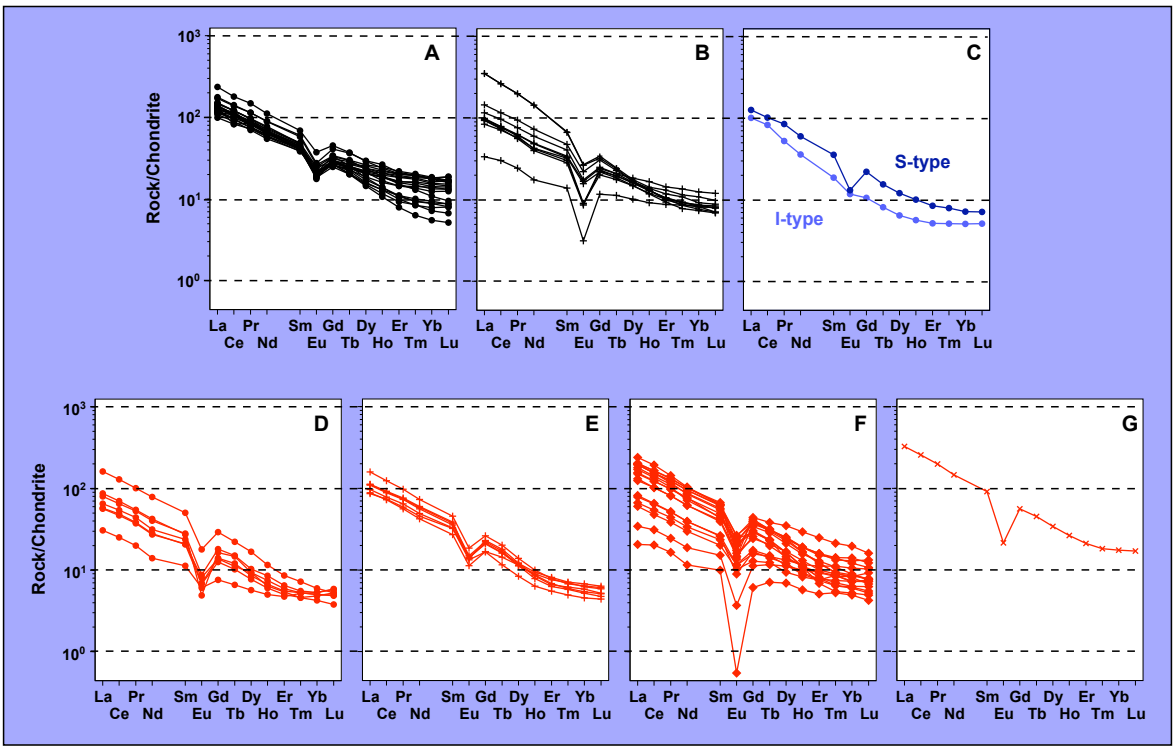


Figure 5.3: Chondrite-normalized REE plots of: A) Metavolcanic rocks of the Ollo de Sapo Domain; B) Metagranites of the Ollo de Sapo Domain; C) References averages of the I and S types granites; D) Metagranites of the Tormes Dome; E) Metagranites of the Sierra de Gredos; F) Metagranites and metavolcanic rocks of the Sierra de Guadarrama; G) Metagranites of the Anatectic Complex of Toledo.

Table 5.1: Alumina saturation index (ASI) and average of the Alumina saturation index (ASI*) of: OSD, Ollo de Sapo Domain; MROS, metavolcanic rocks of the Ollo de Sapo Domain; metagranites of the Ollo de Sapo Domain; SGCD, Schist-Graywacke Complex Domain; MTD, metagranites of the Tormes Dome; MGR, metagranites of the Sierra de Gredos, MGU, metagranites and metavolcanic rocks of the Sierra de Guadarrama; MTO, metagranites of the Anatectic Complex of Toledo.

| Domain | Group | ASI | ASI* |
|---|---|---|---|
| **OSD** | **MROS** | 1.50 | 1.37 |
| | **MOS** | 1.15 | |
| **SGCD** | **MTD** | 1.45 | 1.40 |
| | **MGR** | 1.35 | |
| | **MGU** | 1.40 | |
| | **MTO** | 1.22 | |

The Sr and Nd isotope composition of the metavolcanic rocks of the Ollo de Sapo Formation (Fig. 5.4 and Table 5.2) clusters around $(^{87}Sr/^{86}Sr)_{490Ma} \approx 0.710$ (ranging from 0.707 to 0.713), $\varepsilon Nd_{490Ma} \approx -4.6$ (ranging from -5.8 to -3.3), and $T_{(DM)} \approx 1.8$ Ga (ranging

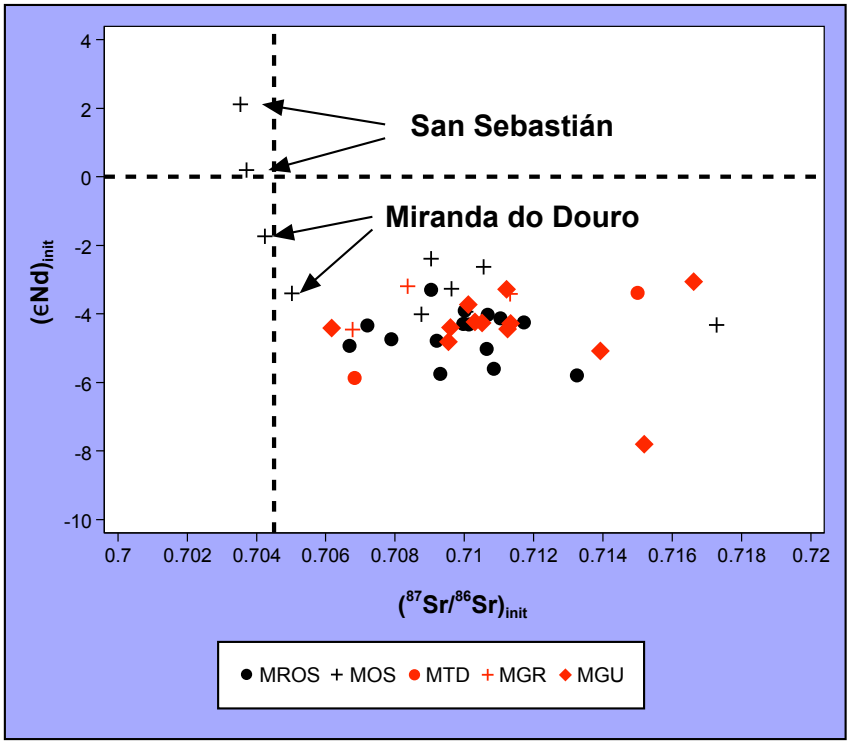


Figure 5.4: $(\epsilon Nd)_{init}$ vs. $(^{87}Sr/^{86}Sr)_{init}$ of the: A) MROS, metavolcanic rocks of Ollo de Sapo Domain; B) MOS, metagranites of the Ollo de Sapo Domain; C) MGR, metagranites of the Sierra de Gredos; D) MGU, metagranites and metavolcanic rocks of the Sierra de Guadarrama, E) MTD, metagranites of the Tormes Dome.

from 1.6 to 2.0), values that suggest they were derived from old continental materials. The metagranites of the Ollo de Sapo Formation have, in general, slightly higher $\varepsilon Nd_{490Ma}$ than the metavolcanic rocks and show a wider range of $(^{87}Sr/^{86}Sr)_{490Ma}$. The isotope composition of two metagranites, Antoñita and Viana do Bolo, overlaps with the metavolcanic rocks, but the other two, Miranda do Douro and San Sebastián, are more primitive, with $(^{87}Sr/^{86}Sr)_{490Ma} \approx 0.704$, $T_{(DM)} \approx 1.3$ Ga and variable $\varepsilon Nd_{490Ma}$ which ranges from -3.4 to -1.7 in Miranda do Douro and from 0.2 to 2.1 in San Sebastián (Fig. 5.4). The San Sebastián metagranite, therefore, besides being the youngest and having the lowest zircon inheritance, also has the most primitive isotope composition of the whole Ollo de Sapo Formation.

The Sr and Nd isotope composition of the metagranites and metavolcanic rocks of the northern Schist-Graywacke Complex Domain are very monotonous and similar to the metavolcanic rocks of the Ollo de Sapo Formation. Neither in Guadarrama, Gredos or Tormes Dome, we have found metagranites with such a primitive isotope composition such as Miranda do Douro or San Sebastián. By contrast, the metagranites of the northern Schist-Graywacke Complex Domain have slightly higher average values of $(^{87}Sr/^{86}Sr)_{490Ma} \approx 0.711$ and $T_{(DM)} \approx 1.9$ (Table 5.2). In detail, the metagranites of the Sierra de Gredos show the most primitive isotope composition having $(^{87}Sr/^{86}Sr)_{490Ma} \approx 0.709$, $\varepsilon Nd_{490Ma} \approx -3.7$ and $T_{(DM)} \approx 1.8$ Ga. The metagranites and the metavolcanic rocks of the Sierra de Guadarrama and the metagranites of the Tormes Dome have $(^{87}Sr/^{86}Sr)_{490Ma} \approx 0.711$ and $T_{(DM)} \approx 1.9$ Ga and slightly variable $\varepsilon Nd_{490Ma}$, -4.5 and -4.6 respectively.

Table 5.2: Average Sr and Nd isotope data of: MROS, metavolcanic rocks of Ollo de Sapo Domain; MOS, metagranites of the Ollo de Sapo Domain; MTD, metagranites of the Tormes Dome; MGR, metagranites of the Sierra de Gredos; MGU, metagranites and metavolcanic rocks of Sierra de Guadarrama

| Group | $(^{87}Sr/^{86}Sr)_{490Ma}$ | $(\epsilon Sr)_{490Ma}$ | $(^{143}Nd/^{144}Nd)_{490Ma}$ | $(\epsilon Nd)_{490Ma}$ | $Nd_{(CHUR)}$ (Ga) | $T_{(DM)}$ (Ga) |
|---|---|---|---|---|---|---|
| **MROS** | 0.7098 | 84 | 0.511771 | -4.6 | 1.0 | 1.8 |
| **MOS** | 0.7082 | 61 | 0.511888 | -2.3 | 0.8 | 1.6 |
| **MTD** | 0.7109 | 99 | 0.511771 | -4.6 | 1.1 | 1.9 |
| **MGR** | 0.7088 | 70 | 0.511818 | -3.7 | 1.0 | 1.8 |
| **MGU** | 0.7113 | 105 | 0.511777 | -4.5 | 1.2 | 1.9 |

# 6. DISCUSSION

# 6. DISCUSSION

## 6.1. The nature of the magmatic sources

The distribution of 627 concordant or nearly concordant ion-microprobe and LA-ICPMS ages for the Cambro-Ordovician rocks of Central Iberia (Figs. 4.2 and 4.26) shows that a significant fraction of zircons contain inherited cores (Fig. 6.1; see section 6.3) and that a significant fraction of these are Ediacaran. Whereas in the Ollo de Sapo Domain and the Tormes Dome the age of the Ediacaran inherited component is unimodal, dominated by 605 Ma to 620 Ma ages, in Guadarrama and the two eastern most metagranites of Gredos, Castellanos and Bercimuelle, besides a widespread 605-620 Ma component, there is another well-represented inherited component with ages at 540-550 Ma and another, which is less abundant, at 570-580 Ma. It is worth mentioning that Gredos is the only area of the Central Iberian zone where orthogneisses with a crystallization age of 540 Ma to 550 Ma have been identified so far (Bea et al., 2003).

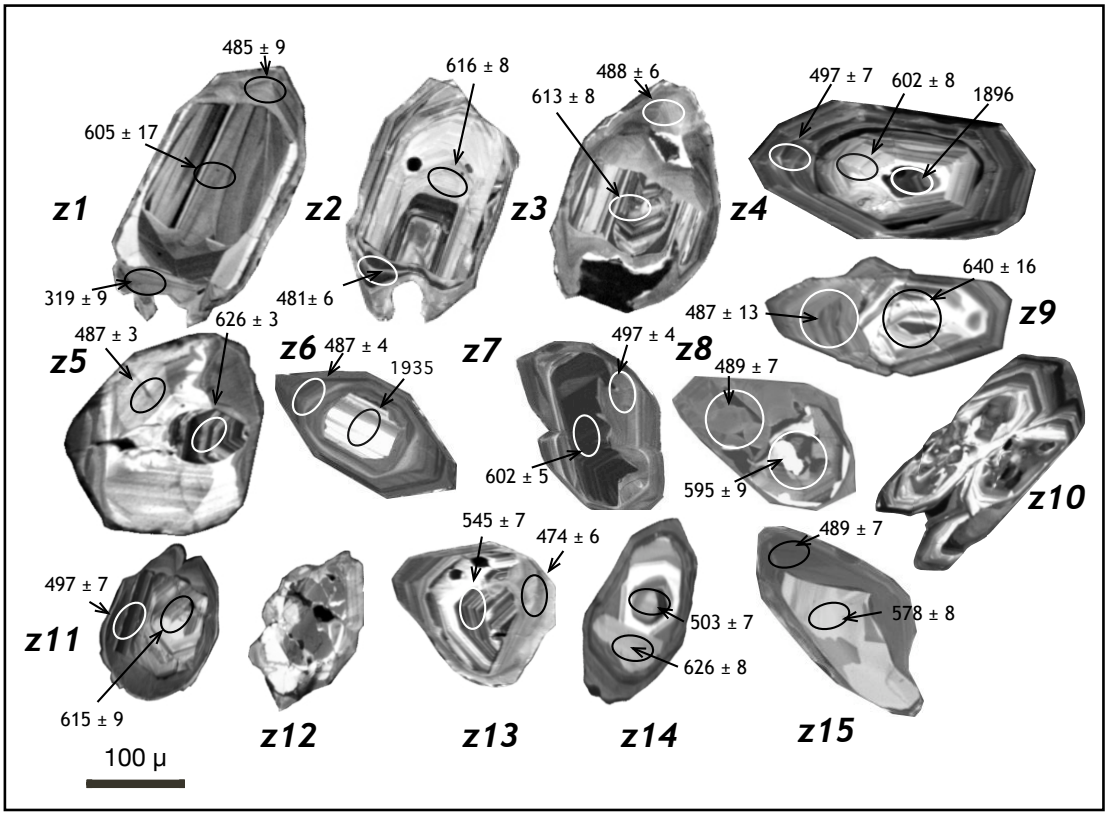


Figure 6.1: Cathodoluminescence images of the representative zircons of the Cambro-Ordovician rocks of Central Iberia. Numbers represent concordant U-Pb ages determined either with ion-microprobe (ellipses) or LA-ICP-MS (circles).

The marked dominance among the inherited cores of the Ediacaran components suggests that the protolith of the Cambro-Ordovician magmas of Iberia mostly consisted of igneous rocks of late Pan-African age, or young (at the time of melting) immature sediments derived from them. In principle, the highly radiogenic Sr and Nd isotope composition of the Cambro-Ordovician igneous rocks might be compatible with derivation from the Cambro-Ediacaran terrigenous series underlying them, either the Angon Formation, the Viana Series or the Schist-Graywacke Complex. Putting aside the fact that the chemical composition of these terrigenous sediments is hardly capable of producing melts with a composition similar to the Cambro-Ordovician igneous rocks, there is compelling evidence derived from zircon studies that negates this possibility. First, the studies of Fernández-Suárez et al. (2000) on detrital zircons of the Cambro-Ediacaran series in the north of the Central Iberian and the Western-Asturian-Leonese Zone indicate

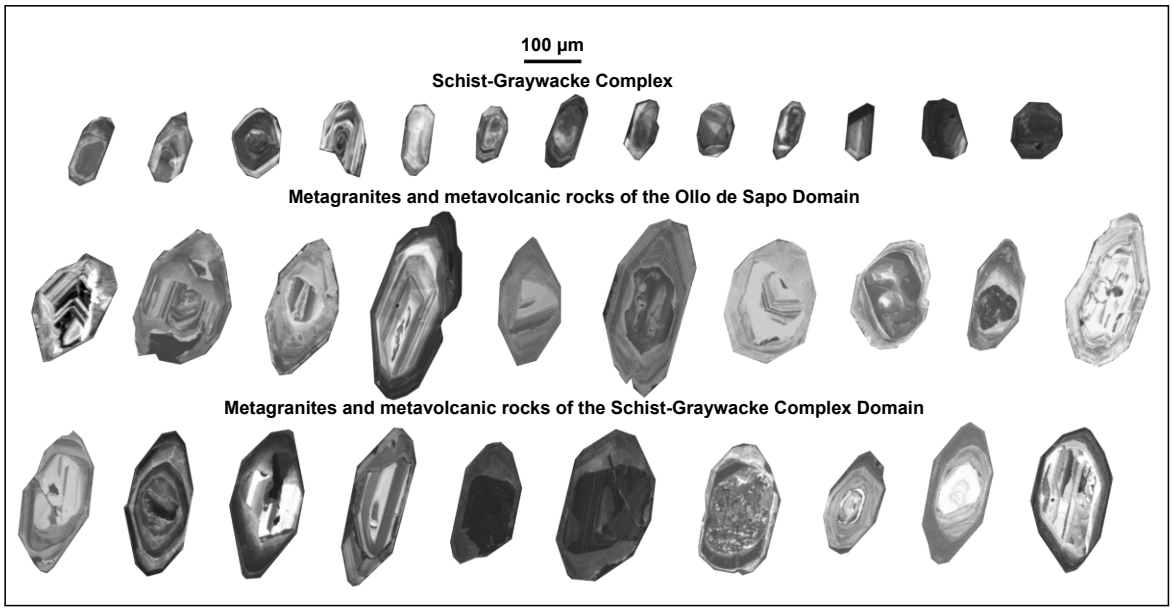


Figure 6.2: Cathodoluminescence images of selected zircons of Schist-Graywacke Complex, metagranites and metavolcanic rocks of the Ollo de Sapo Domain and the north of the Schist-Graywacke Complex Domain. Note the differences of zircon size between the Cambro-Ordovician rocks and the Schist-Graywacke Complex, the latter being smaller than most inherited cores.

that ages between 650 Ma and 950 Ma are among the most abundant, and these ages are not represented in the inherited components of the Cambro-Ordovician metagranites and metavolcanic rocks. Second, our ongoing studies on the materials of the Schist-Graywacke Complex reveal that these rocks contain very few zircons, and that these are very small, smaller even that the inherited cores of the Cambro-Ordovician gneisses (Fig. 6.2), which

must have necessarily been partially dissolved during the Cambro-Ordovician magmatism (see section 6.3.4.). Neither the ages nor the abundance and size of the zircons of the terrigenous series, therefore, are compatible with them being the source of the Cambro-Ordovician magmatism.

Due to vigorous Variscan crustal reworking, intermediate to felsic calc-alkaline igneous rocks of late Pan-African rocks are poorly exposed in Iberia, except for some small dioritic to granitic massifs in the Mérida region to the south of the Central Iberian Zone (Bandrés et al., 2004), and a few granodioritic gneisses in the west of the Ávila batholith (Bea et al., 2003). Calc-alkaline plutonism of Ediacaran age, however, was one of the most important magmatic events of the neighboring Anti-Atlas region of Morocco (Gasquet et al., 2005), a region attached to Iberia during the Ediacaran (Ennih and Liegeois, 2001; Ennih and Liegeois, 2003) but which was subsequently little affected by the Variscan orogeny.

Sr and Nd isotopes are consistent with the idea that late Pan-African rocks similar to those of the Anti-Atlas could have been the source of the Cambro-Ordovician magmatism

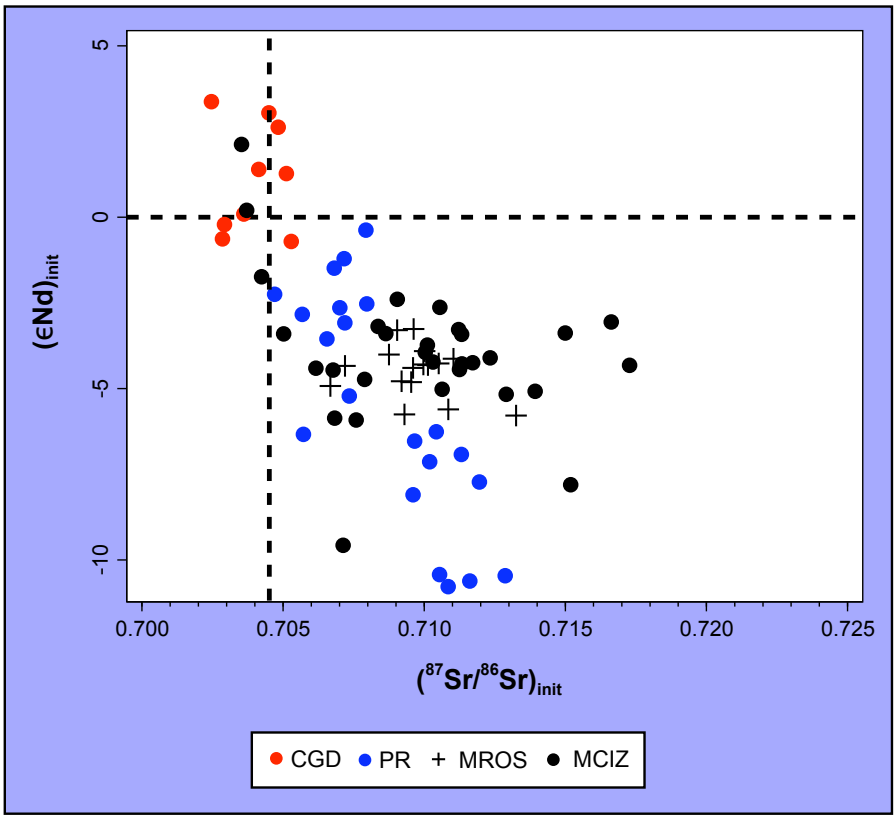


Figure 6.3: $(\epsilon Nd)_{init}$ vs. $(^{87}Sr/^{86}Sr)_{init}$ of the: CGD, Carrascal gabbro-diorites; PR, Pan-African rocks which correspond to Anti-Atlas late-Pan-African granites and volcanics; MROS, metavolcanic rocks of the Ollo de Sapo Domain; MCIZ, metagranites of the Central Iberian Zone.

of Iberia. Figure 6.3 represents the data of the Cambro-Ordovician igneous rocks of the Central Iberian Zone with data from Anti-Atlas late-Pan-African granites and volcanics (Gasquet et al., 2005; unpublished data of P. Montero) recalculated at 490 Ma and data from the Carrascal gabbro-diorites, the only mafic Cambro-Ordovician body of the Central Iberian Zone (Sola et al., 2005; Sola, 2007). Despite the noise caused by the Variscan metamorphism, it is evident in this plot that the Cambro-Ordovician magmas of Iberia can have been generated by partial melting of rocks similar to the Anti-Atlas with little material contribution of mafic magmas except in the most primitive metagranites, Miranda do Douro and, especially, San Sebastián.

## 6.2. The reasons for the abnormally elevated zircon inheritance

The investigations described in Chapter 3 have revealed an unusually large proportion of zircon crystals with pre-magmatic, inherited zircon cores. If we accept that discordant cores such as those shown in Fig. 6.2 are restitic (which was confirmed wherever U-Pb

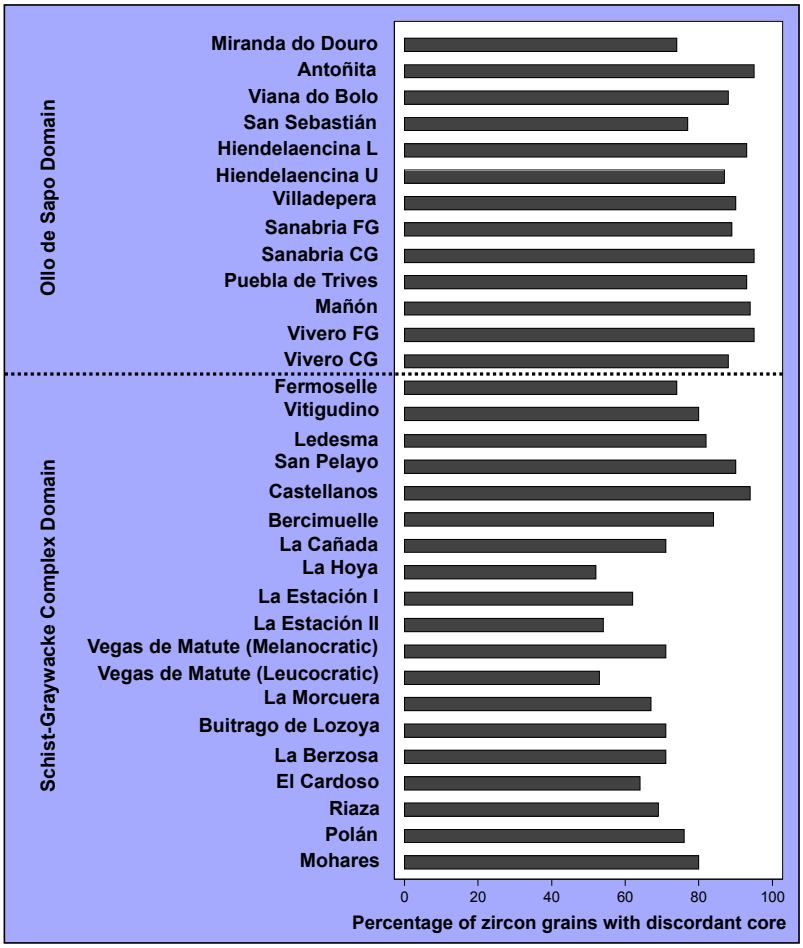


Figure 6.4: Percentage of zircon grains with pre-magmatic cores in 32 Cambro-Ordovician massifs of the Central Iberia. L, lower; U, upper, CG, coarse-grained; and FG, fine-grained.

spot analyses are available), the examination of some 2000 zircons by cathodoluminescence imaging has shown that the proportion of grains with inherited cores varies from 75% to 95% in the metagranites, and from 70% to 80%, locally up to 100%, in the metavolcanic rocks, except in Guadarrama where this number decreases to 50% -70 % (Fig. 6.4). To the authors' knowledge, such a high degree of inheritance is common in low melt-fraction migmatites (e.g. Montero et al., 2004b) or low-T pegmatoid mobilisates (e.g. Gilotti and McClelland, 2005) but is extremely rare in high-level granites or rhyodacitic volcanic rocks.

The solubility of zircon in felsic magmas has been thoroughly studied experimentally by Watson and Harrison (1983) and Harrison and Watson (1983), who have demonstrated that in peraluminous or metaluminous melts solubility only depends of the temperature and composition (basically the silica content) of the magma. This experimental model has been checked on many occasions (e.g. Bea and Montero, 1999) so that it seems to be accurate beyond any reasonable doubt. Since the expected variations in the composition of crustal melts have far less influence that the variations in temperature (for example, melts with 68 % and 72 % of $SiO_2$ dissolve 148 and 131 ppm Zr at 800°C, but dissolve 253 and 223 ppm Zr at 850°C), the first hypothesis that might explain the abnormally elevated zircon inheritance of the Cambro-Ordovician magmas is that they never reached a high enough temperature to dissolve all the zircon present in the source rock, which for some unknown reason was unusually elevated.

To check this hypothesis we consider the zircon saturation temperature, calculated according to the Watson and Harrison (1983) model, with the Ti-in-zircon temperature (Watson and Harrison, 2005; and Watson et al., 2006). Whereas the former represents an estimate of the temperature required to avoid zircon inheritance (Hanchar and Watson, 2003), the later represents a minimum estimate of the temperature attained by the magmas at their locus of melting.

### 6.2.1. Zircon saturation temperatures

The zircon saturation temperature is calculated with the expression:

$$\mathbf{T_{Zr}=12900/(\log(497600/Zr)+3.8+(0.85*(M-1)))-273};\ (1)$$

where:
$T_{Zr}$ is the zircon saturation temperature,

Zr is in ppm,

M=(Ca+Na+K)/(Al*Si/(Si+Ti+Al+Fe+Mg+Mn+Ca+Na+K)), and all major elements are expressed as atomic equivalents.

The application of this expression yielded a slightly skewed unimodal distribution, tailed at lower values due to loss of Zr during crystallization of the granitoids, with the mode value at 815°C (Fig. 6.5). If we exclude the most silicic samples, and hence the most prone to have undergone magmatic differentiation processes, the average $T_{Zr}$ is 822 ± 5°C which would then represent the temperature required to dissolve all zircon present in the rock.

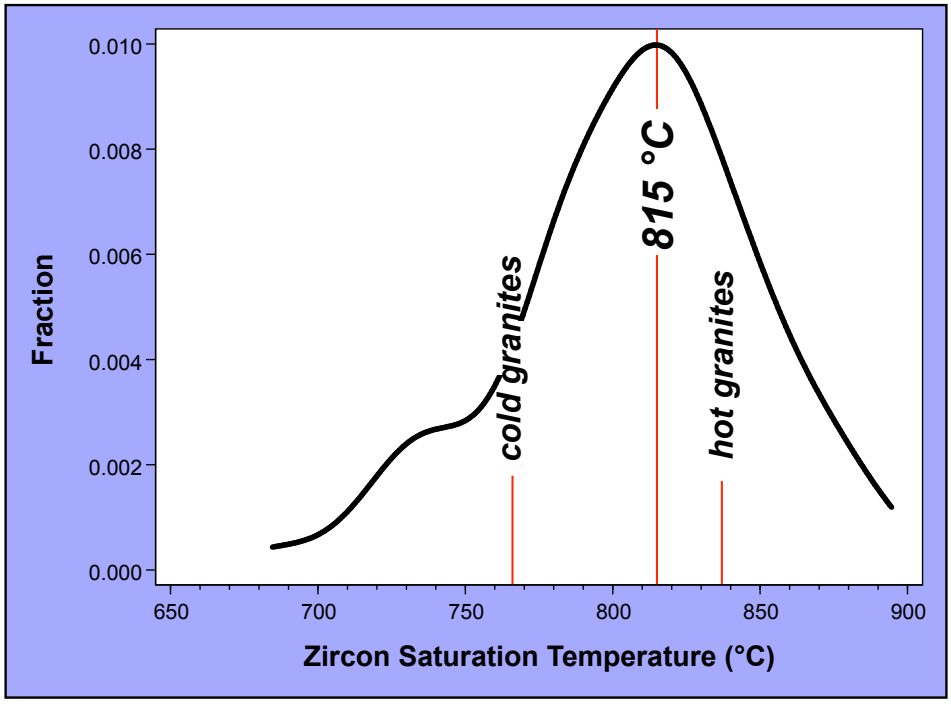


Figure 6.5: Zircon saturation temperature for representative samples of the metavolcanic rocks and metagranites of the Ollo de Sapo Domain and the north of the Schist-Graywacke Complex Domain calculated from data of Table 6.1. The zircon saturation temperature of these samples is compared to the temperature of cold and hot granites.

Miller et al. (2003) have demonstrated that zircon inheritance and zircon saturation temperatures are antithetic. These authors divided North-American granites into "hot" (average $T_{Zr}$ = 837°C, little or no inheritance) and "cold" (average $T_{Zr}$ = 766°C; high zircon inheritance, most often clustering around 50%) types. With minor modifications, this two-fold categorization seems applicable worldwide(e.g., Asrat et al., 2004; Rowe et al., 2007; Bryan et al. 2008), irrespective of granite age and typology, implying that the

inverse relation between inheritance and $T_{Zr}$ is probably a reflection of the conditions that most typically occur during granite petrogenesis. Remarkably, the Central Iberian Cambro-Ordovician igneous rocks do not follow this rule, because they have simultaneously an average high $T_{Zr}$ of 822 °C, characteristic of "hot" granites, and a zircon inheritance that not only matches, but in most cases nearly duplicates that of "cold" granites (Fig. 6.6). As discussed below, this unusual combination suggests disequilibrium processes that do not

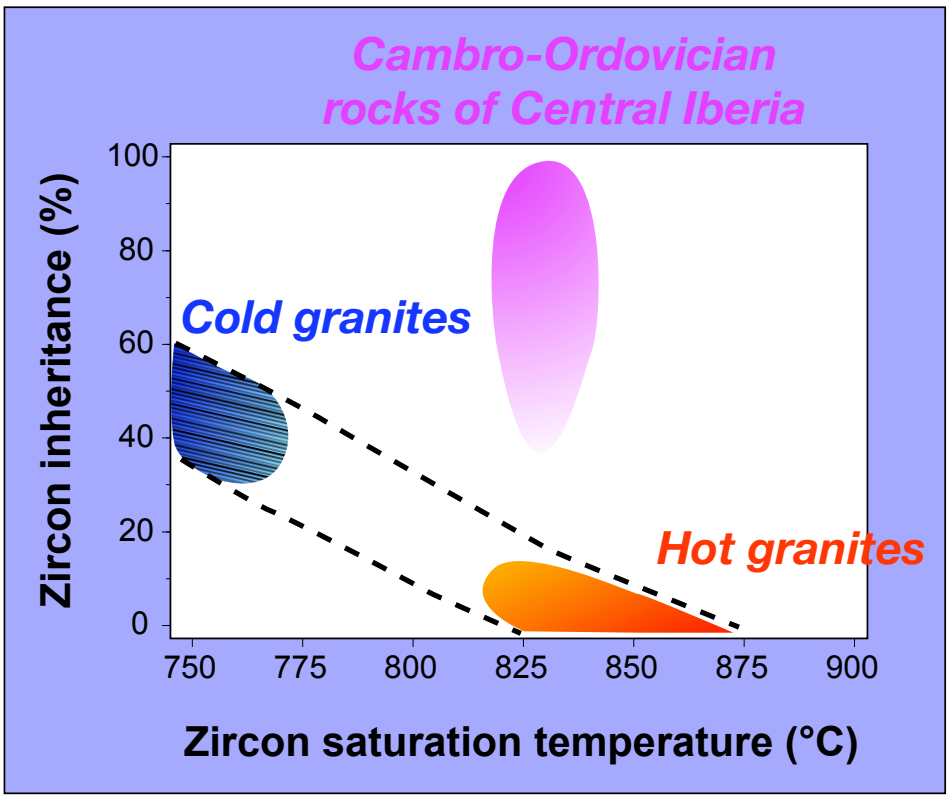


Figure 6.6: Zircon inheritance vs zircon saturation temperature of Cambro-Ordovician rocks of the Central Iberia. These rocks are compared to cold and hot granites of Miller et al. (2003).

normally occur during granite magmas.

To understand the atypical processes involved in the generation of the Iberian Cambro-Ordovician magmas, we must consider the following: Zircon solubility in common crustal melts depends on melt composition and temperature, but it is almost independent of pressure and water content (Watson and Harrison, 1983). Since the variations to be expected in the melt bulk-composition have less influence than the variations to be expected in temperature, the first hypothesis that might explain the abnormally elevated zircon inheritance of the Cambro-Ordovician magmas is that they were never sufficiently

hot to dissolve all the zircon grains entrained from the source, these, for some unspecified reason, being exceptionally abundant.

### 6.2.2. Ti-in-zircon temperatures

The minimum temperature attained by the magma can be estimated by applying the Ti-in-zircon thermometer (Watson and Harrison, 2005; Watson et al., 2006) to the Cambro-Ordovician rims of the zircon grains. To this end, we analyzed the low-abundance (5.5%) but interference-free $^{49}$Ti isotope, plus $^{238}$U, $^{207}$Pb and $^{206}$Pb (to ascertain the age), $^{178}$Hf (to calculate Zr/Hf) and $^{92}$Zr and $^{29}$Si (as internal standards) with a LA-ICPMS system, ablating 60 µm diameter spots to get enough sensitivity. One of the main problems with this geothermometer is the sensitivity to inclusions of Ti-bearing minerals in the ablated volume, something that cannot be totally avoided by careful microscopic examination prior to analyses. For this reason, we filtered out our results excluding analyses that yielded Ti > 100 ppm (≈ 994°C) because higher values are indicative of inclusions and Zr/Hf >45 to avoid residual crystals formed from lower T melts (Bea et al., 2006).

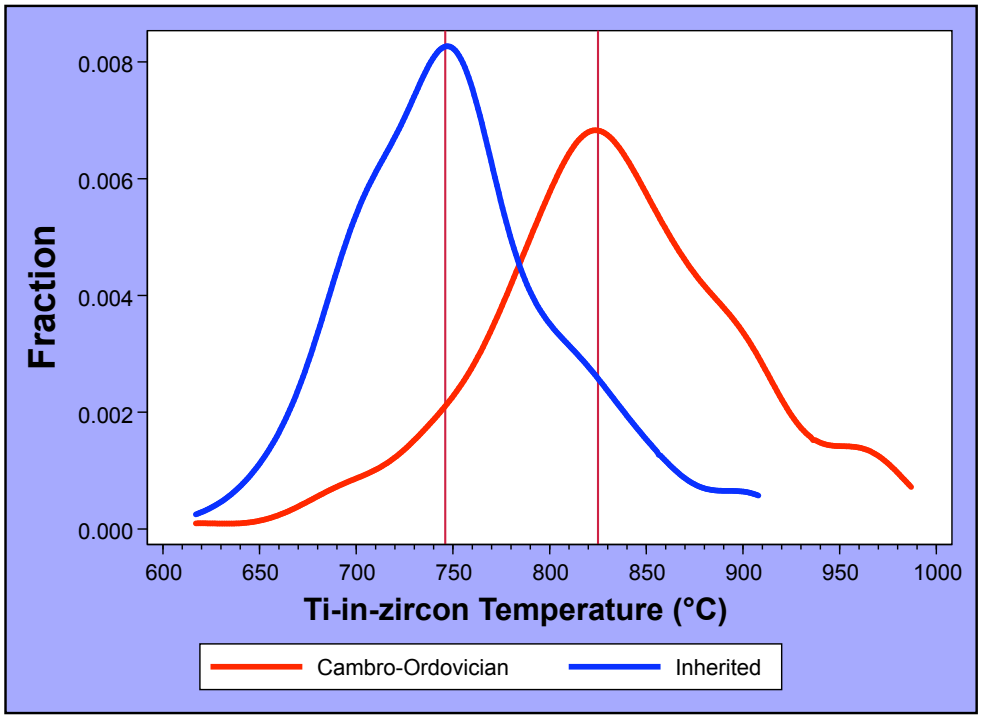


Figure 6.7: Gaussian distribution of the Ti-in-zircon temperature of the Cambro-Ordovician zircons and inherited cores.

With this method we have studied 11 massifs: 2 metavolcanic and 9 metagranitic (Table 6.1). Among these, only one from Guadarrama (La Morcuera metagranite) was included,

the rest of metagranites have zircons with Zr/Hf decreasing from 60 to 20, which strongly suggest that they have undergone magmatic fractionation processes. The results reveal that in all cases the crystallization temperatures of the inherited zircons, which peak at 745°C (Fig. 6.7), are considerably lower than the crystallization temperatures of the neoformed Cambro-Ordovician grains, which peak at 826°C and have some values exceeding 950°C. Remarkably, the average Ti-in-zircon temperature is always higher than the average zircon saturation temperature, except in La Morcuera, where magmatic fractionation almost certainly occurred.

Therefore, if we accept that the Ti-in-zircon temperature represents a minimum estimate of the thermal peak of the magmas (see discussion in section 6.3.3.4), we must conclude that the temperature attained by the Cambro-Ordovician magmas was not lower than 900-950°C, that is, high enough to dissolve all entrained zircons. The reasons why so many of them survived should be, therefore, related to the zircon dissolution kinetics.

Table 6.1: Summary of the Ti-in-zircon and zircon saturation temperatures. $T_{cao}$, Ti-in-zircon temperatures of the Cambro-Ordovician zircons; Tpre-$_{CAO}$, Ti-in-zircon temperatures of pre-Cambro-Ordovician cores; and $T_{Zr}$, zircon saturation temperature.

| Massif | $T_{CAO}$ | $T_{pre\text{-}CAO}$ | $T_{Zr}$ |
|---|---|---|---|
| Vivero | 840 | 767 | 843 |
| Sanabria | 831 | 770 | 843 |
| Viana do Bolo | 828 | 786 | 803 |
| San Sebastian | 844 | 765 | 778 |
| Miranda do Douro | 829 | 754 | 817 |
| Fermoselle | 820 | 744 | 767 |
| Bercimuelle | 827 | 713 | 796 |
| Ledesma | 865 | 795 | 794 |
| Vitigudino | 821 | 732 | 780 |
| Castellanos | 823 | 738 | 802 |
| Morcuera | 814 | 746 | 869 |

### 6.2.3. Zircon dissolution kinetics in the Cambro-Ordovician magmas of Iberia

During partial melting of a rock, the main factors that may hinder or may delay the dissolution of zircon into the melt are: (i) shielding by major minerals, (ii) the small volume of the magma pores surrounding zircon grains, (iii) exceedingly fast heating/ cooling rates.

The first factor, shielding by major minerals, can be easily excluded because the mineral that contains most inclusions of zircon is biotite (Bea, 1996), and this mineral has, necessarily, been involved in anatectic reactions. In the same way, the high mobility of magmas capable of eruption on the Earth's surface implies a total connectivity of melt, excluding therefore the second factor, small volume of melt reservoirs. Accordingly, the most probable hypothesis is that the elevated zircon inheritance was the result of extremely fast heating/cooling rates. To check this hypothesis, we can use the experimental work of Watson (1996).

#### *6.2.3.1. Watson's equation*

Watson's equation (1996, eq. 17) for calculating the instant dissolution rate of spherical zircon crystals is:

$$dr/dt \times 10^{17} = -U([(1.25 \times 1010/r)\exp(-28380/T) + 7.24 \times 108 \exp(-23280/T)]); \quad (2)$$

where:

dr/dt is the instant dissolution rate (cm $s^{-1}$),

r is the radius of a spherical zircon crystal (cm),

T is the absolute temperature (°K),

U is the difference between the current Zr concentration of the melt and the concentration required for zircon saturation according to the experimental model of Watson and Harrison (1983). In partially molten systems, calculating U requires knowledge of the Zr concentration and bulk-rock composition of the protolith, and the volume of the melt reservoirs.

This equation can be used stepwise to calculate the variations of the zircon radius as a function of time for a given heating (or cooling) gradient. This requires inputting: (i) the new T, (ii) the new zircon radius that resulted from the previous step, (iii) the new U value calculated considering the amount of zircon dissolved in the previous step and the change in zircon solubility caused by the variation in T and melt composition.

#### 6.2.3.2. Choice of parameters

The data of Bea et al. (2003) indicate that the 543 Ma Almohalla metagranite contains zircons with maximum dimensions of 300 x 100 x 100 μm and a volume equivalent to a 89 μm radius sphere and an average Zr concentration of 283 ppm. The data of Bandrés et al. (2004) indicate that the Pan-African granitoids of Mérida contain zircon grains with

maximum dimensions of 270 x 100 x 100 µm (a volume equivalent to a 86 µm radius sphere) and have an average concentration of Zr of 125 ppm. This value, however, is probably an underestimate because the samples were analyzed after acid digestion; our XRF data for the same rocks reveal concentrations between 150 and 270 ppm Zr. Additionally, the ca. 600 Ma granites of Morocco, with average XRF Zr concentrations of 227 ppm, contain zircon grains with dimensions most frequently around 150 x 70 x 50 µm (volume equivalent to a 56 µm radius sphere) and only the largest ones reach 300 x 120 x 90 µm (volume equivalent to a 92 µm radius sphere). Neither the zircon grain size, nor the Zr concentration of these rocks are exceptional, but instead are close to what one would expect for common granodiorites and granites.

Mérida, Morocco, and to a lesser extent Almohalla, granitoids can give an idea, at least approximatly, about the grain size distribution of zircon, the Zr concentration and the bulk-rock composition of a potential protolith, needed for the calculations on zircon solution kinetics made in the next section. Therefore, we assumed the following conservative initial conditions:

1. Beginning of melting: 700°C
2. Maximum temperature reached by the magma: 900°C
3. Volume of melt reservoirs: infinite
4. Major elements composition of the melt (to calculate zircon solubility): calculated using the equations of (Winther, 1995) for a granodioritic protolith at 8 kbar and 2% $H_2O$: $SiO_2$ = 70.73; $TiO_2$ = 0.42; $Al_2O_3$ = 14.97; $FeO_{tot.}$ = 1.89; MgO = 0.75; MnO = 0.03; CaO = 1.68; $Na_2O$ = 2.91; $K_2O$ = 4.74.
5. Zr concentration in the protolith = 225 ppm.

**6.2.3.3. Estimation of heating rates**

Figure 6.8 shows the calculated time-temperature coordinates at which spherical zircons with radii of 25 µm, 50 µm, 75 µm, 100 µm, 150 µm and 200 µm will dissolve totally in the melt as a function of the heating rate. The following stands out: Zircons with a spherical radius of 50 µm, i.e. with a volume similar to the population most commonly found in the protolith, would only survive if heating occurred at a rate of 0.1 °C/year or faster. Zircons with a radius of 100 µm, that is with a volume larger than the largest zircons of the protolith, would only survive if the heating rate was 0.025 °C/year or faster. In

summary, the survival of protolith zircons requires less than 10,000 years, probably around 2,000 years, from the beginning of melting (700°C) up to the thermal peak (900°C).

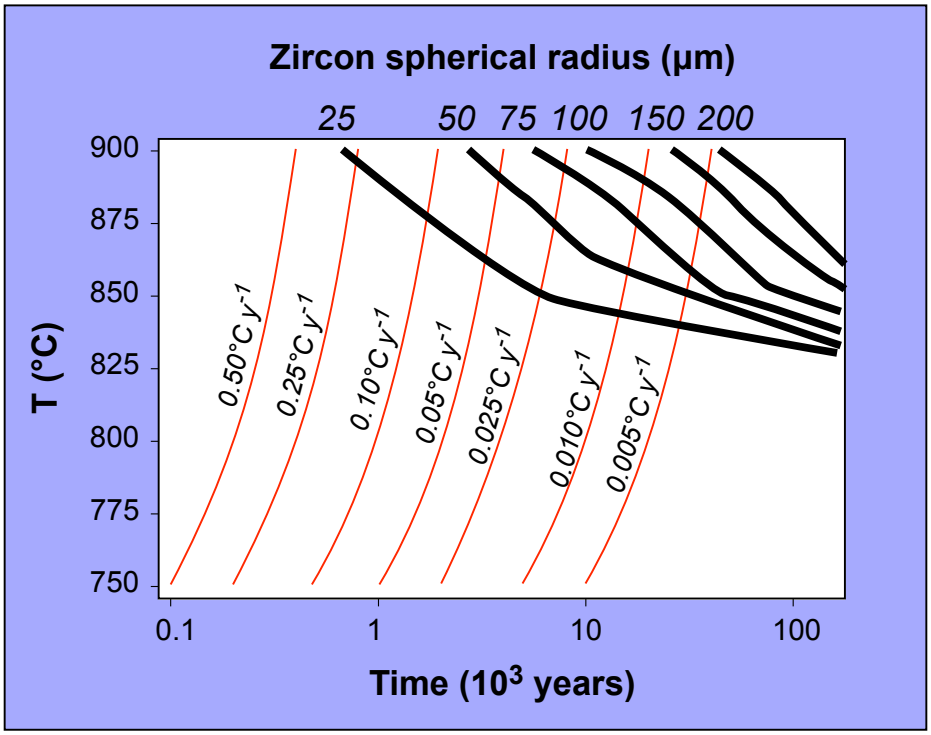


Figure 6.8: Disappearance curves (Black lines) of spherical zircon grains as a function of the heating rate (Red lines) calculated with Watson's equation (1996, eq. 17).

### 6.2.3.4. Estimation of cooling rates

Zircon grains that were partially dissolved during heating will continue dissolving during cooling as long as the melt does not become zircon saturated. Therefore, we calculated again the time-temperature coordinates at which spherical zircon survivors with radii of 20 μm, 40 μm, 60 μm and 80 μm will totally dissolve in the melt as a function of the cooling rate. To estimate the Zr concentration in the melt at 900°C we considered that all protolith zircon grains had a spherical radius of 100 μm and that, during heating, the radius of the dissolving crystal was coupled to the Zr concentration of the melt so that the total concentration of Zr in the system (melt plus crystals) was always equal to that of the protolith: 225 ppm. Results are shown in Fig. 6.9, from which it follows that the survival of 20 μm, 40 μm, 60 μm and 80 μm zircons require linear cooling rates from 900°C to 830°C faster than 0.4°C/year, 0.1 °C year$^{-1}$, 0.05°C/year, and 0.025°C/year, respectively. Since the cooling rates of erupted felsic magmas are often much faster than these (e. g. Harris et al.,

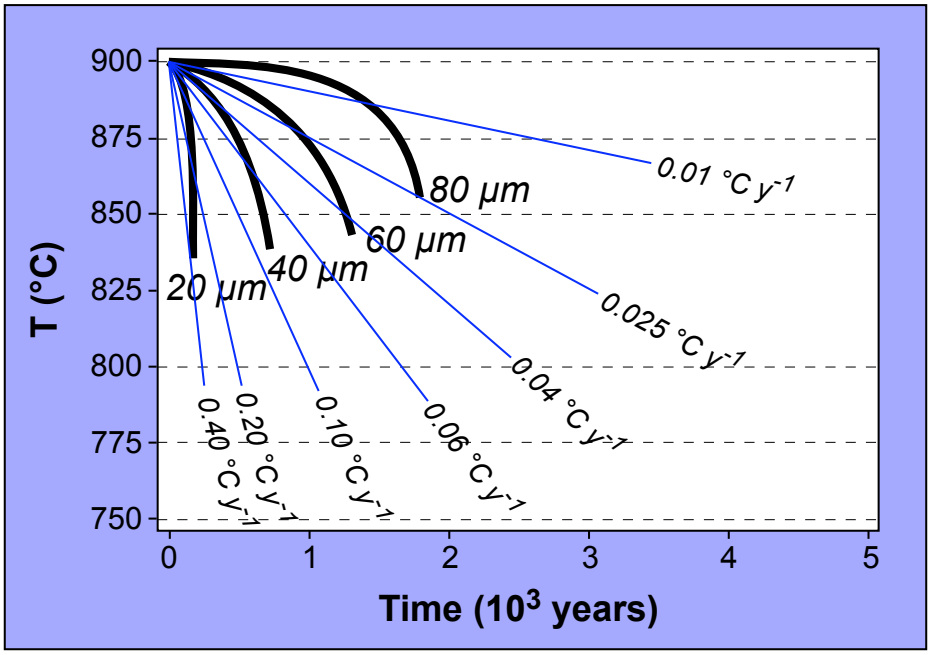


Figure 6.9: Disappearance curves (Black lines) of spherical zircon survivors as a function of the cooling rate (Blue lines) calculated with Watson´s equation.

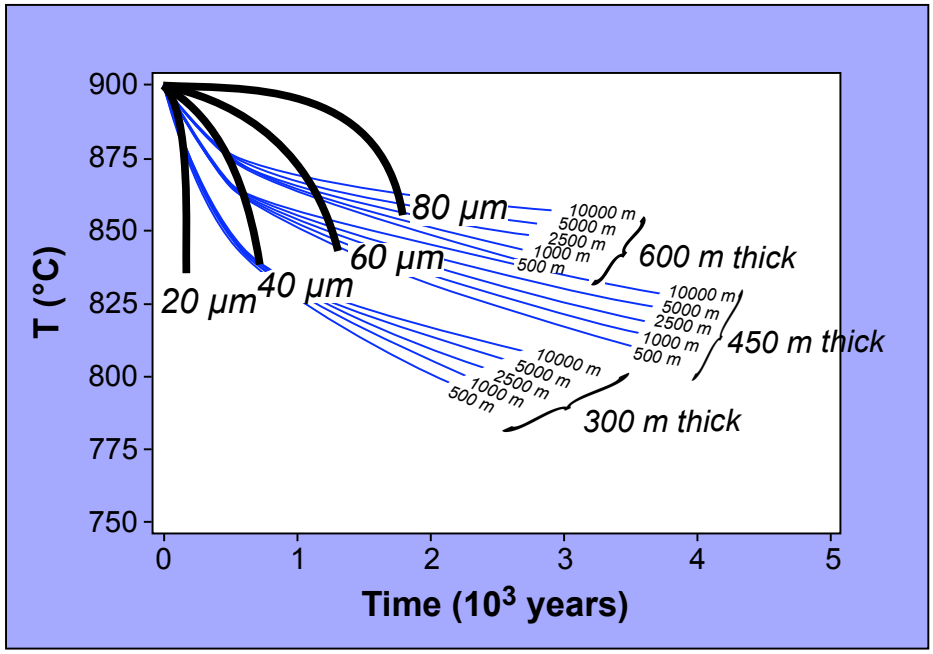


Figure 6.10: Disappearance curves (Black lines) of spherical zircon survivors as a function of the cooling rate calculated as in Fig. 6.9, compared with the 1D cooling curves (Blue lines) of granitic sills of different thickness emplaced at depths from 500 m to 10.000 m.

2002), we can conclude that most survivors would have a chance of cooling with little size reduction if the magma crystallized quickly by being rapidly transported from the melting region to Earth's surface.

The situation, however, is different if the magmas crystallized at depth, such as in the case of the metagranites. According to Iglesias Ponce de Leon and Ribeiro, (1981), González Lodeiro, (1981) and Lancelot et al. (1985), the metagranites of the Ollo de Sapo Formation occur as high-level sills or laccoliths about 300-400 m thick. A similar geometry can be presumed for the metagranites of the north of the Schist-Graywacke Complex Domain except, perhaps, in Guadarrama. To assess the behavior of zircon under these conditions we calculated the 1D cooling paths of granitic sills with the same initial T of 900ºC, different thickness (300 m, 450 m and 600 m) which were emplaced at different depths (500 m, 1000 m, 2500 m, 5000 m and 10000 m), and compared them with the curves of zircon disappearance during cooling as calculated with Watson's equation (1996, eq. 17).

The results of the above are shown in Figure 6.10, from which the following stands out: During cooling of a 300 m thick body, independent of the depth of intrusion (up to 10 km), all zircons with a radius larger than 40 μm will survive. If the sill thickness increases up to 450 m, only zircons with a radius larger than 70 μm would survive. If the sill thickness increases up to 600 m, even the zircons with a radius of 80 μm will disappear unless the sill is emplaced at a depth less than 2 km. It seems, therefore, that the critical parameter governing zircon survival in granite magmas emplaced in the upper crust is the thickness of the magmatic body, with the depth of intrusion seemingly playing a secondary role.

These calculations indicate that the elevated zircon inheritance of the Cambro-Ordovician igneous rocks of Central Iberia resulted from the swiftness of the magmatic pulses, which apparently lasted just a few thousands of years from the beginning of melting to final emplacement. The fact that the fraction of zircons with inherited cores decreases from > 70-80% in all rocks of the Ollo de Sapo Domain and most metagranites of the Schist-Graywacke Complex Domain to about 50% in Guadarrama, can be easily understood because in this area the accumulation of Cambro-Ordovician granitoids occurred at batholitic scale, which undoubtedly resulted in slower cooling rates and, therefore, enhanced zircon dissolution.

### 6.2.3.5. Discussion of results

The applicability of the above calculations to geological systems depends on the validity of the numerical model of zircon dissolution, the proper choice of the initial conditions and model parameters, and the deviations caused by (i) the residence of Zr in minerals other than zircon and (ii) the variable grain size and non-spherical shape of zircon crystals. These circumstances can be evaluated as follows:

Watson's (1996) equation relies on two factors: First, on zircon solubility in silicic melts, which for non-peralkaline liquids depends primarily on the temperature and the melt major-element composition (Watson and Harrison, 1983). Second, on Zr diffusion in the melt, which depends additionally on the $H_2O$ content of the melt (Harrison and Watson, 1983). The equation treats temperature and melt composition as independent variables (the latter for calculating zircon solubility), but it assumes a constant 3% $H_2O$ for the melt. In principle, this assumption might be a serious limitation. In practice, however, it does not critically affect the model. First, because crustal magmas rarely have less than 2-3 % $H_2O$ (e.g., Clemens, 1984; Carrington and Harley, 1996; etc.). Second, because the effects on Zr diffusion mostly occur in the first 2-3% dissolved $H_2O$ (Harrison and Watson, 1983).

It should also be considered that Watson´s equation is a simplification. According to this author, however, it deviates less that 10% from the results of more rigorous, moving boundary, finite-difference methods (Watson, 1996). Therefore, since this deviation is perfectly tolerable for our purposes and nothing indicates that the Cambro-Ordovician magmas of Central Iberia were exceptionally $H_2O$-poor, we can accept the numerical foundation for calculating the curves of zircon disappearance plotted in Figs. 6.8 and 6.9.

The choice of a Pan-African protolith is justified by the dominance of inherited 600-620 Ma ages (Figs. 4.2 and 4.26). Moreover, this choice is not critical because the zircon grain-size distribution and the Zr concentration estimated for this protolith are typical for common granitoids. Only if the protolith had zircons with a spherical radius larger than 150 μm, or a bulk rock concentration of Zr higher than 400-500 ppm, would we expect significant departures from the model. Since such features are mostly limited to peralkaline rocks, and these are unknown among the 600-620 Ma magmatism of north-west Gondwana (e.g. Gasquet et al., 2005), we can safely exclude this possibility. Neither is the major-element composition of the melt critical, because it was necessarily silicic and variations of less than 5% $SiO_2$ have little effect.

In contrast, the determination of the peak temperature reached by the melts is crucial, especially if it were overestimated. The Ti-in-zircon thermometer requires $TiO_2$ activity equal to one (Watson et al., 2006). In the present case, the presence of primary ilmenite and rutile inclusions indicates that such a condition was satisfied. If not, it would have caused underestimation, which would not invalidate our conclusions but, instead, indicate even faster heat-transfer rates. More important, perhaps, is that Ti-in-zircon temperatures can be easily overestimated if there were minute inclusions of Ti-bearing minerals or glass within the analyzed volume. The problem is especially serious when Ti is determined using a LA-ICPMS system such as the one we used here, which to get reasonable $^{49}Ti$ sensitivity requires ablation of craters with a diameter of 60 μm and a depth of about 40 μm. Nevertheless, the careful selection, under the microscope, of the areas to be analyzed and, especially, the nearly Gaussian distribution of the results, notably exempt of outliers (see Fig. 6.7), indicates that inclusions have caused little trouble in the present case. Consequently, we can assume that the maximum temperatures recorded by the Ti-in-zircon thermometer (900-950°C) represent a minimum estimate of the magma's thermal peak, an assumption totally consistent with a large body of experimental data indicating that temperatures of this order are required for generating large volumes of silicic crustal magma in vapor-absent conditions (e.g. Clemens, 2003; and references therein mentioned).

A final consideration is that Watson's equation assumes that all zircon grains are spheres of the same size, and that all Zr resides in zircon. Real rocks, however, have non-spherical zircon crystals, and these are of different shapes and sizes. Real rocks also have a variable fraction of Zr residing in minerals other than zircon such as titanite, amphibole or garnet (e.g., Bea et al., 2006). Certainly, all these differences may affect the zircon dissolution rate. Shapes other than a sphere would increase it, since a sphere represents the smallest surface/volume ratio. Nevertheless, the existence of a large variety of zircon sizes could delay the dissolution of the largest grains because the Zr concentration in the melt would increase rapidly owing to the fast dissolution of the smallest grains. Zircon dissolution would also be delayed if phases other than zircon release Zr to the melt but, on the other hand, it would be accelerated if a Zr-bearing mineral such as garnet appears as a product of melting reactions and extracts Zr from the melt. However, on balance, none of these effects are likely be of great importance and, what is more, they tend to mutually cancel, so we can accept that the results of Watson's equation acceptably match the real situation, i.e. that the magmatic pulses that generated the Central Iberian Cambro-Ordovician magmas were

very fast, probably taking around two thousand years from the beginning of melting until their eruption or emplacement as thin sills or laccoliths at upper crustal levels.

## 6.3. Origin and geodynamic significance of the Cambro-Ordovician magmas of the Central Iberian Zone.

The origin and significance of the Cambro-Ordovician magmatism of Central Iberia has been controversial. Whereas most authors agree that the coeval peralkaline association found in the Ossa Morena and Galicia-Tras-Os-Montes zones was generated in a rifting environment (e.g., Ribeiro 1987; Ribeiro and Floor 1987; Montero et al. 1998; Santos Zalduegui et al. 1995; Montero and Floor 2004a), the peraluminous association, Ollo de Sapo and Guadarrama orthogneisses included, has been interpreted by other authors as evidence of an active margin setting, simply because of the supposed calc-alkaline chemical signature (e.g., Gebauer et al. 1993; Valverde-Vaquero and Dunning 2000; von Raumer et al. 2003; Bea and Navidad 2004).

However, the interpretation of the peraluminous Cambro-Ordovician rocks of Iberia as a product of arc-related magmatism does not find support from chemical, isotopic, and geochronologic or geologic evidence. First, because the link between the geochemical signature and geodynamic setting is not definitive and may be equally explained as a legacy from their protoliths, as proposed for the Cambro-Ordovician rocks of the northern Bohemian Massif by Klimas-August (1990) and Floyd et al. (2000). Second, and more importantly, because the chemical composition of these rocks is not calc-alkaline but alkaline-calcic (Fig. 5.1), and bears no resemblance with the composition of subduction-related igneous rocks with similar $SiO_2$ contents (Figs. 5.2 and 5.3). On the contrary, it shows a striking similarity with the composition of collision-related granites derived from partial melting of old continental materials, which is totally consistent with the high abundance of zircon crystals with old, pre-magmatic, cores. The fact that the most abundant inherited age population, found in all rock types irrespective of their locality is Ediacaran, with a mean age of 605-625 Ma (Figs 4.2 and 4.26) suggests that the source of the Cambro-Ordovician magmas must have been mainly composed of igneous rocks of Ediacaran age, or sediments derived from them. Sr and Nd isotopes point towards the same conclusion. The isotope composition of the metavolcanic rocks and metagranites, with $(^{87}Sr/^{86}Sr)_{init} \approx 0.709\text{-}0.711$, $\varepsilon Nd_{init} \approx -5.8$ to $-3.3$, and $T_{(DM)}$ around 1.8-1.9 Ga, does not reflect the input of juvenile arc-material but indicates derivation from materials with a long

crustal residence. The only exception are two metagranites, Miranda do Douro and San Sebastián, which are isotopically more primitive probably as the result of some hybridization with juvenile mafic magmas similar to the Cambro-Ordovician Carrascal gabbrodiorites at the southern boundary of the Central Iberian Zone (Fig. 6.3). But, as discussed below, this is not an acceptable argument in favor of arc-related magmatism.

The geodynamic environment proposed for the Cambro-Ordovician magmas must be compatible with the following facts:

1. Very fast generation of crustal melts, as revealed by zircon inheritance.
2. Short duration and synchronicity of the magmatism all over the Central Iberian Zone.
3. The lack of coeval regional metamorphism and deformation.

With respect to the first point, it should be considered that the only heating mechanism capable of melting crustal materials at the required rate is the advection of heat by mafic magmas, as revealed by the numerical analysis of Huppert and Sparks (1989). Other crustal-heating mechanisms have much large time-constants, from $10^5$-$10^6$ years for the displacement of isotherms caused by tectonics, burial or erosion (e.g., Chapman and Furlong, 1992; Zen, 1995; Huerta et al., 1999) to 1-3 x $10^7$ years for radiogenic heating (e.g. Vanderhaeghe and Teyssier, 2001; Bea et al., 2003). The analysis of Huppert and Sparks (1989) also predicts that felsic magmas were generated following the intrusion of mafic magmas would have peak-temperatures of 900°C, abundant pre-magmatic crystals and a highly porphyritic character, a set of features found in the Central Iberia Cambro-Ordovician rocks which are difficult to explain by any other mechanism. This gives additional support to the idea that heat for crustal melting was supplied by mantle-derived mafic magmas. Additionally, the imperceptible hybridization between these and the felsic magmas, except perhaps in San Sebastián and Miranda do Douro metagranites suggests that the meltable crustal material directly overlay the mafic intrusions, where the density difference and the quick solidification of the mafic magma at the contact would make mixing unlikely (Huppert and Sparks, 1989). This places the mafic intrusions at the crust-mantle interface. Lastly, the fast melt transport to upper crustal levels points to extensional rather than compressional forces. All these reasons, therefore, strongly suggests that the Central Iberian Cambro-Ordovician magmas were generated during the rifting of a continental crust caused by an upwelling mantle-plume, which likely occurred during the

early Paleozoic fragmentation and dispersal of terranes from the northern margin of west Gondwana (Crowley et al., 2000; Matte, 2001) and ultimately led to the formation of the Iberian microplate. This mechanism would, additionally, explain the synchronicity of the Cambro-Ordovician magmatic event in Central Iberia, the lack of coeval regional metamorphism and deformation, and the short duration of the magmatism throughout this zone.

In this scenario crustal deformation depends to a significant extent on the mechanical coupling between mantle and crust (Burov and Guillou-Frottier, 2005); if the coupling is weak, the concentration of plume-related extension in the mantle lithosphere has little effect on the crust. This might explain the scarcity of contemporaneous deformation. The lack of any Cambro-Ordovician metamorphic imprint in all exposed mid-crustal sections of Central Iberia may also be explained by the swiftness of the generation and emplacement of the crustal magmas. Metamorphism involves conductive heat transfer, an inherently slow process that requires much more than a few thousands of years to be perceptible at a crustal scale. Here, the heat advected to the lower crust by mantle magmas was first consumed by melting reactions and then quickly transported to the uppermost crustal sections by the so-produced magmas causing, therefore, a negligible thermal impact on most of the crustal section above the melting zone except, perhaps, the first lowermost 1000-2000 m.

## 6.4. The age of the Cambro-Ordovician rifting in Iberia

When the geochronological data obtained in this work is combined with all currently available crystallization ages for the Iberian Cambro-Ordovician magmatic rocks (Fig. 6.11, and references therein), the following stands out: In the Central Iberian Zone the oldest crystallization ages of the metavolcanic rocks cluster around 495 Ma, and the youngest around 483 Ma, with the maximum production of magma at 490-485 Ma. After 483 Ma, the magmatic activity was only plutonic and was mostly concentrated in the Guadarrama and Hiendelaencina regions (Fig. 1.8). The exceptions are the 470 Ma San Sebastián metagranite, and the 471 Ma Carrascal massif, spatially associated to the Urra Formation, which is the only Cambro-Ordovician mafic body of Central Iberia (Solá et al. 2005). The last magmatic event in the Central iberian Zone prior to ~495 Ma produced the 543 Ma Almohalla metagranite (Bea et al., 2003) and the 570-580 Ma Merida-Aljucén massif (Bandrés et al. 2004; Talavera et al. 2008a). After ~470 Ma, the magmatic activity

ceased totally until the intrusion of the first Variscan granitoids at ~350 Ma (Montero et al. 2004b).

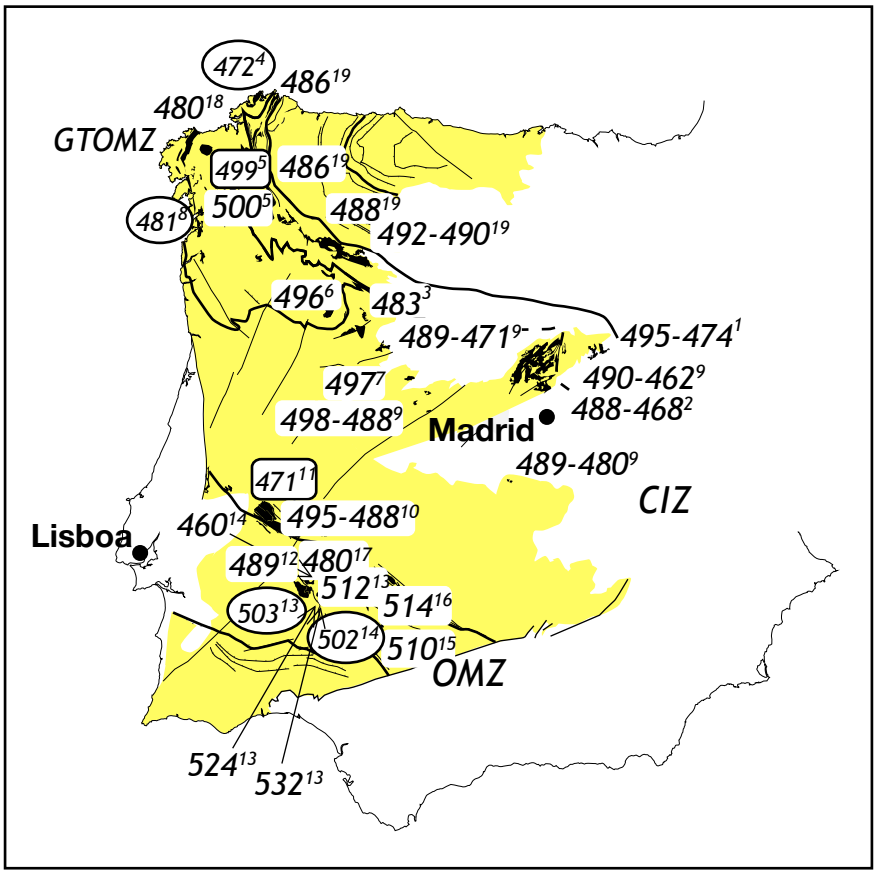


Figure 6.11: Zircon U-Pb crystallization ages of the Iberian Cambro-Ordovician magmas. Numbers within ellipses represent peralkaline rocks. Numbers with squares represent mafic bodies. The rest are felsic peraluminous rocks. Superscripts represent data sources: 1, Montero et al., 2007*; 2, Valverde-Vaquero and Dunning, 2000; 3, Bea et al., 2006*; 4, Valverde-Vaquero et al., 2005; 5, Abati et al., 1999; 6, Dallmeyer and Quesada, 1992; 7, Bea et al., 2009*; 8, Montero et al., 2008; 9, unpublished data of this thesis; 10, Solá et al., 2008; 11, Solá et al., 2005; 12, Schäfer, 1990; 13, Ochsner, 1993; 14, Montero et al., 2000; 15, Montero et al., 1999; 16, Ordóñez Casado, 1998; 17, Expósito Ramos et al., 2003; 18, Talavera et al., 2008b; 19, **Montero et al., in press***. Note the references with * superscript contain data of this thesis.

In the Ossa Morena Zone, to the south (Fig. 6.11), the Cambro-Ordovician magmatism spanned a longer period than in Central Iberia, from 515 Ma to 460 Ma without a clear maximum of magma production, and with an episode of peralkaline magmatism at

500-505 Ma (Ochsner 1993; Salman 2002). In the Galicia-Tras-os-Montes Zone, to the north (Fig. 6.11), despite the lithologies of the Cambro-Ordovician rocks being similar to Ossa Morena, the crystallization ages are akin to Central Iberia, with the oldest clustering around 500-495 Ma (Dallmeyer and Quesada, 1992 and Abati et al., 1999) and the youngest around 470 Ma (Valverde-Vaquero et al., 2005). Remarkably, the Galician peralkaline rocks have ages from 482 Ma (the Galiñeiro massif, Montero et al., 2008) to 475 Ma (alkaline rhyolites of the Schistose Domain, Valverde-Vaquero et al. 2005). Therefore, they are 20-25 Ma younger than their counterparts in Ossa Morena to the south and, in contrast to that zone, apparently closed the Cambro-Ordovician magmatic cycle.

It follows that in the Central Iberian and Galicia-Tras-os-Montes Zones, the Cambro-Ordovician rifting started at ~500-495 Ma, reached a maximum activity between 495-483 Ma, depending on the particular location, and ceased at ~470 Ma. In Ossa Morena, on the other hand, the situation is not so clear, because there was episodic magmatism throughout the Cambrian. The beginning of the rifting would have occurred after the emplacement of the the 532 Ma Culebrín tonalite, the composition of which is hardly compatible with a rifting environment (Salman, 2002), and rifting must have continued to 500-505 Ma, when the peralkaline magmas crystallized (Fig. 6.11 and references therein). In addition, both the 515-510 Ma and the 460 Ma peraluminous granites were probably generated during the Cambro-Ordovician rifting (Exposito Ramos et al., 2003). Therefore, these dates, 515 Ma to 460 Ma, would mark the minimum duration of the rifting in this region. If so, the extension began before, and was longer, than in the rest of Iberia, which suggests that the Ossa Morena crust overlay a zone of the lithospheric mantle that was particularly active during the Lower Paleozoic extension.

# 7. SUMMARY AND CONCLUSIONS

# 7. SUMMARY AND CONCLUSIONS

## 7.1. Summary and conclusions

The Cambro-Ordovician magmatism of the Central Iberian Zone is concentrated in three NW-SE roughly parallel curved lineaments (Fig.1.1A), two of them in the northern half of the Central Iberian Zone, and the other to the south, at the boundary with the Ossa Morena Zone. From north to south, these three lineaments are:

1. The metavolcanic rocks and metagranites of the Ollo de Sapo Domain.

2. The metagranites and metavolcanic rocks of the northern Schist-Graywacke Complex Domain, which are concentrated in four areas: the Tormes Dome, the northwestern part of the Sierra de Gredos, the Sierra de Guadarrama and the Anatectic Complex of Toledo.

3. The Urra Formation, located in Portugal.

This work has concentrated on the two first lineaments. Its main objectives have been to determine accurately the U-Pb (ion microprobe and LA-ICPMS) and/or Pb-Pb (stepwise sequential evaporation) crystallization ages and Sr and Nd isotope geology of these rocks. From these data, the genesis and geodynamic significance of the Cambro-Ordovician magmatism of Central Iberia is discussed.

| ***Metavolcanic rocks of the Ollo de Sapo Formation*** | |
|---|---|
| Vivero | 486 ± 3 Ma |
| Trives | 486 ± 5 Ma |
| Sanabria | 492 ± 4 Ma (lower metavolcanic rocks)<br>490 ± 2 Ma (upper metavolcanic rocks) |
| Villadepera | 483 ± 4 Ma |
| Hiendelaencina | 495 ± 5 Ma (lower metavolcanic rocks)<br>483 ± 3 Ma (upper metavolcanic rocks) |

From north to south, the average crystallization ages of the metavolcanic rocks of the Ollo de Sapo Formation are:

| ***Metagranites associated with the Ollo de Sapo Formation*** | |
|---|---|
| Viana do Bolo (Covelo) (Sanabria region) | 487 ± 4 Ma |
| San Sebastián (Sanabria region) | 470 ± 3 Ma |
| Miranda do Douro (Villadepera region) | 483 ± 3 Ma |
| Antoñita (Hiendelaencina region) | 474 ± 4 Ma |

| ***Tormes Dome*** | |
|---|---|
| Fermoselle | 486 ± 6 Ma |
| Vitigudino | 489 ± 5 Ma |
| Ledesma | 471 ± 7 Ma |
| ***NW Gredos*** | |
| San Pelayo | 492 ± 4 Ma |
| Castellanos | 498 ± 4 Ma |
| Bercimuelle | 488 ± 3 Ma |
| ***Guadarrama*** | |
| La Cañada | 489 ± 9 Ma |
| La Hoya | 478 ± 7 Ma |
| Santa María de la Alameda | 490 ± 5 Ma *(Estación I)*<br>473 ± 8 Ma *(Estación II)* |
| Vegas de Mature | 476 ± 5 Ma *(melanocratic)*<br>484 ± 6 Ma *(leucocratic)* |
| La Morcuera | 482 ± 8 Ma |
| Buitrago de Lozoya | 481 ± 9 Ma |
| La Berzosa *(metavolcanic)* | 462 ± 11 Ma |
| El Cardoso *(metavolcanic)* | 483 ± 6 Ma |
| Riaza *(metavolcanic)* | 475 ± 5 Ma |
| ***Toledo*** | |
| Polán | 480 ± 8 Ma |
| Mochares | 489 ± 7 Ma |

The average crystallization age of the metagranites spatially associated with the metavolcanic rocks of the Ollo de Sapo Formation, again from north to south, are:

The average crystallization age of the metagranites and metavolcanic rocks of the northern area of the Schist-Graywacke Complex are:

These data reveal that in the Ollo de Sapo Domain, the magmatic activity was synchronous and short lived, except in the Hiendelaencina region where was exceptionally prolonged. In the northwest of the Ollo de Sapo Domain and Sanabria and Villadepera regions, the whole magmatic activity occurred at the same time, between 492 and 483 Ma. After this time, there is only one small igneous body in the Sanabria region, San Sebastián metagranite (470 Ma). In the Hiendelaencina region, there are, at least, two volcanic episodes at 495 and 483 Ma, which occurred before the plutonic activity, at 474 Ma.

In the north of the Schist-Graywacke Complex Domain, the Cambro-Ordovician magmatism began in the Sierra de Gredos, where it took place from 498 Ma to 488 Ma. Apparently, the magmatism ceased in this region at the same time that started in the Tormes Dome (489 Ma to 471 Ma), Toledo (489 Ma to 480 Ma) and Guadarrama, where it occurred almost uninterruptedly from 490 Ma to 462 Ma producing the only batholithic accumulation of Cambro-Ordovician granitoids of Iberia.

All the Cambro-Ordovician igneous rocks of the Ollo de Sapo Domain and the north of the Schist-Graywacke Complex Domain belong to the peraluminous association, as defined by Montero et al. (2008). In these regions no rocks of the peralkaline association have been found so far. The rocks from both domains have comparable major and trace element compositions: they are markedly peraluminous, magnesian and alkaline-calcic (Fig. 5.1) characterized by enrichments in the most incompatible elements with a positive Li anomaly and a negative Sr anomaly (compared to the average continental crust, Fig. 5.2), Th and U are elevated, and REE patterns decrease smoothly from La (100-200 x chondrite) to the HREE (5-15 x chondrite) with a constant negative Eu anomaly (Fig. 5.3). Such a composition is typical of granites derived from crustal materials with little, if any, input of juvenile mantle materials.

In the same way, the metavolcanic rocks and some of the metagranites of both areas also have similar Sr and Nd isotope compositions. The metavolcanic rocks of the Ollo de Sapo Formation (Fig. 5.4 and Table 5.2) cluster around $(^{87}Sr/^{86}Sr)_{490Ma} \approx 0.710$, $\varepsilon Nd_{490Ma} \approx -4.6$, and $T_{(DM)} \approx 1.8$ Ga. Two Ollo de Sapo Formation metagranites, Antoñita and Viana do Bolo, have the same composition but the other two, Miranda do Douro and San Sebastián, are more primitive, with $(^{87}Sr/^{86}Sr)_{490Ma} \approx 0.704$, $T_{(DM)} \approx 1.3$ Ga and variable $\varepsilon Nd_{490Ma}$ which ranges from -3.40 to -1.74 in Miranda do Douro and from 0.2 to 2.1 in San Sebastián (Fig. 5.4). The Sr and Nd isotope composition of the metagranites and metavolcanic rocks from the north of the Schist-Graywacke Complex Domain is also similar to the metavolcanic rocks of the Ollo de Sapo Formation, with $(^{87}Sr/^{86}Sr)_{490Ma} \approx 0.711$, $\varepsilon Nd_{490Ma} \approx -3.6$ to -4.7 and $T_{(DM)} \approx 1.9$. These values support the inference drawn from the major and trace element compositions, that the source rocks from which the Cambro-Ordovician magmas of Central Iberia derived were continental crust with little material contribution from mafic magmas, except in the most primitive metagranites, Miranda do Douro and San Sebastián.

One of the most remarkable features of all the studied rocks is the anomalously elevated proportion of zircons with inherited cores, between 70 and 80%, on occasions up to nearly 100% in the Ollo de Sapo Domain, and between 50 and 90% in the north of the Schist-Graywacke Complex Domain. The age distribution of the inherited cores reveals a vast preponderance of Ediacaran components, though there are some differences between the two domains. In both there are: (i) a 605-625 Ma population, which is more abundant in the Ollo de Sapo Domain; (ii) a Cryogenian (650-700 Ma) population; (iii) a Tonian (850-900) population; (iv) an Orosirian (1900-2000 Ma) population, which is more abundant in the Ollo de Sapo Domain; (v) a Neoarchean population; and (vi) a Mesoarchean population. But in the metagranites of the northern Schist-Graywacke Complex Domain we have additionally found two younger populations at 540 Ma and 571 Ma which have not been observed in the Ollo de Sapo Domain. The occurrence of these populations is related to the existence of 540 Ma late Pan-African granitoids such as the Almohalla orthogneiss in the Sierra de Gredos (Bea et al., 2003). The dominance of Ediacaran cores indicates that the magmatic source was dominated by igneous rocks of this age, or immature sediments derived from them. The isotopic composition of the Cambro-Ordovician rocks of Central Iberia is compatible with them being derived from late-Pan-African rocks similar to the ones currently found in the Moroccan Anti-Atlas.

The high proportion of inherited cores was maintained despite the fact that the peak temperature of the magmas, estimated with the Ti-in-zircon geothermometer (Watson and Harrison, 2005; Watson et al., 2006) at 826ºC and some values exceeding the 950ºC, surpassed the rock's zircon saturation temperature, estimated with Watson and Harrison (1983) model at 815ºC. Therefore, according to the calculations of heating and cooling rates estimated with Watson's equation for the kinetics of zircon dissolution (Watson, 1996), abnormally elevated zircon inheritance of the Central Iberia can be explained by swift magmatic pulses, which lasted just a few thousands of years from the beginning of melting to final emplacement and solidification.

The Cambro-Ordovician magmatism of Central Iberia is not a product of arc-related magmatism as has been repeatedly suggested solely because of its supposedly "calc-alkaline" signature. Our data reveal that neither the chemical nor the isotopic composition of these rocks bears any resemblance to the composition of subduction-related igneous rocks with similar $SiO_2$ contents but are, instead, akin to collision-related granites derived from partial melting of old continental materials. This is totally consistent with the high abundance of zircon crystals with old pre-magmatic cores.

The very fast rate of generation of crustal melts revealed by zircon inheritance can only be produced by advective heating caused by mafic magmas. Additionally, the imperceptible hybridization between these and the felsic magmas, except perhaps in San Sebastián and Miranda do Douro metagranites, suggests that the meltable crustal material just overlay the mafic intrusions, where the density difference and the quenching of the mafic magma at the contact would make mixing unlikely (Huppert and Sparks, 1989). This places the mafic intrusions at the crust-mantle interface. Lastly, the fast melt transport to upper crustal levels points to extensional rather than compressional forces. All these reasons, therefore, strongly suggest that the Central Iberian Cambro-Ordovician magmas were generated during rifting of a continental crust caused by an upwelling mantle-plume, which likely occurred during the early Paleozoic fragmentation and dispersal of terranes from the northern margin of west Gondwana (Crowley et al., 2000; Matte, 2001) and ultimately led to the formation of the Iberian microplate. This mechanism would, additionally, explain the synchronicity of the Cambro-Ordovician magmatic event in Central Iberia, the lack of coeval regional metamorphism and deformation, and the short duration of the magmatism throughout this zone.

Finally, when our data are combined with all the available geochronological data from the Central Iberian, Galicia Tras-os-Montes and Ossa Morena Zones, it is possible to determine the timing of the Cambro-Ordovician rifting in Iberia. In Central Iberia and Galicia Tras-os-Montes it started at approximately 500-495 Ma, reached a maximum between 495-483 Ma, depending on the particular area, and finished at approximately 470 Ma. In the Ossa Morena Zone, however, the situation is not so clear because there were many different magmatic episodes during the Cambrian. Our estimate is that 515 Ma to 460 Ma would mark the minimum duration of the Ossa Morena rifting so that in this region the extension started before and was more prolonged than in the rest of Iberia.

## 7.2. Conclusiones

El magmatismo Cambro-Ordovícico de la Zona Centroibérica se concentra en tres bandas curvadas y casi paralelas, con dirección NW-SE (Fig. 1.1A). Dos de ellas se localizan en la mitad norte de la Zona Centroibérica y la tercera se localiza en el sur, en el límite con la Zona de Ossa Morena. De norte a sur, estas tres bandas son:

1. Las rocas metavolcánicas y los metagranitos del Dominio de Ollo de Sapo.

2. Los rocas metavolcánicas y los metagranitos del norte del Domino del Complejo Esquito-Grauváquico, que se localizan en cuatro áreas: en el Domo del Tormes, en el noroeste de la Sierra de Gredos, en la Sierra de Guadarrama y en el Complejo Anatéctico de Toledo.

3. La Formación Urra, situada en Portugal.

Esta tesis se ha concentrado en las dos primeras bandas y sus principales objetivos han sido la determinación precisa de las edades de cristalización U-Pb por microsonda iónica y ablación láser, y/o Pb-Pb por evaporación secuencial, y el estudio de la geología isotópica de Sr y Nd. A partir de estos datos, se ha discutido la posible génesis y el significado geodinámico del magmatismo Cambro-Ordovícico de la Zona Centroibérica.

De norte a sur, las edades de cristalización de las rocas metavolcánicas de la Formación Ollo de Sapo son:

| ***Rocas metavolcánicas de la Formación Ollo de Sapo*** | |
|---|---|
| Vivero | 486 ± 3 Ma |
| Trives | 486 ± 5 Ma |
| Sanabria | 492 ± 4 Ma (Rocas metavolcánicas inferiores)<br>490 ± 2 Ma (Rocas metavolcánicas superiores) |
| Villadepera | 483 ± 4 Ma |
| Hiendelaencina | 495 ± 5 Ma (Rocas metavolcánicas inferiores)<br>483 ± 3 Ma (Rocas metavolcánicas superiores) |

De norte a sur, las edades de cristalización de los metagranitos asociados espacialmente a las rocas metavolcánicas de la Formación Ollo de Sapo son:

| ***Metagranitos asociados a la Formación Ollo de Sapo*** | |
|---|---|
| Viana do Bolo (Covelo) (Región de Sanabria) | 487 ± 4 Ma |
| San Sebastián (Región de Sanabria) | 470 ± 3 Ma |
| Miranda do Douro (Región de Villadepera) | 483 ± 3 Ma |
| Antoñita (Región de Hiendelaencina) | 474 ± 4 Ma |

Las edades de cristalización de los metagranitos y las rocas metavolcánicas de la zona norte del Dominio del Complejo Esquisto-Grauváquico son:

| ***Domo del Tormes*** | |
|---|---|
| Fermoselle | 486 ± 6 Ma |
| Vitigudino | 489 ± 5 Ma |
| Ledesma | 471 ± 7 Ma |
| ***Noroeste de Gredos*** | |
| San Pelayo | 492 ± 4 Ma |
| Castellanos | 498 ± 4 Ma |
| Bercimuelle | 488 ± 3 Ma |
| ***Guadarrama*** | |
| La Cañada | 489 ± 9 Ma |
| La Hoya | 478 ± 7 Ma |
| Santa María de la Alameda | 490 ± 5 Ma *(Estación I)*<br>473 ± 8 Ma *(Estación II)* |
| Vegas de Mature | 476 ± 5 Ma *(melanocrático)*<br>484 ± 6 Ma *(leucocrático)* |
| La Morcuera | 482 ± 8 Ma |
| Buitrago de Lozoya | 481 ± 9 Ma |
| La Berzosa *(Rocas metavolcánicas)* | 462 ± 11 Ma |
| El Cardoso *(Rocas metavolcánicas)* | 483 ± 6 Ma |
| Riaza *(Rocas metavolcánicas)* | 475 ± 5 Ma |
| ***Toledo*** | |
| Polán | 480 ± 8 Ma |
| Mochares | 489 ± 7 Ma |

Estos datos revelan que la actividad magmática en el Dominio de Ollo de Sapo fue sincrónica y de corta duración, excepto en la región de Hiendelaencina donde fue excepcionalmente larga. En el noroeste del Dominio de Ollo de Sapo y en las regiones de Sanabria y Villadepera, la actividad magmática ocurrió al mismo tiempo, entre los 492 y los 483 Ma. Después de este momento, no se observa actividad magmática en estas áreas salvo un pequeño cuerpo ígneo en la región de Sanabria, el metagranito de San Sebastián (470 Ma). En la región de Hiendelaencina, se observan, al menos, dos episodios volcánicos a 495 y a 483 Ma que ocurrieron antes de la actividad plutónica que se produjo a los 474 Ma.

En el norte del Dominio del Complejo Esquito-Grauváquico, el magmatismo Cambro-Ordovícico comienzó en la Sierra de Gredos a los 498 y terminó a los 488 Ma. Aparentemente, el magmatismo cesa en esta región al mismo tiempo que comienza en el Domo del Tormes (entre los 489 y los 471 Ma), Toledo (entre los 489 y los 480 Ma) y Guadarrama, donde tuvo lugar casi ininterrumpidamente desde los 490 a los 462 Ma generando la única acumulación de granitoides Cambro-Ordovícicos en Iberia con dimensiones batolíticas.

Todas las rocas ígneas Cambro-Ordovícicas del Dominio de Ollo de Sapo y del norte del Dominio del Complejo Esquito-Grauváquico pertenecen a la asociación peraluminosa definida por Montero et al. (2008). En estas regiones no se han encontrado rocas de la asociación peralcalina. La composición de elementos mayores y trazas rocas de las rocas de ambos dominios es similar: son marcadamente peraluminosas, magnesianas y alcalino-cálcicas (Fig. 5.1) caracterizadas por un enriquecimiento en los elementos más incompatibles con una anomalía positiva de Li y una anomalía negativa de Sr (comparado con la composición media de la corteza continental, Fig. 5.2), un alto contenido de U y Th y un patrón de REE que decrece suavemente desde el La (100-200 x condrito) a las HREE (5-15 x condrito) con una anomalia negativa de Eu (Fig. 5.3). Esta composición es típica de granitos que proceden de materiales corticales antiguos con una pequeña contribución de materiales jóvenes mantélicos.

La composición isotópica de Sr y Nd de las rocas metavolcánicas y los metagranitos de los dos dominios es similar. Las rocas metavolcánicas de la Formación Ollo de Sapo (Fig. 5.4 y Tabla 5.2) tienen un relación $(^{87}Sr/^{86}Sr)_{490Ma} \approx 0.710$, $\varepsilon Nd_{490Ma} \approx -4.6$, y $T_{(DM)} \approx 1.8$ Ga. Dos de los cuatro metagranitos asociados a la Formación Ollo de Sapo, Antoñita y

Viana do Bolo, tienen la misma composición isotópica que las rocas metavolcánicas mientras que los otros dos metagranitos, Miranda do Douro y San Sebastián son más primitivos, con una relación $^{87}Sr/^{86}Sr_{490Ma} \approx 0.704$, $T_{(DM)} \approx 1.3$ Ga y $\varepsilon Nd_{490Ma}$ variable que oscila entre -3.40 y -1.74 en Miranda do Douro y entre 0.2 y 2.1 en San Sebastián (Fig. 5.4). La composición isotópica de Sr y Nd de los metagranitos y las rocas metavolcánicas del norte del Dominio del Complejo Esquito-Grauváquico es similar a la de las rocas metavolcánicas de la Formación Ollo de Sapo, con una relación $(^{87}Sr/^{86}Sr)_{490Ma} \approx 0.711$, un $\varepsilon Nd_{490Ma}$ que oscila entre -3.6 y -4.7 y un $T_{(DM)} \approx 1.9$. Estos valores apoyan la idea, inferida a partir de la composición de elementos mayores y trazas de estas rocas, de que la fuente de los magmas Cambro-Ordovícicos de Iberia Central fue una corteza continental con una pequeña contribución de magmas máficos, excepto en las rocas más primitivas, Miranda do Douro y San Sebastián.

Una de las características más destacadas de las rocas estudiadas es la elevada proporción de circones con núcleos heredados, que oscila entre un 70 y un 80%, llegando, en ocasiones, a alcanzar el 100 % en el Dominio del Ollo de Sapo, y entre un 50 y un 90 % en el norte del Dominio del Complejo Esquisto-Grauváquico. La distribución de edades de los núcleos heredados pone de manifiesto el predominio de un componente Ediacariense, aunque existen diferencias entre los dos dominios. Ambos tienen: (i) una población de 605-625 Ma, que es más abundante en el Dominio del Ollo de Sapo; (ii) una población Criogeniense (650-700 Ma); (iii) una población Toniense (850-900); (iv) una población Orosiriense (1900-2000 Ma), que es más abundante en el Dominio del Ollo de Sapo; (v) una población Neoarcaica; y (vi) una población Mesoarcaica. Pero en los metagranitos del norte del Dominio del Complejo Esquisto-Grauváquico además se han observado dos poblaciones más jóvenes a 540 y a 571 Ma, que no se han encontrado en el Dominio de Ollo de Sapo. La presencia de estas poblaciones se ha relacionado con la existencia de granitoides Panafricanos como el ortogneis de la Almohalla de la Sierra de Gredos (Bea et al., 2003). La abundancia de núcleos Ediacarienses indica que la fuente magmática estaba compuesta en gran parte por rocas de esta edad o sedimentos inmaduros derivados de ellas. La composición isotópica de las rocas Cambro-Ordovícicas de Iberia Central es compatible con aquellas que han sido derivadas de rocas Panafricanas similares a las que actualmente se encuentran en el Anti-Atlas marroquí.

Una alta proporción de núcleos heredados sobrevivió a pesar de que el pico de temperatura de los magmas, estimada con el geotermómetro de Ti en circón (Watson y

Harrison, 2005; Watson et al., 2006) a 826ºC, excediendo algunos valores los 950ºC, superó la temperatura de saturación de circón en la roca, estimada con el modelo de Watson y Harrison (1983) a 815ºC. Por tanto, de acuerdo con los cálculos de los gradientes de calentamiento y enfriamiento estimados a partir de la ecuación de Watson aplicada a la cinética de disolución de circón (Watson, 1996), la elevada proporción de núcleos heredados de Iberia Central puede explicarse a partir de la existencia de pulsos magmáticos rápidos, que tuvieron una duración de apenas unos pocos miles de años desde el comienzo de la fusión hasta su emplazamiento final y su solidificación.

El magmatismo Cambro-Ordovícico de Iberia Central no es el producto de un magmatismo de arco como se ha sugerido, en repetidas ocasiones, apoyándose en su supuesta signatura "calcoalcalina". Nuestros datos revelan que la composición química e isotópica de estas rocas no se parece a la composición de las rocas ígneas de ambientes de subducción con contenidos similares de $SiO_2$, sino a la composición de granitos de colisión derivados por fusión parcial de materiales continentales antiguos. Esto es compatible con la elevada proporción de circones con núcleos pre-magmáticos antiguos.

La herencia de estos circones apunta hacia una rápida generación de fundidos corticales que sólo pueden producirse por la transferencia de calor procedente de magmas máficos. Además, la inapreciable hibridación entre los magmas máficos y los félsicos, excepto quizá en los metagranitos de San Sebastián y Miranda do Douro, sugieren que el material cortical fértil estaba justo a techo de estas intrusiones máficas, siendo la mezcla entre ambos poco probable debido a la diferencia de densidad y a la rápida solidificación de los magmas máficos (Huppert y Sparks, 1989). El lugar dónde se sitúan las intrusiones máficas se localiza en la interfase corteza-manto. Por último, el rápido transporte del fundido hasta niveles de la corteza superior indican la existencia de fuerzas extensionales y no compresivas. Por tanto, todas estas razones sugieren que los magmas Cambro-Ordovícicos de Iberia Central se generaron durante el rifting de una corteza continental producida durante el ascenso de una pluma mantélica, que probablemente ocurrió durante la fragmentación y la dispersión de terrenos en el margen norte del oeste de Gondwana durante Paleozoico Inferior (Crowley et al., 2000; Matte, 2001) y que llevó a la formación de la microplaca Iberia. Este mecanismo además podría explicar el sincronismo del evento magmático Cambro-Ordovícico, la ausencia de metamorfismo regional y deformación contemporáneo y la corta duración del magmatismo a lo largo de esta zona.

Por último, si se combinan los datos de esta tesis con los datos geocronológicos disponibles de la Zonas Centroibérica, Galicia Tras-os-Montes y Ossa Morena, es posible determinar la duración del rifting Cambro-Ordovícico en Iberia. En Iberia Central y en Galicia Tras-os-Montes, comenzó aproximadamente a 500-495 Ma, alcanzando su máximo entre los 495-483 Ma, dependiendo de la zona en particular, y terminó aproximadamente a 470 Ma. En la zona de Ossa-Morena, la situación no es tan clara porque se observan diferentes episodios magmáticos durante el Cámbrico. Nuestras estimaciones señalan que la duración mínima del rifting en Ossa Morena sería de unos 55 Ma, comenzando a 515 Ma y finalizando a 460 Ma. Por lo tanto, en esta región la extensión comenzó antes y duró algo más que en el resto de Iberia.

# REFERENCES

# REFERENCES

Abati, J., Dunning, G.R., Arenas, R., Diaz-Garcia, F., Gonzalez-Cuadra, P., Martinez-Catalan, J.R. and Andonaegui, P. (1999). Early Ordovician orogenic event in Galicia (NW Spain): evidence from U-Pb ages in the uppermost unit of the Ordenes Complex. *Earth and Planetary Science Letters* **165**, 213–228.

Álvarez Nava, H., García Casquero, J.L., Gil Toja, A., Hernández Urroz, J., Lorenzo Álvarez, S., López Díaz, F., Mira López, M., Monteserín, V., Nozal, F., Pardo, M., Picart J., Robles, R., Santamaría, J. and Sõle, F.J. (1988). Unidades litoestratigráficas de los materiales precámbrico-cámbricos en la mitad suroriental de la Zona Centro-Ibérica. *II Congreso Geológico de España* **1**, 19–22.

Álvaro, M., Apalategui, O., Baena, J., Balcells, R., Barnolas, A., Barrera, J.L., Bellido, F., Cueto, L.A., Díaz de Neira, A., Elízaga, E., Fernández-Gianotti, J.R., Ferreiro, E., Gabaldón, , García-Sansegundo, J., Gómez, J.A., Heredia, N., Hernández-Urroz, J., Hernández-Samaniego, A., Lendínez, A., Leyva, F., López-Olmedo, F.L., Lorenzo, S., Martín, L., Martín, D., Martín-Serrano, A., Matas, J., Monterserín, V., Nozal, F., Olive, A., Ortega, E., Piles, E., Ramírez, J.I., Robador, A., Roldán, F., Rodríguez, L.R., Ruiz, P., Ruiz, M.T., Sánchez-Carretero, R. and Teixell, A. (1994). *Mapa geológico de la Península Ibérica, Baleares y Canarias.* Escala 1:1.000.000. Instituto Tecnológico Geominero de España.

Anthonioz, M. and Ferragne, A. (1967). Sur la présence d'orthogneiss en Galice moyenne (Nord-Ouest de l'Espagne). *Comptes Rendus de l'Academie des Sciences de Paris* **265**, 848–851.

Arenas, R., Farias, ,P. Gallastegui, G., Gil Ibarguchi, J.I., González Lodeiro, F., Klein, E., Marquínez, J., Martín Parra, L.M., Martínez Catalán, J.R., Ortega, E., Pablo Maciá, J.G.d., Peinado, M. and Rodríguez-Fernández, L.R. (1988). Características geológicas y significado de los dominios que componen la Zona de Galicia-Trás-os-Montes. *II Congreso Geológico de España* **1**, 75–84.

Arias, D., Farias, P. and Marcos, A. (2002). Estratigrafía y estructura del Antiforme del Ollo de Sapo en el área de Viana do Bolo-A Gudiña (Provincia de Orense, NO de España): nuevos datos sobre la posición estratigráfica de la Formación porfiroide Ollo de Sapo. *Trabajos de Geología* **23**, 9–19.

Asrat, A., Barbey P., Ludden, J.N., Reisberg, L., Gleizes, G. and Ayalew, D. (2004). Petrology and Isotope Geochemistry of the Pan-African Negash Pluton, Northern Ethiopia: Mafic-Felsic Magma Interactions during the construction of shallow-level calc-alkaline plutons. *Journal of Petrology* **45**, 1147–1179.

Azor, A., González Lodeiro, F. and Simancas, F. (1994). Tectonic evolution of the boundary between the Central Iberian and Ossa-Morena Zones (Variscan belt, southwest Spain. *Tectonics* **13**, 45–61.

Bandrés, A., Eguíluz, L., Pin, C., Paquette, J.L., Ordóñez, B., Le Févre, B., Ortega, L.A. and Gil Ibarguchi, I. (2004). The northern Ossa-Morena Cadomian batholith (Iberian Massif): magmatic arc origin and early evolution. *International Journal of Earth Sciences* **93**, 860–885.

Barbey, P., Cheilletz, A. and Laumonier, B. (2001). The Canigou orthogneisses (Eastern Pyrenees, France, Spain): an early Ordovician rapakivi granite laccolith and its contact aureole. *Comptes Rendus Hebdomadaires de l'Academie des Sciences s. II Fascicule a Sciences de La Terre et des Planetes* **332**, 129–136.

Bard, J., Capdevila, R. and Matte, P. (1970). Les grands traits stratigraphiques, tectoniques, métamorphiques et plutoniques des Sierras de Gredos et de Guadarrama (Espagne centrale). *Comptes Rendus de l'Academie des Sciences* s. *D* **270**, 2630–2633.

Bea, F., Ibarra, I. and Pereira, M.D. (1990). Migmatización metatexítica y fenómenos anatécticos en la Formación Almohalla, Complejo Anatéctico de la Peña Negra. *Boletín Geológico y Minero* **101-102**, 187–209.

Bea, F. (1996). Residence of REE, Y, Th and U in granites and crustal protoliths: implications for the chemistry of crustal melts. *Journal of Petrology* **37**, 521–552.

Bea, F. and Montero, P. (1999). Behavior of accessory phases and redistribution of Zr, REE, Y, Th and U during metamorphism and partial melting of metapelites in the lower crust: an example from the Kinzigite Formation of Ivrea-Verbano, NW Italy. *Geochimica et Cosmochimica Acta* **63**, 1133–1153.

Bea, F., Montero, P. and Zinger, T. (2003). The Nature and Origin of the Granite Source Layer of Central Iberia: evidence from Trace Element, Sr and Nd Isotopes and Zircon Age Patterns. *Journal of Geology* **111**, 579–595.

Bea, F. and Navidad, M. (2004). El magmatismo prevarisco. In: Vera, J.A. (ed.) *Geología de España*. Sociedad Geológica de España and Instituto Geológico y Minero de España, 92–96.

Bea, F., Montero, P., Talavera, C. and Zinger, T. (2006a) A revised Ordovician age for the oldest magmatism of Central Iberia: U-Pb ion microprobe and LA-ICPMS dating of the Miranda do Douro orthogneiss. *Geologica Acta* **4**, 395–401.

Bea, F., Montero, P. and Ortega, M. (2006b). A LA-ICPMS evaluation of Zr reservoirs in common crustal rocks: implications for Zr and Hf geochemistry and zircon-forming processes. *Canadian Mineralogist* **44**, 693–714.

Bea, F., Montero, P., Gonzalez Lodeiro, F. and Talavera, C. (2007). Zircon inheritance reveals exceptionally fast crustal magma generation processes in Central Iberia during the Cambro-Ordovician. *Journal of Petrology* **48**, 2327–2339.

Bea, F., Pesquera, A., Montero, P., Torres-Ruiz, J. and Gil-Crespo, P.P. (in press). Tourmaline $^{40}Ar/^{39}Ar$ chronology of tourmaline-rich rocks from Central Iberia dates the main Variscan deformation phases. *Geologica Acta*

Bernardo de Sousa, M. (1984). Consideraçoes sobre a estratigrafia do Complexo Xisto-Grauváquico (CXG) e sua relaçao com o Paleozóico Inferior. *Cuadernos Geología Ibérica* **9**, 9–36.

Bischoff, L., Lenz, H., Müller, P. and Schmidt, K. (1978). Geochemische und geochronologische Untersuchungen an Metavulkaniten und Orthogneisen der östlichen Sierra de Guadarrama (Spanien). *Neues Jahrbuch fur Geologie und Paläeontologie Abhandlungen* **155**, 275–299.

Blatrix, P. and Burg, J. (1981). $^{40}Ar/^{39}Ar$ dates from Sierra Morena (Southern Spain): Variscan metamorphism and Cadomian Orogeny. *Neues Jahrbuch fur Mineralogie-Monatshefte* **10**, 470–478.

Bryan, S.E., Ferrari, L., Reiners, P.W., Allen, C.M., Petrone, C.M., Ramos-Rosique, A. and Campbell, I.H. (2008). New insights into crustal contributions to large-volume

rhyolite generation in the Mid-Tertiary Sierra Madre Occidental Province, Mexico, revealed by U-Pb geochronology. *Journal of Petrology* **49**, 47–77.

Bultynck, P. and Soers, E. (1971). Le Silurien supérieur et le Dévonien inférieur de la Sierra de Guadarrama (Espagne Central). *Bulletin de l'Institut Royal des Sciences Naturelles de Belgique* **47**, 1–22.

Burov, E. and Guillou-Frottier, L. (2005). The plume head-continental lithosphere interaction using a tectonically realistic formulation for the lithosphere. *Geophysics Journal International* **161**, 469–490.

Capdevila, R., Matte, P. and Paredes, J. (1971). La nature du Précambrien et ses relations avec le Paleozoïque dans la Sierra Morena centrale (Sud de l'Espagne). *Comptes Rendus de l'Academie des Sciences de Paris* **273**, 1359–1362.

Capote, R. and Fernández Casals, M.J. (1975). Las séries anteordovícicas del Sistema Central. *Boletín Geológico y Minero* **86**, 21–35.

Capote, R., Fernández-Casals, M.J., González Lodeiro, F. and Iglesias Ponce de León, M. (1977). El límite entre las zonas Asturoccidental-Leonesa y Galaico-Castellana en el Sistema Central. *Boletín del Instituto Geológico y Minero de España* **88**, 517–520.

Capote, R., Casquet, C. and Fernández Casals, M.J. (1981). La tectónica Hercínica de cabalgamientos en el Sistema Central. *Cuadernos Geología Ibérica* **7**, 455–469.

Carls, P. (1969). Zur Einstufung des Devons der östlichen Guadarrama Spanien. *Senckenbergiana Lethaea* **50**, 67–78.

Carls, P. (1977). The Silurian-Devonian boundary in northeastern and central Spain. In: *The Silurian-Devonian boundary*, IUGS Series A 5, 143–158.

Carrington da Costa, J. (1950). Noticia sobre uma carta geologica do Buçaco, de Nery Delgado. *Comunicaçoes dos Serviços Geológicos de Portugal (Lisboa)*, 1–27.

Carrington, D. and Harley, S.L. (1996). Cordierite as a monitor of fluid and melt $H_2O$ contents in the lower crust: an experimental calibration. *Geology* **24**, 647–650.

Castro, A., Corretge, L.G., Elbiad, M., Elhmidi, H., Fernández, C. and Douce, A.E. (2000). Experimental Constraints on Hercynian Anatexis in the Iberian Massif, Spain. *Journal of petrology* **41**, 1471–1488.

Castro, A., Douce, A.E., Corretge, L.G., de la Rosa, J.D., El-Biad, M. and El-Hmidi, H. (1999). Origin of peraluminous granites and granodiorites, Iberian massif, Spain: an experimental test of granite petrogenesis. *Contributions to Mineralogy and Petrology* **135**, 255–276.

Chapman, D.S. and Furlong, K. (1992). Thermal state of the continental lower crust. In: Fountain, D.M., Arculus, R. and Kay, R.W. (eds.) *Continental Lower Crust*. Elsevier, 179–199.

Clemens, J.D. (1984). Water contents of silicic to intermediate magmas. *Lithos* **17**, 272–287.

Clemens, J.D. (2003). S-type granitic magmas - petrogenetic issues, models and evidence. *Earth-Science Reviews* **61**, 1–18.

Cortázar, D. (1874). Datos geológicos de las provincias de Zamora y Orense. *Boletín de la Comisión del Mapa Geológico de España* **1**.

Cózar, P. and Rodríguez, S. (1999). Propuesta de nueva nomenclatura para las unidades del Carbonífero Inferior del sector Norte del área del Guadiato (Córdoba). *Boletín Geológico y Minero* **110**, 237–254.

Crowley, Q.G., Floyd, A., Winchester, J.A., Franke, W. and Holland, J.G. (2000). Early Paleozoic rift-related magmatism in Variscan Europe: fragmentation of the Armorican Terrane Assemblage. *Terra Nova* **12**, 171–180.

Delaperriere, E. and Respaut, J. (1995). Un âge ordovicien de l'orthogneiss de la Preste par la méthode d'évaporation directe du plomb sur monozircon remet en question l'existence d'un socle précambrien dans le Massif du Canigou (Pyrénées Orientales, France). *Comptes Rendus de l'Academie des Sciences de Paris s. II* **320**, 1179–1185.

Dallmeyer, R.D. and Quesada, C. (1992). Cadomian vs. Variscan evolution of the Ossa-Morena Zone (SW Iberia): field and $^{40}Ar/^{39}Ar$ mineral age constraints. *Tectonophysics* **216**, 339–364.

Deloule, E., Alexandrov, P., Cheilletz, A., Laumonier, B. and Barbey, P. (2002). In-situ U-Pb zircon ages for Early Ordovician magmatism in the eastern Pyrenees, France: the Canigou orthogneisses. *International Journal of Earth Sciences* **91**, 398–405.

Dias, G., Simoes, P.P., Ferreira, N. and Leterrier, J. (2002). Mantle and crustal sources in the genesis of late-Hercynian granitoids (NW Portugal): geochemical and Sr-Nd isotopic constraints. *Gondwana Research* **5**, 287–305.

Diez Balda, M.A. (1986). *El Complejo Esquisto-Grauwáckico, las series Paleozoicas, y la estructura Hercínica al sur de Salamanca.* Thesis, Universidad de Salamanca, 162 p.

Díez Balda, M.A., Vegas, R. and González Lodeiro, F. (1990). Central-Iberian Zone. Autochthonous Sequences. Structure. In: Dallmeyer, R.D. and Martínez García, E. (eds.) *Pre-Mesozoic Geology of Iberia*. Springer-Verlag, 172–188.

Diez Balda, M.A., Martínez Catalán, J.R. and Ayarza, P. (1995). Syn-collisional extensional collapse parallel to the orogenic trend in a domain of steep tectonics: the Salamanca Detachment Zone (Central Iberian Zone, Spain). *Journal of Structural Geology* **17**, 163–182.

Díez Montes, A. (2006). *La geología del Dominio "Ollo de Sapo" en las comarcas de Sanabria y Terra do Bolo.* Thesis, Universidad de Salamanca and Instituto Geológico y Minero de España, 496 p.

Drot, J. and Matte, P. (1967). Sobre la presencia de capas del Devoniano en el límite de Galicia y León (NW de España). *Notas y Comunicaciones del Instituto Geológico y Minero de España* **93**, 87–92.

Ennih, N. and Liegeois, J. (2001). The Morocan Anti-Atlas: the West Africa craton passive margin with limited Pan-African activity. Implications for the northern limit of the craton. *Precambrian Research* **112**, 289–302.

Ennih, N. and Liegeois, J. (2003). The Morocan Anti-Atlas: the West Africa craton passive margin with limited Pan-African activity. Implications for the northern limit of the craton: reply to comments by E. H. Bouougri. *Precambrian Research* **120**, 185–189.

Escuder Viruete, J., Arenas, R. and Martínez Catalán, J.R. (1994). Tectonothermal evolution associated with Variscan crustal extension in the Tormes gneissic dome (NW Salamanca, Iberian Massif, Spain). *Tectonophysics* **238**, 117–138.

Escuder Viruete, J., Indares, A. and Arenas, R. (2000). P-T paths derived from garnet growth zoning in an extensional setting: an example from the Tormes Gneissic Dome (Iberian Massif, Spain). *Journal of Petrology* **41**, 1488–1518.

Exposito Ramos, I., Simancas, J.F., González Lodeiro, F., Bea, F., Montero, P. and Salman, K. (2003). Metamorphic and deformational imprint on Cambrian-Lower Ordovician rifting in the Ossa-Morena Zone (Iberian Massif, Spain). *Journal of Structural Geology* **25**, 2077–2087.

Farias, P., Gallastegui, G., González-Lodeiro, F., Marquínez, J., Martín-Parra, L.M., Martínez Catalán, J.R., de Pablo Maciá, J.G. and Rodríguez Fernández, L.R. (1987). Aportaciones al conocimiento de la litoestratigrafía y estructura de Galicia Central. *Memorias do Musen e Laboratorio Mineralógico e Geológico, Faculdade de Ciências, Universidade do Porto* **1**, 411–431.

Fernández Casals, M.J. and Capote, R. (1971). Los gneises gl andulares del Guadarrama oriental. *Boletín de la Real Sociedad Española de Historia Natural. Sección Geológica* **69**, 69–80.

Fernández Casals, M.J. (1974). Significado Geotectónico de la Fm Neises de la Morcuera. *Stvdia Geológica Salamanticensia* **7**, 87–106.

Fernández Rodríguez, C. (1991). *Estudio de los procesos de deformación en la Zona de Cizalla de Hiendelaencina (Sistema Central Español)*. Thesis, Universidad Complutense de Madrid, 522 p.

Fernández-Suarez, J., Gutierrez-Alonso, G., Jenner, G. and Tubrett, M.N. (1999, Crustal sources in Lower Palaeozoic rocks from NW Iberia: insights from laser ablation U–Pb ages of detrital zircons. *Journal of the Geological Society* **156**, 1065–1068.

Fernández-Suárez, J., Gutiérrez-Alonso, G., Jenner, G.A. and Turbrett, M. (2000). New ideas on the Proterozoic-Early Paleozoic evolution of NW Iberia: insights from U-Pb detrital zircon ages. *Precambrian Research* **102**,m185–206.

Ferragne, A. (1968). Sur l'existence d'un socle précambrien dans la région de Viana del Bollo (Galice méridionale, Nord-ouest de l'Espagne. *Comptes Rendus de l'Academie des Sciences de Paris* **266**, 2375–2379.

Floyd, A., Winchester, J.A., Seston, R., Kryza, R. and Crowley, Q.G. (2000). Review of geochemical variation in Lower Palaeozoic metabasites from the NE Bohemian Masif: intracratonic rifting and plume-ridge interaction. In: Franke, W. (ed.) *Orogenic Processes: Quantification and Modelling in the Variscan Belt*, 155–174.

Friedl, G., Finger, F., Paquette, J.L., von Quadt, A., McNaughton, N.J. and Fletcher, I.R. (2004). Pre-Variscan geological events in the Austrian part of the Bohemian Massif deduced from U-Pb zircon ages. *International Journal of Earth Sciences* **93**, 802–823.

Frost, B.R., Barnes, C.G., Collins, W.J., Arculus, R.J., Ellis, D.J. and Frost, C.D. (2001). A geochemical classification for granitic rocks. *Journal of Petrology* **42**, 2033–2048.

Gasquet, D., Levresse, G., Cheillez, A., Azizi-Samir, M.R. and Mouttaqi, A. (2005). Contribution to a geodynamic reconstruction of the Anti-Atlas Morocco) during Pan-African times with the emphasis on inversion tectonics and metallogenic activity at the Precambrian-Cambrian transition. *Precambrian Research* **140**, 157–182.

García de Figuerola, L.C. and Franco González, M. (1975). Las formaciones infraordovícicas y el borde de las granodioritas al Este de Guijuelo (Salamanca). *Estudios Geológicos* **31**, 487–500.

García-Alcalde, J.L., Arbizu, M.A., Pardo Alonso, M. and García López, S. (1984). El límite Devónico-Carbonífero en el área de Guadalmez-Santa Eufemia (Provs. de Ciudad Real y Córdoba, Sierra Morena, España). *I Congreso Geológico de España* **1**, 421–430.

García Cacho, L. (1973). *Evolución temporal del metamorfismo y procesos de blastesis sucesiva en el sector oriental del Sistema Central Español.* Thesis, Universidad Complutense de Madrid, 319 p.

García-Hidalgo, J.F. (1985). *Estratigrafía y sedimentología del Alcudiense Superior en los anticlinorios de Ibor y Navezuelas-Robledollano.* Thesis*,* Universidad Complutense de Madrid, 190 p.

Gebauer, D., Martínez-García, E. and Hepburn, J.C. (1993). Geodynamic significance, age and origin of the Ollo de Sapo Augengneiss (NW Iberian Massif, Spain). *Abstracts with Programs - Geological Society of America* **25** (6), 342.

Gilotti, J.A. and McClelland, W.C. (2005). Leucogranites and the Time of Extension in the East Greenland Caledonides. *Journal of Geology* **113**, 399–417.

González Clavijo, E. and Martínez Catalán, J.R. (2002). Stratigraphic record of preorogenic to synorogenic sedimentation and tectonic evolution of imbricate units in the Alcañices synform (northwestern Iberian Massif). In: Martínez Catalán, J.R., Hatcher Jr., R.D., R. Arenas, R. and Díaz García, F. (eds.) *Variscan-Appalachian dynamics: The building of the late Paleozoic basement.* Geological Society of America, Special Paper **364**, 17–35.

González Lodeiro, F., Martínez-Catalán, F., Macaya, J. R. and Álvarez, F. (1988). Sobre la estructura del Antiforme de El Cardoso y el Sinforme de Majaelrayo y su relación con la Falla de Berzosa. *Geogaceta* **4**, 11–13.

González Lodeiro, F. (1980). *Estudio geológico estructural de la terminación oriental de la Sierra del Guadarrama (Sistema Central Español).* Thesis*,* Universidad de Salamanca, 334 p.

González Lodeiro, F. (1981a). La estructura del anticlinorio del "Ollo de Sapo" en la región de Hiendelaencina (extremo oriental del Sistema Central Español): *Cuadernos Geología Ibérica* **7**, 535–545.

González Lodeiro, F. (1981b). Posición de las series infraordovícicas en el extremo oriental del Sistema Central y su correlación. *Cuadernos Laboratorio Xeoloxico de Laxe* **2**, 125–134.

González Lodeiro, F., Díez Balda, M.A. and Vegas, R. (2004). Las deformaciones pre-variscas. In: Vera, J.A. (ed.) *Geología de España*, Sociedad Geológica de España and Instituto Geológico de España, 83.

Govindaraju, K. (1994). Compilation of working values and sample description for 383 geostandards. *Geostandards and Geoanalytical research* **18**, 1-158.

Govindaraju, K., Potts, J., Webb, C. and Watson, J.S. (1994). Report on Whin Sill Dolerite WS-E from England and Pitscurrie Micrograbbro PM-S from Scotland: assessment by one hundred and four international laboratories. *Geostandards Newsletters* **XVIII**, 211–300.

Gutierrez Marco, J.C., Robardet, M., Rábano, I., Sarmiento, G.N., San José Lancha, M.A., Herranz, P. and Pieren Pidal, A. (2002). Ordovician. In: Gibbons, W. and Moreno, T. (eds.) *The Geology of Spain*, Geological Society of London, 31–49.

Gutiérrez-Marco, J. C., Aramburu, C., Arbizu, M., Bernárdez, E., Hacar Rodríguez, M., Méndez-Bedia, I., Montesinos López, R., Rábano, I., Truyols, J. and Villas, E. (1999). Revisión bioestratigráfica de las pizarras del Ordovícico Medio en el noroeste de España (zonas Cantábrica, Asturoccidental-Leonesa y Centroibérica septentrional). *Acta Geológica Hispánica* **34**, 3–87.

Gutiérrez-Marco, J.C. and Robardet, M. (1991). Découverte de la zone à Parakidograptus acuminatus (base du Ll andovery) dans le Silurien du synclinorium de Truchas (Zone Asturo-léonaise, NO de l'Espagne): conséquences stratigraphiques et paléogéographiques au passage Ordovicien-Silurien. *Comptes Rendus de l'Academie des Sciences de Paris* **312**, 729–734.

Hanchar, J.M. and Watson, E.B. (2003). Zircon saturation thermometry. In: Hanchar, J.M. and Hoskin, W.O. (eds.). *Zircon*. *Reviews in Mineralogy 53*. Mineralogical Society of America and Geochemical Sociecty, 89–112.

Harris, A.J.L., Flynn, L., Matias, O. and Rose, W.I. (2002). The thermal stealth flows of Santiaguito dome, Guatemala: implications for the cooling and emplacement of dacitic block-lava flow. *Bulletin of Geological Society of America* **114**, 553–546.

Harrison, T.M. and Watson, E.B. (1983). Kinetics of zircon dissolution and zirconium diffussion in granitic melts of variable water content. *Contributions to Mineralogy and Petrology* **84**, 67–72.

Helbing, H. and Tiepolo, M. (2005). Age determination of Ordovician magmatism in NE Sardinia and its bearing on Variscan basement evolution. *Journal of the Geological Society* **162**, 689–700.

Hernández Sampelayo, P. (1922). *Hierros de Galicia, I.* Memorias del Instituto Geológico y Minero de España IV, 483 p.

Herranz, P., San José, M.A. and Vilas, L. (1977). Ensayo de correlación del Precámbrico entre los Montes de Toledo y el Valle de Matachel. *Estudios Geológicos* **33**, 327–342.

Huerta, A.D., Royden, L.H. and Hodges, K. (1999). The effects of accretion, erosion and radiogenic heat on the metamorphic evolution of collisional orogens. *Journal Metamorphic Geology* **17**, 349–366.

Huppert, H.E. and Sparks, S.J. (1989). The Generation of Granitic Magmas by Intrusion of Basalt into Continental Crust. *Journal of Petrology* **29**, 599–624.

Iglesias Ponce de León, M. and Ribeiro, A. (1981). Position stratigraphique de la formation Ollo de Sapo dans la région de Zamora (Espagne)-Miranda do Douro (Portugal). *Comunicaçoes Servicio Geologico de Portugal* **67**, 141–146.

Julivert, M., Fontboté, J.M., Ribeiro, A. and Nabais-Conde, L.E. (1972). Mapa tectónico de la Península Ibérica y Baleares. Escala: 1:1.000.000. *Memoria explicativa del Instituto Geológico y Minero de España*, **113.**

Klimas-August, K. (1990). Genesis of gneisses and granites from the eastern part of the Izera metamorphic complex in the light of studies on zircons from selected geological profiles. *Geologia Sudetica* **24**, 1–71.

Kober, B. (1987). Single-zircon evaporation combined with $Pb^{+}$ emitter-bedding for $^{207}Pb/^{206}Pb$ age investigations using thermal ion mass spectrometry and implications to zirconology. *Contributions to Mineralogy and Petrology* **96**, 63–71.

Lancelot, J.R., Allegret, A. and Iglesias Ponce de León, M. (1985). Outline of Upper Precambrian and Lower paleozoic evolution of the Iberian Peninsula according to U-Pb dating of zircons. *Earth and Planetary Science Letters* **74**, 325–337.

Linares, E., Pellitero, E. and Saavedra, J. (1987). Primeras edades radimétricas en el área Estanno-Wolframífera de Morille-Martinamor (Centro-Oeste de España). *Boletín Geológico y Minero* **XCVIII-V**, 640–646.

Llopis, N., San José, M.A. y Herranz, P. (1970). Notas sobre una discordancia posiblemente precámbrica al SE de la provincia de Badajoz y sobre la edad de las series paleozoicas circundantes. *Boletín Geológico y Minero* **81**, 586–592.

Lotze, F. (1945). Zur Gliederung der Varisziden der Iberischen Meseta. *Geotektonische Forschungen* **6**, 78–92.

Lotze, F. (1956). Über Sardischen bewegungen in Spanien und ihre Beziehungen zur assyntischen faltung. *Geotektonische Symposium H. Stille*, 129–139.

Macaya, J., González-Lodeiro, F., Martínez-Catalán, J.R. and Álvarez, F. (1991). Continuous deformation, ductile thrusting and backfolding of cover and basament in the Sierra de Guadarrama, Hercynian orogen of Central Spain. *Tectonophysics* **191**, 291–309.

Macpherson, J. (1883). Estudio micrográfico de algunas rocas de la provincia de Zamora: grauwackas cámbricas. In: Puig y Larraz, G. (ed.) *Descripción física y geológica de la provincia de Zamora*, 466–475.

Mamet, B. and Martínez, C. (1981). Late Vissean microfossils of the Las Calderas Bajas limestone (Córdoba, Spain). *Revista Española de Micropaleontología* **13**, 105–118.

Martínez Catalán, J.R. (1985). Estratigrafía y estructura del Domo de Lugo (Sector Oeste de la Zona Asturoccidental-leonesa). *Corpus Geologicum Gallaeciae (2ª Serie)* **2**, 1–291.

Martínez Catalán, J.R. and González Clavijo, E. (2004). Secuencia sinorogénica. In: Vera, J.A. (ed.) *Geología de España*. Sociedad Geológica de España and Instituto Geológico y Minero de España, 75.

Martínez García, E. and Corretgé, G. (1970). Nota sobre la serie metamórfica de Porto-Villavieja (Provincias de Zamora y Orense). *Stvdia Geológica Salamanticensia* **1**, 47–58.

Martínez García, E. (1971). Esquema geológico del Noroeste de la provincia de Zamora. *I Congreso Hispano-Luso-Americano Geología Económico* ***1***, 273–286.

Martínez García, E. (1973). Deformación y Metamorfismo en la zona de Sanabria (Provincias de Zamora, León y Orense, Noroeste de España). *Stvdia Geológica Salamanticensia* **V**, 7–106.

Martínez Poyatos, D., Gutierrez Marco, J.C., Pardo Alonso, M., Rábano, I. and Sarmiento, G. (2004). La secuencia paleozoica postcámbrica. In: Vera, J.A. (ed.) *Geología de España*. Sociedad Geológica de España and Instituto Geológico y Minero de España, 81–83.

Matte, P. (1963). Sur la structure du Paléozoïque de la Sierra de Caurel (NW de l'Espagne). *Compte Rendu Sommaire des séances de la Société Géologique de France,* 243–245.

Matte, P. (1968). La structure de la virgation hercynienne de Galice (Espagne). *Revue de Géologie Alpine* **44**, 1–128.

Matte, P. (2001). The Variscan collage and orogeny (480-290 Ma) and the tectonic definition of the Armorica microplate: a review. *Terra Nova* **13**, 122–128.

Mazur, S., Turniak, K. and Brocker, M. (2004). Neoproterozoic and Cambro-Ordovician magmatism in the Variscan Klodzko Metamorphic Complex (West Sudetes, Pol and): new insights from U/Pb zircon dating. *International Journal of Earth Sciences* **93**, 758–772.

Miller, C.F., McDowell, S.M. and Mapes, R.W. (2003). Hot and cold granites? Implications of zircon saturation temperatures and preservation of inheritance. *Geology* **31**, 529–532.

Montero, P. and Bea, F. (1998). Accurate determination of $^{87}Rb/^{86}Sr$ and $^{143}Sm/^{144}Nd$ ratios by inductively-coupled-plasma mass spectrometry in isotope geoscience: an alternative to isotope dilution analysis. *Analytica Chimica Acta* **358**, 227–233.

Montero, P., Salman, K., Zinger, T. and Bea, F. (1999). Rb-Sr and single-zircon grain $^{207}Pb/^{206}Pb$ chronology of Monesterio granodiorite and related migmatites. Evidence of a late Cambrian melting event in the Ossa Morena zone, Iberian Massif. *Estudios Geológicos* **55**, 3–8.

Montero, P., Salman, K., Bea, F., Azor, A., Expósito Ramos, I., González Lodeiro, F., Martínez Poyatos, D. and Simancas, J.F. (2000). New data on the Geochronology of the Ossa-Morena Zone, Iberian Massif. In: *Variscan-Appalachian dyamics: The building of the Upper Paleozoic basement,* 136–138.

Montero, M. P. and Floor, P. (2004a). Los complejos alcalinos prevariscos (magmatismo del Palezoico Inferior en las unidades basales). In: Vera, J.A. (ed.) *Geología de España*. Sociedad Geológica de España and Instituto Geológico y Minero de España, 149–150.

Montero, P., Bea, F., Zinger, T.F., Scarrow, J.H., Molina, J.F. and Whitehouse, M.J. (2004b). 55 Million Years of Continuous Anatexis in Central Iberia: Single Zircon Dating of the Peña Negra Complex. *Journal of the Geological Society* **161**, 255–264.

Montero, P., Bea, F., González-Lodeiro, F., Talavera, C. and Whitehouse, M. (2007). Zircon crystallization age and protolith history of the metavolcanic rocks and metagranites of the Ollo de Sapo Domain in central Spain. Implications for the Neoproterozoic to Early-Paleozoic evolution of Iberia. *Geological Magazine* **144**, 963–976.

Montero, M.P., Bea, F., Corretge, G., Floor, and Whitehouse, M.J. (in rev.). U-Pb ion microprobe dating and Sr and Nd isotope geology of the Galiñeiro Igneous Complex. A model for the peralkaline/calc-alkaline duality of the Cambro-Ordovician magmatic rocks of Iberia. *Lithos.*

Montero, M.P., Talavera, C., Bea, F., González Lodeiro, F. and Whitehouse, M. (in press). Zircon Geochronology of the Ollo de Sapo Formation and the age of the Cambro-Ordovician rifting in Iberia. *The journal of Geology.*

Navidad, M. (1978). Las series glandulares "Ollo de Sapo" en los sectores nord-occidental y centro-oriental del Macizo Ibérico. *Estudios Geológicos* **34**, 511–528.

Navidad, M. (1979). Las series gl andulares del sector central del Macizo Ibérico (Guadarrama centro-occidental). *Estudios Geológicos* **35**, 31–48.

Navidad, M. and López Ramos, C. (1981). Los ortogneises de "El Vellón-Pedrezuela" (Sistema Central Español). *Estudios Geológicos* **37**, 97–107.

Navidad, M. and Peinado, M. (1981). Ortogneises y metasedimetos de la Formación Infrabasal al Ollo de Sapo (Macizo de Hiendelaencina, Guadarrama Oriental). *Cuadernos Geología Ibérica* **7**, 183–189.

Ochsner, A. (1993). *U-Pb Geochronology of the Upper Proterozoic - Lower Paleozoic Geodynamic Evolution in the Ossa-Morena Zone (SW Iberia): Constraints on the Timing of Cadomian Orogeny.* Thesis, Eidgenössische Technische Hochschule, Zurich, 249 p.

Ordoñez Casado, B. (1998). *Geochronological studies of the Pre-Mesozoic basament of the Iberian Massif: the Ossa-Morena Zone and the Allochthonous Complexes within the Central Iberian Zone.* Thesis, Eidgenössische Technische Hochschule, Zurich, 235 p.

Ortega Gironés, E. and González Lodeiro, F. (1986). La discordancia intra-Alcudiense en el dominio meridional de la Zona Centroibérica. *Breviora Geológica Astúrica* **27**, 27–32.

Ortega, L.A., Pin, C., Menéndez, M. and Gil Ibarguchi, J.I. (2000). Geoquímica isotópica Nd-Sr del gneis de Ollo de Sapo: Implicaciones sobre la formación de corteza continental en el Noroeste de la zona Centroibérica. *Cuadernos Laboratorio Xeoloxico de Laxe* **25**, 273–276.

Palacios, T. (1989). Microfósiles de pared orgánica del Proterozoico Superior (región central de la Península Ibérica). *Memorias del Museo Paleontológico de la Universidad de Zaragoza* **3**, 1–91.

Parga-Pondal, I., Matte, P. and Capdevila, R. (1964). Introduction a la geologie de l'Ollo de Sapo', Formation porphyrode antesilurienne du nord ouest de l'Espagne. *Notas y Comunicaciones del Instituto Geológico y Minero de España* **76**, 119–153.

Pearce, N.J.G., Perkins, W.T., Westgate, J.A., Gorton, M., Jackson, S.E., Neal, C.R. and Chenery, S. (1997). A Compilation of New and Published Major and Trace Element Data for NIST SRM 610 and NIST SRM 612 Glass Reference Materials. *Geostandards Newsletters* **21**, 115–144.

Peinado, M. and Álvaro, M. (1981). Magmatismo pre e intrahercínico en el sector metamórfico de El Escorial (Sistema Central Español). *Cuadernos Geología Ibérica* **7**, 201–216.

Pérez Estaún, A. (1978). Estratigrafía y estructura de la rama Sur de la Zona Asturoccidental-Leonesa. *Memorias del Instituto Geológico y Minero de España* **92**, 1–149.

Pérez-Estaún**,** A., Bea, F., Bastida, F., Marcos, A., Martínez Catalán, J.R., Martínez Poyatos, D., Arenas, R., Díaz García, F., Azor, A., Simancas, J.F. and González-Lodeiro, F. (2004). La cordillera Varisca Europea: El Macizo Ibérico. In: Vera, J.A. (ed.) *Geología de España*. Sociedad Geológica de España and Instituto Geológico y Minero de España, 21–25.

Pieren, A. (2000). *Las sucesiones anteordovícicas de la región oriental de la provincia de Badajoz y área contigua de la de Ciudad Real*. Thesis, Universidad Complutense de Madrid, 379 p.

Priem, H.N.A., Boelrijk, N.A.I.M., Verschure, R.H., Hebeda, E.H. and Verdumen, E.A.T. (1970). Dating events of acid plutonism through the Paleozoic of the Western Iberian Peninsula. *Eclogae Geologica Helvetica* **63**, 255–274.

Puschmann, H. (1967). Zum Problem der Schichtlücken im devon der Sierra Morena (Spanien). *Geologische Rundschau* **56**, 528–542.

Ribeiro, M.L. (1987). Petrogenesis of early Paleozoic peralkaline ryolites from the Macedo de Cavaleiros region (NW de Portugal). *Geologische Rundschau* **76**, 147–168.

Ribeiro, M.L. and Floor, P. (1987). Magmatismo peralcalino no Macizo Hesperico: Sua distribuiçao e significado geodinamico. In Bea, F., Carnicero, A., Gonzalo, J.C., López Plaza, M. and Rodríguez Alonso, M.D. (eds.) *Geología de los granitoides y rocas asociadas del Macizo Hespérico*. Rueda, 211–221.

Riemer, W. (1963). Entwicklung des Paläozoikums in der Südlichen Provinz Lugo (Spanien). *Neues Jahrbuch für Geologie und Paläontologie. Abhandlungen* **117**, 273–285.

Robardet, M. (1981). Late Ordovician tillites in the Iberian Peninsula. In: Hambrey, M.J. and Harlant, W.B. (eds.) *Earth Pre-Pleistocene Glacial Record.* Cambridge University Press, 585–589.

Robles, R. and Álvarez Nava, H. (1988). Los materiales precámbrico-cámbricos del Domo de las Hurdes: Existencia de tres series sedimentarias separadas por discordancias, SO de Salamanca (Zona Centro-Ibérica). *II Congreso Geológico de España* **1**, 185–188.

Rodríguez Alonso, M.D. (1985). El Complejo Esquisto-Grauwáckico y el Paleozoico en el Centro-Oeste Español. *Acta Salamanticensia* **51**, 1–174.

Rodríguez Alonso, M.D., Díez Balda, M.A., Parejón, A., Pereira, A., Liñán, E., López Díaz, F., Moreno, F., Gómez Vintaned, J.A., González Lodeiro, F., Martínez Poyatos, D. and Vegas, R. (2004). La secuencia litoestratigráfica del Neoproterozoico-Cámbrico Inferior. In: Vera, J.A. (ed.) *Geología de España*. Sociedad Geológica de España and Instituto Geológico y Minero de España, 78–81.

Rodríguez, L.**,** Mira, M. and Ortega, E. (1990). Mapa y memoria explicativa de la Hoja nº 833 (Hinojosa del Duque) del Mapa geológico Nacional a escala 1:50.000 (2ª Serie).

Roger, F., Respaut, J., Brunel, M., Matte, P. and Paquette, J.L. (2004). U-Pb dating of Augen orthogneisses from the axial zone of the Montague Noire (Southern of Massif Central): new witness of Ordovician magmatism into the Variscan Belt. *Comptes Rendus Geoscience* **336**, 19–28.

Rowe, M.C., Wolf, J.A., Gardner, J.N., Ramos, F.C., Teasdale, R. and Heikoop, C.E. (2007). Development of a continental volcanic field: petrogenesis of pre-caldera intermediate and silicic rocks and origin of the Bandelier Magmas, Jemez Mountains (New Mexico, USA). *Journal of petrology* **48**, 2063–2091.

Saavedra, J., Pellitero, E., García Sánchez, A. and Fernández Turiel, J.L. (1984). Rasgos petrográficos y geoquímicos de los granitoides y rocas metamórficas. *Estudios Geológicos* **40**, 15–21.

Salman, K. (2002). *Estudio petrológico, geoquímico y geocronológico de los granitoides del área Monesterio-Cala, Zona de Ossa-Morena (Macizo Ibérico).* Thesis, Universidad de Granada, 232 p.

San José, M.A., Pieren, A., García Hidalgo, F.J., Vilas, L., Herranz, P., Peláez, J.R. and Perejón, A. (1990). Ante-Ordovician stratigraphy. In: Dallmeyed, R.D. and Martínez-García, E. (eds.) *Pre-Mesozoic geology of Iberia*. Springer-Verlag, 145–159.

San Miguel de la Cámara, M. and Lobato Díez, M. (1955). Datos sobre la petrografía de los alrededores del Lago de Sanabria en la provincia de Zamora. *Estudios Geológicos* **27-28**, 371–382.

Sánchez García, T., Bellido, F. and Quesada, C. (2003). Geodynamic setting and geochemical signatures of Cambrian_ordovician rift-related igneous rocks (Ossa-Morena Zone, SW Iberia). *Tectonophysics* **365**, 233–255.

Santos Zalduegui, J.F., Schärer, U. and Gil Ibarguchi, L. (1995). Isotope constraints on the age and origin of magmatism and metamorphism in the Malpica-Tuy allochton, Galicia, NW España. *Chemical Geology* **121**, 91–103.

Schäfer, G. (1969). Geologie und Petrographie im östlichen Kastilischen Hauptscheidegebirge (Sierra de Guadarrama, Spanien). *Münsters Forschungen zur Geologie und Paläontologie* **10**, 1–207.

Schäfer, H.J. (1990). *Geochronological Investigations in the Ossa-Morena Zone, SW Spain*. Thesis, Eidgenössische Technische Hochschule, Zurich, 153 p.

Schaltegger, U., Abrecht, J. and Corfu, F. (2003). The Ordovician orogeny in the Alpine basement: constraints from geochronology and geochemisty in the Aar Massif (Central Alps). *Schweizerische Mineralogische und Petrographische Mitteilungen* **83**, 183–195.

Schaltegger, U. and Gebauer, D. (1999). Pre-Alpine geochronology of the Central, Western and Southern Alps. *Schweizerische Mineralogische und Petrographische Mitteilungen* **79**, 79–87.

Schroeder, E. (1930). Das Grenzgebiete von Guadarrama und Hesperichen Ketten (Zentralspanien). *Abhandlungen der Gesellschaft Wissenschagten zu Göttingen, Math.-Phys* **XVI.**

Soers, E. (1972). Stratigraphie et géologie structurale de la partie orientale de la Sierra de Guadarrama (Espagne Centrale). *Stvdia Geológica Salamanticensia* **4**, 7–88.

Sola, A.R., Montero, P., Riberiro, M.L., Neiva, A.M.R., Zinger, T. and Bea, F. (2005). Pb/Pb age of the Carrascal Massif, central Portugal. *Geochimica et Cosmochimica Acta* **69**, A856–A856.

Sola, A.R. (2007). *Relaçoes petrogeoquímicas dos Maciços Graníticos do NE Alentejano.* Thesis, Universidade de Coimbra, 405 p.

Sola, A.R., Pereira, M.F., Williams, I.S., Ribeiro, M.L., Neiva, A.M.R., Montero, P., Bea, F. and Zinger, T. (2008). New insights from U-Pb zircon dating of Early Ordovician magmatism on the northern Gondwana margin: the Urra Formation (SW Iberian Massif, Portugal). *Tectonophysics* **461**, 114–129

Stacey, J.S. and Kramers, J.D. (1975). Approximation of terrestrial lead isotope evolution by a two-stage model. *Earth and Planetary Science Letters* **26**, 207–221.

Steiger, R.H. and Jäger, E. (1977). Subcommision on Geochronology. Convention on the use of decay constants in geo- and cosmochronology. *Earth and Planetary Science Lettters* **36**, 359–362.

Talavera, C., Montero, M.P., Bea, F. and Whitehouse, M. (in press). A revised Ordovician age for the Sisargas orhogneiss, Galicia (Spain). Zircon U-Pb ion-microprobe and LA-ICPMS dating. *Geologica Acta* **6***,* 313-317.

Talavera, C., Montero, P. and Bea, F. (2008). Precise single-zircon Pb-Pb dating reveals that Aljucén (Mérida) is the oldest plutonic body of the Central Iberian Zone. *Geo-Temas* **10**, 249–252.

Vacas, J.M. and Martínez Catalán, J.R. (1987). El sinforme de Alcañices en la transversal de Manzanal del Barco. *Stvdia Geológica Salamanticensia* **24**, 151–175.

Valladares, M.I., Barba, , Colmenero, J.R., Armenteros, I. and Ugidos, J.M. (1998). La sucesión sedimentaria del Precámbrico Superior-Cámbrico Inferior en el sector

dentral de la Zona Centro Ibérica: litoestratigrafía, geoquímica y facies sedimentarias. *Revista de la Sociedad Geológica de España* **11**, 271–283.

Valladares, M.I., Ugidos, J.M., Barba, P. and Colmenero, J.R. (2002a). Contrasting geochemical features of the central Iberia zone shales (Iberian Massif, Spain): implications for the evolution of Neoproterozoic-Lower Cambrian sediments and their sources in other peri-Gondwanan areas. *Tectonophysics* **352**, 121–132.

Valladares, M.I., Barba, P. and Ugidos, J.M. (2002b). Precambrian. In: Gibbons, W. and Moreno, T. (eds.) *The Geology of Spain*. Geological Society of London, 7–16.

Valverde-Vaquero, and Dunning, G.R. (2000). New U-Pb ages for Early Ordovician magmatism in Central Spain. *Journal of the Geological Society* **157**, 15–26.

Valverde-Vaquero, P., Marcos, A., Farias, P. and Gallastegui, G. (2005). U-Pb dating of Ordovician felsic volcanism in the Schistose Domain of the Galicia-Trás-os-Montes Zone near Cabo Ortegal (NW Spain). *Geologica Acta* **3**, 27–37.

Vanderhaeghe, O. and Teyssier, C. (2001). Crustal-scale rheological transitions during late-orogenic collapse. *Tectonophysics* **335**, 211–288.

Vialette, Y., Casquet, C., Fúster, J.M., Ibarrola, E., Navidad, M., Peinado, M. and Villaseca, C. (1987). Geochronological study of orthogneisses from the Sierra de Guadarrama (Spanish Central System). *Neues Jahrbuch für Mineralogie-Monatshefte* **10**, 465–479.

Vidal, G., Jensen, S. and Palacios, T. (1994). Neoproterozoic (Vendian) ichnofossils from Lower Alcudian strata in central Spain. *Geological Magazine* **131**, 169–179.

Villaseca, C., Barbero, L. and Rogers, G. (1998). Crustal origin of Hercynian peraluminous granitic batholiths of Central Spain: petrological, geochemical and isotopic (Sr, Nd) constraints. *Lithos* **43**, 55–79.

von Raumer, J.F., Stampfli, G.M. and Bussy, F. (2003). Gondwana-derived microcontinents — the constituents of the Variscan and Alpine collisional orogens. *Tectonophysics* **365**, 7–22.

Wagner, R.H. and Utting, J. (1967). Sur le terrain houllier de Puertollano (province de Ciudad Real, Espagne). *Comptes Rendus de l'Academie des Sciences de Paris* **264**, 5–8.

Watson, E.B. and Harrison, T.M. (1983). Zircon saturation revisited: temperature and composition effects in a variety of crustal magma types. *Earth and Planetary Science Letters* **64**, 295–304.

Watson, E.B. (1996). Dissolution, growth and survival of zircons during crustal fusion: Kinetic principles, geological models and implications for isotopic inheritance. *Transactions of the Royal Society of Edinburgh: Earth Science* **87**, 43–56.

Watson, E.B. and Harrison, T.M. (2005). Zircon thermometer reveals minimum melting conditions on earliest Earth. *Science* **308**, 841–844.

Watson, E.B., Wark, D. and Thomas, J. (2006). Crystallization thermometers for zircon and rutile. *Contributions to Mineralogy and Petrology* **151**, 413–433.

Whitehouse, M.J., Kamber, B.S. and Moorbath, S. (1999). Age significance of U-Th-Pb zircon data from early Archaean rocks of west Greenl and a reassessment based on combined ion-microprobe and imaging studies. *Chemical Geology* **160**, 201–224.

Wiedenbeck, M., Allé, P., Corfu, F., Griffin, W.L., Meier, M., Oberli, F., von Quadt, A., Roddick, J.C. and Spiegel, W. (1995). Three natural zircon standards for U-Th-Pb Lu-Hf trace element and REE analysis. *Geostandards Newsletter* **19**, 1–23.

Wildberg, H.G., Bischoff, L. and Baumann, A. (1989). U-Pb ages of zircons from meta-igneous and meta-sedimentary rocks of the Sierra de Guadarrama: implications for the Central Iberia crustal evolution. *Contributions to Mineralogy and Petrology* **103**, 253–262.

Winther, K.T. (1995). A model for estimating the composition of partial melts. *Mineralogy and Petrology* **53**, 189–195.

Zeck, H., Wingate, M.T.D., Pooley, G.D. and Ugidos, J.M. (2004). A Sequence of Pan-African and Hercynian Events Recorded in Zircons from an orthogneiss from the Hercynian Belt of Western Central Iberia—an Ion Microprobe U–Pb Study. *Journal of Petrology* **45**, 1613–1629.

Zeck, H., Whitehouse, M.J. and Ugidos, J.M. (2007). 496 ± 3 Ma zircon ion microprobe age for pre-Hercynian granite, Central Iberian Zone, NE Portugal (earlier claimed 618 ± 9 Ma). *Geological Magazine* **144**, 21–31.

Zen, E.A. (1995). Crustal magma generation and low-pressure high-temperature regional metamorphism in an extensional environment; Possible application to the Lachlan Belt, Australia. *American Journal of Science* **295**, 851–874.

# APPENDIX

# 9. APPENDIX

## 9.1. Tables of the geochronological data

### 9.1.1. The Ollo de Sapo Domain

Table 4.2: U-Pb laser ablation results of the Vivero metavolcanic rocks.

| | Element concentration (ppm) | | | Isotope ratios | | | | Ages (Ma) | | | |
|---|---|---|---|---|---|---|---|---|---|---|---|
| **Grain** | **U** | **Th** | **Pb** | **($^{207}Pb/^{206}Pb)_{meas}$** | **σ (%)** | **($^{206}Pb/^{238}U)_{meas}$** | **σ (%)** | **$^{206}Pb/^{238}U$** | **$^{207}Pb/^{235}U$** | **$^{207}Pb/^{206}Pb$** | **($^{206}Pb/^{238}U)_{cor}$** |
| LA014a | 99 | 78 | 11 | 0.06806 | 5.24 | 0.09905 | 2.15 | 609 | 667 | 870 | 603 ± 14 |
| LA018a | 312 | 69 | 122 | 0.16145 | 2.89 | 0.37122 | 1.83 | 2035 | 2260 | 2471 | - |
| LA020a | 377 | 91 | 126 | 0.15277 | 2.54 | 0.31572 | 3.37 | 1769 | 2066 | 2377 | - |
| LA022a | 717 | 529 | 76 | 0.06096 | 6.12 | 0.09677 | 6.06 | 596 | 604 | 638 | 595 ± 38 |
| LA024a | 306 | 50 | 36 | 0.06759 | 4.07 | 0.12088 | 3.8 | 736 | 766 | 856 | 732 ± 30 |
| LA026a | 277 | 55 | 21 | 0.05865 | 4.48 | 0.07832 | 1.7 | 486 | 498 | 554 | 485 ± 9 |
| LA036a | 319 | 37 | 24 | 0.05907 | 4.75 | 0.07775 | 2.63 | 483 | 498 | 570 | 481 ± 13 |
| LA038a | 221 | 129 | 24 | 0.06196 | 3.2 | 0.10014 | 2.87 | 615 | 628 | 673 | 614 ± 19 |
| LA044a | 353 | 364 | 73 | 0.07441 | 2.75 | 0.17422 | 2.6 | 1035 | 1041 | 1053 | - |
| LA046a | 439 | 572 | 180 | 0.11847 | 2.41 | 0.30947 | 4.26 | 1738 | 1829 | 1933 | - |
| LA058a | 272 | 35 | 28 | 0.07343 | 2.46 | 0.10487 | 3.7 | 643 | 735 | 1026 | 633 ± 25 |
| LA062a | 309 | 26 | 28 | 0.0668 | 3.91 | 0.09643 | 5.36 | 594 | 645 | 832 | 588 ± 33 |
| LA070a | 239 | 134 | 26 | 0.06127 | 4.38 | 0.10031 | 3.63 | 616 | 623 | 649 | 616 ± 23 |
| LA072a | 271 | 75 | 22 | 0.06595 | 2.59 | 0.0798 | 2.45 | 495 | 554 | 805 | 489 ± 13 |
| LA074a | 513 | 48 | 39 | 0.05729 | 4.36 | 0.08067 | 3.48 | 500 | 501 | 503 | 500 ± 18 |
| LA080a | 211 | 46 | 18 | 0.06163 | 4.33 | 0.08546 | 1.95 | 529 | 554 | 661 | 526 ± 11 |
| LA082a | 365 | 29 | 27 | 0.06009 | 2.7 | 0.07914 | 2.19 | 491 | 512 | 607 | 489 ± 11 |
| LA092a | 791 | 342 | 65 | 0.06406 | 4.35 | 0.07908 | 3.8 | 491 | 538 | 744 | 486 ± 19 |
| LA094a | 926 | 2724 | 108 | 0.06645 | 3.47 | 0.07419 | 2.69 | 461 | 527 | 821 | 455 ± 13 |
| LA096a | 365 | 53 | 26 | 0.06583 | 4.74 | 0.07253 | 2.31 | 451 | 514 | 801 | 446 ± 11 |
| LA104a | 252 | 57 | 19 | 0.06025 | 4.64 | 0.0784 | 3.64 | 487 | 509 | 613 | 485 ± 18 |
| LA106a | 305 | 96 | 24 | 0.06326 | 4.49 | 0.07816 | 3.77 | 485 | 528 | 717 | 481 ± 19 |
| LA108a | 322 | 36 | 93 | 0.11883 | 3.04 | 0.29165 | 3.71 | 1650 | 1781 | 1939 | - |
| LA110a | 288 | 54 | 60 | 0.12593 | 4.63 | 0.20122 | 5.09 | 1182 | 1526 | 2042 | - |
| LA116a | 452 | 383 | 37 | 0.06214 | 3.73 | 0.0742 | 3.28 | 1838 | 1886 | 1940 | 458 ± 16 |
| LA120a | 272 | 152 | 117 | 0.16182 | 3.83 | 0.38335 | 2.76 | 461 | 500 | 679 | - |
| LA122a | 307 | 135 | 92 | 0.11905 | 2.27 | 0.27846 | 2.61 | 2092 | 2292 | 2475 | - |
| LAa1 | 362 | 153 | 29 | 0.05803 | 2.54 | 0.07842 | 1.72 | 1584 | 1744 | 1942 | 486 ± 9 |
| LAa3 | 210 | 67 | 16 | 0.05874 | 4.47 | 0.07812 | 2.16 | 487 | 495 | 531 | 484 ± 11 |
| LAa4 | 1606 | 560 | 727 | 0.19353 | 4.57 | 0.41111 | 6.55 | 485 | 498 | 558 | - |
| LAa5b | 376 | 129 | 37 | 0.06124 | 2.55 | 0.09673 | 1.89 | 2220 | 2521 | 2773 | 594 ± 12 |
| LAa5c | 407 | 183 | 40 | 0.0633 | 3.21 | 0.09484 | 1.54 | 595 | 606 | 648 | 581 ± 9 |
| LAa8b | 117 | 36 | 13 | 0.0629 | 4.16 | 0.11103 | 2.01 | 584 | 612 | 718 | 678 ± 14 |
| LAa8c | 116 | 57 | 14 | 0.06434 | 3.22 | 0.11055 | 1.65 | 679 | 685 | 705 | 674 ± 12 |
| LAa6 | 861 | 709 | 390 | 0.12207 | 1.6 | 0.38057 | 2.68 | 676 | 694 | 753 | - |
| LAa7c | 1395 | 424 | 704 | 0.16915 | 2.03 | 0.46443 | 2.56 | 2079 | 2033 | 1987 | - |
| LAa9 | 201 | 44 | 22 | 0.06208 | 3.88 | 0.11294 | 4.77 | 2459 | 2509 | 2549 | 690 ± 35 |
| LAbz1 | 380 | 206 | 39 | 0.05672 | 6.38 | 0.09691 | 5.33 | 690 | 687 | 677 | 599 ± 33 |
| LAbz3 | 746 | 91 | 75 | 0.06258 | 2.72 | 0.10483 | 3.54 | 596 | 573 | 481 | 642 ± 24 |
| LAbz5b | 568 | 208 | 59 | 0.06208 | 3.33 | 0.10152 | 2.54 | 623 | 635 | 677 | 622 ± 17 |
| LAbz5c | 488 | 197 | 52 | 0.06088 | 3.2 | 0.10409 | 1.87 | 638 | 638 | 635 | 638 ± 13 |
| LAbz6 | 161 | 60 | 16 | 0.05998 | 4.6 | 0.09535 | 1.66 | 587 | 590 | 603 | 587 ± 10 |
| LAbz7 | 189 | 211 | 113 | 0.16903 | 1.84 | 0.46611 | 2.22 | 2467 | 2512 | 2548 | - |

| | | | | | | | | | | | |
|---|---|---|---|---|---|---|---|---|---|---|---|
| LAbz8c | 520 | 43 | 183 | 0.11972 | 3.19 | 0.35461 | 2.35 | 1957 | 1954 | 1952 | - |
| LAbz8b | 529 | 50 | 171 | 0.1229 | 1.94 | 0.32685 | 4.48 | 1823 | 1907 | 1999 | - |
| LAbz9 | 543 | 177 | 269 | 0.19904 | 3.36 | 0.43269 | 1.92 | 2318 | 2595 | 2818 | - |
| LAz2 | 468 | 136 | 36 | 0.06008 | 6.37 | 0.08036 | 5.75 | 498 | 518 | 607 | 496 ± 30 |
| LAz3 | 815 | 74 | 60 | 0.05948 | 4.72 | 0.07711 | 2.89 | 479 | 498 | 585 | 477 ± 14 |
| LAz4 | 665 | 116 | 50 | 0.05689 | 5.84 | 0.07823 | 2.36 | 486 | 486 | 487 | 486 ± 12 |
| LAz6 | 767 | 251 | 73 | 0.06152 | 5.47 | 0.09405 | 3.26 | 579 | 596 | 658 | 578 ± 20 |
| LAz9 | 560 | 250 | 100 | 0.07334 | 4.5 | 0.17077 | 2.33 | 1016 | 1019 | 1023 | - |
| LAz10 | 1288 | 393 | 121 | 0.05979 | 3.62 | 0.09415 | 5.88 | 580 | 583 | 596 | 580 ± 36 |
| LAz11 | 255 | 102 | 20 | 0.0575 | 2.58 | 0.07809 | 5.06 | 485 | 489 | 511 | 484 ± 25 |
| LAz12 | 204 | 110 | 17 | 0.05843 | 5.05 | 0.07812 | 3.44 | 485 | 496 | 546 | 484 ± 17 |
| LAz14 | 3744 | 342 | 1692 | 0.19907 | 6.37 | 0.43128 | 6.42 | 2312 | 2592 | 2819 | - |
| LAz15 | 891 | 126 | 66 | 0.0593 | 7.81 | 0.07779 | 11 | 483 | 500 | 578 | 481 ± 55 |
| LAz17 | 1094 | 121 | 81 | 0.05946 | 3.73 | 0.07838 | 3.49 | 486 | 504 | 584 | 485 ± 18 |
| LAz17c | 622 | 666 | 77 | 0.06057 | 2.64 | 0.10195 | 2.54 | 626 | 625 | 624 | 626 ± 17 |
| LAz20 | 219 | 116 | 25 | 0.06247 | 3.75 | 0.10508 | 3.21 | 644 | 654 | 690 | 643 ± 22 |

Table 4.3: Single-grain stepwise evaporation $^{207}Pb/^{206}Pb$ data of the Vivero metavolcanic rocks.

| Grain | Step | $(^{204}Pb/^{206}Pb)_{meas}$ | $(^{207}Pb/^{206}Pb)_{meas}$ | $(^{207}Pb/^{206}Pb)_{cor}$ | 2 σ | Age (Ma) |
|---|---|---|---|---|---|---|
| z1 | 1 | 0.000152 | 0.059006 | 0.056932 | 0.5 | 489 ± 11 |
| | 2 | 0.000165 | 0.063833 | 0.061439 | 1.2 | 660 ± 26 |
| | 3 | 0.000046 | 0.066605 | 0.066103 | 0.6 | 810 ± 12 |
| z2 | 1 | 0.000237 | 0.05788 | 0.054555 | 0.5 | 394 ± 11 |
| | 2 | 0.000187 | 0.058143 | 0.055553 | 0.6 | 435 ± 13 |
| | 3 | 0.000051 | 0.067341 | 0.056737 | 0.6 | 481 ± 13 |
| | 4 | 0.000052 | 0.057351 | 0.056732 | 0.3 | 481 ± 7 |
| z3 | 1 | 0.000153 | 0.060463 | 0.058383 | 0.6 | 544 ± 13 |
| | 2 | 0.000101 | 0.059621 | 0.058296 | 1.2 | 541 ± 34 |
| z8 | 1 | 0.000054 | 0.057895 | 0.057248 | 0.39 | 501 ± 8 |
| | 2 | 0.000054 | 0.058647 | 0.058003 | 1.1 | 530 ± 24 |
| | 3 | 0.000048 | 0.059031 | 0.058476 | 0.6 | 548 ± 13 |
| | 4 | 0.00003 | 0.059561 | 0.059269 | 0.22 | 577 ± 5 |
| | 5 | 0.00004 | 0.060027 | 0.059591 | 0.7 | 589 ± 15 |
| z11 | 1 | 0.000074 | 0.058099 | 0.057161 | 0.4 | 498 ± 18 |
| | 2 | 0.000083 | 0.058506 | 0.057439 | 0.6 | 508 ± 9 |
| | 3 | 0.000099 | 0.058903 | 0.057604 | 0.6 | 515 ± 9 |
| | 4 | 0.000127 | 0.066386 | 0.064713 | 0.5 | 765 ± 10 |
| | 5 | 0.000085 | 0.091242 | 0.090274 | 0.3 | 1431 ± 6 |
| | 6 | 0.000031 | 0.112577 | 0.112429 | 0.4 | 1839 ± 7 |
| | 7 | 0.000031 | 0.112644 | 0.112497 | 0.27 | 1840 ± 5 |
| | 8 | 0.000033 | 0.112651 | 0.112477 | 0.18 | 1840 ± 3 |
| z12 | 1 | 0.000097 | 0.057345 | 0.056068 | 0.7 | 455 ± 16 |
| | 2 | 0.00008 | 0.058024 | 0.057006 | 0.3 | 492 ± 6 |
| | 3 | 0.000059 | 0.057554 | 0.056833 | 0.3 | 485 ± 6 |
| | 4 | 0.000047 | 0.057488 | 0.056942 | 0.2 | 489 ± 4 |
| | 5 | 0.000047 | 0.057334 | 0.056788 | 0.18 | 483 ± 4 |
| | 6 | 0.000086 | 0.059345 | 0.058237 | 0.2 | 539 ± 4 |
| | 7 | 0.000053 | 0.060508 | 0.059885 | 0.5 | 599 ± 11 |
| | 8 | 0.000056 | 0.060632 | 0.059966 | 0.3 | 602 ± 6 |
| z2 | 1 | 0.000145 | 0.05879 | 0.056818 | 0.6 | 484 ± 13 |
| | 2 | 0.00002 | 0.057197 | 0.057044 | 0.5 | 493 ± 11 |
| | 3 | 0.000018 | 0.056876 | 0.056751 | 0.25 | 482 ± 6 |
| | 4 | 0.000025 | 0.057038 | 0.056812 | 0.4 | 484 ± 9 |
| z3 | 1 | 0.000107 | 0.055268 | 0.053841 | 0.7 | 364 ± 15 |
| | 2 | 0.0001 | 0.056073 | 0.054747 | 0.4 | 402 ± 9 |
| | 3 | 0.000037 | 0.05736 | 0.05696 | 0.4 | 490 ± 9 |
| | 4 | 0.000034 | 0.057206 | 0.056849 | 0.5 | 486 ± 11 |
| | 5 | 0.000039 | 0.057458 | 0.057029 | 0.36 | 493 ± 8 |
| | 6 | 0.000417 | 0.066205 | 0.060312 | 0.4 | 615 ± 9 |
| | 7 | 0.00016 | 0.062191 | 0.060018 | 0.35 | 604 ± 7 |
| z4 | 1 | 0.000076 | 0.059324 | 0.058362 | 0.6 | 543 ± 13 |
| | 2 | 0.000082 | 0.059437 | 0.058388 | 1 | 544 ± 22 |
| z5 | 1 | 0.000236 | 0.060108 | 0.056813 | 0.5 | 484 ± 11 |
| z6 | 1 | 0.000026 | 0.12187 | 0.12182006 | 0.19 | 1983 ± 4 |
| | 2 | 0.000048 | 0.1212 | 0.12085538 | 0.22 | 1968 ± 4 |
| | 3 | 0.000056 | 0.189127 | 0.188927 | 0.29 | 2733 ± 5 |
| z7 | 1 | 0.000155 | 0.076139 | 0.07411095 | 0.24 | 1044 ± 5 |
| | 2 | 0.000111 | 0.091553 | 0.09022258 | 0.29 | 1430 ± 5 |
| | 3 | 0.00034 | 0.107858 | 0.10344833 | 0.6 | 1678 ± 7 |
| | 4 | 0.000144 | 0.120999 | 0.11935885 | 0.38 | 1947 ± 4 |

Table 4.4: U-Pb laser ablation (LA) and ion microprobe (IM) results of the Trives metavolcanic rocks. Analyses references ending in b mean rims and c mean cores.

| | Element concentration (ppm) | | | Isotope ratios | | | | Ages (Ma) | | | |
|---|---|---|---|---|---|---|---|---|---|---|---|
| **Grain** | **U** | **Th** | **Pb** | $(^{207}Pb/^{206}Pb)_{meas}$ | **σ (%)** | $(^{206}Pb/^{238}U)_{meas}$ | **σ (%)** | $^{206}Pb/^{238}U$ | $^{207}Pb/^{235}U$ | $^{207}Pb/^{206}Pb$ | $(^{206}Pb/^{238}U)_{cor}$ |
| ***Laser-Ablation ICPMS data*** | | | | | | | | | | | |
| LA008 | 296 | 161 | 111 | 0.123 | 1.79 | 0.344 | 2.53 | 1908 | 1952 | 1998 | - |
| LA014 | 181 | 228 | 20 | 0.061 | 1.79 | 0.091 | 2.53 | 559 | 574 | 633 | 558 ± 14 |
| LA018 | 366 | 77 | 28 | 0.06 | 1.79 | 0.079 | 2.53 | 492 | 516 | 621 | 490 ± 12 |
| LA020 | 582 | 140 | 45 | 0.061 | 1.79 | 0.079 | 2.53 | 492 | 519 | 641 | 490 ± 12 |
| LA022 | 606 | 152 | 47 | 0.059 | 1.79 | 0.078 | 2.53 | 486 | 499 | 557 | 485 ± 12 |
| LA024 | 265 | 110 | 25 | 0.06 | 1.79 | 0.091 | 2.53 | 563 | 568 | 592 | 562 ± 14 |
| LA032 | 253 | 238 | 29 | 0.062 | 1.79 | 0.099 | 2.53 | 611 | 626 | 682 | 609 ± 15 |
| LA042 | 272 | 116 | 28 | 0.066 | 1.79 | 0.1 | 2.53 | 613 | 653 | 795 | 608 ± 15 |
| LA044 | 89 | 33 | 9 | 0.063 | 1.79 | 0.103 | 2.53 | 633 | 652 | 719 | 631 ± 16 |
| LA046 | 345 | 32 | 26 | 0.06 | 1.79 | 0.079 | 2.53 | 492 | 509 | 586 | 491 ± 12 |
| LA050 | 249 | 117 | 95 | 0.127 | 1.79 | 0.356 | 2.53 | 1965 | 2011 | 2059 | - |
| LA062c | 49 | 70 | 6 | 0.064 | 1.79 | 0.1 | 2.53 | 613 | 642 | 745 | 610 ± 15 |
| LA062b | 102 | 84 | 9 | 0.059 | 1.79 | 0.079 | 2.53 | 492 | 502 | 550 | 491 ± 12 |
| LA074a | 635 | 346 | 53 | 0.064 | 1.79 | 0.08 | 2.53 | 497 | 540 | 725 | 493 ± 12 |
| LA078a | 1004 | 402 | 101 | 0.062 | 1.79 | 0.099 | 2.53 | 606 | 624 | 686 | 605 ± 15 |
| LA080a | 631 | 148 | 48 | 0.06 | 1.79 | 0.078 | 2.53 | 484 | 504 | 598 | 482 ± 12 |
| LA010a2 | 589 | 173 | 61 | 0.065 | 1.79 | 0.1 | 2.53 | 617 | 654 | 784 | 613 ± 15 |
| LA018a6 | 522 | 542 | 48 | 0.058 | 1.79 | 0.074 | 2.53 | 459 | 473 | 538 | 458 ± 11 |
| LA020a7 | 276 | 26 | 21 | 0.06 | 1.79 | 0.079 | 2.53 | 490 | 513 | 620 | 487 ± 12 |
| LA022a8 | 722 | 70 | 55 | 0.061 | 1.79 | 0.08 | 2.53 | 495 | 524 | 652 | 493 ± 12 |
| LA032a11 | 708 | 139 | 54 | 0.062 | 1.79 | 0.077 | 2.53 | 480 | 518 | 688 | 477 ± 12 |
| LA036a13 | 807 | 44 | 62 | 0.058 | 1.79 | 0.082 | 2.53 | 510 | 517 | 545 | 509 ± 13 |
| LA038a14 | 2337 | 213 | 224 | 0.063 | 1.79 | 0.101 | 2.53 | 618 | 637 | 706 | 616 ± 15 |
| LA040a15 | 510 | 103 | 37 | 0.057 | 1.79 | 0.076 | 2.53 | 473 | 479 | 508 | 472 ± 12 |
| LA044a17 | 470 | 55 | 38 | 0.062 | 1.79 | 0.083 | 2.53 | 512 | 541 | 662 | 510 ± 13 |
| LA062a24 | 341 | 70 | 26 | 0.057 | 1.79 | 0.079 | 2.53 | 492 | 492 | 489 | 492 ± 12 |
| ***Ion-microprobe data*** | | | | | | | | | | | |
| IMZ1c | n.d. | n.d. | n.d. | 0.1221 | 1.43 | 0.3754 | 1.4 | 2055 | 2022 | 1988 | - |
| IMz2c | n.d. | n.d. | n.d. | 0.0614 | 1.12 | 0.0995 | 1.63 | 612 | 620 | 652 | 611 ± 10 |
| IMz3b | n.d. | n.d. | n.d. | 0.0607 | 1.07 | 0.0797 | 1.07 | 494 | 519 | 627 | 492 ± 5 |
| IMz3b2 | n.d. | n.d. | n.d. | 0.06 | 0.47 | 0.0754 | 0.49 | 468 | 492 | 603 | 466 ± 2 |
| IMz4c | n.d. | n.d. | n.d. | 0.0623 | 1.73 | 0.0995 | 1.05 | 612 | 627 | 684 | 610 ± 6 |
| IMz4b | n.d. | n.d. | n.d. | 0.0575 | 1.23 | 0.0793 | 0.79 | 492 | 495 | 509 | 492 ± 4 |
| IMz9c2 | n.d. | n.d. | n.d. | 0.0563 | 1.28 | 0.0803 | 0.58 | 498 | 492 | 464 | 499 ± 3 |
| IMz7c | n.d. | n.d. | n.d. | 0.0638 | 0.56 | 0.1051 | 0.61 | 644 | 665 | 734 | 642 ± 4 |
| IMz12c | n.d. | n.d. | n.d. | 0.0594 | 1.3 | 0.0783 | 1.1 | 486 | 503 | 583 | 485 ± 5 |
| IMz10c | n.d. | n.d. | n.d. | 0.0582 | 2.61 | 0.0797 | 1.18 | 495 | 502 | 536 | 494 ± 6 |
| IMz16c2 | n.d. | n.d. | n.d. | 0.0616 | 1.55 | 0.0797 | 1.15 | 495 | 525 | 662 | 492 ± 6 |

Table 4.5: U-Pb laser ablation (LA) and ion microprobe (IM) results of the lower metavolcanic rocks of Sanabria region. Analyses references ending in b mean rims and c mean cores.

| | Element concentration (ppm) | | | Isotope ratios | | | | Ages (Ma) | | | |
|---|---|---|---|---|---|---|---|---|---|---|---|
| **Grain** | **U** | **Th** | **Pb** | $(^{207}Pb/^{206}Pb)_{meas}$ | **σ (%)** | $(^{206}Pb/^{238}U)_{meas}$ | **σ (%)** | $^{206}Pb/^{238}U$ | $^{207}Pb/^{235}U$ | $^{207}Pb/^{206}Pb$ | $(^{206}Pb/^{238}U)_{cor}$ |
| ***Laser-Ablation ICPMS data*** | | | | | | | | | | | |
| LAbz10b | 439 | 47 | 32 | 0.062 | 2.7 | 0.076 | 2.55 | 472 | 508 | 676 | 469 ± 12 |
| LAbz11b | 772 | 118 | 59 | 0.063 | 2.7 | 0.08 | 2.55 | 498 | 538 | 712 | 494 ± 12 |
| LAbz13 | 570 | 123 | 43 | 0.058 | 2.7 | 0.081 | 2.55 | 501 | 505 | 522 | 500 ± 13 |
| LAbz14 | 605 | 31 | 64 | 0.065 | 2.7 | 0.113 | 2.55 | 690 | 708 | 768 | 688 ± 17 |
| LAbz15 | 451 | 68 | 34 | 0.06 | 2.7 | 0.079 | 2.55 | 491 | 513 | 611 | 489 ± 12 |
| LAbz3 | 879 | 486 | 165 | 0.075 | 2.7 | 0.174 | 2.55 | 1034 | 1049 | 1080 | - |
| LAbz3b | 522 | 111 | 51 | 0.061 | 2.7 | 0.097 | 2.55 | 600 | 605 | 627 | 599 ± 15 |
| LAbz4 | 593 | 92 | 214 | 0.165 | 2.7 | 0.343 | 2.55 | 1903 | 2207 | 2504 | - |
| LAbz5 | 208 | 39 | 19 | 0.059 | 2.7 | 0.092 | 2.55 | 570 | 568 | 562 | 570 ± 14 |
| LAbz8 | 454 | 28 | 33 | 0.062 | 2.7 | 0.077 | 2.55 | 476 | 510 | 665 | 473 ± 12 |
| LAbz8b | 522 | 41 | 39 | 0.06 | 2.7 | 0.08 | 2.55 | 495 | 512 | 587 | 493 ± 12 |
| LAbz9 | 422 | 325 | 174 | 0.121 | 2.7 | 0.356 | 2.55 | 1961 | 1965 | 1970 | - |
| LAc1 | 255 | 26 | 25 | 0.061 | 2.7 | 0.099 | 2.55 | 609 | 618 | 654 | 608 ± 15 |
| LAc10 | 467 | 50 | 35 | 0.058 | 2.7 | 0.08 | 2.55 | 496 | 502 | 530 | 496 ± 12 |
| LAc11 | 340 | 27 | 25 | 0.056 | 2.7 | 0.079 | 2.55 | 487 | 484 | 470 | 488 ± 12 |
| LAc3 | 251 | 91 | 89 | 0.158 | 2.7 | 0.315 | 2.55 | 1766 | 2093 | 2433 | - |
| LAc4 | 148 | 23 | 25 | 0.11 | 2.7 | 0.165 | 2.55 | 986 | 1273 | 1796 | 939 ± 23 |
| LAc6 | 242 | 28 | 19 | 0.059 | 2.7 | 0.08 | 2.55 | 498 | 509 | 561 | 497 ± 12 |
| LAc7 | 65 | 25 | 23 | 0.159 | 2.7 | 0.315 | 2.55 | 1766 | 2099 | 2443 | - |
| LAa10 | 929 | 35 | 67 | 0.059 | 2.7 | 0.078 | 2.55 | 483 | 497 | 566 | 481 ± 12 |
| LAa11 | 405 | 217 | 48 | 0.062 | 2.7 | 0.11 | 2.55 | 672 | 675 | 684 | 672 ± 17 |
| LAa2 | 289 | 46 | 28 | 0.062 | 2.7 | 0.099 | 2.55 | 606 | 617 | 658 | 605 ± 15 |
| LAa4 | 274 | 23 | 21 | 0.062 | 2.7 | 0.08 | 2.55 | 495 | 529 | 678 | 492 ± 12 |
| LAa5 | 358 | 270 | 73 | 0.076 | 2.7 | 0.179 | 2.55 | 1060 | 1070 | 1089 | - |
| LAa5b | 343 | 42 | 25 | 0.059 | 2.7 | 0.078 | 2.55 | 483 | 499 | 573 | 481 ± 12 |
| LAa6 | 169 | 41 | 16 | 0.068 | 2.7 | 0.094 | 2.55 | 581 | 641 | 859 | 575 ± 14 |
| LAa8 | 442 | 128 | 118 | 0.142 | 2.7 | 0.246 | 2.55 | 1417 | 1789 | 2256 | - |
| LAa9 | 195 | 60 | 19 | 0.059 | 2.7 | 0.099 | 2.55 | 609 | 601 | 569 | 610 ± 15 |
| LAa9b | 491 | 123 | 48 | 0.061 | 2.7 | 0.098 | 2.55 | 602 | 607 | 626 | 602 ± 15 |
| ***Ion-microprobe data*** | | | | | | | | | | | |
| IMPz1b | n.d | n.d | n.d | 0.0583 | 1.15 | 0.079 | 0.35 | 490 | 499 | 540 | 490 ± 2 |
| IMPz1c | n.d | n.d | n.d | 0.0827 | 1.95 | 0.1811 | 1.45 | 1073 | 1138 | 1263 | - |
| IMPz5b | n.d | n.d | n.d | 0.063 | 0.53 | 0.0796 | 0.41 | 494 | 534 | 707 | 490 ± 2 |
| IMPz12b | n.d | n.d | n.d | 0.0625 | 1.43 | 0.0799 | 1.4 | 495 | 532 | 691 | 492 ± 7 |
| IMPz7b | n.d | n.d | n.d | 0.0583 | 1.12 | 0.0792 | 1.63 | 491 | 500 | 541 | 491 ± 8 |

Table 4.6: Single-grain stepwise evaporation $^{207}Pb/^{206}Pb$ data of the lower metavolcanic rocks of the Sanabria region.

| Grain | Step | $(^{204}Pb/^{206}Pb)_{meas}$ | $(^{207}Pb/^{206}Pb)_{meas}$ | $(^{207}Pb/^{206}Pb)_{cor}$ | 2σ | Age (Ma) |
|---|---|---|---|---|---|---|
| z1 | 1 | 0.000025 | 0.106876 | 0.10679323 | 0.8 | 1745 ± 14 |
| | 2 | 0.000097 | 0.137302 | 0.13636582 | 0.4 | 2182 ± 6 |
| | 3 | 0.000086 | 0.142068 | 0.14129601 | 0.6 | 2243 ± 10 |
| | 4 | 0.000006 | 0.234751 | 0.23525394 | 0.5 | 3088 ± 8 |
| | 5 | 0.00021 | 0.249008 | 0.24734885 | 0.5 | 3168 ± 8 |
| z2 | 1 | 0.000024 | 0.074321 | 0.07415859 | 2.5 | 1046 ± 49 |
| | 2 | 0.000063 | 0.136121 | 0.13562584 | 0.8 | 2172 ± 14 |
| | 3 | 0.000071 | 0.155188 | 0.15466218 | 0.7 | 2398 ± 12 |
| | 4 | 0.000061 | 0.159199 | 0.15881523 | 0.39 | 2443 ± 12 |
| | 5 | 0.000067 | 0.164715 | 0.16427656 | 0.28 | 2500 ± 5 |

Table 4.7: U-Pb laser ablation (LA) and ion microprobe (IM) results of the upper metavolcanic rocks of Sanabria region. Analyses references ending in b mean rims and c mean cores.

| | Element concentration (ppm) | | | Isotope ratios | | | | Ages (Ma) | | | |
|---|---|---|---|---|---|---|---|---|---|---|---|
| **Grain** | **U** | **Th** | **Pb** | $(^{207}Pb/^{206}Pb)_{meas}$ | **σ (%)** | $(^{206}Pb/^{238}U)_{meas}$ | **σ (%)** | $^{206}Pb/^{238}U$ | $^{207}Pb/^{235}U$ | $^{207}Pb/^{206}Pb$ | $(^{206}Pb/^{238}U)_{cor}$ |
| ***Laser-Ablation ICPMS data*** | | | | | | | | | | | |
| LA020a | 277 | 214 | 54 | 0.122 | 1.96 | 0.162 | 2.45 | 970 | 1336 | 1984 | 908 ± 22 |
| LA022a | 199 | 188 | 96 | 0.168 | 1.96 | 0.395 | 2.45 | 2148 | 2353 | 2536 | - |
| LA026a | 584 | 89 | 55 | 0.067 | 1.96 | 0.1 | 2.45 | 616 | 667 | 846 | 610 ± 15 |
| LA038a | 747 | 37 | 55 | 0.059 | 1.96 | 0.079 | 2.45 | 489 | 503 | 565 | 488 ± 12 |
| LA042c | 153 | 98 | 16 | 0.064 | 1.96 | 0.099 | 2.45 | 607 | 640 | 757 | 604 ± 14 |
| LA042b | 279 | 113 | 22 | 0.06 | 1.96 | 0.079 | 2.45 | 490 | 511 | 606 | 488 ± 12 |
| LA056a | 134 | 131 | 17 | 0.064 | 1.96 | 0.114 | 2.45 | 698 | 712 | 758 | 696 ± 17 |
| LA058a | 605 | 297 | 64 | 0.063 | 1.96 | 0.101 | 2.45 | 618 | 636 | 699 | 616 ± 15 |
| LA060a | 442 | 166 | 44 | 0.06 | 1.96 | 0.096 | 2.45 | 592 | 596 | 609 | 592 ± 14 |
| LA066a | 247 | 221 | 128 | 0.169 | 1.96 | 0.42 | 2.45 | 2260 | 2415 | 2548 | - |
| LA068a | 53 | 115 | 27 | 0.121 | 1.96 | 0.339 | 2.45 | 1881 | 1924 | 1971 | - |
| LA082a | 1557 | 244 | 118 | 0.06 | 1.96 | 0.078 | 2.45 | 487 | 510 | 616 | 485 ± 12 |
| LA084a | 557 | 100 | 51 | 0.061 | 1.96 | 0.096 | 2.45 | 591 | 603 | 651 | 590 ± 14 |
| LA088a | 309 | 95 | 25 | 0.062 | 1.96 | 0.079 | 2.45 | 493 | 526 | 674 | 490 ± 12 |
| LA090a | 240 | 180 | 30 | 0.069 | 1.96 | 0.103 | 2.45 | 633 | 694 | 897 | 627 ± 15 |
| LA096a | 52 | 59 | 7 | 0.064 | 1.96 | 0.104 | 2.45 | 635 | 657 | 732 | 633 ± 15 |
| LA108a | 293 | 146 | 25 | 0.059 | 1.96 | 0.08 | 2.45 | 495 | 511 | 585 | 494 ± 12 |
| LA110a | 150 | 254 | 20 | 0.061 | 1.96 | 0.098 | 2.45 | 600 | 609 | 644 | 599 ± 14 |
| LA112a | 58 | 60 | 7 | 0.059 | 1.96 | 0.097 | 2.45 | 599 | 592 | 566 | 599 ± 14 |
| LA124a | 68 | 62 | 22 | 0.148 | 1.96 | 0.251 | 2.45 | 1444 | 1840 | 2323 | - |
| ***Ion-microprobe data*** | | | | | | | | | | | |
| IMPz1 | n.d. | n.d. | n.d. | 0.255 | 0.46 | 0.6186 | 0.9 | 3105 | 3173 | 3216 | - |
| IMPz2c | n.d. | n.d. | n.d. | 0.0591 | 0.95 | 0.0783 | 0.96 | 486 | 501 | 570 | 485 ± 5 |
| IMPz3c | n.d. | n.d. | n.d. | 0.0634 | 0.82 | 0.0796 | 0.63 | 494 | 536 | 721 | 490 ± 3 |
| IMPz4c | n.d. | n.d. | n.d. | 0.2009 | 0.28 | 0.4957 | 0.94 | 2595 | 2732 | 2834 | - |
| IMPz7c | n.d. | n.d. | n.d. | 0.0596 | 1.22 | 0.1027 | 0.51 | 631 | 622 | 590 | 631 ± 3 |
| IMPz13 | n.d. | n.d. | n.d. | 0.0572 | 2.02 | 0.0785 | 0.92 | 487 | 489 | 500 | 487 ± 4 |
| IMP13c | n.d. | n.d. | n.d. | 0.1177 | 0.31 | 0.3532 | 0.75 | 1950 | 1936 | 1922 | - |
| IMP18b | n.d. | n.d. | n.d. | 0.0572 | 0.86 | 0.0785 | 0.64 | 487 | 489 | 499 | 487 ± 3 |
| IMP18c | n.d. | n.d. | n.d. | 0.0695 | 1 | 0.1032 | 0.46 | 633 | 698 | 913 | 626 ± 3 |
| IMP19c | n.d. | n.d. | n.d. | 0.231 | 1.51 | 0.5719 | 2.03 | 2916 | 3001 | 3059 | - |
| IMP15c | n.d. | n.d. | n.d. | 0.0627 | 0.49 | 0.0994 | 0.69 | 611 | 630 | 697 | 609 ± 4 |
| IMPz6b | n.d. | n.d. | n.d. | 0.0572 | 0.31 | 0.0787 | 0.6 | 488 | 490 | 500 | 488 ± 3 |

Table 4.8: Single-grain stepwise evaporation $^{207}Pb/^{206}Pb$ data of the upper metavolcanic rocks of the Sanabria region.

| Grain | Step | $(^{204}Pb/^{206}Pb)_{meas}$ | $(^{207}Pb/^{206}Pb)_{meas}$ | $(^{207}Pb/^{206}Pb)_{cor}$ | 2σ | Age (Ma) |
|---|---|---|---|---|---|---|
| z1 | 1 | 0.000006 | 0.095317 | 0.09546472 | 1.1 | 1537 ± 21 |
| | 2 | 0.000002 | 0.164924 | 0.16529885 | 1.1 | 2511 ± 18 |
| | 3 | 0.000003 | 0.18207 | 0.182475 | 0.3 | 2675 ± 5 |
| | 4 | 0.000001 | 0.185691 | 0.18612911 | 0.3 | 2705 ± 5 |
| z3 | 1 | 0.000159 | 0.058964 | 0.05678859 | 0.8 | 483 ± 17 |
| | 2 | 0.000157 | 0.059065 | 0.05691939 | 0.4 | 488 ± 8 |
| | 3 | 0.000133 | 0.058891 | 0.05709528 | 0.5 | 495 ± 11 |
| | 4 | 0.000101 | 0.059957 | 0.05863314 | 0.37 | 553 ± 8 |
| | 5 | 0.000103 | 0.059991 | 0.05863814 | 0.27 | 554 ± 5 |
| z1 | 1 | 0.001563 | 0.079676 | 0.05708818 | 1.5 | 495 ± 33 |
| | 2 | 0.0002864 | 0.0610698 | 0.05704238 | 0.4 | 493 ± 9 |
| | 3 | 0.00026789 | 0.06075226 | 0.05699445 | 0.3 | 491 ± 6 |
| | 4 | 0.0001 | 0.058269 | 0.05695249 | 0.24 | 490 ± 5 |
| | 5 | 0.000112 | 0.058436 | 0.05694494 | 0.28 | 489 ± 6 |
| z4 | 1 | 0.000143 | 0.058881 | 0.05693909 | 0.6 | 489 ± 13 |
| z3 | 1 | 0.000045 | 0.058083 | 0.05756832 | 0.7 | 513 ± 15 |
| | 2 | 0.000109 | 0.059846 | 0.05840504 | 0.8 | 545 ± 17 |
| | 3 | 0.000071 | 0.060443 | 0.05955791 | 0.7 | 587 ± 15 |
| | 4 | 0.000038 | 0.060492 | 0.060008688 | 0.7 | 607 ± 15 |
| | 5 | 0.000106 | 0.061433 | 0.06004269 | 0.5 | 605 ± 11 |
| z4 | 1 | 0.000021 | 0.057034 | 0.0568661 | 0.8 | 486 ± 17 |
| | 2 | 0.000171 | 0.059417 | 0.05706862 | 0.6 | 494 ± 13 |
| | 3 | 0.000015 | 0.057281 | 0.05720126 | 0.5 | 499 ± 11 |
| | 4 | 0.00014 | 0.059611 | 0.05771662 | 0.6 | 519 ± 13 |
| z5 | 1 | 0.000041 | 0.057264 | 0.05680502 | 1 | 484 ± 22 |
| | 2 | 0.000151 | 0.060953 | 0.05890497 | 0.5 | 563 ± 10 |
| | 3 | 0.00006 | 0.059835 | 0.05910778 | 0.7 | 571 ± 15 |
| | 4 | 0.000367 | 0.0604401 | 0.05922245 | 0.5 | 575 ± 11 |

Table 4.9: U-Pb laser ablation (LA) and ion microprobe (IM) results of the Villadepera metavolcanic rocks. Analyses references ending in b mean rims and c mean cores.

| | Element concentration (ppm) | | | Isotope ratios | | | | Ages (Ma) | | | |
|---|---|---|---|---|---|---|---|---|---|---|---|
| Grain | U | Th | Pb | $(^{207}Pb/^{206}Pb)_{meas}$ | σ (%) | $(^{206}Pb/^{238}U)_{meas}$ | σ (%) | $^{206}Pb/^{238}U$ | $^{207}Pb/^{235}U$ | $^{207}Pb/^{206}Pb$ | $(^{206}Pb/^{238}U)_{cor}$ |
| ***Laser-Ablation ICPMS data*** | | | | | | | | | | | |
| z2 | 165 | 78 | 13 | 0.054 | 2.38 | 0.078 | 1.97 | 484 | 465 | 373 | 486 ± 10 |
| z3 | 60 | 75 | 27 | 0.122 | 2.38 | 0.351 | 1.97 | 1939 | 1963 | 1989 | - |
| z5 | 703 | 52 | 55 | 0.082 | 2.38 | 0.077 | 1.97 | 480 | 639 | 1249 | 465 ± 10 |
| z6 | 127 | 46 | 10 | 0.058 | 2.38 | 0.078 | 1.97 | 482 | 489 | 523 | 481 ± 10 |
| z7 | 440 | 174 | 58 | 0.064 | 2.38 | 0.129 | 1.97 | 783 | 776 | 757 | 784 ± 16 |
| z8 | 163 | 81 | 18 | 0.061 | 2.38 | 0.104 | 1.97 | 639 | 639 | 638 | 639 ± 13 |
| z9 | 93 | 61 | 38 | 0.159 | 2.38 | 0.357 | 1.97 | 1969 | 2214 | 2450 | - |
| z10 | 195 | 103 | 21 | 0.061 | 2.38 | 0.103 | 1.97 | 632 | 636 | 650 | 631 ± 13 |
| z11 | 233 | 76 | 30 | 0.089 | 2.38 | 0.115 | 1.97 | 705 | 893 | 1394 | 682 ± 15 |
| z12 | 1279 | 351 | 169 | 0.08 | 2.38 | 0.126 | 1.97 | 768 | 889 | 1204 | 753 ± 16 |
| z15 | 164 | 73 | 13 | 0.056 | 2.38 | 0.076 | 1.97 | 473 | 468 | 443 | 474 ± 10 |
| z16 | 139 | 69 | 33 | 0.142 | 2.38 | 0.203 | 1.97 | 1194 | 1631 | 2251 | - |
| z17 | 258 | 83 | 20 | 0.055 | 2.38 | 0.077 | 1.97 | 479 | 466 | 406 | 480 ± 10 |
| z18 | 439 | 43 | 44 | 0.061 | 2.38 | 0.105 | 1.97 | 645 | 642 | 634 | 645 ± 13 |
| z19 | 124 | 97 | 78 | 0.207 | 2.38 | 0.505 | 1.97 | 2636 | 2779 | 2885 | - |
| ***Ion-microprobe data*** | | | | | | | | | | | |
| z1a | 239 | 24 | 20 | 0.0562 | 1.21 | 0.0786 | 1.34 | 488 | 483 | 463 | 488 ± 7 |
| z1b | 279 | 38 | 24 | 0.0561 | 1.01 | 0.0778 | 1.34 | 483 | 479 | 456 | 484 ± 7 |
| z2a | 299 | 16 | 24 | 0.0569 | 0.96 | 0.0763 | 1.35 | 474 | 477 | 489 | 474 ± 7 |
| z2b | 123 | 97 | 14 | 0.0594 | 1.41 | 0.0883 | 1.39 | 545 | 553 | 583 | 545 ± 8 |
| z3 | 527 | 375 | 51 | 0.1208 | 1.06 | 0.0839 | 1.34 | 519 | 888 | 1968 | 478 ± 7 |
| z4a | 291 | 29 | 24 | 0.0565 | 1 | 0.0771 | 1.34 | 479 | 478 | 472 | 479 ± 7 |
| z4c | 314 | 28 | 27 | 0.0586 | 0.94 | 0.0781 | 1.36 | 485 | 497 | 551 | 484 ± 7 |
| z4d | 349 | 21 | 30 | 0.0571 | 0.91 | 0.0786 | 1.34 | 488 | 489 | 494 | 488 ± 7 |
| z5 | 92 | 23 | 11 | 0.0625 | 2 | 0.1001 | 1.34 | 615 | 632 | 692 | 613 ± 9 |
| z6a | 543 | 78 | 46 | 0.057 | 0.72 | 0.0776 | 1.35 | 482 | 484 | 493 | 482 ± 7 |
| z6b | 369 | 88 | 32 | 0.0571 | 1 | 0.0778 | 1.36 | 483 | 485 | 496 | 483 ± 7 |
| z7 | 239 | 161 | 103 | 0.1194 | 0.46 | 0.3243 | 1.34 | 1811 | 1875 | 1948 | - |
| z8c | 156 | 65 | 17 | 0.0597 | 1.46 | 0.0928 | 1.34 | 572 | 576 | 591 | 572 ± 8 |
| z8b | 674 | 44 | 48 | 0.0558 | 0.73 | 0.0661 | 1.34 | 413 | 418 | 445 | 412 ± 6 |

Table 4.10: U-Pb laser ablation (LA) and ion microprobe (IM) results of the lower metavolcanic rocks of the Hiendelaencina region. Analyses references ending in b mean rims and c mean cores.

| | | Element concentration (ppm) | | | Isotope ratios | | | | Ages (Ma) | | | |
|---|---|---|---|---|---|---|---|---|---|---|---|---|
| **Sample** | **Grain** | **U** | **Th** | **Pb** | **($^{207}Pb/^{206}Pb)_{meas}$** | **σ (%)** | **($^{206}Pb/^{238}U)_{meas}$** | **σ (%)** | **$^{206}Pb/^{238}U$** | **$^{207}Pb/^{235}U$** | **$^{207}Pb/^{206}Pb$** | **($^{206}Pb/^{238}U)_{cor}$** |
| ***Laser-Ablation ICPMS data*** | | | | | | | | | | | | |
| T-21 | a1 | 430 | 258 | 44 | 0.063 | 2.38 | 0.093 | 1.97 | 575 | 603 | 712 | 572 ± 12 |
| | a2 | 495 | 148 | 41 | 0.058 | 2.38 | 0.083 | 1.97 | 516 | 522 | 544 | 516 ± 11 |
| | a3b | 346 | 58 | 29 | 0.059 | 2.38 | 0.087 | 1.97 | 539 | 544.6 | 569 | 538 ± 11 |
| | a6b | 476 | 118 | 54 | 0.086 | 2.38 | 0.106 | 1.97 | 651 | 826 | 1333 | 631 ± 13 |
| | a6c | 68 | 72 | 21 | 0.114 | 2.38 | 0.236 | 1.97 | 1366 | 1576 | 1870 | 1317 ± 29 |
| | a9 | 495 | 152 | 50 | 0.06 | 2.38 | 0.101 | 1.97 | 618 | 616 | 607 | 618 ± 13 |
| | bz1 | 274 | 74 | 41 | 0.073 | 2.38 | 0.147 | 1.97 | 883 | 922 | 1015 | 878 ± 18 |
| | bz10 | 1291 | 377 | 138 | 0.063 | 2.38 | 0.106 | 1.97 | 651 | 667 | 720 | 649 ± 13 |
| | bz3 | 362 | 125 | 48 | 0.069 | 2.38 | 0.129 | 1.97 | 780 | 810 | 895 | 776 ± 16 |
| | bz4 | 643 | 292 | 55 | 0.064 | 2.38 | 0.081 | 1.97 | 503 | 549 | 745 | 499 ± 10 |
| | bz5 | 495 | 269 | 52 | 0.067 | 2.38 | 0.096 | 1.97 | 590 | 645 | 841 | 585 ± 12 |
| | bz7b | 513 | 42 | 37 | 0.059 | 2.38 | 0.076 | 1.97 | 472 | 486 | 552 | 471 ± 10 |
| | bz9 | 63 | 47 | 9 | 0.069 | 2.38 | 0.131 | 1.97 | 792 | 819 | 891 | 789 ± 16 |
| | c1 | 145 | 31 | 18 | 0.064 | 2.38 | 0.125 | 1.97 | 759 | 750.6 | 727 | 759 ± 16 |
| | c4 | 363 | 309 | 43 | 0.065 | 2.38 | 0.103 | 1.97 | 630 | 664 | 780 | 623 ± 13 |
| T-22 | a11 | 312 | 138 | 39 | 0.067 | 2.38 | 0.12 | 1.97 | 731 | 760 | 847 | 728 ± 15 |
| | a12 | 208 | 55 | 16 | 0.059 | 2.38 | 0.079 | 1.97 | 489 | 500 | 549 | 488 ± 10 |
| | a15 | 608 | 663 | 74 | 0.062 | 2.38 | 0.102 | 1.97 | 625 | 637 | 679 | 624 ± 13 |
| | a16 | 401 | 121 | 39 | 0.061 | 2.38 | 0.098 | 1.97 | 604 | 611 | 635 | 604 ± 12 |
| | a17 | 202 | 69 | 20 | 0.06 | 2.38 | 0.097 | 1.97 | 596 | 594 | 589 | 596 ± 12 |
| | a20 | 427 | 123 | 134 | 0.117 | 2.38 | 0.304 | 1.97 | 1710 | 1803 | 1913 | 1681 ± 38 |
| | a21 | 700 | 724 | 67 | 0.06 | 2.38 | 0.08 | 1.97 | 497 | 514 | 591 | 495 ± 10 |
| | a5 | 530 | 934 | 71 | 0.061 | 2.38 | 0.099 | 1.97 | 606 | 610 | 627 | 605 ± 12 |
| | a7 | 96 | 71 | 12 | 0.069 | 2.38 | 0.115 | 1.97 | 700 | 746 | 889 | 695 ± 14 |
| | a8 | 174 | 132 | 49 | 0.114 | 2.38 | 0.245 | 1.97 | 1412 | 1606 | 1870 | 1366 ± 30 |
| | a9 | 422 | 207 | 52 | 0.069 | 2.38 | 0.118 | 1.97 | 717 | 765 | 905 | 712 ± 15 |
| | bz10 | 66 | 68 | 10 | 0.193 | 2.38 | 0.097 | 1.97 | 594 | 1294 | 2772 | 494 ± 13 |
| | bz11 | 458 | 102 | 37 | 0.06 | 2.38 | 0.082 | 1.97 | 508 | 527 | 614 | 506 ± 10 |
| | bz12 | 425 | 252 | 46 | 0.061 | 2.38 | 0.102 | 1.97 | 626 | 630 | 647 | 625 ± 13 |
| | bz2 | 257 | 78 | 25 | 0.065 | 2.38 | 0.1 | 1.97 | 615 | 650 | 771 | 612 ± 13 |
| | bz6 | 404 | 50 | 36 | 0.06 | 2.38 | 0.094 | 1.97 | 576 | 582 | 607 | 576 ± 12 |
| | bz8 | 682 | 1113 | 74 | 0.065 | 2.38 | 0.081 | 1.97 | 500 | 553 | 779 | 495 ± 10 |
| | bz9 | 377 | 241 | 38 | 0.061 | 2.38 | 0.095 | 1.97 | 584 | 599 | 654 | 583 ± 12 |
| ***Ion-microprobe data*** | | | | | | | | | | | | |

| | | | | | | | | | | | | |
|---|---|---|---|---|---|---|---|---|---|---|---|---|
| T-22 | z26a | 201 | 119 | 82 | 0.1199 | 1.59 | 0.3158 | 1.38 | 1769 | 1856 | 1954 | - |
| | z26b | 238 | 150 | 107 | 0.1234 | 0.6 | 0.3455 | 1.34 | 1913 | 1958 | 2007 | - |
| | z28c | 381 | 277 | 71 | 0.068 | 0.58 | 0.1456 | 1.37 | 876 | 874 | 869 | 876 ± 12 |
| | z28b | 469 | 286 | 83 | 0.0676 | 0.53 | 0.1407 | 1.34 | 849 | 851 | 858 | 848 ± 11 |
| | z31b | 410 | 36 | 36 | 0.0575 | 0.91 | 0.0813 | 1.35 | 504 | 505 | 510 | 504 ± 7 |
| | z31c | 418 | 250 | 50 | 0.0675 | 0.79 | 0.0939 | 1.36 | 579 | 638 | 855 | 573 ± 8 |
| | z32a | 277 | 46 | 25 | 0.0573 | 1.01 | 0.0801 | 1.34 | 497 | 498 | 502 | 497 ± 7 |
| | z32b | 295 | 395 | 42 | 0.0607 | 0.87 | 0.0979 | 1.34 | 602 | 608 | 629 | 602 ± 8 |
| | z32c | 635 | 72 | 58 | 0.0575 | 0.8 | 0.0839 | 1.34 | 519 | 518 | 510 | 520 ± 7 |
| | z33 | 200 | 63 | 26 | 0.0629 | 1.35 | 0.1136 | 1.34 | 694 | 696 | 704 | 693 ± 10 |
| | z35 | 538 | 41 | 68 | 0.063 | 0.68 | 0.1154 | 1.36 | 704 | 705 | 709 | 704 ± 10 |

Table 4.11: Single-grain stepwise evaporation $^{207}Pb/^{206}Pb$ data of the lower metavolcanic rocks of the Hiendelaencina region.

| Grain | Step | $(^{204}Pb/^{206}Pb)_{meas}$ | $(^{207}Pb/^{206}Pb)_{meas}$ | $(^{207}Pb/^{206}Pb)_{cor}$ | 2σ | Age (Ma) |
|---|---|---|---|---|---|---|
| z2 | 1 | 0.000061 | 0.057628 | 0.0568784 | 1.2 | 487 ± 26 |
| | 2 | 0.00005 | 0.0577351 | 0.0571456 | 0.5 | 497 ± 11 |
| | 3 | 0.000048 | 0.057726 | 0.071664 | 0.6 | 498 ± 13 |
| | 4 | 0.000074 | 0.059441 | 0.0585085 | 0.4 | 549 ± 8 |
| | 5 | 0.000058 | 0.05906 | 0.0583592 | 0.5 | 543 ± 11 |
| z3 | 1 | 0.00002 | 0.057176 | 0.0570231 | 0.5 | 492 ± 11 |
| | 2 | 0.000017 | 0.058337 | 0.058231 | 0.18 | 539 ± 4 |
| | 3 | 0.000016 | 0.058252 | 0.0581603 | 0.24 | 536 ± 6 |
| | 4 | 0.000027 | 0.059315 | 0.0590663 | 0.3 | 569 ± 6 |
| | 5 | 0.000032 | 0.059181 | 0.0588591 | 0.29 | 562 ± 7 |
| | 6 | 0.000031 | 0.059129 | 0.0588215 | 0.35 | 560 ± 7 |
| | 7 | 0.000033 | 0.060362 | 0.0600291 | 0.2 | 605 ± 5 |
| z4 | 1 | 0.000018 | 0.057281 | 0.0571575 | 0.18 | 498 ± 4 |
| | 2 | 0.000016 | 0.057235 | 0.0571406 | 0.3 | 497 ± 7 |
| | 3 | 0.000015 | 0.056952 | 0.0568714 | 0.3 | 487 ± 7 |
| | 4 | 0.000018 | 0.057216 | 0.0570923 | 0.3 | 495 ± 7 |

Table 4.12: U-Pb laser ablation (LA) and ion microprobe (IM) results of the upper metavolcanic rocks of the Hiendelaencina region. Analyses references ending in b mean rims and c mean cores.

| | Element concentration (ppm) | | | Isotope ratios | | | | Ages (Ma) | | | |
|---|---|---|---|---|---|---|---|---|---|---|---|
| **Grain** | **U** | **Th** | **Pb** | $(^{207}Pb/^{206}Pb)_{meas}$ | **σ (%)** | $(^{206}Pb/^{238}U)_{meas}$ | **σ (%)** | $^{206}Pb/^{238}U$ | $^{207}Pb/^{235}U$ | $^{207}Pb/^{206}Pb$ | $(^{206}Pb/^{238}U)_{cor}$ |
| ***Laser-Ablation ICPMS data*** | | | | | | | | | | | |
| a1 | 49 | 29 | 8 | 0.072 | 1.7 | 0.144 | 2.5 | 868 | 902 | 987 | 863 ± 22 |
| a2 | 224 | 78 | 17 | 0.059 | 1.7 | 0.077 | 2.5 | 479 | 497 | 577 | 478 ± 12 |
| a4 | 426 | 100 | 37 | 0.086 | 1.7 | 0.084 | 2.5 | 517 | 699 | 1340 | 499 ± 13 |
| a5 | 583 | 52 | 42 | 0.06 | 1.7 | 0.076 | 2.5 | 472 | 496 | 608 | 470 ± 12 |
| bz1 | 166 | 126 | 13 | 0.072 | 1.7 | 0.064 | 2.5 | 397 | 498 | 991 | 388.7 |
| bz2 | 192 | 80 | 19 | 0.061 | 1.7 | 0.099 | 2.5 | 609 | 617 | 649 | 608 ± 15 |
| bz5 | 205 | 117 | 34 | 0.072 | 1.7 | 0.155 | 2.5 | 931 | 947 | 986 | 929 ± 23 |
| bz6 | 449 | 153 | 44 | 0.06 | 1.7 | 0.097 | 2.5 | 595 | 599 | 614 | 594 ± 15 |
| bz7 | 509 | 233 | 48 | 0.06 | 1.7 | 0.091 | 2.5 | 563 | 570 | 597 | 562 ± 14 |
| c2 | 130 | 74 | 20 | 0.067 | 1.7 | 0.14 | 2.5 | 846 | 841 | 827 | 846 ± 21 |
| c3 | 308 | 378 | 39 | 0.063 | 1.7 | 0.1 | 2.5 | 616 | 640 | 724 | 614 ± 15 |
| c4 | 302 | 35 | 24 | 0.066 | 1.7 | 0.082 | 2.5 | 509 | 568 | 812 | 504 ± 13 |
| b8 | 268 | 40 | 22 | 0.064 | 1.7 | 0.085 | 2.5 | 526 | 565 | 728 | 522 ± 13 |
| ***Ion-microprobe data*** | | | | | | | | | | | |
| z21 | 2707 | 987 | 220 | 0.0797 | 0.67 | 0.0768 | 1.34 | 477 | 621 | 1189 | 463 ± 6 |
| z22 | 485 | 40 | 39 | 0.0647 | 0.95 | 0.0753 | 1.34 | 468 | 522 | 763 | 463 ± 6 |
| z23 | 354 | 131 | 41 | 0.0613 | 0.8 | 0.1004 | 1.34 | 617 | 624 | 651 | 616 ± 8 |
| z24 | 201 | 21 | 22 | 0.0617 | 1.1 | 0.0975 | 1.68 | 600 | 613 | 663 | 599 ± 10 |
| z26b | 275 | 7 | 23 | 0.0564 | 1.13 | 0.0795 | 1.35 | 493 | 488 | 467 | 493 ± 7 |
| z27 | 196 | 38 | 17 | 0.0561 | 1.44 | 0.0785 | 1.34 | 488 | 482 | 457 | 488 ± 7 |
| z28 | 335 | 30 | 29 | 0.0581 | 1.13 | 0.0795 | 1.34 | 493 | 500 | 533 | 493 ± 7 |
| z29a | 258 | 32 | 23 | 0.0567 | 1.4 | 0.0797 | 1.34 | 495 | 492 | 482 | 495 ± 7 |
| z30b2 | 1184 | 43 | 100 | 0.0626 | 0.6 | 0.0796 | 1.34 | 494 | 531 | 694 | 491 ± 7 |
| z30c | 300 | 148 | 34 | 0.0608 | 0.92 | 0.094 | 1.34 | 579 | 590 | 633 | 578 ± 8 |
| z31 | 367 | 53 | 31 | 0.0568 | 1.15 | 0.0774 | 1.34 | 481 | 481 | 485 | 481 ± 7 |
| z32 | 510 | 71 | 44 | 0.0574 | 0.87 | 0.078 | 1.34 | 484 | 488 | 507 | 484 ± 7 |
| z33b | 375 | 44 | 34 | 0.0555 | 0.86 | 0.0829 | 1.34 | 513 | 499 | 432 | 515 ± 7 |
| z33c | 349 | 6 | 29 | 0.057 | 0.95 | 0.0776 | 1.34 | 482 | 484 | 492 | 482 ± 7 |

Table 4.13: Single-grain stepwise evaporation $^{207}Pb/^{206}Pb$ data of the upper metavolcanic rocks of the Hiendelaencina region.

| Grain | Step | $(^{204}Pb/^{206}Pb)_{meas}$ | $(^{207}Pb/^{206}Pb)_{meas}$ | $(^{207}Pb/^{206}Pb)_{cor}$ | 2σ | Age (Ma) |
|---|---|---|---|---|---|---|
| z1 | 1 | 0.000095 | 0.057097 | 0.055849 | 0.16 | 446 ± 4 |
| | 2 | 0.000096 | 0.056903 | 0.055639 | 0.14 | 438 ± 3 |
| | 3 | 0.000131 | 0.06254 | 0.060791 | 0.19 | 632 ± 9 |
| | 4 | 0.000055 | 0.087353 | 0.086792 | 0.6 | 1356 ± 12 |
| | 5 | 0.000031 | 0.123167 | 0.123052 | 0.3 | 2001 ± 5 |
| z2 | 2 | 0.000046 | 0.057234 | 0.056702 | 0.2 | 480 ± 4 |
| | 3 | 0.000044 | 0.057274 | 0.056771 | 0.4 | 483 ± 8 |
| | 4 | 0.000066 | 0.057731 | 0.056909 | 0.4 | 488 ± 9 |
| | 5 | 0.000073 | 0.057722 | 0.056798 | 0.3 | 484 ± 6 |
| z3 | 1 | 0.000047 | 0.056651 | 0.056102 | 0.4 | 456 ± 9 |
| | 2 | 0.000084 | 0.059604 | 0.058526 | 0.2 | 549 ± 5 |
| | 3 | 0.000057 | 0.058511 | 0.057823 | 0.2 | 523 ± 4 |
| z4 | 1 | 0.000218 | 0.058588 | 0.055546 | 0.2 | 434 ± 5 |
| | 2 | 0.000118 | 0.058199 | 0.056619 | 0.5 | 477 ± 11 |
| | 3 | 0.000042 | 0.057149 | 0.056675 | 0.4 | 479 ± 9 |
| | 4 | 0.000071 | 0.057847 | 0.056952 | 0.2 | 490 ± 5 |
| z1 | 1 | 0.000041 | 0.057459 | 0.057001 | 0.9 | 492 ± 19 |
| | 2 | 0.00003 | 0.060404 | 0.060115 | 0.14 | 608 ± 3 |
| | 3 | 0.000028 | 0.065274 | 0.065028 | 0.6 | 775 ± 13 |
| | 4 | 0.000073 | 0.074735 | 0.073874 | 0.14 | 1038 ± 3 |
| z6 | 1 | 0.000211 | 0.058848 | 0.055911 | 0.4 | 449 ± 9 |

Table 4.14: Rb-Sr data of a sliced K-feldspar megacryst from the upper metavolcanic rocks of the Hiendelaencina region.

| Sample | $^{87}Rb/^{86}Sr$ | error | $^{87}Sr/^{86}Sr$ | error |
|---|---|---|---|---|
| Fto-8 | 1.66714 | 1.2 | 0.72401 | 0.002 |
| Fto-3 | 1.714108 | 1.2 | 0.724281 | 0.002 |
| Fto-7 | 1.768224 | 1.2 | 0.724439 | 0.002 |
| Fto-9 | 1.86337 | 1.2 | 0.725494 | 0.002 |
| Fto-10 | 2.208603 | 1.2 | 0.727668 | 0.002 |

Table 4.15: U-Pb laser ablation (LA) results of the Viana do Bolo metagranite.

| | Element concentration (ppm) | | | Isotope ratios | | | | Ages (Ma) | | | |
|---|---|---|---|---|---|---|---|---|---|---|---|
| **Grain** | **U** | **Th** | **Pb** | $(^{207}Pb/^{206}Pb)_{meas}$ | **σ (%)** | $(^{206}Pb/^{238}U)_{meas}$ | **σ (%)** | $^{206}Pb/^{238}U$ | $^{207}Pb/^{235}U$ | $^{207}Pb/^{206}Pb$ | $(^{206}Pb/^{238}U)_{cor}$ |
| LA010a | 295 | 51 | 60 | 0.13006 | 2.38 | 0.19283 | 1.97 | 1137 | 1518 | 2099 | - |
| LA018a | 396 | 90 | 39 | 0.06305 | 2.38 | 0.09878 | 1.97 | 607 | 629 | 710 | 605 ± 13 |
| LA024a | 443 | 190 | 36 | 0.05948 | 2.38 | 0.077 | 1.97 | 478 | 497 | 585 | 477 ± 10 |
| LA026a | 465 | 449 | 55 | 0.06501 | 2.38 | 0.10131 | 1.97 | 622 | 656 | 775 | 619 ± 13 |
| LA032a | 669 | 43 | 49 | 0.05816 | 2.38 | 0.07769 | 1.97 | 482 | 492 | 536 | 482 ± 10 |
| LA034a | 958 | 51 | 72 | 0.05952 | 2.38 | 0.07848 | 1.97 | 487 | 505 | 586 | 485 ± 10 |
| LA038a | 580 | 130 | 45 | 0.0586 | 2.38 | 0.07784 | 1.97 | 483 | 495 | 552 | 482 ±10 |
| LA042a | 665 | 38 | 48 | 0.05975 | 2.38 | 0.0767 | 1.97 | 476 | 497 | 595 | 475 ± 10 |
| LA048a | 586 | 92 | 69 | 0.09227 | 2.38 | 0.11814 | 2.31 | 720 | 932 | 1473 | 694 ± 17 |
| LA050a | 346 | 63 | 27 | 0.06096 | 2.38 | 0.08019 | 2.31 | 497 | 523 | 638 | 495 ± 12 |
| LA066a | 1208 | 70 | 90 | 0.06338 | 2.38 | 0.07735 | 2.31 | 480 | 524 | 721 | 476 ± 11 |
| LA070a | 800 | 80 | 59 | 0.06682 | 2.38 | 0.07578 | 2.31 | 471 | 538 | 832 | 465 ± 11 |
| LA072a | 1105 | 109 | 82 | 0.06017 | 2.38 | 0.07785 | 2.31 | 483 | 506 | 610 | 481 ± 11 |
| LA074a | 1401 | 66 | 111 | 0.05951 | 2.38 | 0.08364 | 2.31 | 518 | 531 | 586 | 517 ± 12 |
| LA082a | 467 | 261 | 55 | 0.06492 | 2.38 | 0.09891 | 2.31 | 608 | 644 | 772 | 604 ± 14 |
| LA086a | 142 | 51 | 49 | 0.1538 | 2.38 | 0.29704 | 2.31 | 1677 | 2018 | 2389 | - |
| LA088a | 834 | 102 | 82 | 0.07225 | 2.38 | 0.09857 | 2.31 | 606 | 695 | 993 | 597 ± 14 |

Table 4.16: Single-grain stepwise evaporation $^{207}Pb/^{206}Pb$ data of the Viana do Bolo metagranite.

| Grain | Step | $(^{204}Pb/^{206}Pb)_{meas}$ | $(^{207}Pb/^{206}Pb)_{meas}$ | $(^{207}Pb/^{206}Pb)_{cor}$ | 2σ | Age (Ma) |
|---|---|---|---|---|---|---|
| z10 | 1 | 0.00099 | 0.071097 | 0.056835 | 0.29 | 485 ± 6 |
| | 2 | 0.0001 | 0.059067 | 0.05775391 | 0.17 | 520 ± 3 |
| z11 | 1 | 0.00009 | 0.0582815 | 0.05711106 | 0.29 | 496 ± 6 |
| | 2 | 0.000099 | 0.058908 | 0.05760882 | 0.4 | 515 ± 9 |
| | 3 | 0.000117 | 0.06058 | 0.05902574 | 0.3 | 586 ± 6 |
| | 4 | 0.000022 | 0.059983 | 0.05980885 | 0.4 | 597 ± 8 |
| | 5 | 0.000014 | 0.06011 | 0.06005242 | 0.8 | 605 ± 17 |
| | 6 | 0.000011 | 0.060304 | 0.06029051 | 0.6 | 614 ± 13 |
| z12 | 1 | 0.000144 | 0.06226 | 0.06032564 | 0.2 | 615 ± 4 |
| | 2 | 0.000093 | 0.06355 | 0.06235744 | 0.4 | 686 ± 8 |
| | 3 | 0.000106 | 0.064836 | 0.06346038 | 0.4 | 724 ± 8 |
| | 4 | 0.000102 | 0.065683 | 0.0643689 | 0.6 | 754 ± 12 |
| z14 | 1 | 0.000804 | 0.06732 | 0.05574436 | 0.17 | 442 ± 4 |
| | 2 | 0.000818 | 0.068705 | 0.0569469 | 0.18 | 489 ± 4 |
| | 3 | 0.000807 | 0.068533 | 0.05693467 | 0.14 | 489 ± 3 |
| | 4 | 0.00081 | 0.068596 | 0.05695437 | 0.18 | 490 ± 4 |
| | 5 | 0.000496 | 0.06518 | 0.0581182 | 0.2 | 534 ± 4 |
| | 6 | 0.000021 | 0.059115 | 0.05895295 | 0.19 | 565 ± 4 |
| | 7 | 0.0000349 | 0.0603465 | 0.0599859 | 0.47 | 603 ± 10 |
| z15 | 1 | 0.0002877 | 0.0609035 | 0.05685662 | 0.5 | 486 ± 11 |
| | 2 | 0.000287 | 0.062176 | 0.0581493 | 0.35 | 535 ± 7 |
| | 3 | 0.0002832 | 0.0622224 | 0.05825162 | 0.4 | 539 ± 9 |
| | 4 | 0.000296 | 0.062586 | 0.05843082 | 0.43 | 546 ± 9 |
| z2 | 1 | 0.000427 | 0.06607 | 0.06002957 | 0.6 | 605 ± 12 |
| | 2 | 0.00015513 | 0.062120658 | 0.06001846 | 1.3 | 604 ± 19 |
| z3 | 1 | 0.000281 | 0.060927 | 0.0569785 | 0.13 | 491 ± 3 |
| | 2 | 0.000316 | 0.061506 | 0.05704912 | 0.22 | 493 ± 4 |
| | 3 | 0.00031 | 0.061427 | 0.05705743 | 0.14 | 494 ± 3 |
| | 4 | 0.000288915 | 0.061248872 | 0.05718697 | 0.16 | 499 ± 4 |
| | 5 | 0.000384 | 0.064168 | 0.05873839 | 0.21 | 557 ± 4 |
| z4 | 1 | 0.000082 | 0.05892 | 0.05786886 | 0.22 | 525 ± 5 |
| | 2 | 0.000075 | 0.058991 | 0.05804219 | 0.24 | 531 ± 6 |
| | 3 | 0.000073 | 0.059085 | 0.0581657 | 0.3 | 536 ± 7 |
| | 4 | 0.00003 | 0.060276 | 0.05998646 | 0.7 | 603 ± 15 |
| | 5 | 0.00006 | 0.062046 | 0.06132653 | 0.37 | 651 ± 8 |
| | 6 | 0.000048 | 0.062518 | 0.06197421 | 0.7 | 673 ± 15 |
| | 7 | 0.00007 | 0.062877 | 0.06201542 | 0.7 | 675 ± 15 |
| | 8 | 0.000024 | 0.062416 | 0.06221974 | 0.5 | 682 ± 11 |
| z5 | 1 | 0.000357 | 0.061728 | 0.05667152 | 0.42 | 479 ± 9 |
| | 2 | 0.000295 | 0.061555 | 0.0574063 | 0.36 | 507 ± 8 |
| | 3 | 0.000248 | 0.061435 | 0.05797336 | 0.28 | 529 ± 6 |
| | 4 | 0.000325 | 0.064432 | 0.05986783 | 0.58 | 599 ± 10 |
| | 5 | 0.000188 | 0.062659 | 0.06008108 | 1.2 | 606 ± 26 |
| z6 | 1 | 0.000323 | 0.061188 | 0.05662576 | 0.38 | 477 ± 8 |
| | 2 | 0.0004 | 0.062468 | 0.05678711 | 0.7 | 483 ± 15 |
| | 3 | 0.000518 | 0.064565 | 0.0571724 | 1 | 498 ± 22 |
| | 4 | 0.000438 | 0.064052 | 0.05782938 | 0.4 | 523 ± 8 |
| | 5 | 0.000778 | 0.069402 | 0.05824747 | 0.51 | 539 ± 11 |
| | 6 | 0.000515 | 0.065597 | 0.05826099 | 0.6 | 539 ± 13 |
| z7 | 1 | 0.000459 | 0.061779 | 0.05522252 | 0.25 | 421 ± 5 |
| | 2 | 0.000055506 | 0.058913424 | 0.05824843 | 0.6 | 539 ± 13 |

| | | | | | | |
|---|---|---|---|---|---|---|
| z8 | 1 | 0.000361159 | 0.060940015 | 0.05581572 | 0.9 | 445 ± 20 |
| | 2 | 0.000169 | 0.059037 | 0.05671573 | 0.6 | 480 ± 13 |
| | 3 | 0.000105 | 0.059027 | 0.05764078 | 0.5 | 516 ± 11 |
| | 4 | 0.000167448 | 0.060360697 | 0.05806949 | 0.6 | 532 ± 13 |
| | 5 | 0.000164 | 0.06047866 | 0.05823844 | 0.5 | 539 ± 11 |
| z9 | 1 | 0.00012 | 0.058605 | 0.05699785 | 1.3 | 491 ± 28 |

Table 4.17: U-Pb laser ablation (LA) and ion microprobe (IM) results of the San Sebastián metagranite. Analyses references ending in b mean rims and c mean cores.

| | Element concentration (ppm) | | | Isotope ratios | | | | Ages (Ma) | | | |
|---|---|---|---|---|---|---|---|---|---|---|---|
| **Grain** | **U** | **Th** | **Pb** | $(^{207}Pb/^{206}Pb)_{meas}$ | **σ (%)** | $(^{206}Pb/^{238}U)_{meas}$ | **σ (%)** | $^{206}Pb/^{238}U$ | $^{207}Pb/^{235}U$ | $^{207}Pb/^{206}Pb$ | $(^{206}Pb/^{238}U)_{cor}$ |
| ***Laser-Ablation ICPMS data*** | | | | | | | | | | | |
| z25b | 1495 | 74 | 124 | 0.0567 | 0.46 | 0.0766 | 0.85 | 476 | 476 | 478 | 476 ± 4 |
| z26m | 171 | 206 | 18 | 0.0577 | 1.35 | 0.0745 | 0.88 | 463 | 473 | 519 | 462 ± 4 |
| z30b | 724 | 53 | 61 | 0.0575 | 1.03 | 0.0765 | 0.83 | 475 | 481 | 510 | 474 ± 4 |
| z30c | 171 | 38 | 15 | 0.0576 | 1.53 | 0.0763 | 0.83 | 474 | 481 | 514 | 474 ± 4 |
| z30c2 | 36 | 86 | 5 | 0.0579 | 3.93 | 0.0753 | 1.01 | 468 | 478 | 527 | 467 ± 6 |
| z36b | 796 | 79 | 66 | 0.0572 | 0.71 | 0.0755 | 0.83 | 469 | 474 | 498 | 469 ± 4 |
| ***SHRIMP data*** | | | | | | | | | | | |
| z4.1 | 636 | 59 | 44 | 0.0562 | 1.2 | 0.0749 | 2.2 | 465 | 464 | 459 | 465 ± 10 |
| z5.1 | 326 | 122 | 23 | 0.056 | 1.7 | 0.076 | 2.2 | 472 | 469 | 454 | 473 ± 10 |
| z7.1 | 1612 | 190 | 115 | 0.0573 | 0.7 | 0.076 | 2.2 | 472 | 477 | 501 | 472 ± 10 |
| z2.2 | 55 | 97 | 6 | 0.0572 | 4.1 | 0.0749 | 1.6 | 466 | 471 | 498 | 466 ± 9 |

Table 4.18: Single-grain stepwise evaporation $^{207}Pb/^{206}Pb$ data of the San Sebastián metagranite.

| Grain | Step | $(^{204}Pb/^{206}Pb)_{meas}$ | $(^{207}Pb/^{206}Pb)_{meas}$ | $(^{207}Pb/^{206}Pb)_{cor}$ | 2σ | Age (Ma) |
|---|---|---|---|---|---|---|
| z1 | 1 | 0.000072 | 0.057101 | 0.0561888 | 0.5 | 460 ± 11 |
| z4 | 1 | 0.000043 | 0.068459 | 0.0680007 | 0.6 | 869 ± 13 |
| | 2 | 0.000032 | 0.078264 | 0.0779999 | 0.33 | 1147 ± 7 |
| | 3 | 0.00003 | 0.060333 | 0.0901323 | 0.2 | 1428 ± 4 |
| | 4 | 0.000057 | 0.103189 | 0.1026552 | 0.5 | 1673 ± 9 |
| | 5 | 0.118152 | 0.000061 | 0.0117617 | 0.21 | 1920 ± 4 |
| | 6 | 0.000028 | 0.143633 | 0.143619 | 0.19 | 2271 ± 3 |
| | 7 | 0.000027 | 0.148659 | 0.148673 | 0.2 | 2331 ± 4 |
| | 8 | 0.000031 | 0.147794 | 0.147754 | 0.2 | 2320 ± 4 |
| z3 | 1 | 0.000062 | 0.056942 | 0.0561607 | 0.4 | 459 ± 9 |
| | 2 | 0.000083 | 0.057348 | 0.0563122 | 0.4 | 465 ± 9 |
| z9 | 1 | 0.000021 | 0.055909 | 0.0557379 | 0.6 | 442 ± 13 |
| | 2 | 0.000015 | 0.056753 | 0.0566718 | 0.8 | 479 ± 17 |

Table 4.19: U-Pb laser ablation (LA) and ion microprobe (IM) results of the Miranda do Douro metagranite. Analyses references ending in b mean rims and c mean cores.

| | Element concentration (ppm) | | | Isotope ratios | | | | Ages (Ma) | | | |
|---|---|---|---|---|---|---|---|---|---|---|---|
| **Grain** | **U** | **Th** | **Pb** | $(^{207}Pb/^{206}Pb)_{meas}$ | **σ (%)** | $(^{206}Pb/^{238}U)_{meas}$ | **σ (%)** | $^{206}Pb/^{238}U$ | $^{207}Pb/^{235}U$ | $^{207}Pb/^{206}Pb$ | $(^{206}Pb/^{238}U)_{cor}$ |
| ***Laser-Ablation ICPMS data*** | | | | | | | | | | | |
| z20 | 455 | 73 | 34 | 0.066 | 2.38 | 0.077 | 1.97 | 476 | 537 | 804 | 471 ± 10 |
| z22 | 2439 | 889 | 144 | 0.067 | 2.38 | 0.057 | 1.97 | 360 | 433 | 847 | 353 ± 7 |
| z24 | 362 | 123 | 34 | 0.059 | 2.38 | 0.092 | 1.97 | 568 | 570 | 578 | 568 ± 12 |
| z25 | 425 | 140 | 55 | 0.066 | 2.38 | 0.127 | 1.97 | 772 | 784 | 819 | 770 ± 16 |
| z26 | 624 | 200 | 56 | 0.059 | 2.38 | 0.089 | 1.97 | 549 | 551 | 559 | 549 ± 11 |
| z27 | 309 | 223 | 20 | 0.061 | 2.38 | 0.058 | 1.97 | 366 | 405 | 631 | 363 ± 8 |
| z30c | 577 | 100 | 132 | 0.174 | 2.38 | 0.198 | 1.97 | 1166 | 1778 | 2598 | - |
| z30b | 603 | 47 | 47 | 0.057 | 2.38 | 0.083 | 1.97 | 512 | 507 | 482 | 513 ± 11 |
| z31 | 409 | 176 | 24 | 0.065 | 2.38 | 0.056 | 1.97 | 350 | 413 | 785 | 344 ± 7 |
| z33 | 233 | 147 | 16 | 0.085 | 2.38 | 0.059 | 1.97 | 367 | 533 | 1323 | 353 ± 8 |
| z35 | 388 | 55 | 31 | 0.057 | 2.38 | 0.083 | 1.97 | 513 | 508 | 489 | 513 ± 10 |
| z38c | 575 | 471 | 36 | 0.064 | 2.38 | 0.054 | 1.97 | 338 | 393 | 729 | 334 ± 7 |
| z38b | 630 | 397 | 35 | 0.042 | 2.38 | 0.053 | 1.97 | 331 | 270 | -99 | 336 ± 7 |
| ***Ion-microprobe data*** | | | | | | | | | | | |
| z-9c | 1447 | 68 | 95 | 0.0774 | 0.48 | 0.0625 | 1.34 | 391 | 519 | 1133 | 380 ± 5 |
| z-9b | 332 | 41 | 23 | 0.0754 | 0.86 | 0.0662 | 1.34 | 413 | 532 | 1080 | 403 ± 6 |
| z-10 | 293 | 23 | 25 | 0.0577 | 0.99 | 0.0785 | 1.34 | 487 | 492 | 517 | 487 ± 7 |
| z-10b | 351 | 34 | 29 | 0.0566 | 1.13 | 0.0775 | 1.34 | 481 | 480 | 476 | 481 ± 7 |
| z-11 | 257 | 26 | 21 | 0.0562 | 1.06 | 0.0771 | 1.34 | 479 | 476 | 462 | 479 ± 7 |
| z-12 | 346 | 28 | 29 | 0.0567 | 0.9 | 0.0778 | 1.35 | 483 | 482 | 478 | 483 ± 7 |
| z-13b | 1529 | 44 | 89 | 0.0931 | 0.53 | 0.0579 | 1.34 | 363 | 564 | 1489 | 345 ± 5 |
| z-13c | 569 | 139 | 61 | 0.0699 | 0.59 | 0.0952 | 1.34 | 586 | 661 | 924 | 579 ± 8 |
| z-14 | 339 | 71 | 29 | 0.0574 | 0.92 | 0.0769 | 1.34 | 478 | 483 | 508 | 477 ± 7 |
| z-15b | 636 | 75 | 39 | 0.0686 | 0.7 | 0.0576 | 1.34 | 361 | 442 | 887 | 354 ± 5 |
| z-15c | 830 | 204 | 92 | 0.06 | 0.73 | 0.0978 | 1.34 | 601 | 602 | 605 | 601 ± 8 |
| z-16 | 580 | 219 | 70 | 0.0608 | 0.68 | 0.1026 | 1.35 | 630 | 630 | 632 | 630 ± 9 |
| z-17 | 396 | 42 | 30 | 0.0637 | 0.83 | 0.0709 | 1.34 | 442 | 492 | 732 | 437 ± 6 |
| z-19c | 516 | 77 | 398 | 0.2445 | 0.26 | 0.5984 | 1.34 | 3024 | 3100 | 3149 | - |
| z-19b | 128 | 53 | 94 | 0.2425 | 0.74 | 0.5444 | 1.34 | 2802 | 3000 | 3137 | - |

Table 4.20: Single-grain stepwise evaporation $^{207}Pb/^{206}Pb$ data of the Antoñita metagranite.

| Grain | Step | $(^{204}Pb/^{206}Pb)_{meas}$ | $(^{207}Pb/^{206}Pb)_{meas}$ | $(^{207}Pb/^{206}Pb)_{cor}$ | 2σ | Age (Ma) |
|---|---|---|---|---|---|---|
| z1 | 1 | 0.000068 | 0.060095 | 0.084187 | 1 | 579 ± 22 |
| z10 | 1 | 0.000012 | 0.056627 | 0.0565893 | 1.2 | 476 ± 26 |
| | 2 | 0.000075 | 0.05834 | 0.0573887 | 0.14 | 507 ± 4 |
| | 3 | 0.000075 | 0.058436 | 0.0585766 | 0.32 | 551 ± 7 |
| | 4 | 0.000071 | 0.060229 | 0.0593431 | 0.5 | 580 ± 11 |
| | 5 | 0.000062 | 0.060336 | 0.0595814 | 0.28 | 588 ± 6 |
| | 6 | 0.000049 | 0.060391 | 0.0598257 | 0.4 | 597 ± 9 |
| z11 | 1 | 0.000302 | 0.058943 | 0.0546703 | 0.21 | 399 ± 5 |
| | 2 | 0.000294 | 0.059071 | 0.054917 | 0.21 | 409 ± 5 |
| | 3 | 0.000072 | 0.05723 | 0.0563183 | 0.17 | 465 ± 4 |
| | 4 | 0.000075 | 0.057273 | 0.0560318 | 0.26 | 465 ± 6 |
| | 5 | 0.000074 | 0.057373 | 0.0564326 | 0.28 | 469 ± 7 |
| | 6 | 0.000067 | 0.058651 | 0.0578175 | 0.47 | 523 ± 10 |
| | 7 | 0.000078 | 0.059429 | 0.0584381 | 0.9 | 546 ± 20 |
| z12 | 1 | 0.000166 | 0.06091 | 0.0586429 | 0.5 | 554 ± 11 |
| z14 | 1 | 0.000115 | 0.0566 | 0.0550566 | 0.48 | 415 ± 10 |
| | 2 | 0.000053 | 0.057141 | 0.0565065 | 0.7 | 472 ± 15 |
| | 3 | 0.00005 | 0.05905 | 0.0584657 | 0.5 | 547 ± 11 |
| z15 | 1 | 0.00047 | 0.061913 | 0.0551959 | 0.6 | 420 ± 13 |
| | 2 | 0.000647 | 0.062187 | 0.0555173 | 0.29 | 433 ± 6 |
| | 3 | 0.000131 | 0.058439 | 0.05667 | 0.21 | 479 ± 5 |
| | 4 | 0.00013 | 0.058545 | 0.0567914 | 0.18 | 483 ± 4 |
| | 5 | 0.000117 | 0.059865 | 0.0583075 | 0.16 | 541 ± 3 |
| z2 | 1 | 0.000038 | 0.056395 | 0.0559771 | 1.5 | 451 ± 33 |
| | 2 | 0.00018 | 0.059013 | 0.0565307 | 0.6 | 473 ± 13 |
| | 3 | 0.000089 | 0.05895 | 0.0577969 | 0.7 | 522 ± 15 |
| | 4 | 0.000081 | 0.061906 | 0.0608819 | 1.4 | 635 ± 30 |
| z4 | 1 | 0.000356 | 0.060216 | 0.0551602 | 1.3 | 419 ± 28 |
| | 2 | 0.000082 | 0.057463 | 0.0564061 | 0.4 | 468 ± 8 |
| | 3 | 0.000087 | 0.057508 | 0.0563782 | 0.4 | 467 ± 9 |
| | 4 | 0.000037 | 0.056707 | 0.0563046 | 0.38 | 463 ± 8 |
| | 5 | 0.000045 | 0.057042 | 0.0569524 | 0.31 | 473 ± 7 |
| z5 | 1 | 0.000047 | 0.05574 | 0.0551884 | 0.4 | 420 ± 10 |
| | 2 | 0.000017 | 0.056737 | 0.0566266 | 0.15 | 477 ± 3 |
| | 3 | 0.000018 | 0.056935 | 0.0568106 | 0.26 | 484 ± 6 |
| | 4 | 0.000019 | 0.057071 | 0.0567427 | 0.6 | 482 ± 13 |
| z6 | 1 | 0.0000332 | 0.0567942 | 0.0564469 | 0.3 | 470 ± 7 |
| | 2 | 0.000044 | 0.0567365 | 0.056232 | 0.4 | 462 ± 9 |
| | 3 | 0.000036 | 0.086829 | 0.0865335 | 0.52 | 1350 ± 10 |
| z7 | 1 | 0.000024 | 0.057011 | 0.0567993 | 1.3 | 484 ± 29 |
| | 2 | 0.000049 | 0.057606 | 0.0570314 | 1.5 | 493 ± 32 |
| | 3 | 0.000041 | 0.060191 | 0.0597413 | 1.4 | 594 ± 30 |
| z9 | 1 | 0.000086 | 0.10472 | 0.1037929 | 0.6 | 1693 ± 11 |
| | 2 | 0.000018 | 0.15779 | 0.1579451 | 0.24 | 2434 ± 4 |
| | 3 | 0.000016 | 0.180637 | 0.1808804 | 0.16 | 2661 ± 3 |
| | 4 | 0.000024 | 0.18337 | 0.1835241 | 0.4 | 2685 ± 7 |

Table 4.21: Rb-Sr data of the Antoñita metagranite.

| Sample | $^{87}Rb/^{86}Sr$ | error | $^{87}Sr/^{86}Sr$ | error |
|---|---|---|---|---|
| CT-9 | 4.839 | 1.2 | 0.743294 | 0.002 |
| CT-10 | 5.45 | 1.2 | 0.74794 | 0.002 |
| CT-11 | 6.15 | 1.2 | 0.753283 | 0.002 |
| CT-4 | 22.086 | 1.2 | 0.860977 | 0.002 |

## 9.1.2. Tables of geochronological data of the Schist-Graywacke Complex Domain

Table 4.22: U-Pb ion microprobe results of the Fermoselle metagranite. Analyses references ending in b mean rims and c mean cores.

| | Element concentration (ppm) | | | Isotope ratios | | | | Ages (Ma) | | | |
|---|---|---|---|---|---|---|---|---|---|---|---|
| Grain | U | Th | Pb | $(^{207}Pb/^{206}Pb)_{meas}$ | σ (%) | $(^{206}Pb/^{238}U)_{meas}$ | σ (%) | $^{206}Pb/^{238}U$ | $^{207}Pb/^{235}U$ | $^{207}Pb/^{206}Pb$ | $(^{206}Pb/^{238}U)_{cor}$ |
| z17b | 298 | 26 | 25 | 0.056 | 1.15 | 0.0765 | 3.3 | 475 | 472 | 453 | 476 ± 15 |
| z22b | 410 | 139 | 70 | 0.0691 | 1.24 | 0.1438 | 2.02 | 866 | 876 | 902 | 865 ± 18 |
| z22c | 187 | 77 | 36 | 0.0715 | 1.42 | 0.1629 | 2.55 | 973 | 972 | 971 | 973 ± 25 |
| z23c | 78 | 27 | 8 | 0.0587 | 2.49 | 0.092 | 2.06 | 568 | 565 | 557 | 568 ± 12 |
| z29c | 288 | 92 | 26 | 0.0574 | 1.16 | 0.0801 | 1.35 | 497 | 499 | 508 | 497 ± 7 |
| z31b | 261 | 60 | 23 | 0.0562 | 1 | 0.0782 | 1.6 | 486 | 481 | 459 | 486 ± 8 |
| z31c | 715 | 196 | 54 | 0.0559 | 0.71 | 0.0653 | 1.35 | 408 | 414 | 449 | 407 ± 6 |
| z32b | 520 | 40 | 44 | 0.0571 | 0.57 | 0.0775 | 1.36 | 481 | 484 | 495 | 481 ± 7 |
| z33b | 386 | 31 | 33 | 0.0561 | 0.67 | 0.0787 | 1.35 | 488 | 482 | 455 | 489 ± 7 |
| z33c | 446 | 208 | 43 | 0.0571 | 0.77 | 0.0789 | 1.43 | 489 | 490 | 494 | 489 ± 7 |

Table 4.23: U-Pb SIMS results of the Vitigudino metagranite. Analyses references ending in b mean rims and c mean cores.

| | Element concentration (ppm) | | | Isotope ratios | | | | Ages (Ma) | | | |
|---|---|---|---|---|---|---|---|---|---|---|---|
| Grain | U | Th | Pb | $(^{207}Pb/^{206}Pb)_{meas}$ | σ (%) | $(^{206}Pb/^{238}U)_{meas}$ | σ (%) | $^{206}Pb/^{238}U$ | $^{207}Pb/^{235}U$ | $^{207}Pb/^{206}Pb$ | $(^{206}Pb/^{238}U)_{cor}$ |
| z1c | 289 | 65 | 24 | 0.0553 | 1.73 | 0.0764 | 1.64 | 475 | 466 | 425 | 476 ± 8 |
| z7c | 944 | 448 | 102 | 0.0596 | 0.8 | 0.0923 | 1.35 | 569 | 573 | 590 | 569 ± 8 |
| z10b | 322 | 27 | 27 | 0.0569 | 1.17 | 0.0767 | 1.5 | 476 | 479 | 489 | 476 ± 7 |
| z10c | 162 | 119 | 19 | 0.0585 | 1.63 | 0.0955 | 1.36 | 588 | 580 | 550 | 589 ± 8 |
| z15c | 141 | 102 | 18 | 0.0614 | 2.02 | 0.105 | 1.35 | 643 | 646 | 654 | 643 ± 9 |
| z1 | 510 | 48 | 44 | 0.0588 | 0.91 | 0.0798 | 1.47 | 495 | 507 | 561 | 494 ± 7 |
| z2 | 369 | 58 | 39 | 0.075 | 0.97 | 0.1712 | 1.63 | 1019 | 1035 | 1069 | - |
| z3 | 598 | 49 | 45 | 0.0747 | 0.74 | 0.1702 | 1.48 | 1013 | 1028 | 1059 | - |
| z4 | 316 | 40 | 27 | 0.0592 | 0.84 | 0.0791 | 1.5 | 491 | 506 | 574 | 489 ± 7 |
| z5 | 510 | 42 | 46 | 0.064 | 0.68 | 0.0968 | 1.47 | 596 | 627 | 743 | 593 ± 9 |
| z6 | 436 | 39 | 37 | 0.0562 | 1.04 | 0.0788 | 1.48 | 489 | 484 | 462 | 489 ± 7 |
| z7 | 722 | 76 | 68 | 0.0582 | 0.53 | 0.0859 | 1.47 | 531 | 532 | 536 | 531 ± 8 |
| z8 | 641 | 49 | 56 | 0.058 | 0.68 | 0.0803 | 1.47 | 498 | 504 | 529 | 497 ± 7 |
| z9 | 396 | 52 | 35 | 0.0575 | 0.76 | 0.0798 | 1.49 | 495 | 498 | 512 | 495 ± 7 |
| z10 | 199 | 37 | 17 | 0.0581 | 1.03 | 0.0795 | 1.47 | 493 | 500 | 533 | 493 ± 7 |
| z11 | 762 | 59 | 67 | 0.0582 | 0.52 | 0.0801 | 1.47 | 497 | 504 | 538 | 496 ± 7 |
| z12 | 359 | 72 | 29 | 0.0621 | 0.91 | 0.0969 | 1.48 | 596 | 614 | 679 | 595 ± 9 |
| z13 | 633 | 274 | 72 | 0.0594 | 0.56 | 0.0957 | 1.47 | 589 | 587 | 580 | 589 ± 9 |
| z14 | 175 | 66 | 19 | 0.06 | 1.23 | 0.0922 | 1.47 | 569 | 576 | 603 | 568 ± 9 |

Table 4.24: U-Pb ion microprobe results of the Ledesma metagranite. Analyses references ending in b mean rims and c mean cores.

| | Element concentration (ppm) | | | Isotope ratios | | | | Ages (Ma) | | | |
|---|---|---|---|---|---|---|---|---|---|---|---|
| **Grain** | **U** | **Th** | **Pb** | **($^{207}Pb/^{206}Pb)_{meas}$** | **σ (%)** | **($^{206}Pb/^{238}U)_{meas}$** | **σ (%)** | **$^{206}Pb/^{238}U$** | **$^{207}Pb/^{235}U$** | **$^{207}Pb/^{206}Pb$** | **($^{206}Pb/^{238}U)_{cor}$** |
| z17b | 443 | 29 | 36 | 0.0595 | 1.26 | 0.0774 | 1.95 | 481 | 499 | 584 | 479 ± 9 |
| z18c | 525 | 606 | 81 | 0.0624 | 0.61 | 0.1064 | 3.29 | 652 | 660 | 688 | 651 ± 21 |
| z19b | 512 | 32 | 40 | 0.0573 | 1.08 | 0.0737 | 1.95 | 459 | 466 | 504 | 458 ± 9 |
| z22b | 496 | 4 | 40 | 0.0574 | 1.12 | 0.0764 | 1.95 | 475 | 480 | 508 | 474 ± 9 |
| z22c | 39 | 20 | 11 | 0.0784 | 2.85 | 0.2247 | 2.56 | 1306 | 1251 | 1156 | - |
| z29b | 374 | 38 | 31 | 0.0583 | 1.05 | 0.0764 | 1.35 | 474 | 486 | 542 | 473 ± 7 |
| z29c | 484 | 117 | 51 | 0.0589 | 1.02 | 0.0943 | 1.61 | 581 | 578 | 565 | 582 ± 9 |
| z29m | 131 | 37 | 13 | 0.06 | 1.8 | 0.0883 | 1.35 | 546 | 557 | 605 | 545 ± 8 |
| z30b | 481 | 42 | 39 | 0.0584 | 1.25 | 0.0763 | 1.36 | 474 | 486 | 546 | 473 ± 7 |
| z30c | 502 | 432 | 100 | 0.0703 | 0.59 | 0.1565 | 1.36 | 937 | 934 | 936 | 938 ± 13 |
| z31c | 686 | 340 | 66 | 0.0562 | 0.61 | 0.0804 | 1.36 | 499 | 492 | 459 | 499 ± 7 |
| z33c | 439 | 200 | 53 | 0.0615 | 0.82 | 0.1019 | 1.35 | 625 | 633 | 658 | 625 ± 9 |
| z34c | 800 | 189 | 91 | 0.0607 | 0.61 | 0.1004 | 1.38 | 617 | 620 | 629 | 617 ± 9 |

Table 4.25: U-Pb LA-ICPMS, SIMS and SHRIMP results of the San Pelayo metagranite. Analyses references ending in b mean rims and c mean cores.

| | Element concentration (ppm) | | | Isotope ratios | | | | Ages (Ma) | | | |
|---|---|---|---|---|---|---|---|---|---|---|---|
| **Grain** | **U** | **Th** | **Pb** | **($^{207}Pb/^{206}Pb)_{meas}$** | **σ (%)** | **($^{206}Pb/^{238}U)_{meas}$** | **σ (%)** | **$^{206}Pb/^{238}U$** | **$^{207}Pb/^{235}U$** | **$^{207}Pb/^{206}Pb$** | **($^{206}Pb/^{238}U)_{cor}$** |
| ***Laser-Ablation ICPMS data*** | | | | | | | | | | | |
| z49 | 209 | 95 | 23 | 0.062 | 2.38 | 0.104 | 1.97 | 639 | 646 | 670 | 639 ± 13 |
| z51 | 186 | 183 | 23 | 0.059 | 2.38 | 0.104 | 1.97 | 640 | 623 | 562 | 642 ± 13 |
| z52 | 100 | 31 | 31 | 0.118 | 2.38 | 0.298 | 1.97 | 1683 | 1791 | 1919 | - |
| z53 | 733 | 343 | 52 | 0.059 | 2.38 | 0.07 | 1.97 | 435 | 455 | 559 | 433 ± 9 |
| z54 | 228 | 329 | 27 | 0.059 | 2.38 | 0.094 | 1.97 | 578 | 578 | 579 | 578 ± 12 |
| z55 | 332 | 56 | 104 | 0.122 | 2.38 | 0.311 | 1.97 | 1745 | 1855 | 1980 | - |
| z56 | 333 | 79 | 24 | 0.057 | 2.38 | 0.075 | 1.97 | 467 | 472 | 496 | 466 ± 10 |
| z57 | 114 | 156 | 14 | 0.063 | 2.38 | 0.096 | 1.97 | 589 | 615 | 712 | 586 ± 12 |
| ***SIMS data*** | | | | | | | | | | | |
| z27 | 39 | 24 | 5 | 0.0596 | 2.26 | 0.0951 | 1.34 | 585 | 586 | 587.7 | 585 ± 9 |
| z28b | 776 | 18 | 65 | 0.0568 | 0.56 | 0.0791 | 1.34 | 491 | 490 | 484.9 | 491 ± 7 |
| z28c | 307 | 72 | 41 | 0.0638 | 0.7 | 0.1176 | 1.35 | 717 | 721 | 734.3 | 717 ± 10 |
| z29 | 166 | 51 | 29 | 0.071 | 0.79 | 0.1523 | 1.34 | 914 | 927 | 958.3 | 912 ± 12 |
| z30 | 196 | 94 | 25 | 0.062 | 0.96 | 0.1047 | 1.39 | 642 | 649 | 672.3 | 641 ± 9 |
| z31 | 680 | 29 | 58 | 0.0562 | 0.71 | 0.0803 | 1.34 | 498 | 491 | 459.1 | 498 ± 7 |
| z32 | 687 | 176 | 64 | 0.0565 | 0.61 | 0.0822 | 1.34 | 509 | 503 | 471.3 | 510 ± 7 |
| z33 | 133 | 167 | 19 | 0.0587 | 1.19 | 0.097 | 1.36 | 597 | 589 | 557.1 | 598 ± 8 |
| z33b | 103 | 91 | 14 | 0.059 | 1.82 | 0.0976 | 1.37 | 600 | 594 | 567.9 | 601 ± 9 |
| ***SHRIMP data*** | | | | | | | | | | | |
| z1.1 | 2191 | 21 | 161 | 0.0601 | 0.6 | 0.0796 | 2.2 | 491 | 486 | 463.1 | 492 ± 11 |
| z1.2 | 274 | 218 | 107 | 0.1153 | 0.8 | 0.3347 | 3.1 | 1861 | 1872 | 1883.1 | - |
| z2.1 | 601 | 25 | 43 | 0.0571 | 1.2 | 0.0778 | 2.2 | 482 | 480 | 465.9 | 483 ± 11 |
| z2.2 | 180 | 70 | 17 | 0.0595 | 2 | 0.0944 | 2.3 | 580 | 568 | 519.7 | 581 ± 14 |
| z3.1 | 238 | 118 | 27 | 0.0622 | 1.6 | 0.1094 | 2.2 | 668 | 651 | 593.5 | 669 ± 15 |
| z4.1 | 1816 | 42 | 134 | 0.0564 | 0.7 | 0.0805 | 2.2 | 498 | 488 | 438.9 | 499 ± 11 |
| z4.2 | 1568 | 171 | 132 | 0.0606 | 0.7 | 0.0902 | 2.3 | 556 | 556 | 555.3 | 556 ± 13 |
| z5.1 | 586 | 58 | 43 | 0.0579 | 1.3 | 0.0776 | 2.2 | 481 | 483 | 492.9 | 481 ± 11 |
| z5.2 | 514 | 15 | 38 | 0.0556 | 1.3 | 0.0799 | 2.2 | 495 | 476 | 388.9 | 496 ± 11 |
| z6.1 | 1141 | 169 | 357 | 0.1228 | 0.3 | 0.3108 | 2.2 | 1744 | 1861 | 1993.5 | - |
| z6.2 | 1316 | 33 | 96 | 0.057 | 0.8 | 0.0798 | 2.2 | 494 | 484 | 437.9 | 495 ± 11 |
| z7.1 | 493 | 142 | 251 | 0.1713 | 0.7 | 0.4719 | 2.3 | 2491 | 2534 | 2567.5 | - |
| z7.2 | 956 | 47 | 65 | 0.0631 | 1 | 0.0724 | 2.2 | 447 | 453 | 479.9 | 447 ± 10 |
| z8.1 | 502 | 23 | 36 | 0.0564 | 1.3 | 0.0788 | 2.2 | 489 | 483 | 456.3 | 489 ± 11 |
| z8.2 | 158 | 60 | 17 | 0.0591 | 1.9 | 0.109 | 2.3 | 666 | 635 | 528.5 | 669 ± 16 |
| z10.1 | 1720 | 12 | 109 | 0.0558 | 0.8 | 0.0699 | 2.2 | 435 | 434 | 424.9 | 435 ± 10 |
| z10.2 | 379 | 130 | 36 | 0.0584 | 1.3 | 0.095 | 2.3 | 584 | 567 | 500.3 | 586 ± 13 |
| z11.1 | 878 | 69 | 80 | 0.06 | 0.8 | 0.0981 | 2.2 | 603 | 600 | 587.9 | 603 ± 13 |

Table 4.26: U-Pb LA-ICPMS and SIMS results of the Castellanos metagranite. Analyses references ending in b mean rims and c mean cores.

| | Element concentration (ppm) | | | Isotope ratios | | | | Ages (Ma) | | | |
|---|---|---|---|---|---|---|---|---|---|---|---|
| **Grain** | **U** | **Th** | **Pb** | **($^{207}Pb/^{206}Pb)_{meas}$** | **σ (%)** | **($^{206}Pb/^{238}U)_{meas}$** | **σ (%)** | **$^{206}Pb/^{238}U$** | **$^{207}Pb/^{235}U$** | **$^{207}Pb/^{206}Pb$** | **($^{206}Pb/^{238}U)_{cor}$** |
| ***Laser-Ablation ICPMS data*** | | | | | | | | | | | |
| z5c | 491 | 167 | 46 | 0.06 | 1.2 | 0.092 | 2.2 | 569 | 578 | 614 | 568 ± 12 |
| z6b | 862 | 3 | 60 | 0.056 | 1.2 | 0.075 | 2.2 | 469 | 465 | 445 | 469 ± 10 |
| z7b | 586 | 202 | 58 | 0.062 | 1.2 | 0.097 | 2.2 | 596 | 610 | 661 | 594 ± 13 |
| z7c | 589 | 234 | 61 | 0.062 | 1.2 | 0.099 | 2.2 | 607 | 620 | 668 | 606 ± 13 |
| z8 | 677 | 34 | 51 | 0.059 | 1.2 | 0.081 | 2.2 | 500 | 509 | 552 | 499 ± 11 |
| z10b | 544 | 258 | 45 | 0.056 | 1.2 | 0.08 | 2.2 | 495 | 485 | 435 | 496 ± 11 |
| z10c | 444 | 176 | 37 | 0.057 | 1.2 | 0.081 | 2.2 | 500 | 498 | 487 | 501 ± 11 |
| z12c | 301 | 136 | 32 | 0.06 | 1.2 | 0.102 | 2.2 | 627 | 618 | 587 | 627 ± 14 |
| z15c | 365 | 76 | 28 | 0.06 | 1.2 | 0.079 | 2.2 | 489 | 508 | 593 | 488 ± 11 |
| z16 | 383 | 243 | 46 | 0.06 | 1.2 | 0.108 | 2.2 | 663 | 649 | 600 | 664 ± 14 |
| z41a | 238 | 68 | 23 | 0.061 | 1.2 | 0.088 | 2.2 | 543 | 558 | 621 | 542 ± 12 |
| z41a | 186 | 64 | 18 | 0.059 | 1.2 | 0.09 | 2.2 | 557 | 560 | 574 | 556 ± 12 |
| z42a | 375 | 73 | 32 | 0.057 | 1.2 | 0.081 | 2.2 | 504 | 502 | 492 | 504 ± 11 |
| z42b | 256 | 63 | 22 | 0.056 | 1.2 | 0.082 | 2.2 | 507 | 500 | 467 | 508 ± 11 |
| z45 | 391 | 348 | 50 | 0.061 | 1.2 | 0.1 | 2.2 | 612 | 614 | 622 | 612 ± 13 |
| z46a | 543 | 59 | 44 | 0.057 | 1.2 | 0.081 | 2.2 | 501 | 499 | 490 | 501 ± 11 |
| z46b | 645 | 40 | 52 | 0.059 | 1.2 | 0.08 | 2.2 | 496 | 507 | 559 | 495 ± 11 |
| z47 | 271 | 89 | 37 | 0.064 | 1.2 | 0.124 | 2.2 | 751 | 747 | 734 | 752 ± 16 |
| z48 | 412 | 143 | 46 | 0.06 | 1.2 | 0.103 | 2.2 | 630 | 623 | 597 | 631 ± 14 |
| ***SIMS data*** | | | | | | | | | | | |
| z-11c | 198 | 120 | 76 | 0.1127 | 0.52 | 0.2967 | 1.4 | 1675 | 1752 | 1844 | - |
| z-11b | 982 | 81 | 99 | 0.0587 | 0.82 | 0.0896 | 1.41 | 553 | 553 | 555 | 553 ± 8 |
| z-12 | 966 | 21 | 79 | 0.057 | 0.83 | 0.0777 | 1.34 | 482 | 484 | 492 | 482 ± 7 |
| z-13 | 305 | 110 | 32 | 0.0602 | 1.16 | 0.091 | 1.34 | 561 | 571 | 609 | 560 ± 8 |
| z-14 | 29 | 73 | 33 | 0.2467 | 0.64 | 0.6006 | 1.45 | 3032 | 3112 | 3164 | - |
| z-15 | 2403 | 888 | 274 | 0.0601 | 0.3 | 0.0977 | 1.34 | 601 | 602 | 606 | 601 ± 8 |
| z-16 | 190 | 46 | 45 | 0.1377 | 1.06 | 0.1929 | 1.69 | 1137 | 1563 | 2198 | - |
| z-17 | 485 | 214 | 58 | 0.06 | 0.63 | 0.0997 | 1.34 | 612 | 611 | 604 | 613 ± 8 |
| z-18 | 1040 | 62 | 91 | 0.0569 | 0.54 | 0.0815 | 1.34 | 505 | 502 | 489 | 505 ± 7 |
| z-19 | 320 | 16 | 27 | 0.057 | 1.05 | 0.0801 | 1.34 | 496 | 496 | 492 | 497 ± 7 |
| z-20 | 380 | 200 | 38 | 0.0565 | 0.99 | 0.0815 | 1.34 | 505 | 499 | 471 | 505 ± 7 |
| z-21b | 895 | 3 | 77 | 0.0571 | 0.53 | 0.081 | 1.34 | 502 | 501 | 497 | 502 ± 7 |
| z-21a | 1281 | 57 | 99 | 0.0578 | 0.88 | 0.0794 | 1.34 | 492 | 498 | 523 | 492 ± 7 |
| z-22 | 461 | 221 | 59 | 0.0614 | 0.63 | 0.1048 | 1.34 | 643 | 645 | 654 | 643 ± 9 |
| z-23 | 516 | 143 | 52 | 0.0579 | 0.76 | 0.0873 | 1.34 | 540 | 537 | 528 | 540 ± 7 |
| z-24a | 913 | 3 | 84 | 0.0573 | 0.59 | 0.0872 | 1.34 | 539 | 532 | 502 | 540 ± 7 |
| z-24b | 221 | 44 | 21 | 0.0583 | 1.06 | 0.0851 | 1.34 | 527 | 530 | 542 | 526 ± 7 |
| z-25 | 386 | 262 | 55 | 0.0618 | 0.73 | 0.1117 | 1.34 | 683 | 679 | 668 | 683 ± 9 |

Table 4.27: U-Pb LA-ICPMS and SIMS results of the Bercimuelle metagranite. Analyses references ending in b mean rims and c mean cores.

| | Element concentration (ppm) | | | Isotope ratios | | | | Ages (Ma) | | | |
|---|---|---|---|---|---|---|---|---|---|---|---|
| **Grain** | **U** | **Th** | **Pb** | $(^{207}Pb/^{206}Pb)_{meas}$ | **σ (%)** | $(^{206}Pb/^{238}U)_{meas}$ | **σ (%)** | $^{206}Pb/^{238}U$ | $^{207}Pb/^{235}U$ | $^{207}Pb/^{206}Pb$ | $(^{206}Pb/^{238}U)_{cor}$ |
| ***Laser-ablation-ICPMS data*** | | | | | | | | | | | |
| z1b | 510 | 35 | 66 | 0.107 | 1.7 | 0.135 | 2.5 | 814 | 1100 | 1720 | 774 ± 20 |
| z1c | 299 | 79 | 132 | 0.174 | 1.7 | 0.417 | 2.5 | 2245 | 2430 | 2588 | - |
| z2b | 1585 | 67 | 124 | 0.057 | 1.7 | 0.088 | 2.5 | 542 | 524 | 443 | 544 ± 14 |
| z2c | 1169 | 533 | 136 | 0.065 | 1.7 | 0.113 | 2.5 | 689 | 702 | 741 | 688 ± 17 |
| z3b | 1397 | 434 | 112 | 0.06 | 1.7 | 0.083 | 2.5 | 511 | 517.7 | 548 | 510 ± 13 |
| z5b | 256 | 73 | 26 | 0.06 | 1.7 | 0.105 | 2.5 | 640 | 622.1 | 558 | 642 ± 16 |
| z5c | 442 | 113 | 43 | 0.06 | 1.7 | 0.102 | 2.5 | 626 | 612 | 562 | 627 ± 16 |
| z6b | 594 | 37 | 43 | 0.058 | 1.7 | 0.082 | 2.5 | 505 | 501 | 482 | 506 ± 13 |
| z6c | 423 | 39 | 31 | 0.055 | 1.7 | 0.078 | 2.5 | 482 | 458.9 | 343 | 485 ± 12 |
| z7b | 420 | 38 | 31 | 0.054 | 1.7 | 0.078 | 2.5 | 484 | 452.6 | 297 | 487 ± 12 |
| z7c | 790 | 163 | 59 | 0.057 | 1.7 | 0.08 | 2.5 | 494 | 486.3 | 451 | 494 ± 12 |
| z8b | 163 | 54 | 19 | 0.063 | 1.7 | 0.119 | 2.5 | 723 | 706.9 | 656 | 725 ± 18 |
| z8c | 331 | 159 | 42 | 0.066 | 1.7 | 0.122 | 2.5 | 741 | 742.3 | 746 | 741 ± 19 |
| z9b | 109 | 17 | 35 | 0.121 | 1.7 | 0.334 | 2.5 | 1854 | 1900.3 | 1952 | - |
| z9c | 116 | 19 | 36 | 0.121 | 1.7 | 0.322 | 2.5 | 1796 | 1867.7 | 1948 | - |
| z20a | 443 | 18 | 36 | 0.054 | 1.7 | 0.078 | 2.5 | 485 | 457 | 318 | 487 ± 12 |
| z20b | 533 | 195 | 57 | 0.06 | 1.7 | 0.099 | 2.5 | 607 | 592 | 537 | 608 ± 15 |
| z21b | 546 | 162 | 56 | 0.062 | 1.7 | 0.097 | 2.5 | 594 | 599 | 617 | 593 ± 15 |
| z22b | 1058 | 284 | 99 | 0.054 | 1.7 | 0.078 | 2.5 | 483 | 457 | 327 | 485 ± 12 |
| z22c | 1587 | 260 | 152 | 0.059 | 1.7 | 0.089 | 2.5 | 548 | 540 | 507 | 549 ± 14 |
| z23b | 647 | 76 | 57 | 0.058 | 1.7 | 0.081 | 2.5 | 499 | 493 | 463 | 499 ± 13 |
| z23c | 261 | 82 | 27 | 0.06 | 1.7 | 0.097 | 2.5 | 595 | 587 | 558 | 596 ± 15 |
| z25c | 622 | 29 | 64 | 0.061 | 1.7 | 0.105 | 2.5 | 641 | 632 | 602 | 642 ± 16 |
| z26b | 436 | 63 | 38 | 0.054 | 1.7 | 0.078 | 2.5 | 481 | 449 | 291 | 484 ± 12 |
| z26bb | 391 | 52 | 35 | 0.061 | 1.7 | 0.089 | 2.5 | 547 | 554 | 584 | 546 ± 14 |
| z27b | 389 | 48 | 66 | 0.122 | 1.7 | 0.157 | 2.5 | 940 | 1303 | 1965 | 880 ± 23 |
| z27c | 435 | 81 | 105 | 0.144 | 1.7 | 0.217 | 2.5 | 1262 | 1685 | 2261 | - |
| z28b | 708 | 113 | 54 | 0.059 | 1.7 | 0.077 | 2.5 | 479 | 483 | 501 | 478 ± 12 |
| z28bb | 605 | 66 | 47 | 0.058 | 1.7 | 0.078 | 2.5 | 481 | 482 | 488 | 481 ± 12 |
| z28c | 610 | 94 | 49 | 0.059 | 1.7 | 0.079 | 2.5 | 487 | 492 | 514 | 486 ± 12 |
| z29b | 615 | 45 | 209 | 0.173 | 1.7 | 0.309 | 2.5 | 1734 | 2148 | 2571 | - |
| z29bb | 903 | 54 | 467 | 0.198 | 1.7 | 0.466 | 2.5 | 2462 | 2650 | 2796 | - |
| z29c | 269 | 58 | 136 | 0.185 | 1.7 | 0.444 | 2.5 | 2364 | 2542 | 2686 | - |
| z30b | 525 | 166 | 55 | 0.059 | 1.7 | 0.102 | 2.5 | 623 | 599 | 508 | 626 ± 16 |
| z30bb | 432 | 23 | 39 | 0.058 | 1.7 | 0.096 | 2.5 | 592 | 567.9 | 471 | 595 ± 15 |
| z30c | 436 | 378 | 59 | 0.06 | 1.7 | 0.113 | 2.5 | 691 | 661 | 562 | 694 ± 17 |
| z31c | 523 | 84 | 45 | 0.057 | 1.7 | 0.079 | 2.5 | 488 | 475.8 | 420 | 489 ± 12 |

| | | | | | | | | | | | |
|---|---|---|---|---|---|---|---|---|---|---|---|
| z31b | 879 | 73 | 76 | 0.055 | 1.7 | 0.091 | 2.5 | 560 | 525 | 372 | 564 ± 14 |
| z33b | 496 | 122 | 42 | 0.057 | 1.7 | 0.089 | 2.5 | 548 | 526 | 435 | 550 ± 14 |
| z33bb | 609 | 124 | 52 | 0.056 | 1.7 | 0.087 | 2.5 | 538 | 515 | 413 | 540 ± 14 |
| z33c | 739 | 247 | 65 | 0.056 | 1.7 | 0.078 | 2.5 | 484 | 471 | 407 | 486 ± 12 |
| z34a | 248 | 77 | 22 | 0.058 | 1.7 | 0.079 | 2.5 | 489 | 488 | 480 | 489 ± 12 |
| z36b | 462 | 58 | 39 | 0.056 | 1.7 | 0.078 | 2.5 | 484 | 468 | 389 | 485 ± 12 |
| z36bb | 574 | 201 | 52 | 0.058 | 1.7 | 0.088 | 2.5 | 541 | 525.6 | 460 | 542 ± 14 |
| z36c | 477 | 95 | 41 | 0.057 | 1.7 | 0.088 | 2.5 | 542 | 523.1 | 440 | 544 ± 14 |
| z38a | 548 | 186 | 58 | 0.059 | 1.7 | 0.103 | 2.5 | 630 | 606.4 | 518 | 633 ± 16 |
| z38b | 461 | 137 | 49 | 0.06 | 1.7 | 0.104 | 2.5 | 634 | 613.8 | 540 | 636 ± 16 |
| ***Ion-microprobe data*** | | | | | | | | | | | |
| z2 | 1500 | 584 | 184 | 0.0603 | 0.36 | 0.1044 | 1.34 | 640 | 634 | 613 | 641 ± 8 |
| z6 | 459 | 27 | 38 | 0.057 | 0.78 | 0.0781 | 1.34 | 485 | 486 | 492 | 485 ± 7 |
| z7 | 638 | 93 | 56 | 0.0573 | 0.68 | 0.0793 | 1.34 | 492 | 494 | 504 | 492 ± 7 |
| z8a | 300 | 10 | 25 | 0.0573 | 0.96 | 0.0783 | 1.34 | 486 | 489 | 501 | 486 ± 7 |
| z8b | 482 | 8 | 40 | 0.0569 | 0.76 | 0.0789 | 1.34 | 489 | 489 | 489 | 489 ± 7 |
| z9a | 72 | 24 | 11 | 0.0652 | 1.45 | 0.1259 | 1.34 | 765 | 769 | 781 | 764 ± 11 |
| z9b | 184 | 109 | 29 | 0.0642 | 0.95 | 0.1248 | 1.35 | 758 | 756 | 750 | 758 ± 10 |
| z10 | 268 | 11 | 22 | 0.0572 | 1.01 | 0.0781 | 1.34 | 485 | 488 | 500 | 485 ± 9 |

Table 4.28: U-Pb LA-ICPMS and SIMS results of the La Cañada metagranite. Analyses references ending in b mean rims and c mean cores.

| | Element concentration (ppm) | | | Isotope ratios | | | | Ages (Ma) | | | |
|---|---|---|---|---|---|---|---|---|---|---|---|
| **Grain** | **U** | **Th** | **Pb** | **($^{207}Pb/^{206}Pb)_{meas}$** | **σ (%)** | **($^{206}Pb/^{238}U)_{meas}$** | **σ (%)** | **$^{206}Pb/^{238}U$** | **$^{207}Pb/^{235}U$** | **$^{207}Pb/^{206}Pb$** | **($^{206}Pb/^{238}U)_{cor}$** |
| ***Laser-Ablation ICPMS data*** | | | | | | | | | | | |
| z2 | 4369 | 1240 | 278 | 0.061 | 2.77 | 0.067 | 3.45 | 412 | 416 | 439 | 419 ± 14 |
| z3 | 281 | 95 | 20 | 0.075 | 9.41 | 0.072 | 5.66 | 436 | 409 | 263 | 438 ± 26 |
| z4 | 232 | 281 | 85 | 0.121 | 2.31 | 0.272 | 7 | 1525 | 1608 | 1718 | - |
| z6 | 685 | 39 | 36 | 0.058 | 3.01 | 0.056 | 2.5 | 350 | 321 | 114 | 352 ± 9 |
| z16 | 1129 | 139 | 64 | 0.077 | 15.36 | 0.056 | 8.23 | 338 | 329 | 266 | 338 ± 29 |
| z17 | 1423 | 253 | 88 | 0.066 | 4.69 | 0.061 | 4.93 | 377 | 379 | 392 | 377 ± 19 |
| z18 | 2804 | 1320 | 205 | 0.094 | 11.57 | 0.064 | 11.8 | 379 | 378 | 375 | 378 ± 43 |
| z27 | 1533 | 623 | 116 | 0.061 | 2.51 | 0.071 | 2.68 | 437 | 405 | 222 | 440 ± 12 |
| ***Ion-microprobe data*** | | | | | | | | | | | |
| z39b | 542 | 54 | 45 | 0.057 | 0.97 | 0.0772 | 1.05 | 479 | 481 | 491 | 479 ± 5 |
| z39m | 1621 | 609 | 193 | 0.0624 | 0.46 | 0.1022 | 1.05 | 627 | 641 | 688 | 626 ± 7 |
| z41c | 562 | 328 | 54 | 0.0582 | 0.89 | 0.0788 | 1.1 | 489 | 498 | 536 | 489 ± 6 |
| z43b | 2698 | 95 | 230 | 0.0569 | 0.42 | 0.0802 | 1.05 | 497 | 496 | 489 | 497 ± 5 |
| z43c | 104 | 132 | 14 | 0.0591 | 1.84 | 0.0961 | 1.06 | 591 | 587 | 572 | 592 ± 7 |
| z44m | 300 | 296 | 37 | 0.0602 | 1.11 | 0.0902 | 1.05 | 557 | 568 | 611 | 556 ± 6 |
| z45b | 998 | 64 | 84 | 0.0559 | 0.69 | 0.0787 | 1.05 | 488 | 481 | 447 | 489 ± 5 |
| z45c | 1504 | 370 | 161 | 0.0594 | 0.62 | 0.0942 | 1.26 | 581 | 581 | 583 | 581 ± 7 |
| z48c | 208 | 71 | 22 | 0.0582 | 1.74 | 0.0897 | 1.08 | 554 | 550 | 536 | 554 ± 6 |
| z49b | 369 | 32 | 30 | 0.0573 | 1.1 | 0.0764 | 1.06 | 475 | 480 | 503 | 474 ± 5 |
| z49c | 339 | 157 | 214 | 0.1818 | 0.38 | 0.4819 | 1.05 | 2536 | 2610 | 2670 | - |
| z50m | 433 | 395 | 54 | 0.0598 | 0.94 | 0.0933 | 1.05 | 575 | 579 | 596 | 575 ± 6 |
| z51b | 361 | 9 | 31 | 0.0575 | 1.11 | 0.0812 | 1.06 | 504 | 505 | 511 | 503 ± 6 |

Table 4.29: U-Pb SIMS results of La Hoya metagranite. Analyses references ending in b mean rims and c mean cores.

| | Element concentration (ppm) | | | Isotope ratios | | | | Ages (Ma) | | | |
|---|---|---|---|---|---|---|---|---|---|---|---|
| **Grain** | **U** | **Th** | **Pb** | **($^{207}Pb/^{206}Pb)_{meas}$** | **σ (%)** | **($^{206}Pb/^{238}U)_{meas}$** | **σ (%)** | **$^{206}Pb/^{238}U$** | **$^{207}Pb/^{235}U$** | **$^{207}Pb/^{206}Pb$** | **($^{206}Pb/^{238}U)_{cor}$** |
| z2 | 215 | 30 | 18 | 0.05695 | 1.3 | 0.0768 | 1.06 | 477 | 479 | 490 | 477 ± 5 |
| z5 | 765 | 55 | 62 | 0.05681 | 0.71 | 0.0753 | 1.06 | 468 | 471 | 484 | 468 ± 5 |
| z8 | 222 | 130 | 21 | 0.05743 | 1.3 | 0.0755 | 1.05 | 469 | 476 | 508 | 469 ± 5 |
| z12b | 1502 | 54 | 101 | 0.05546 | 0.54 | 0.063 | 1.05 | 394 | 399 | 431 | 393 ± 4 |
| z14 | 432 | 629 | 51 | 0.05739 | 0.87 | 0.0774 | 1.05 | 480 | 485 | 507 | 480 ± 5 |
| z15c | 353 | 532 | 42 | 0.05593 | 1.15 | 0.0777 | 1.09 | 483 | 477 | 450 | 483 ± 6 |
| z16b | 547 | 4 | 46 | 0.05712 | 0.74 | 0.0789 | 1.05 | 490 | 491 | 496 | 489 ± 5 |
| z16c | 43 | 68 | 8 | 0.06412 | 2.25 | 0.1166 | 1.05 | 711 | 719 | 746 | 710 ± 8 |

Table 4.30: U-Pb SIMS results of the La Estación metagranite. Analyses references ending in b mean rims and c mean cores.

| | Element concentration (ppm) | | | Isotope ratios | | | | Ages (Ma) | | | |
|---|---|---|---|---|---|---|---|---|---|---|---|
| Grain | U | Th | Pb | $(^{207}Pb/^{206}Pb)_{meas}$ | σ (%) | $(^{206}Pb/^{238}U)_{meas}$ | σ (%) | $^{206}Pb/^{238}U$ | $^{207}Pb/^{235}U$ | $^{207}Pb/^{206}Pb$ | $(^{206}Pb/^{238}U)_{cor}$ |
| z24b | 2306 | 105 | 197 | 0.0565 | 0.4 | 0.08 | 0.91 | 496 | 492 | 472 | 496 ± 4 |
| z26b | 2458 | 23 | 205 | 0.0571 | 0.38 | 0.0789 | 0.92 | 489 | 491 | 496 | 489 ± 4 |
| z29b | 913 | 46 | 75 | 0.0568 | 0.61 | 0.0769 | 0.95 | 477 | 479 | 484 | 477 ± 5 |
| z29c | 271 | 128 | 32 | 0.0603 | 0.95 | 0.0989 | 0.93 | 608 | 610 | 616 | 608 ± 6 |
| z30c | 583 | 976 | 73 | 0.0564 | 0.76 | 0.079 | 0.92 | 490 | 486 | 466 | 490 ± 5 |
| z30m | 497 | 25 | 41 | 0.056 | 0.86 | 0.0774 | 0.92 | 480 | 475 | 451 | 481 ± 5 |
| z32b | 765 | 10 | 65 | 0.0568 | 0.92 | 0.0808 | 0.84 | 501 | 498 | 482 | 501 ± 4 |
| z32c | 414 | 212 | 49 | 0.0599 | 0.93 | 0.0972 | 0.83 | 598 | 599 | 602 | 598 ± 5 |
| z33b | 409 | 38 | 35 | 0.0563 | 1.16 | 0.08 | 0.88 | 496 | 491 | 466 | 497 ± 5 |
| z33c | 631 | 238 | 115 | 0.0693 | 0.55 | 0.154 | 0.83 | 924 | 919 | 909 | 924 ± 8 |
| z34b | 586 | 51 | 50 | 0.0566 | 0.89 | 0.0795 | 0.84 | 493 | 490 | 475 | 493 ± 4 |
| z35c | 254 | 200 | 26 | 0.0567 | 1.34 | 0.0779 | 0.84 | 484 | 483 | 481 | 484 ± 4 |
| z36b | 360 | 43 | 31 | 0.0575 | 1.08 | 0.0798 | 0.84 | 495 | 498 | 510 | 495 ± 4 |
| z36c | 95 | 44 | 12 | 0.0607 | 1.76 | 0.1054 | 0.89 | 646 | 642 | 630 | 646 ± 6 |

Table 4.31: U-Pb SIMS results of the La Estación II metagranite. Analyses references ending in b mean rims and c mean cores.

| | Element concentration (ppm) | | | Isotope ratios | | | | Ages (Ma) | | | |
|---|---|---|---|---|---|---|---|---|---|---|---|
| Grain | U | Th | Pb | $(^{207}Pb/^{206}Pb)_{meas}$ | σ (%) | $(^{206}Pb/^{238}U)_{meas}$ | σ (%) | $^{206}Pb/^{238}U$ | $^{207}Pb/^{235}U$ | $^{207}Pb/^{206}Pb$ | $(^{206}Pb/^{238}U)_{cor}$ |
| z39b | 1150 | 51 | 96 | 0.0567 | 0.55 | 0.0777 | 1.06 | 482 | 482 | 478 | 482 ± 5 |
| z40b | 3626 | 93 | 288 | 0.0584 | 0.3 | 0.0764 | 1.05 | 475 | 487 | 545 | 474 ± 5 |
| z47b | 518 | 68 | 44 | 0.0576 | 0.99 | 0.0774 | 0.92 | 481 | 487 | 515 | 480 ± 5 |
| z48c | 352 | 322 | 34 | 0.0573 | 1.24 | 0.0734 | 0.92 | 457 | 465 | 503 | 456 ± 5 |
| z49b | 734 | 72 | 60 | 0.0558 | 1.11 | 0.0751 | 0.93 | 467 | 463 | 443 | 467 ± 5 |
| z49c | 669 | 557 | 67 | 0.0571 | 0.86 | 0.077 | 0.93 | 479 | 481 | 494 | 478 ± 5 |

Table 4.32: U-Pb SIMS results of the melanocric metagranites of Vegas de Matute. Analyses references ending in b mean rims and c mean cores.

| | Element concentration (ppm) | | | Isotope ratios | | | | Ages (Ma) | | | |
|---|---|---|---|---|---|---|---|---|---|---|---|
| **Grain** | **U** | **Th** | **Pb** | **($^{207}Pb/^{206}Pb)_{meas}$** | **σ (%)** | **($^{206}Pb/^{238}U)_{meas}$** | **σ (%)** | **$^{206}Pb/^{238}U$** | **$^{207}Pb/^{235}U$** | **$^{207}Pb/^{206}Pb$** | **($^{206}Pb/^{238}U)_{cor}$** |
| z48b | 244 | 11 | 20 | 0.0568 | 1.86 | 0.0757 | 1.2 | 470 | 473 | 482 | 470 ± 6 |
| z48c | 191 | 95 | 20 | 0.0587 | 2.62 | 0.0911 | 1.2 | 562 | 561 | 556 | 562 ± 8 |
| z49b | 481 | 65 | 39 | 0.0579 | 1.27 | 0.0757 | 1.2 | 470 | 480 | 526 | 469 ± 6 |
| z50b | 400 | 45 | 34 | 0.0561 | 1.11 | 0.0792 | 1.2 | 491 | 485 | 455 | 492 ± 6 |
| z50c | 92 | 212 | 26 | 0.0734 | 1.35 | 0.1697 | 1.3 | 1011 | 1015 | 1024 | - |
| z52b | 713 | 38 | 69 | 0.059 | 0.85 | 0.0906 | 1.25 | 559 | 561 | 568 | 559 ± 7 |
| z52c | 201 | 100 | 23 | 0.0597 | 1.34 | 0.0973 | 1.2 | 599 | 598 | 594 | 599 ± 8 |
| z53b | 479 | 70 | 45 | 0.0576 | 0.74 | 0.0856 | 1.42 | 530 | 527 | 515 | 530 ± 8 |
| z53c | 407 | 206 | 45 | 0.0589 | 0.95 | 0.0929 | 1.2 | 573 | 571 | 563 | 573 ± 7 |
| z54c | 17 | 18 | 9 | 0.121 | 1.48 | 0.3484 | 1.3 | 1927 | 1948 | 1971 | - |
| z55c | 787 | 161 | 72 | 0.0564 | 0.44 | 0.0816 | 1.36 | 505 | 499 | 469 | 506 ± 7 |
| z57c | 369 | 343 | 39 | 0.0565 | 0.67 | 0.0772 | 1.21 | 479 | 478 | 475 | 479 ± 6 |
| z58b | 325 | 29 | 27 | 0.0571 | 0.71 | 0.077 | 1.24 | 478 | 481 | 496 | 478 ± 6 |
| z59b | 224 | 15 | 19 | 0.0565 | 0.87 | 0.0766 | 1.22 | 476 | 475 | 473 | 476 ± 6 |
| z59c | 383 | 166 | 41 | 0.0599 | 1.28 | 0.0884 | 1.22 | 546 | 557 | 602 | 545 ± 7 |
| z60 | 371 | 26 | 30 | 0.0565 | 0.78 | 0.0757 | 1.2 | 470 | 471 | 473 | 470 ± 6 |
| z61b | 298 | 23 | 24 | 0.0571 | 0.8 | 0.0757 | 1.2 | 470 | 475 | 497 | 470 ± 6 |
| z61c | 94 | 39 | 10 | 0.0593 | 1.51 | 0.0922 | 1.2 | 569 | 571 | 579 | 569 ± 7 |
| z63b | 292 | 24 | 24 | 0.0574 | 0.82 | 0.077 | 1.35 | 478 | 483 | 506 | 478 ± 7 |
| z63c | 107 | 83 | 14 | 0.0615 | 1.14 | 0.0992 | 1.22 | 610 | 620 | 656 | 609 ± 8 |

Table 4.33: U-Pb SIMS results of the leucocratic metagranite of Vegas de Matute. Analyses references ending in b mean rims and c mean cores.

| | Element concentration (ppm) | | | Isotope ratios | | | | Ages (Ma) | | | |
|---|---|---|---|---|---|---|---|---|---|---|---|
| Grain | U | Th | Pb | $(^{207}Pb/^{206}Pb)_{meas}$ | σ (%) | $(^{206}Pb/^{238}U)_{meas}$ | σ (%) | $^{206}Pb/^{238}U$ | $^{207}Pb/^{235}U$ | $^{207}Pb/^{206}Pb$ | $(^{206}Pb/^{238}U)_{cor}$ |
| z45b | 271 | 32 | 24 | 0.0581 | 1.74 | 0.0813 | 2.05 | 504 | 509 | 533 | 503 ± 11 |
| z44b | 985 | 89 | 85 | 0.0573 | 1.27 | 0.081 | 2.05 | 502 | 502 | 503 | 502 ± 10 |
| z33c | 223 | 277 | 25 | 0.0559 | 1.38 | 0.0767 | 1.96 | 477 | 472 | 448 | 477 ± 10 |
| z35c | 126 | 21 | 11 | 0.058 | 1.78 | 0.0766 | 1.95 | 476 | 485 | 530 | 475 ± 10 |
| z1b | 331 | 114 | 28 | 0.0796 | 1.14 | 0.0789 | 1.48 | 477 | 490 | 548 | 476 ± 7 |
| z2c | 297 | 41 | 20 | 0.0702 | 0.94 | 0.0595 | 1.47 | 365 | 366 | 370 | 365 ± 6 |
| z3b | 335 | 80 | 26 | 0.0931 | 0.7 | 0.0623 | 1.47 | 371 | 372 | 378 | 371 ± 6 |
| z4b | 3098 | 110 | 275 | 0.0602 | 0.7 | 0.0777 | 1.47 | 480 | 478 | 470 | 480 ± 7 |
| z4c | 564 | 152 | 51 | 0.1044 | 1.28 | 0.07 | 1.48 | 411 | 418 | 454 | 409 ± 7 |
| z6c | 844 | 84 | 71 | 0.0788 | 0.67 | 0.0715 | 1.47 | 433 | 431 | 424 | 432 ± 7 |
| z8c | 1352 | 77 | 112 | 0.0597 | 0.45 | 0.0765 | 1.48 | 473 | 471 | 462 | 473 ± 7 |
| z9b | 1315 | 68 | 112 | 0.0592 | 0.39 | 0.0788 | 1.47 | 487 | 482 | 457 | 488 ± 7 |
| z10c | 1552 | 365 | 158 | 0.0823 | 0.29 | 0.0788 | 1.47 | 475 | 484 | 529 | 473 ± 7 |
| z10b | 1051 | 169 | 101 | 0.0758 | 0.81 | 0.0802 | 1.49 | 486 | 490 | 504 | 486 ± 7 |
| z11b | 2060 | 140 | 174 | 0.1192 | 1.14 | 0.0648 | 1.48 | 372 | 366 | 326 | 372 ± 6 |
| z12c | 312 | 44 | 26 | 0.0593 | 0.98 | 0.0794 | 1.49 | 490 | 479 | 425 | 491 ± 7 |
| z15c | 456 | 88 | 39 | 0.0593 | 0.8 | 0.0786 | 1.48 | 486 | 484 | 472 | 486 ± 7 |
| z20c | 380 | 54 | 32 | 0.0581 | 0.84 | 0.0776 | 1.48 | 481 | 479 | 470 | 481 ± 7 |

Table 4.34: U-Pb SIMS results of the Morcuera metagranite. Analyses references ending in b mean rims and c mean cores.

| | Element concentration (ppm) | | | Isotope ratios | | | | Ages (Ma) | | | |
|---|---|---|---|---|---|---|---|---|---|---|---|
| Grain | U | Th | Pb | $(^{207}Pb/^{206}Pb)_{meas}$ | σ (%) | $(^{206}Pb/^{238}U)_{meas}$ | σ (%) | $^{206}Pb/^{238}U$ | $^{207}Pb/^{235}U$ | $^{207}Pb/^{206}Pb$ | $(^{206}Pb/^{238}U)_{cor}$ |
| z42b | 243 | 51 | 21 | 0.0583 | 1.28 | 0.0785 | 0.84 | 487 | 497 | 543 | 486 ± 4 |
| z42c | 153 | 80 | 20 | 0.061 | 1.37 | 0.1064 | 0.83 | 652 | 649 | 638 | 652 ± 6 |
| z48b | 259 | 32 | 22 | 0.0553 | 1.2 | 0.0794 | 0.84 | 492 | 481 | 426 | 494 ± 4 |
| z48c | 179 | 162 | 25 | 0.0621 | 1.41 | 0.1035 | 0.83 | 635 | 644 | 679 | 634 ± 6 |
| z50c | 177 | 96 | 20 | 0.0583 | 1.31 | 0.0927 | 0.84 | 571 | 566 | 542 | 572 ± 5 |
| z53b | 603 | 62 | 49 | 0.0571 | 0.74 | 0.0753 | 0.83 | 468 | 472 | 494 | 468 ± 4 |
| z54b | 463 | 46 | 40 | 0.0569 | 0.87 | 0.0786 | 0.83 | 488 | 488 | 489 | 488 ± 4 |
| z54c | 205 | 47 | 28 | 0.0652 | 1.19 | 0.1193 | 0.83 | 726 | 740 | 782 | 725 ± 7 |
| z55 | 370 | 30 | 31 | 0.0575 | 1.01 | 0.0777 | 0.84 | 483 | 488 | 512 | 482 ± 4 |
| z57 | 296 | 40 | 25 | 0.0575 | 1.07 | 0.0767 | 0.84 | 477 | 483 | 512 | 476 ± 4 |
| z58b | 321 | 30 | 29 | 0.0577 | 1.34 | 0.0833 | 0.85 | 516 | 517 | 520 | 516 ± 5 |
| z59c | 483 | 165 | 58 | 0.0613 | 0.71 | 0.1029 | 0.84 | 632 | 635 | 648 | 631 ± 5 |

Table 4.35: U-Pb SIMS results of the Buitrago de Lozoya metagranite. Analyses references ending in b mean rims and c mean cores.

| | Element concentration (ppm) | | | Isotope ratios | | | | Ages (Ma) | | | |
|---|---|---|---|---|---|---|---|---|---|---|---|
| Grain | U | Th | Pb | $(^{207}Pb/^{206}Pb)_{meas}$ | σ (%) | $(^{206}Pb/^{238}U)_{meas}$ | σ (%) | $^{206}Pb/^{238}U$ | $^{207}Pb/^{235}U$ | $^{207}Pb/^{206}Pb$ | $(^{206}Pb/^{238}U)_{cor}$ |
| z10b | 506 | 14 | 42 | 0.0574 | 1.4 | 0.0774 | 1.98 | 481 | 486 | 509 | 480 ±10 |
| z11b | 778 | 109 | 74 | 0.0593 | 0.82 | 0.0868 | 1.98 | 537 | 545 | 578 | 536 ± 11 |
| z11c | 513 | 111 | 50 | 0.0604 | 1.14 | 0.0882 | 1.95 | 545 | 560 | 619 | 544 ± 11 |
| z13c | 88 | 71 | 10 | 0.0598 | 2.05 | 0.0912 | 2.03 | 563 | 569 | 596 | 562 ± 12 |
| z14b | 297 | 7 | 24 | 0.0572 | 1.09 | 0.0754 | 1.63 | 468 | 474 | 499 | 468 ± 8 |
| z16c | 119 | 62 | 71 | 0.18 | 0.51 | 0.4518 | 1.63 | 2403 | 2541 | 2653 | - |
| z17c | 120 | 170 | 25 | 0.0667 | 1.04 | 0.1389 | 1.65 | 838 | 835 | 827 | 839 ± 14 |
| z23b | 450 | 37 | 38 | 0.0566 | 1.09 | 0.0787 | 1.63 | 488 | 486 | 475 | 488 ± 8 |
| z23c | 339 | 283 | 45 | 0.0607 | 0.72 | 0.1019 | 1.66 | 625 | 626 | 628 | 625 ± 10 |
| z27b | 372 | 34 | 32 | 0.0562 | 0.81 | 0.0786 | 1.63 | 488 | 483 | 462 | 488 ± 8 |
| z27c | 254 | 103 | 32 | 0.0621 | 0.78 | 0.1065 | 1.64 | 652 | 658 | 678 | 652 ± 11 |

Table 4.36: U-Pb SIMS results of the La Berzosa metavolcanic rocks. Analyses references ending in b mean rims and c mean cores.

| | Element concentration (ppm) | | | Isotope ratios | | | | Ages (Ma) | | | |
|---|---|---|---|---|---|---|---|---|---|---|---|
| Grain | U | Th | Pb | $(^{207}Pb/^{206}Pb)_{meas}$ | σ (%) | $(^{206}Pb/^{238}U)_{meas}$ | σ (%) | $^{206}Pb/^{238}U$ | $^{207}Pb/^{235}U$ | $^{207}Pb/^{206}Pb$ | $(^{206}Pb/^{238}U)_{cor}$ |
| z1b | 333 | 46 | 28 | 0.0561 | 1.4 | 0.0765 | 2 | 475 | 472 | 457 | 475 ± 10 |
| z2 | 197 | 106 | 18 | 0.0596 | 2.02 | 0.0777 | 1.95 | 483 | 502 | 591 | 481 ± 10 |
| z4b | 311 | 84 | 26 | 0.0562 | 1.97 | 0.0731 | 1.98 | 455 | 456 | 461 | 455 ± 9 |
| z4b2 | 127 | 59 | 11 | 0.0571 | 1.14 | 0.0733 | 0.68 | 456 | 463 | 495 | 456 ± 3 |
| z6c | 64 | 45 | 9 | 0.0634 | 2.62 | 0.1129 | 2 | 690 | 697 | 721 | 689 ± 15 |
| z8c | 143 | 40 | 86 | 0.1832 | 0.61 | 0.4758 | 0.66 | 2509 | 2606 | 2682 | - |
| z9b | 334 | 29 | 31 | 0.062 | 0.93 | 0.0869 | 1.96 | 537 | 564 | 674 | 535 ± 10 |
| z11c | 240 | 179 | 33 | 0.0611 | 1.15 | 0.1035 | 1.95 | 635 | 636 | 642 | 635 ± 12 |
| z14c | 90 | 60 | 42 | 0.1206 | 0.94 | 0.3494 | 1.96 | 1932 | 1948 | 1965 | - |
| z15c | 307 | 119 | 35 | 0.06 | 0.96 | 0.0963 | 1.95 | 593 | 595 | 604 | 593 ± 11 |
| z15b | 207 | 21 | 17 | 0.0641 | 1.25 | 0.0744 | 1.98 | 463 | 513 | 746 | 458 ± 9 |
| z16c | 331 | 283 | 42 | 0.0594 | 1.14 | 0.098 | 1.68 | 603 | 598 | 580 | 603 ± 10 |
| z18b | 556 | 293 | 67 | 0.0624 | 0.79 | 0.1 | 1.7 | 615 | 631 | 690 | 613 ± 10 |
| z18c | 367 | 154 | 44 | 0.0634 | 0.74 | 0.1017 | 1.64 | 625 | 646 | 723 | 622 ± 10 |
| z19b | 607 | 50 | 47 | 0.0642 | 0.81 | 0.0726 | 1.65 | 452 | 504 | 748 | 447 ± 7 |

Table 4.37: U-Pb SIMS results of the El Cardoso metavolcanic rocks. Analyses references ending in b mean rims and c mean cores.

| | Element concentration (ppm) | | | Isotope ratios | | | | Ages (Ma) | | | |
|---|---|---|---|---|---|---|---|---|---|---|---|
| Grain | U | Th | Pb | $(^{207}Pb/^{206}Pb)_{meas}$ | σ (%) | $(^{206}Pb/^{238}U)_{meas}$ | σ (%) | $^{206}Pb/^{238}U$ | $^{207}Pb/^{235}U$ | $^{207}Pb/^{206}Pb$ | $(^{206}Pb/^{238}U)_{cor}$ |
| z1c | 177 | 117 | 22 | 0.0622 | 1.8 | 0.0994 | 1.52 | 610 | 618 | 646 | 609 ± 10 |
| z4b | 235 | 20 | 20 | 0.0583 | 1.22 | 0.0787 | 1.49 | 487 | 485 | 473 | 488 ± 7 |
| z4c | 530 | 224 | 197 | 0.1192 | 0.48 | 0.3024 | 1.47 | 1703 | 1812 | 1941 | - |
| z5c | 345 | 408 | 33 | 0.0623 | 1.07 | 0.0782 | 1.49 | 483 | 488 | 514 | 482 ± 7 |
| z7c | 307 | 922 | 20 | 0.0755 | 0.93 | 0.0526 | 1.47 | 323 | 340 | 461 | 321 ± 5 |
| z8c | 587 | 21 | 50 | 0.0573 | 0.64 | 0.0791 | 1.48 | 491 | 492 | 496 | 491 ± 7 |
| z10c | 1380 | 1224 | 146 | 0.0576 | 0.51 | 0.0796 | 1.49 | 494 | 496 | 509 | 493 ± 7 |
| z11c | 713 | 631 | 69 | 0.0584 | 0.62 | 0.0776 | 1.48 | 481 | 482 | 485 | 481 ± 7 |
| z15c | 1848 | 1379 | 191 | 0.0566 | 0.43 | 0.0784 | 1.49 | 486 | 482 | 462 | 487 ± 7 |
| z16c | 59 | 17 | 10 | 0.0693 | 1.31 | 0.144 | 1.54 | 866 | 868 | 873 | 866 ± 14 |
| z16b | 497 | 180 | 62 | 0.0638 | 0.55 | 0.1078 | 1.49 | 659 | 669 | 703 | 658 ± 10 |
| z24b | 318 | 134 | 34 | 0.0637 | 0.86 | 0.0978 | 3.36 | 601 | 630 | 733 | 599 ± 19 |
| z26b | 289 | 19 | 25 | 0.0559 | 1.06 | 0.0791 | 3.31 | 491 | 483 | 448 | 492 ± 16 |
| z30b | 188 | 120 | 16 | 0.0578 | 1.35 | 0.0748 | 3.29 | 465 | 476 | 528 | 464 ± 15 |
| z32b | 268 | 31 | 22 | 0.0574 | 1.2 | 0.0761 | 3.29 | 473 | 479 | 507 | 472 ± 15 |

Table 4.38: U-Pb SIMS results of the Riaza metavolcanic rocks. Analyses references ending in b mean rims and c mean cores.

| | Element concentration (ppm) | | | Isotope ratios | | | | Ages (Ma) | | | |
|---|---|---|---|---|---|---|---|---|---|---|---|
| Grain | U | Th | Pb | $(^{207}Pb/^{206}Pb)_{meas}$ | σ (%) | $(^{206}Pb/^{238}U)_{meas}$ | σ (%) | $^{206}Pb/^{238}U$ | $^{207}Pb/^{235}U$ | $^{207}Pb/^{206}Pb$ | $(^{206}Pb/^{238}U)_{cor}$ |
| z21c | 975 | 49 | 366 | 0.1214 | 0.54 | 0.3303 | 1.49 | 1840 | 1905 | 1976 | - |
| z22c | 221 | 273 | 30 | 0.0614 | 1.01 | 0.0936 | 1.47 | 576 | 580 | 596 | 575 ± 9 |
| z23c | 1068 | 316 | 136 | 0.078 | 0.38 | 0.1073 | 1.47 | 646 | 664 | 724 | 643 ± 9 |
| z23b | 493 | 35 | 40 | 0.0584 | 0.83 | 0.0765 | 1.47 | 473 | 464 | 420 | 474 ± 7 |
| z24c | 365 | 251 | 45 | 0.0834 | 0.63 | 0.0915 | 1.47 | 548 | 554 | 575 | 547 ± 8 |
| z25b | 504 | 69 | 40 | 0.0656 | 0.86 | 0.0766 | 1.49 | 471 | 471 | 473 | 470 ± 7 |
| z32c | 295 | 39 | 24 | 0.063 | 0.99 | 0.0769 | 1.47 | 473 | 463 | 415 | 474 ± 7 |
| z33c | 234 | 189 | 31 | 0.0642 | 0.87 | 0.0991 | 1.48 | 606 | 599 | 575 | 606 ± 9 |
| z35c | 148 | 116 | 19 | 0.0613 | 1.13 | 0.0969 | 1.54 | 596 | 600 | 618 | 595 ± 9 |
| z35b | 440 | 228 | 53 | 0.0599 | 0.73 | 0.0976 | 1.47 | 600 | 594 | 574 | 600 ± 9 |
| z35b2 | 415 | 30 | 35 | 0.0567 | 0.93 | 0.0784 | 1.58 | 486 | 476 | 430 | 487 ± 8 |
| z4c | 145 | 125 | 21 | 0.0609 | 1.29 | 0.1042 | 1.99 | 639 | 638 | 637 | 639 ± 13 |
| z5b | 341 | 15 | 28 | 0.0574 | 1.24 | 0.0771 | 1.96 | 479 | 484 | 506 | 479 ± 9 |
| z5c | 189 | 75 | 20 | 0.0576 | 1.26 | 0.0881 | 1.95 | 544 | 539 | 517 | 545 ± 11 |
| z6b | 246 | 23 | 20 | 0.0575 | 1.12 | 0.0754 | 1.95 | 469 | 476 | 510 | 468 ± 9 |
| z9b | 222 | 73 | 23 | 0.0593 | 0.87 | 0.0869 | 0.71 | 537 | 545 | 577 | 537 ± 4 |
| z13b | 121 | 93 | 15 | 0.0591 | 1.47 | 0.0964 | 1.95 | 594 | 589 | 569 | 594 ± 12 |

Table 4.39: U-Pb SIMS results of the Polán metagranite. Analyses references ending in b mean rims and c mean cores.

| | Element concentration (ppm) | | | Isotope ratios | | | | Ages (Ma) | | | |
|---|---|---|---|---|---|---|---|---|---|---|---|
| Grain | U | Th | Pb | $(^{207}Pb/^{206}Pb)_{meas}$ | σ (%) | $(^{206}Pb/^{238}U)_{meas}$ | σ (%) | $^{206}Pb/^{238}U$ | $^{207}Pb/^{235}U$ | $^{207}Pb/^{206}Pb$ | $(^{206}Pb/^{238}U)_{cor}$ |
| z1a | 476 | 297 | 57 | 0.0597 | 0.68 | 0.0953 | 1.34 | 587 | 588 | 592 | 587 ± 8 |
| z1b | 639 | 142 | 61 | 0.058 | 0.66 | 0.0842 | 1.34 | 521 | 522 | 528 | 521 ± 7 |
| z2c | 360 | 30 | 30 | 0.056 | 0.85 | 0.0774 | 1.54 | 480 | 476 | 452 | 481 ± 7 |
| z3a | 435 | 55 | 35 | 0.0551 | 0.99 | 0.0746 | 1.35 | 464 | 456 | 414 | 465 ± 6 |
| z3b | 565 | 54 | 47 | 0.0563 | 0.72 | 0.076 | 1.34 | 472 | 471 | 466 | 472 ± 6 |
| z5 | 282 | 28 | 24 | 0.0565 | 0.95 | 0.0793 | 1.46 | 492 | 489 | 473 | 493 ± 7 |
| z6 | 400 | 36 | 34 | 0.0567 | 1.17 | 0.0778 | 1.34 | 483 | 483 | 481 | 483 ± 7 |
| z7 | 382 | 149 | 35 | 0.0566 | 1.04 | 0.0775 | 1.34 | 481 | 480 | 475 | 481 ± 7 |
| z10 | 340 | 36 | 26 | 0.056 | 0.96 | 0.0689 | 1.34 | 430 | 433 | 454 | 429 ± 6 |

Table 4.40: U-Pb SIMS results of the Mohares metagranite. Analyses references ending in b mean rims and c mean cores.

| | Element concentration (ppm) | | | Isotope ratios | | | | Ages (Ma) | | | |
|---|---|---|---|---|---|---|---|---|---|---|---|
| Grain | U | Th | Pb | $(^{207}Pb/^{206}Pb)_{meas}$ | σ (%) | $(^{206}Pb/^{238}U)_{meas}$ | σ (%) | $^{206}Pb/^{238}U$ | $^{207}Pb/^{235}U$ | $^{207}Pb/^{206}Pb$ | $(^{206}Pb/^{238}U)_{cor}$ |
| z11 | 643 | 822 | 73 | 0.0574 | 0.64 | 0.0795 | 1.34 | 493 | 496 | 509 | 493 ± 7 |
| z14 | 314 | 49 | 27 | 0.0573 | 0.94 | 0.0771 | 1.34 | 479 | 483 | 503 | 478 ± 7 |
| z16c | 912 | 73 | 78 | 0.0557 | 0.61 | 0.0794 | 1.34 | 493 | 483 | 439 | 494 ± 7 |
| z17 | 396 | 75 | 35 | 0.0564 | 0.84 | 0.0794 | 1.34 | 492 | 488 | 467 | 493 ± 7 |

## 9.2. Tables of the geochemical data

### 9.2.1. The Ollo de Sapo Domain

Table 5.3: Major elements and trace elements of the metavolcanic rocks of the Ollo de Sapo Domain.

| Sample | T1 | T2 | T3 | T4 | T5 | T6 | T7 | T8 | T9 | T10 |
|---|---|---|---|---|---|---|---|---|---|---|
| **Locality** | Vivero | | Mañón | | | | Puebla de Trives | | | |
| **$SiO_2$** | 66.53 | 66.47 | 64.94 | 66.8 | 66.33 | 66.7 | 66.19 | 67.86 | 66.8 | 66.29 |
| **$TiO_2$** | 0.61 | 0.74 | 0.71 | 0.56 | 0.61 | 0.62 | 0.59 | 0.51 | 0.55 | 0.61 |
| **$Al_2O_3$** | 16.13 | 15.74 | 16.18 | 15.8 | 15.43 | 15.25 | 16.47 | 16.27 | 16.28 | 15.79 |
| **$FeO_t$** | 3.61 | 3.68 | 4.09 | 3.3 | 3.35 | 3.53 | 3.52 | 2.85 | 3.12 | 3.73 |
| **MgO** | 1.63 | 1.91 | 1.89 | 1.7 | 1.73 | 1.79 | 1.66 | 1.63 | 1.47 | 1.82 |
| **MnO** | 0.04 | 0.05 | 0.05 | 0.04 | 0.05 | 0.05 | 0.05 | 0.04 | 0.04 | 0.06 |
| **CaO** | 0.37 | 1.16 | 0.67 | 1.38 | 1.4 | 1.23 | 1.05 | 0.69 | 1.22 | 1.48 |
| **$Na_2O$** | 2.73 | 2.42 | 2.64 | 2.86 | 2.74 | 2.85 | 2.87 | 2.13 | 3.01 | 2.75 |
| **$K_2O$** | 4.95 | 4.09 | 4.21 | 4.18 | 4.36 | 4.31 | 5.12 | 5.26 | 4.53 | 4.18 |
| **$P_2O_5$** | 0.232 | 0.211 | 0.229 | 0.228 | 0.232 | 0.234 | 0.231 | 0.215 | 0.216 | 0.219 |
| **Li** | 73 | 67 | 64 | 56 | 62 | 59 | 89 | 57 | 50 | 76 |
| **Rb** | 170 | 160 | 141 | 143 | 145 | 152 | 186 | 197 | 160 | 160 |
| **Cs** | 7.05 | 7.81 | 4.90 | 6.49 | 5.87 | 6.74 | 9.12 | 4.97 | 4.15 | 24.0 |
| **Be** | 2.40 | 2.85 | 2.67 | 2.22 | 2.87 | 2.68 | 2.91 | 2.93 | 2.46 | 2.34 |
| **Sr** | 46.1 | 147 | 63.4 | 157 | 141 | 138 | 144 | 112 | 152 | 131 |
| **Ba** | 851 | 655 | 693 | 763 | 800 | 766 | 908 | 820 | 892 | 646 |
| **Sc** | 10.3 | 12.9 | 12.3 | 9.82 | 10.5 | 10.3 | 9.59 | 8.78 | 8.53 | 11.1 |
| **V** | 67.2 | 82.2 | 78.7 | 66.3 | 69.0 | 67 | 58.6 | 57.5 | 54.6 | 70.1 |
| **Cr** | 53.8 | 63.7 | 59.7 | 49.5 | 57.2 | 53.5 | 46.8 | 51.8 | 45.5 | 56.0 |
| **Co** | 25.1 | 57.5 | 26.5 | 29.4 | 27.9 | 27.4 | 40.1 | 32.0 | 34.2 | 32.6 |
| **Ni** | 20.0 | 16.5 | 27.3 | 17.1 | 22.7 | 20.5 | 17.2 | 15.7 | 10.6 | 21.5 |
| **Cu** | 16.0 | 11.5 | 25.9 | 12.6 | 21 | 20 | 10.9 | 1.4 | 10.2 | 12.9 |
| **Zn** | 44.4 | 66.6 | 65.9 | 46.8 | 48.8 | 52.0 | 78.3 | 45.8 | 54.4 | 80.3 |
| **Ga** | 21.2 | 20.6 | 21.2 | 20.8 | 21.1 | 20.5 | 21.7 | 23.8 | 20.9 | 21.5 |
| **Y** | 25.7 | 20.5 | 22.2 | 27.4 | 29.7 | 34.6 | 18.5 | 15.0 | 28.9 | 38.3 |
| **Nb** | 10.9 | 12.2 | 11.481 | 10.3 | 11.1 | 10.9 | 11.1 | 11 | 10.5 | 11.3 |
| **Ta** | 0.92 | 1.12 | 1.00 | 0.89 | 1.01 | 0.99 | 1.01 | 1.10 | 0.99 | 1.07 |
| **Zr** | 209 | 225 | 213 | 183 | 197 | 191 | 196 | 187 | 189 | 193 |
| **Hf** | 6.30 | 7.40 | 6.30 | 5.60 | 6.00 | 6.00 | 6.30 | 5.90 | 6.30 | 6.20 |
| **Mo** | 0.70 | 0.41 | 0.78 | 0.89 | 0.80 | 0.73 | 0.38 | 0.21 | 0.22 | 0.37 |
| **Sn** | 5.13 | 6.05 | 4.08 | 4.6 | 4.47 | 4.47 | 5.52 | 6.81 | 5.74 | 8.78 |
| **Tl** | 0.97 | 0.83 | 0.80 | 0.76 | 0.75 | 0.83 | 1.13 | 1.00 | 0.88 | 0.91 |
| **Pb** | 23.2 | 34.5 | 22.1 | 18.8 | 23.2 | 20.7 | 29.5 | 17.3 | 25.3 | 20.4 |
| **U** | 3.84 | 2.80 | 3.61 | 3.12 | 3.45 | 3.5 | 2.93 | 3.52 | 3.26 | 3.73 |
| **Th** | 13.0 | 13.8 | 13.6 | 9.83 | 11.8 | 11.6 | 14.0 | 14.2 | 12.8 | 12.4 |
| **La** | 28.2 | 42.1 | 28.4 | 27.6 | 30.6 | 30.7 | 31.8 | 32.5 | 35.9 | 33.2 |
| **Ce** | 60.5 | 86.8 | 72.9 | 65.4 | 65.6 | 66.5 | 68.4 | 67.6 | 74.3 | 67.8 |
| **Pr** | 7.66 | 10.6 | 7.53 | 7.16 | 7.97 | 7.82 | 8.16 | 8.39 | 9.01 | 8.37 |
| **Nd** | 29.0 | 40.9 | 29.3 | 27.4 | 30.5 | 30 | 30.5 | 30.8 | 33.9 | 32.8 |
| **Sm** | 6.33 | 8.58 | 6.09 | 5.92 | 6.60 | 6.50 | 6.90 | 6.52 | 7.22 | 7.12 |
| **Eu** | 1.13 | 1.48 | 1.13 | 1.04 | 1.16 | 1.13 | 1.24 | 1.06 | 1.39 | 1.17 |
| **Gd** | 5.60 | 6.67 | 5.22 | 5.4 | 5.53 | 5.71 | 5.26 | 5.33 | 6.57 | 6.78 |
| **Tb** | 0.89 | 0.92 | 0.82 | 0.86 | 0.88 | 0.97 | 0.80 | 0.73 | 1.08 | 1.08 |
| **Dy** | 5.24 | 4.50 | 4.62 | 5.04 | 5.10 | 5.85 | 3.94 | 3.56 | 5.78 | 6.43 |
| **Ho** | 0.91 | 0.76 | 0.9 | 1.03 | 1.02 | 1.19 | 0.70 | 0.58 | 1.04 | 1.34 |
| **Er** | 2.32 | 1.72 | 2.3 | 2.65 | 2.61 | 3.22 | 1.59 | 1.26 | 2.45 | 3.50 |
| **Tm** | 0.34 | 0.23 | 0.35 | 0.39 | 0.40 | 0.48 | 0.21 | 0.16 | 0.32 | 0.50 |
| **Yb** | 1.99 | 1.42 | 2.3 | 2.29 | 2.46 | 2.80 | 1.26 | 0.89 | 1.75 | 2.98 |
| **Lu** | 0.31 | 0.20 | 0.32 | 0.35 | 0.36 | 0.39 | 0.20 | 0.13 | 0.23 | 0.42 |

Table 5.3: Major elements and trace elements of the metavolcanic rocks of the Ollo de Sapo Domain (Continuation).

| Sample | T12 | T13 | T15 | T16 | T17 | T18 | T19 | T20 | T21 | T22 |
|---|---|---|---|---|---|---|---|---|---|---|
| Locality | Sanabria | | | | | | Villadepera | | Hiendelaencina | |
| $SiO_2$ | 58.70 | 66.65 | 67.05 | 67.50 | 69.06 | 66.84 | 70.67 | 68.02 | 68.06 | 72.24 |
| $TiO_2$ | 1.05 | 0.69 | 0.52 | 0.54 | 0.61 | 0.5 | 0.54 | 0.68 | 0.5 | 0.38 |
| $Al_2O_3$ | 18.07 | 16.52 | 15.62 | 15.7 | 16.4 | 15.56 | 14.44 | 15.34 | 15.76 | 14.87 |
| $FeO_t$ | 6.24 | 3.45 | 2.93 | 2.99 | 2.38 | 3.19 | 3.45 | 3.73 | 3.32 | 2.59 |
| MgO | 3.33 | 1.53 | 1.53 | 1.49 | 1.47 | 1.51 | 0.92 | 1.44 | 1.49 | 1.15 |
| MnO | 0.09 | 0.02 | 0.04 | 0.04 | 0.02 | 0.04 | 0.04 | 0.05 | 0.04 | 0.24 |
| CaO | 1.45 | 0.05 | 0.98 | 0.91 | 0.18 | 1.48 | 1.08 | 1.28 | 1.38 | 0.99 |
| $Na_2O$ | 2.82 | 0.37 | 2.82 | 2.96 | 0.1 | 2.75 | 3.35 | 2.17 | 2.73 | 2.83 |
| $K_2O$ | 3.17 | 6.68 | 5.17 | 4.68 | 6.28 | 4.55 | 4.08 | 4.39 | 4.18 | 3.10 |
| $P_2O_5$ | 0.21 | 0.19 | 0.21 | 0.22 | 0.19 | 0.22 | 0.19 | 0.25 | 0.18 | 0.15 |
| Li | 52 | 57 | 48 | 57 | 77 | 54 | 263 | 122 | 42 | 26 |
| Rb | 92.7 | 290 | 186 | 162 | 228 | 160 | 206 | 174 | 159 | 126 |
| Cs | 4.09 | 8.69 | 5.32 | 5.93 | 5.54 | 5.27 | 50.7 | 20.6 | 4.86 | 2.78 |
| Be | 4.23 | 2.72 | 2.44 | 2.62 | 2.86 | 2.66 | 2.30 | 2.91 | 2.22 | 2.71 |
| Sr | 207 | 42 | 113 | 166 | 16 | 167 | 125 | 129 | 136 | 168 |
| Ba | 1063 | 1098 | 931 | 909 | 656 | 707 | 753 | 757 | 712 | 863 |
| Sc | 20.0 | 10.9 | 8.21 | 8.37 | 9.50 | 7.40 | 8.77 | 9.38 | 7.13 | 6.39 |
| V | 129 | 67.2 | 51.2 | 52.8 | 57.1 | 48.6 | 53.0 | 63.3 | 61.3 | 49.4 |
| Cr | 106 | 62.2 | 43.4 | 42.7 | 41.8 | 46.7 | 41.8 | 46.7 | 57.1 | 47.7 |
| Co | 28.8 | 27.4 | 21.3 | 30.5 | 19.2 | 33.1 | 72.9 | 60.4 | 128 | 105 |
| Ni | 35.2 | 12.8 | 15.7 | 15.6 | 12.9 | 15.0 | 16.2 | 22.1 | 16.4 | 10.5 |
| Cu | 27.7 | 15.1 | 10.1 | 14.7 | 1.6 | 14.6 | 16.6 | 15.4 | 6.7 | 11.5 |
| Zn | 119 | 70.4 | 46.8 | 46.6 | 37 | 52.7 | 78.1 | 74.7 | 41.5 | 40.0 |
| Ga | 25.0 | 23.4 | 19.5 | 20.9 | 24.4 | 19.0 | 18.4 | 22.0 | 20.0 | 18.1 |
| Y | 36.2 | 40.9 | 34.0 | 33.6 | 34 | 32.5 | 17.8 | 21.6 | 28.2 | 19.0 |
| Nb | 14.3 | 13.3 | 10.0 | 10.3 | 12.2 | 9.23 | 10.0 | 11.3 | 10.5 | 8.4 |
| Ta | 1.06 | 1.29 | 0.93 | 0.96 | 1.08 | 0.87 | 0.98 | 1.17 | 1.14 | 0.90 |
| Zr | 290 | 242 | 191 | 165 | 209 | 179 | 182 | 217 | 162 | 134 |
| Hf | 8.50 | 7.70 | 6.00 | 5.20 | 6.60 | 5.50 | 5.00 | 5.00 | 5.19 | 3.60 |
| Mo | 0.95 | 0.30 | 0.73 | 0.69 | 0.66 | 0.64 | 0.22 | 0.63 | 0.56 | 0.40 |
| Sn | 2.03 | 7.19 | 5.53 | 4.95 | 6.29 | 4.88 | 3.23 | 4.6 | 4.07 | 2.91 |
| Tl | 0.52 | 1.74 | 1.06 | 0.97 | 1.08 | 0.94 | 1.16 | 0.97 | 0.92 | 0.62 |
| Pb | 22.9 | 18.9 | 26.4 | 29.4 | 6.56 | 28.1 | 48.3 | 18.9 | 22.1 | 21.7 |
| U | 2.15 | 4.56 | 3.72 | 2.86 | 3.94 | 3.60 | 2.73 | 3.12 | 3.42 | 3.22 |
| Th | 16.7 | 16.8 | 13.6 | 14.2 | 13.9 | 11.8 | 12.1 | 12.5 | 11.2 | 10.3 |
| La | 55.8 | 40.4 | 25.7 | 34.7 | 23.4 | 28 | 30.4 | 35.2 | 26.8 | 31.3 |
| Ce | 111 | 84.6 | 54.7 | 74.4 | 50.6 | 58.0 | 63.6 | 74.3 | 58.7 | 50.6 |
| Pr | 13.8 | 10.6 | 6.51 | 8.82 | 6.74 | 6.93 | 7.73 | 8.99 | 7.04 | 7.84 |
| Nd | 50.8 | 41.2 | 25.0 | 31.8 | 26.5 | 28.5 | 29.7 | 35.4 | 26.5 | 29.0 |
| Sm | 10.2 | 8.93 | 5.76 | 6.82 | 6.27 | 6.29 | 6.11 | 7.07 | 5.70 | 6.01 |
| Eu | 2.10 | 1.55 | 1.15 | 1.31 | 0.99 | 1.20 | 1.04 | 1.16 | 1.22 | 1.46 |
| Gd | 9.00 | 8.19 | 5.68 | 6.15 | 5.93 | 5.79 | 4.93 | 6.02 | 5.07 | 5.26 |
| Tb | 1.34 | 1.32 | 0.91 | 1.03 | 0.97 | 0.91 | 0.73 | 0.83 | 0.86 | 0.75 |
| Dy | 7.14 | 7.28 | 5.43 | 5.86 | 6.29 | 5.29 | 3.70 | 4.24 | 5.05 | 3.83 |
| Ho | 1.31 | 1.44 | 1.14 | 1.14 | 1.24 | 1.07 | 0.64 | 0.76 | 1.01 | 0.71 |
| Er | 3.28 | 3.39 | 2.96 | 3.12 | 3.25 | 2.95 | 1.49 | 1.76 | 2.55 | 1.76 |
| Tm | 0.48 | 0.48 | 0.46 | 0.45 | 0.48 | 0.43 | 0.21 | 0.25 | 0.37 | 0.23 |
| Yb | 2.95 | 2.89 | 2.87 | 2.61 | 2.83 | 2.52 | 1.15 | 1.5 | 2.14 | 1.44 |
| Lu | 0.46 | 0.46 | 0.40 | 0.41 | 0.42 | 0.37 | 0.17 | 0.21 | 0.33 | 0.22 |

Table 5.4: Major elements and trace elements of the metagranites of the Ollo de Sapo Domain.

| Sample | T24 | T25 | T26 | T27 | T28 | T29 | T31 | T33 | T34 | T35 |
|---|---|---|---|---|---|---|---|---|---|---|
| Locality | Viana do Bolo | | San Sebastián | | Miranda do Douro | | Antoñita | | | |
| SiO2 | 66.24 | 73.41 | 74.8 | 74.83 | 65.54 | 64.62 | 76 | 70.25 | 71.46 | 72.37 |
| TiO2 | 0.79 | 0.29 | 0.23 | 0.22 | 0.67 | 0.62 | 0.09 | 0.43 | 0.32 | 0.35 |
| Al2O3 | 14.83 | 13.72 | 12.29 | 12.74 | 15.79 | 16.07 | 12.88 | 15.07 | 14.45 | 13.92 |
| FeOt | 4.71 | 1.45 | 1.26 | 1.26 | 4.25 | 3.83 | 1.14 | 2.61 | 2.1 | 2.36 |
| MgO | 2.49 | 0.45 | 0.25 | 0.25 | 2.62 | 2.23 | 0.12 | 0.89 | 0.59 | 0.77 |
| MnO | 0.08 | 0.03 | 0.02 | 0.02 | 0.1 | 0.1 | 0.01 | 0.04 | 0.03 | 0.03 |
| CaO | 1.75 | 0.74 | 0.84 | 0.96 | 2.88 | 2.93 | 0.41 | 0.91 | 0.8 | 1.08 |
| Na2O | 2.78 | 2.92 | 3.12 | 3.05 | 3.1 | 3.21 | 2.29 | 2.55 | 2.74 | 3.14 |
| K2O | 3.43 | 5.25 | 5.75 | 5.54 | 3.36 | 4.03 | 5.83 | 5.39 | 5.27 | 4.28 |
| P2O5 | 0.25 | 0.17 | 0.19 | 0.18 | 0.35 | 0.35 | 0.152 | 0.196 | 0.174 | 0.173 |
| Li | 187 | 111 | 34 | 40 | 159 | 102 | 15 | 35 | 21 | 51 |
| Rb | 139 | 218 | 189 | 194 | 217 | 241 | 207 | 217 | 189 | 182 |
| Cs | 8.93 | 22.7 | 3.81 | 4.29 | 15.9 | 14.5 | 5.72 | 6.77 | 3.97 | 9.23 |
| Be | 2.51 | 5.06 | 3.76 | 4.09 | 5.01 | 5.91 | 0.92 | 2.26 | 2.06 | 2.36 |
| Sr | 169 | 53.4 | 103 | 135 | 307 | 339 | 25.9 | 123 | 101 | 82.9 |
| Ba | 665 | 359 | 227 | 240 | 799 | 904 | 59.4 | 724 | 615 | 459 |
| Sc | 17.4 | 3.78 | 2.16 | 2.07 | 9.96 | 9.89 | 1.77 | 6.00 | 4.21 | 3.96 |
| V | 116 | 16.6 | 10.4 | 10.3 | 66.5 | 65.7 | 9.15 | 43.0 | 30.9 | 32.4 |
| Cr | 83.7 | 5.39 | 13.4 | 12.2 | 107 | 83.0 | 20.6 | 46.0 | 32.4 | 35.1 |
| Co | 41.0 | 79.3 | 58.6 | 54.5 | 73.2 | 66.2 | 35.2 | 37.8 | 25.8 | 34.2 |
| Ni | 34.0 | 2.68 | 1.99 | 2.03 | 40.8 | 33.8 | 0.16 | 9.80 | 7.30 | 8.04 |
| Cu | 23.4 | 6.10 | 0.39 | 0.88 | 18.1 | 14.6 | 3.09 | 6.47 | 10.6 | 2.44 |
| Zn | 94.8 | 39.3 | 18.2 | 20.7 | 84.3 | 77.0 | 27.3 | 49.5 | 43.7 | 40.8 |
| Ga | 21.9 | 19 | 21.6 | 22.7 | 23.7 | 24 | 15.1 | 20.9 | 17.2 | 18 |
| Y | 18.3 | 18.4 | 21.1 | 21.2 | 22.1 | 24.0 | 13.5 | 18.1 | 25.0 | 16.1 |
| Nb | 14.3 | 9.52 | 20.4 | 21.4 | 12.9 | 11.8 | 6.65 | 10.6 | 7.89 | 7.95 |
| Ta | 1.22 | 1.47 | 1.56 | 1.82 | 1.36 | 1.23 | 0.91 | 1.10 | 0.90 | 0.59 |
| Zr | 203 | 136 | 151 | 152 | 248 | 232 | 68.4 | 194 | 136 | 151 |
| Hf | 5.70 | 4.30 | 5.10 | 5.20 | 5.40 | 5.70 | 2.63 | 6.05 | 4.31 | 4.97 |
| Mo | 1.00 | 0.15 | 2.36 | 3.57 | 0.73 | 0.78 | 0.11 | 0.37 | 0.32 | 0.36 |
| Sn | 5.36 | 14.3 | 1.80 | 1.86 | 6.89 | 7.45 | 7.49 | 8.43 | 6.20 | 7.14 |
| Tl | 0.79 | 1.31 | 0.77 | 0.75 | 1.54 | 1.47 | 1.14 | 1.2 | 1.1 | 1.03 |
| Pb | 18.3 | 20.6 | 13.6 | 14.1 | 32.0 | 40.8 | 25.1 | 23.4 | 23.9 | 22.0 |
| U | 2.40 | 2.56 | 3.57 | 6.08 | 3.07 | 8.29 | 2.22 | 3.96 | 3.44 | 3.21 |
| Th | 11.0 | 10.6 | 13.2 | 13.8 | 35.8 | 33.5 | 6.86 | 12.1 | 9.82 | 10.1 |
| La | 34.5 | 20.0 | 23.5 | 22.2 | 82.9 | 83.2 | 7.96 | 27.5 | 22.7 | 22.2 |
| Ce | 71.1 | 43.8 | 48.1 | 45.1 | 161 | 161 | 18.5 | 59.2 | 48.3 | 46.7 |
| Pr | 8.74 | 5.27 | 5.57 | 5.22 | 18.4 | 18.5 | 2.26 | 7.04 | 5.86 | 5.79 |
| Nd | 33.5 | 19.5 | 19.2 | 18.2 | 65.8 | 65.7 | 7.97 | 27.4 | 22.4 | 22.1 |
| Sm | 7.03 | 4.76 | 4.45 | 4.19 | 9.87 | 10.0 | 2.06 | 6.04 | 5.05 | 4.9 |
| Eu | 1.25 | 0.51 | 0.50 | 0.49 | 1.50 | 1.52 | 0.18 | 0.99 | 0.94 | 0.89 |
| Gd | 6.10 | 4.00 | 4.63 | 4.43 | 6.44 | 6.80 | 2.32 | 4.97 | 4.81 | 4.34 |
| Tb | 0.83 | 0.64 | 0.70 | 0.71 | 0.87 | 0.89 | 0.41 | 0.75 | 0.75 | 0.67 |
| Dy | 4.15 | 3.66 | 3.99 | 3.94 | 4.09 | 4.34 | 2.49 | 4.03 | 4.54 | 3.68 |
| Ho | 0.72 | 0.66 | 0.71 | 0.71 | 0.75 | 0.78 | 0.50 | 0.7 | 0.91 | 0.64 |
| Er | 1.64 | 1.62 | 1.69 | 1.68 | 1.88 | 2.09 | 1.40 | 1.60 | 2.30 | 1.50 |
| Tm | 0.21 | 0.23 | 0.23 | 0.23 | 0.27 | 0.28 | 0.21 | 0.22 | 0.34 | 0.19 |
| Yb | 1.23 | 1.4 | 1.33 | 1.39 | 1.47 | 1.74 | 1.34 | 1.30 | 2.01 | 1.18 |
| Lu | 0.17 | 0.21 | 0.17 | 0.19 | 0.22 | 0.24 | 0.20 | 0.20 | 0.30 | 0.17 |

## 9.2.2. The Schist-Graywacke Complex Domain

Table 5.5: Major elements and trace elements of the metagranites of the Tormes Dome.

| Sample | T36 | T37 | T38 | T39 | T40 | T41 | T42 |
|---|---|---|---|---|---|---|---|
| Locality | Vitigudino | | Fermoselle | | | Ledesma | |
| $SiO_2$ | 74.67 | 72.37 | 75.64 | 74.57 | 73.41 | 77 | 68.83 |
| $TiO_2$ | 0.23 | 0.24 | 0.16 | 0.27 | 0.12 | 0.1 | 0.56 |
| $Al_2O_3$ | 13.51 | 14.79 | 13.82 | 13.7 | 15.04 | 12.63 | 15.62 |
| $FeO_t$ | 2.04 | 2.39 | 1.74 | 2.35 | 1.17 | 0.88 | 4.05 |
| MgO | 0.52 | 0.79 | 0.68 | 0.61 | 0.36 | 0.21 | 1.47 |
| MnO | 0.03 | 0.05 | 0.02 | 0.03 | 0.01 | 0.01 | 0.07 |
| CaO | 0.68 | 0.82 | 0.66 | 0.63 | 0.35 | 0.59 | 1.08 |
| $Na_2O$ | 2.34 | 2.38 | 1.94 | 2.28 | 1.94 | 2.16 | 1.7 |
| $K_2O$ | 4.82 | 4.44 | 4.06 | 4.07 | 6.27 | 5.49 | 3.77 |
| $P_2O_5$ | 0.17 | 0.16 | 0.173 | 0.14 | 0.11 | 0.129 | 0.192 |
| Li | 63 | 82 | 32 | 71 | 73 | 30 | 86 |
| Rb | 237 | 230 | 172 | 253 | 242 | 218 | 188 |
| Cs | 8.43 | 13.1 | 4.59 | 14.2 | 10.4 | 8.70 | 11.2 |
| Be | 0.56 | 0.78 | 0.75 | 2.23 | 2.03 | 2.73 | 3.47 |
| Sr | 46.3 | 30.8 | 54.8 | 54.1 | 43.6 | 51.4 | 108 |
| Ba | 202 | 120 | 208 | 188 | 224 | 166 | 504 |
| Sc | 4.74 | 5.30 | 2.31 | 5.23 | 4.51 | 2.02 | 9.00 |
| V | 19.3 | 20.9 | 11.1 | 19.3 | 13.8 | 6.00 | 60.1 |
| Cr | 11.1 | 19.5 | 5.01 | 17.7 | 13.1 | 1.01 | 40.3 |
| Co | 38.5 | 93.8 | 47.5 | 113 | 83.2 | 39.6 | 48.2 |
| Ni | 6.37 | 9.34 | 3.68 | 11.8 | 6.94 | 2.11 | 22.2 |
| Cu | 5.17 | 1.89 | 2.55 | 1.96 | 1.50 | 5.06 | 16.1 |
| Zn | 66.1 | 61.3 | 18.6 | 49.4 | 33.6 | 37.3 | 70.0 |
| Ga | 18.0 | 20.6 | 13.4 | 20.1 | 17.7 | 14.0 | 21.8 |
| Y | 11.4 | 9.57 | 11.5 | 12.0 | 8.35 | 7.52 | 17.4 |
| Nb | 9.42 | 10.9 | 3.89 | 8.34 | 5.89 | 5.86 | 11.9 |
| Ta | 1.07 | 1.42 | 0.39 | 1.31 | 0.71 | 0.52 | 1.06 |
| Zr | 104 | 114 | 86.5 | 119 | 63.3 | 73.6 | 198 |
| Hf | 3.60 | 2.34 | 3.10 | 4.50 | 2.50 | 2.70 | 6.20 |
| Mo | 0.08 | 0 | 0.09 | 0.49 | 0.00 | 0.10 | 0.51 |
| Sn | 4.95 | 5.24 | 3.68 | 5.22 | 5.92 | 3.79 | 5.44 |
| Tl | 1.33 | 1.33 | 1.00 | 1.50 | 1.44 | 1.21 | 1.06 |
| Pb | 23.0 | 18.7 | 18.3 | 21.7 | 21.7 | 33.1 | 20.0 |
| U | 3.89 | 5.15 | 1.86 | 4.95 | 2.20 | 2.41 | 3.94 |
| Th | 9.74 | 13.0 | 8.39 | 12.9 | 8.98 | 5.74 | 16.6 |
| La | 15.4 | 18.9 | 13.4 | 20.5 | 13.6 | 7.27 | 38.2 |
| Ce | 33.2 | 40.0 | 28.6 | 42.9 | 29.8 | 15.4 | 79.0 |
| Pr | 4.11 | 4.91 | 3.48 | 5.06 | 3.56 | 1.85 | 9.40 |
| Nd | 14.4 | 18.5 | 12.5 | 19.3 | 12.8 | 6.42 | 36.1 |
| Sm | 3.52 | 4.15 | 3.11 | 4.06 | 3.06 | 1.67 | 7.48 |
| Eu | 0.39 | 0.28 | 0.46 | 0.49 | 0.38 | 0.34 | 1.01 |
| Gd | 2.79 | 3.25 | 2.75 | 3.61 | 2.51 | 1.51 | 5.83 |
| Tb | 0.43 | 0.53 | 0.40 | 0.55 | 0.37 | 0.24 | 0.80 |
| Dy | 2.10 | 2.29 | 2.30 | 2.55 | 1.89 | 1.40 | 4.15 |
| Ho | 0.37 | 0.35 | 0.41 | 0.47 | 0.33 | 0.28 | 0.63 |
| Er | 0.89 | 0.87 | 0.95 | 1.04 | 0.80 | 0.76 | 1.38 |
| Tm | 0.13 | 0.11 | 0.13 | 0.14 | 0.11 | 0.13 | 0.18 |
| Yb | 0.81 | 0.69 | 0.81 | 0.86 | 0.78 | 0.86 | 0.96 |
| Lu | 0.12 | 0.09 | 0.12 | 0.14 | 0.13 | 0.15 | 0.13 |

Table 5.6: Major elements and trace elements of the metagranites of the Sierra de Gredos.

| Sample | T43 | T44 | T45 | T46 | T47 | T48 | T49 |
|---|---|---|---|---|---|---|---|
| Locality | San Pelayo | Castellanos | | Bercimuelle | | | |
| $SiO_2$ | 71.80 | 70.33 | 68.54 | 69.98 | 68.54 | 70.19 | 69.71 |
| $TiO_2$ | 0.38 | 0.36 | 0.59 | 0.46 | 0.39 | 0.42 | 0.45 |
| $Al_2O_3$ | 14.37 | 15.35 | 15.24 | 15.35 | 16.02 | 15.02 | 15.29 |
| $FeO_t$ | 2.19 | 2.16 | 3.5 | 2.97 | 2.56 | 2.86 | 3.14 |
| MgO | 0.93 | 0.69 | 1.47 | 1.13 | 1.02 | 1.06 | 1.14 |
| MnO | 0.04 | 0.03 | 0.05 | 0.05 | 0.04 | 0.05 | 0.05 |
| CaO | 0.89 | 0.79 | 1.07 | 0.87 | 0.5 | 0.89 | 0.93 |
| $Na_2O$ | 2.93 | 3.99 | 2.66 | 2.68 | 2.96 | 2.85 | 2.75 |
| $K_2O$ | 4 | 4.7 | 4.26 | 4.42 | 5.18 | 4.54 | 4.43 |
| $P_2O_5$ | 0.23 | 0.2 | 0.15 | 0.22 | 0.26 | 0.25 | 0.23 |
| Li | 134 | 100 | 137 | 115 | 55 | 93 | 107 |
| Rb | 229 | 151 | 196 | 241 | 248 | 235 | 217 |
| Cs | 22.1 | 17.4 | 14.5 | 17.8 | 8.5 | 10.2 | 10.7 |
| Be | 1.32 | 1.55 | 2.62 | 2.00 | 1.74 | 1.89 | 1.78 |
| Sr | 76.9 | 78.1 | 116 | 83.2 | 75.2 | 84.2 | 91.5 |
| Ba | 341 | 421 | 570 | 429 | 479 | 414 | 424 |
| Sc | 7.97 | 4.47 | 10.7 | 7.26 | 7.49 | 7.77 | 7.55 |
| V | 39.0 | 29.7 | 67.2 | 44.9 | 41.3 | 46.3 | 48.7 |
| Cr | 31.8 | 25.9 | 51.4 | 36.0 | 33.9 | 41.3 | 39.5 |
| Co | 74.5 | 94.5 | 72.8 | 79.1 | 76.8 | 80.7 | 76.6 |
| Ni | 7.64 | 5.41 | 11.5 | 14.2 | 11.6 | 14.0 | 20.1 |
| Cu | 16.6 | 22 | 10.6 | 12.9 | 14.8 | 13.0 | 22.8 |
| Zn | 51.2 | 49.9 | 73.1 | 64.5 | 58.4 | 70.6 | 65.5 |
| Ga | 19.0 | 17.6 | 21.2 | 19.4 | 20.4 | 19.0 | 19.8 |
| Y | 14.6 | 9.64 | 14.9 | 13.7 | 14.1 | 13.2 | 13.0 |
| Nb | 10.2 | 8.48 | 11.5 | 10.8 | 11.2 | 11.2 | 10.9 |
| Ta | 1.32 | 0.86 | 1.25 | 1.44 | 1.90 | 1.31 | 1.20 |
| Zr | 122 | 134 | 191 | 142 | 136 | 131 | 138 |
| Hf | 3.90 | 4.20 | 4.90 | 4.50 | 4.40 | 4.20 | 4.30 |
| Mo | 0.32 | 0.35 | 0.77 | 0.43 | 0.25 | 0.59 | 0.52 |
| Sn | 13.2 | 2.38 | 6.38 | 7.05 | 15.9 | 4.53 | 5.25 |
| Tl | 1.30 | 0.87 | 1.15 | 1.52 | 1.40 | 1.42 | 1.28 |
| Pb | 21.0 | 28.4 | 25.0 | 23.7 | 24.7 | 25.5 | 24.9 |
| U | 4.22 | 3.14 | 3.91 | 7.15 | 4.25 | 6.11 | 7.89 |
| Th | 9.39 | 8.27 | 17.0 | 10.9 | 10.0 | 11.7 | 11.2 |
| La | 20.9 | 20.4 | 37.6 | 25.9 | 22.9 | 26.7 | 26.5 |
| Ce | 44.3 | 45.1 | 75.8 | 54.0 | 47.9 | 56.7 | 55.7 |
| Pr | 5.22 | 5.46 | 9.06 | 6.79 | 5.99 | 7.09 | 6.91 |
| Nd | 19.4 | 20.9 | 33.5 | 25.7 | 22.6 | 27.5 | 26.7 |
| Sm | 4.02 | 4.78 | 6.74 | 5.29 | 4.85 | 5.74 | 5.53 |
| Eu | 0.64 | 0.75 | 1.04 | 0.79 | 0.81 | 0.8 | 0.84 |
| Gd | 3.35 | 3.32 | 5.23 | 4.26 | 4.14 | 4.56 | 4.42 |
| Tb | 0.52 | 0.42 | 0.73 | 0.59 | 0.58 | 0.65 | 0.61 |
| Dy | 2.84 | 2.06 | 3.40 | 2.79 | 2.96 | 2.99 | 2.78 |
| Ho | 0.49 | 0.35 | 0.55 | 0.43 | 0.51 | 0.46 | 0.47 |
| Er | 1.22 | 0.88 | 1.26 | 1.01 | 1.30 | 1.06 | 1.10 |
| Tm | 0.17 | 0.12 | 0.17 | 0.14 | 0.18 | 0.15 | 0.15 |
| Yb | 1.01 | 0.73 | 1.03 | 0.84 | 1.09 | 0.94 | 0.87 |
| Lu | 0.15 | 0.11 | 0.15 | 0.12 | 0.16 | 0.13 | 0.13 |

Table 5.7: Major elements and trace elements of the metagranites of the Sierra de Guadarrama.

| **Sample** | **T51** | **T52** | **T53** | **T54** | **T56** | **T57** | **T58** | **T59** | **T60** | **T61** | **T63** | **T64** |
|---|---|---|---|---|---|---|---|---|---|---|---|---|
| **Locality** | Navas del Marqués | Santa Maria de la Alameda | La Hoya | La Estación | | La Estación II | Vegas de Matute (Melanocratic) | | Vegas de Matute (Leucocratic) | La Morcuera | Buitrago de Lozoya | Prádena del Rincón |
| **$SiO_2$** | 72.30 | 71.05 | 74.23 | 69.46 | 73.72 | 71.80 | 62.67 | 64.41 | 75.45 | 70.16 | 69.61 | 75.59 |
| **$TiO_2$** | 0.27 | 0.51 | 0.24 | 0.39 | 0.22 | 0.41 | 0.91 | 0.75 | 0.08 | 0.54 | 0.45 | 0.13 |
| **$Al_2O_3$** | 14.77 | 14.13 | 13.12 | 15.83 | 13.54 | 13.71 | 16.67 | 16.79 | 13.64 | 14.58 | 15.29 | 13.32 |
| **$FeO_t$** | 2.11 | 3.42 | 1.63 | 3.19 | 1.82 | 2.85 | 6.47 | 4.91 | 1.34 | 3.44 | 3.22 | 1.4 |
| **MgO** | 0.87 | 0.76 | 0.39 | 1.35 | 0.59 | 0.65 | 2.44 | 2.14 | 0.09 | 1.00 | 1.19 | 0.23 |
| **MnO** | 0.03 | 0.04 | 0.02 | 0.0 | 0.02 | 0.0 | 0.10 | 0.07 | 0.03 | 0.04 | 0.04 | 0.02 |
| **CaO** | 0.63 | 1.24 | 0.91 | 1.06 | 0.53 | 0.98 | 1.48 | 1.46 | 0.34 | 0.97 | 1.07 | 0.46 |
| **$Na_2O$** | 2.25 | 2.64 | 2.31 | 2.33 | 1.98 | 2.29 | 1.98 | 2.12 | 2.8 | 2.32 | 2.23 | 2.53 |
| **$K_2O$** | 4.96 | 4.78 | 5.48 | 4.12 | 5.46 | 5.68 | 3.55 | 3.66 | 4.99 | 4.7 | 4.92 | 5.01 |
| **$P_2O_5$** | 0.16 | 0.12 | 0.08 | 0.16 | 0.14 | 0.13 | 0.20 | 0.20 | 0.25 | 0.26 | 0.17 | 0.17 |
| **Li** | 70 | 79 | 34 | 101 | 38 | 76 | 68 | 94 | 164 | 89.7 | 77.5 | 64.0 |
| **Rb** | 213 | 222 | 165 | 191 | 184 | 248 | 111 | 129 | 511 | 158 | 185 | 270 |
| **Cs** | 10.1 | 11.7 | 3.71 | 7.24 | 3.71 | 7.44 | 5.82 | 5.42 | 10.8 | 10.3 | 8.76 | 5.72 |
| **Be** | 2.41 | 1.13 | 1.52 | 2.36 | 1.14 | 2.53 | 2.76 | 3.36 | 0.40 | 3.60 | 0.78 | 1.03 |
| **Sr** | 81.1 | 83.1 | 142 | 117 | 93.9 | 72.0 | 183 | 189 | 9.66 | 92.8 | 120 | 55.6 |
| **Ba** | 383 | 398 | 501 | 485 | 472 | 405 | 947 | 906 | 18.8 | 520 | 549 | 171 |
| **Sc** | 4.19 | 6.24 | 2.69 | 5.36 | 4.04 | 5.17 | 17.6 | 11.1 | 3.21 | 6.01 | 7.51 | 2.99 |
| **V** | 22.7 | 33.6 | 15.6 | 37.8 | 20.1 | 26.9 | 107 | 81.6 | 5.26 | 37.6 | 49.0 | 7.77 |
| **Cr** | 9.92 | 12.2 | 2.30 | 25.9 | 9.09 | 6.31 | 79.22 | 54.9 | 1.12 | 16.3 | 30.6 | 1.03 |
| **Co** | 78.0 | 153 | 104 | 89.8 | 83.7 | 104 | 81.8 | 59.7 | 95.5 | 95.0 | 69.2 | 81.4 |
| **Ni** | 18.5 | 5.10 | 17.8 | 10.7 | 134 | 3.19 | 33.6 | 23.9 | 0.31 | 6.23 | 31.66 | 1.47 |
| **Cu** | 6.30 | 3.57 | 1.86 | 14.0 | 17.6 | 5.71 | 36.5 | 25.5 | 2.38 | 12.9 | 13.2 | 2.18 |
| **Zn** | 33.7 | 58.8 | 29.3 | 59.9 | 37.7 | 47.6 | 105.5 | 91.3 | 23.3 | 70.3 | 65.2 | 35.4 |
| **Ga** | 19.6 | 21.9 | 16.0 | 21.7 | 16.8 | 20.6 | 23 | 22.7 | 24.0 | 20.7 | 19.9 | 18.1 |
| **Y** | 13.0 | 25.2 | 16.5 | 21.5 | 18.5 | 24.0 | 29 | 27.2 | 10.1 | 49.5 | 16.3 | 15.6 |
| **Nb** | 7.11 | 21.4 | 9.24 | 8.82 | 6.28 | 19.6 | 13.6 | 12.9 | 12.2 | 15.4 | 9.60 | 7.16 |
| **Ta** | 0.98 | 1.64 | 0.64 | 0.76 | 0.69 | 1.76 | 1.16 | 0.97 | 1.65 | 1.76 | 0.85 | 0.90 |
| **Zr** | 108 | 326 | 198 | 156 | 101 | 278 | 287 | 246 | 54.1 | 298 | 164 | 69.6 |
| **Hf** | 3.50 | 8.20 | 6.40 | 4.90 | 3.30 | 7.80 | 8.60 | 7.30 | 2.40 | 8.40 | 4.90 | 2.60 |
| **Mo** | 0.28 | 0.48 | 0.25 | 0.46 | 0.12 | 0.37 | 1.24 | 1.12 | 0.17 | 0.29 | 0.59 | 0.24 |
| **Sn** | 5.88 | 3.40 | 2.80 | 3.34 | 5.07 | 5.66 | 3.26 | 3.44 | 7.12 | 8.1 | 4.8 | 13.4 |
| **Tl** | 1.10 | 1.10 | 0.74 | 0.98 | 1.03 | 1.23 | 0.62 | 0.80 | 2.47 | 0.82 | 0.98 | 1.46 |
| **Pb** | 27.8 | 24.8 | 38.7 | 22.9 | 28.6 | 23.4 | 24.0 | 23.3 | 11.7 | 23.7 | 28.4 | 19.9 |
| **U** | 3.34 | 3.37 | 2.68 | 2.48 | 2.53 | 3.40 | 2.9 | 2.26 | 2.35 | 2.86 | 3.30 | 10.0 |
| **Th** | 10.0 | 28.3 | 23.8 | 12.4 | 8.4 | 24.5 | 16.7 | 16.3 | 8.10 | 23.8 | 12.7 | 7.00 |
| **La** | 19.4 | 57.1 | 40.5 | 31.0 | 15.9 | 46.8 | 48.3 | 46.3 | 4.90 | 47.9 | 29.7 | 8.18 |
| **Ce** | 40.3 | 118.3 | 83.6 | 62.7 | 33.3 | 95.2 | 100 | 94.7 | 12.5 | 101 | 62.8 | 19.1 |
| **Pr** | 4.85 | 13.4 | 9.56 | 7.54 | 4.08 | 10.9 | 12.2 | 11.4 | 1.54 | 12.44 | 7.54 | 2.29 |
| **Nd** | 18.0 | 47.5 | 32.9 | 28.2 | 15.5 | 39.1 | 46.7 | 43.6 | 5.31 | 46.04 | 28.66 | 8.59 |
| **Sm** | 3.93 | 9.49 | 6.60 | 6.09 | 3.48 | 8.10 | 9.44 | 9.09 | 1.48 | 10.0 | 5.80 | 2.26 |
| **Eu** | 0.66 | 0.98 | 1.14 | 0.91 | 0.65 | 0.77 | 1.46 | 1.50 | 0.03 | 0.81 | 0.83 | 0.21 |
| **Gd** | 3.47 | 7.97 | 5.85 | 4.86 | 3.16 | 6.83 | 8.38 | 7.70 | 1.22 | 8.82 | 5.15 | 2.25 |
| **Tb** | 0.55 | 1.16 | 0.83 | 0.74 | 0.53 | 1.04 | 1.13 | 1.08 | 0.26 | 1.39 | 0.72 | 0.42 |
| **Dy** | 2.82 | 6.0 | 4.07 | 4.15 | 3.25 | 5.22 | 5.96 | 5.67 | 1.71 | 8.62 | 3.60 | 2.75 |
| **Ho** | 0.49 | 0.92 | 0.60 | 0.71 | 0.64 | 0.86 | 1.04 | 0.90 | 0.31 | 1.61 | 0.60 | 0.55 |
| **Er** | 1.19 | 1.92 | 1.10 | 1.62 | 1.79 | 2.07 | 2.44 | 2.00 | 0.82 | 4.00 | 1.31 | 1.52 |
| **Tm** | 0.16 | 0.23 | 0.14 | 0.22 | 0.28 | 0.27 | 0.35 | 0.23 | 0.13 | 0.53 | 0.17 | 0.21 |
| **Yb** | 0.97 | 1.41 | 0.84 | 1.37 | 1.70 | 1.44 | 1.96 | 1.31 | 0.79 | 3.15 | 1.02 | 1.19 |
| **Lu** | 0.13 | 0.19 | 0.12 | 0.20 | 0.25 | 0.19 | 0.27 | 0.17 | 0.11 | 0.40 | 0.16 | 0.18 |

Table 5.8: Major elements and trace elements of the metavolcanic rocks of the Sierra de Guadarrama (Continuation).

| Sample | T66 | T67 | T68 | T69 | T70 | T71 |
|---|---|---|---|---|---|---|
| Locality | La Berzosa | | El Cardoso | | | Riaza |
| $SiO_2$ | 72.51 | 76.37 | 66.58 | 65.72 | 65.1 | 72.75 |
| $TiO_2$ | 0.35 | 0.05 | 0.80 | 0.79 | 0.79 | 0.29 |
| $Al_2O_3$ | 14.7 | 13.01 | 15.96 | 16.48 | 16.24 | 13.9 |
| $FeO_t$ | 2.54 | 1.2 | 4.97 | 5.05 | 5.14 | 2.28 |
| MgO | 0.64 | 0.09 | 1.84 | 1.9 | 2.21 | 0.74 |
| MnO | 0.03 | 0.06 | 0.07 | 0.06 | 0.07 | 0.03 |
| CaO | 0.67 | 0.40 | 1.56 | 1.66 | 1.25 | 0.75 |
| $Na_2O$ | 2.04 | 2.14 | 2.32 | 2.36 | 2.48 | 2.23 |
| $K_2O$ | 4.5 | 5.94 | 3.74 | 3.87 | 3.95 | 4.64 |
| $P_2O_5$ | 0.16 | 0.17 | 0.20 | 0.20 | 0.20 | 0.15 |
| Li | 55.2 | 19.28 | 58.7 | 58.7 | 55 | 40.4 |
| Rb | 147 | 245 | 154 | 155 | 145 | 229 |
| Cs | 7.28 | 4.21 | 5.47 | 5.11 | 4.42 | 11.4 |
| Be | 2.64 | 1.32 | 2.35 | 2.36 | 2.13 | 1.74 |
| Sr | 159 | 65.0 | 237 | 223 | 168 | 73.7 |
| Ba | 688 | 776 | 925 | 832 | 773 | 250 |
| Sc | 14.4 | 4.52 | 13.3 | 12.9 | 13.7 | 4.45 |
| V | 99.1 | 17.7 | 85.8 | 84.6 | 91.3 | 28.4 |
| Cr | 80.6 | 15.9 | 61.1 | 58.0 | 69.2 | 15.8 |
| Co | 79.3 | 84.6 | 42.4 | 40.0 | 32.4 | 88.4 |
| Ni | 24.3 | 5.22 | 42.6 | 25.1 | 28.9 | 7.89 |
| Cu | 16.9 | 4.14 | 24.7 | 20.1 | 24.4 | 2.49 |
| Zn | 80.4 | 27.1 | 93.0 | 93.0 | 87.9 | 43.9 |
| Ga | 21.8 | 17.1 | 22.5 | 22.7 | 22.4 | 18.9 |
| Y | 14.3 | 12.8 | 26.8 | 30.4 | 19.0 | 15.2 |
| Nb | 12.3 | 6.35 | 12.6 | 12.7 | 12.0 | 7.63 |
| Ta | 1.11 | 1.19 | 1.01 | 1.00 | 1.04 | 0.97 |
| Zr | 170 | 59.0 | 227 | 225 | 219 | 116 |
| Hf | 5.20 | 2.40 | 6.40 | 6.30 | 6.10 | 3.70 |
| Mo | 0.37 | 0.25 | 0.80 | 1.22 | 0.92 | 0.34 |
| Sn | 5.88 | 13.0 | 4.64 | 4.75 | 4.44 | 7.83 |
| Tl | 0.90 | 1.35 | 0.86 | 0.91 | 0.83 | 1.26 |
| Pb | 21.6 | 27.8 | 22.3 | 18.5 | 19.7 | 19.0 |
| U | 3.59 | 5.82 | 3.51 | 3.41 | 3.39 | 4.04 |
| Th | 13.4 | 8.33 | 13.0 | 12.8 | 12.3 | 9.00 |
| La | 35.7 | 14.3 | 46.5 | 42.5 | 37.0 | 18.7 |
| Ce | 75.0 | 29.5 | 94.2 | 86.4 | 76.1 | 39.6 |
| Pr | 9.22 | 3.60 | 11.6 | 10.5 | 9.09 | 4.76 |
| Nd | 35.2 | 13.6 | 43.4 | 40.0 | 34.9 | 18.2 |
| Sm | 6.41 | 2.98 | 9.25 | 8.44 | 7.28 | 3.84 |
| Eu | 1.36 | 0.58 | 1.29 | 1.26 | 1.18 | 0.51 |
| Gd | 5.76 | 2.58 | 7.29 | 7.81 | 6.06 | 3.34 |
| Tb | 0.85 | 0.45 | 1.13 | 1.11 | 0.85 | 0.51 |
| Dy | 3.38 | 2.32 | 6.20 | 6.24 | 4.03 | 2.97 |
| Ho | 0.63 | 0.45 | 1.03 | 1.04 | 0.61 | 0.51 |
| Er | 1.28 | 1.22 | 2.56 | 2.57 | 1.48 | 1.24 |
| Tm | 0.16 | 0.21 | 0.33 | 0.35 | 0.21 | 0.18 |
| Yb | 0.99 | 1.15 | 2.09 | 2.27 | 1.34 | 1.18 |
| Lu | 0.14 | 0.19 | 0.33 | 0.30 | 0.23 | 0.18 |

Table 5.9: Major elements and trace elements of the metagranite of the Anatectic Complex of Toledo.

| **Sample** | **T74** |
|---|---|
| **Locality** | Mohares |
| **$SiO_2$** | 72.91 |
| **$TiO_2$** | 0.68 |
| **$Al_2O_3$** | 12.50 |
| **$FeO_t$** | 3.60 |
| **MgO** | 0.94 |
| **MnO** | 0.03 |
| **CaO** | 1.44 |
| **$Na_2O$** | 2.29 |
| **$K_2O$** | 3.59 |
| **$P_2O_5$** | 0.19 |
| **Li** | 46 |
| **Rb** | 185 |
| **Cs** | 2.46 |
| **Be** | 0.91 |
| **Sr** | 81.9 |
| **Ba** | 478 |
| **Sc** | 6.36 |
| **V** | 47.6 |
| **Cr** | 15.0 |
| **Co** | 99.8 |
| **Ni** | 8.57 |
| **Cu** | 12.0 |
| **Zn** | 76.3 |
| **Ga** | 21.2 |
| **Y** | 35.3 |
| **Nb** | 27.0 |
| **Ta** | 1.39 |
| **Zr** | 406 |
| **Hf** | 12.8 |
| **Mo** | 1.47 |
| **Sn** | 0.79 |
| **Tl** | 1.00 |
| **Pb** | 21.8 |
| **U** | 4.27 |
| **Th** | 44.5 |
| **La** | 77.4 |
| **Ce** | 158 |
| **Pr** | 18.4 |
| **Nd** | 66.9 |
| **Sm** | 13.6 |
| **Eu** | 1.21 |
| **Gd** | 11.1 |
| **Tb** | 1.64 |
| **Dy** | 8.39 |
| **Ho** | 1.44 |
| **Er** | 3.38 |
| **Tm** | 0.45 |
| **Yb** | 2.83 |
| **Lu** | 0.42 |

## 9.3. Table of Sr and Nd isotopic data

Table 5.10: Sr and Nd isotopes of the: MROS, metavolcanic rocks of the Ollo de Sapo Domain; MOS, metagranites of the Ollo de Sapo Domain; MTD, metagranites of the Tormes Dome; MGR, metagranites of the Sierra de Gredos; MGU, metagranites and metavolcanic rocks of the Sierra de Guadarrama

| Sample | Group | $(^{87}Sr/^{86}Sr)_{now}$ | $(^{143}Nd/^{144}Nd)_{now}$ | $(^{87}Sr/^{86}Sr)_{490Ma}$ | $(\epsilon Sr)_{490Ma}$ | $(^{143}Nd/^{144}Nd)_{490Ma}$ | $(\epsilon Nd)_{490Ma}$ | $Nd_{(CHUR)}$ (Ga) | $T_{(DM)}$ (Ga) |
|---|---|---|---|---|---|---|---|---|---|
| **T-2** | MROS | 0.72983 | 0.512172 | 0.70789 | 56 | 0.511765 | -4.7 | 1.0 | 1.7 |
| **T-4** | MROS | 0.73008 | 0.512208 | 0.7117 | 111 | 0.511789 | -4.2 | 1.0 | 1.7 |
| **T-5** | MROS | 0.73142 | 0.51217 | 0.7106 | 95 | 0.511750 | -5.0 | 1.1 | 1.8 |
| **T-6** | MROS | 0.73230 | 0.512203 | 0.71014 | 88 | 0.511786 | -4.3 | 1.0 | 1.7 |
| **T-7** | MROS | 0.73521 | 0.512258 | 0.70904 | 73 | 0.51184 | -3.3 | 0.9 | 1.6 |
| **T-8** | MROS | 0.74630 | 0.512206 | 0.71104 | 101 | 0.511795 | -4.1 | 1.0 | 1.7 |
| **T-10** | MROS | 0.73389 | 0.512183 | 0.70920 | 75 | 0.511762 | -4.8 | 1.1 | 1.8 |
| **T-12** | MROS | 0.71901 | 0.512177 | 0.70997 | 86 | 0.511787 | -4.3 | 0.9 | 1.6 |
| **T-15** | MROS | 0.74444 | 0.512159 | 0.70930 | 76 | 0.511712 | -5.8 | 1.3 | 2.0 |
| **T-16** | MROS | 0.73305 | 0.512126 | 0.7133 | 133 | 0.511710 | -5.8 | 1.2 | 1.9 |
| **T-18** | MROS | 0.73018 | 0.512148 | 0.71085 | 98 | 0.511720 | -5.6 | 1.2 | 1.9 |
| **T-19** | MROS | 0.73857 | 0.512199 | 0.70719 | 46 | 0.511785 | -4.3 | 1.0 | 1.7 |
| **T-20** | MROS | 0.73302 | 0.512174 | 0.70668 | 39 | 0.511755 | -5 | 1.1 | 1.8 |
| **T-21** | MROS | 0.73272 | 0.512219 | 0.71067 | 96 | 0.511800 | -4.0 | 1.0 | 1.7 |
| **T-22** | MROS | 0.72429 | 0.512214 | 0.71002 | 87 | 0.511807 | -3.9 | 0.9 | 1.6 |
| **T-24** | MOS | 0.72535 | 0.512209 | 0.70876 | 69 | 0.511802 | -4.0 | 0.9 | 1.7 |
| **T-25** | MOS | 0.74058 | 0.512565 | 0.70353 | -5.6 | 0.512115 | 2.1 | 0.2 | 1.2 |
| **T-26** | MOS | 0.73273 | 0.512463 | 0.70371 | -3.0 | 0.51202 | 0.20 | 0.5 | 1.4 |
| **T-27** | MOS | 0.7999 | 0.512258 | 0.7173 | 190 | 0.511785 | -4.3 | 1.2 | 2.0 |
| **T-28** | MOS | 0.71892 | 0.512136 | 0.70502 | 16 | 0.511832 | -3.4 | 0.8 | 1.3 |
| **T-29** | MOS | 0.7179 | 0.512232 | 0.70424 | 4.5 | 0.511918 | -1.7 | 0.6 | 1.2 |
| **T-31** | MOS | 0.86098 | 0.512407 | 0.70905 | 73 | 0.511884 | -2.4 | 1.0 | 2.2 |
| **T-33** | MOS | 0.74329 | 0.512268 | 0.70963 | 81 | 0.511840 | -3.3 | 0.9 | 1.7 |
| **T-34** | MOS | 0.7479 | 0.512244 | 0.71004 | 87 | 0.51181 | -3.9 | 1.0 | 1.8 |
| **T-35** | MOS | 0.75328 | 0.512307 | 0.71055 | 94 | 0.511872 | -2.6 | 0.8 | 1.6 |
| **T-37** | MTD | 0.84616 | 0.512278 | 0.71500 | 157 | 0.511834 | -3.4 | 0.9 | 1.8 |
| **T-39** | MTD | 0.79199 | 0.512152 | 0.70683 | 41 | 0.511707 | -5.9 | 1.3 | 2.0 |
| **T-45** | MGR | 0.77014 | 0.512208 | 0.70678 | 41 | 0.511778 | -4.5 | 1.0 | 1.8 |
| **T-46** | MGR | 0.76471 | 0.512264 | 0.71133 | 105 | 0.511832 | -3.4 | 0.9 | 1.7 |
| **T-48** | MGR | 0.74529 | 0.512276 | 0.70837 | 63 | 0.511844 | -3.2 | 0.9 | 1.7 |
| **T-51** | MGU | 0.76120 | 0.512209 | 0.70616 | 32 | 0.511781 | -4.4 | 1.0 | 1.8 |
| **T-53** | MGU | 0.74091 | 0.512246 | 0.71663 | 180.5 | 0.511850 | -3.1 | 0.8 | 1.5 |
| **T-56** | MGU | 0.75353 | 0.512231 | 0.71134 | 105 | 0.511788 | -4.3 | 1.1 | 1.9 |
| **T-59** | MGU | 0.72419 | 0.512212 | 0.71011 | 88 | 0.511816 | -3.7 | 0.9 | 1.6 |
| **T-61** | MGU | 0.74710 | 0.512268 | 0.71122 | 104 | 0.511839 | -3.3 | 0.9 | 1.7 |
| **T-63** | MGU | 0.74376 | 0.512188 | 0.71125 | 104 | 0.511779 | -4.4 | 1.0 | 1.7 |
| **T-64** | MGU | 0.81822 | 0.512169 | 0.71519 | 160 | 0.511607 | -7.8 | 3.3 | 3.8 |
| **T-66** | MGU | 0.72812 | 0.512179 | 0.71031 | 91 | 0.511790 | -4.2 | 0.9 | 1.6 |
| **T-67** | MGU | 0.78285 | 0.512191 | 0.71393 | 142 | 0.511747 | -5.1 | 1.2 | 1.9 |
| **T-68** | MGU | 0.72393 | 0.512185 | 0.71051 | 94 | 0.511788 | -4.3 | 0.9 | 1.6 |
| **T-70** | MGU | 0.72758 | 0.512166 | 0.70954 | 80 | 0.511760 | -4.8 | 1.0 | 1.7 |
| **T-71** | MGU | 0.7746 | 0.512212 | 0.70961 | 81 | 0.511782 | -4.4 | 1.0 | 1.8 |